Small RNA-Seq and real time qPCR to reveal Islet-miRNA modulation under stress and transplantation conditions

Aljani, Bssam

Awarding institution:
King's College London

Technische Universität Dresden
DFG-Center for Regenerative Therapies Dresden
AG Bonifacio

Small RNA-Seq and real time qPCR to reveal Islet-miRNA modulation under stress and transplantation conditions

D i s s e r t a t i o n s s c h r i f t

zur Erlangung des akademischen Grades
Doctor of Philosophy (Ph.D.)
vorgelegt
der Medizinischen Fakultät Carl Gustav Carus
der Technischen Universität Dresden

von

Bssam Aljani, M.D.
aus Syrien

Dresden 2021

1. Gutachter: Prof. Dr. Ezio Bonifacio

2. Gutachter: Prof. Dr. Michele Solimena

Tag der mündlichen Prüfung: (Verteidigungstermin): 05.10.2021

gez.: Prof. Dr. Kaomei Guan
Vorsitzender der Promotionskommission

Intelligence is the ability to adapt to change

Stephen Hawking (1942-2018)

Acknowledgments

First, I am deeply grateful to my principle supervisor Prof. Ezio Bonifacio who gave an exceptional opportunity to work on a very exciting project. Thank you for believing in me and for the guidance and support throughout the four years. Thank you for making me feel at home since the first day at the CRTD. Thank you for the scientific and non-scientific conversations which I enjoyed a lot.

I would like to extend my sincere thanks to Dr. Anne Eugster. Thank you for your patience and guidance. Thank you for your advice and dedication during writing my thesis.

I would like to thank Prof. Michele Solimena for his advice and guidance in the thesis advisory committee meetings.

I would like to thank the lab members of Bonifacio group. Marc Weigelt and Anne Karasinsky for their help in the animal experiments. Annett Lindner for helping me in the biomark work. Virag Sharma for his help in the NGS data analysis.

I would like to thank my co-supervisor at King's College London Prof. Peter Jones. Thank you for helping me to settle in at Guy's Campus and for the fruitful talks. Without your guidance I could not have been able to achieve my experiments at King's.

I would like to thank Prof. Stefan Bornstein the chair of the IRTG program. The funding of the Transcampus was essential to complete this work at TUD and KCL.

I am grateful to my dear parents. Without your support, I would not have been able to achieve my thesis. Especial thanks to my friends for the extensive support and encouragement all the way.

Contents

List of Figures

List of Tables

Abbreviations

3’UTR	Three prime untranslated region
AB	Antibody
Ago	Argonaute
Akt	Protein kinase B (PKB)
ALT	Alanine Aminotransferase
ANOVA	Analysis of variance
APCs	Antigen-presenting cells
AST	Aspartate Transaminase
ATP/ADP	adenosine tri/diphosphate
AUC	Areas under the ROC curve
BL6	Black 6
BSA	Bovine serum albumin
CA	Aggressive cytokines mix
cCas3	cleaved caspase-3
CCR4-Not	Carbon Catabolite Repression—Negative On TATA-less
cDNA	Complementary DNA
CEA	Carcinoembryonic antigen
CM	Mild cytokines mix
CNS	central nervous system
Cq	Quantification cycle
DAPI	4’,6-diamidino-2-phenylindole
dATP	Deoxyadenosine triphosphate
DCP	Decapping protein
dCTP	Deoxycytidine triphosphate
DDX6	DEAD box protein 6
DGCR8	DiGeorge critical region 8 protein
dGTP	Deoxyguanosine triphosphate
dSTZ	diabetic STZ-treated
EDC	Enhancer of decapping
EDTA	Ethylenediaminetetraacetic acid
ELISA	Enzyme-linked immunosorbent assay
EPITA	European Pancreas and Islet Transplantation Association
ER	Endoplasmic reticulum
ErnB	EGF receptor family
FBS	Fetal bovine serum

FC	Fold change
FCS	Fetal calf serum
GAD65	glutamic acid decarboxylase 65 kDa
GADA	Glutamic acid decarboxylase antibodies
GC	Guanine-cytosine
GLUT	Glucose transporter
GSIS	Glucose-stimulated insulin secretion
GW182	glycine-tryptophan 182kDa
H	Hypoxia
HbA1c	Hemoglobin A1c
HCA	Hypoxia+Aggressive cytokines mix
HCL	hydrochloride
HCM	Hypoxia+Mild cytokines mix
HDL	High density lipoproteins
HIF-1α	Hypoxia-inducible factor-1α
HLA	Human leukocyte antigen
HMGB1	High-mobility group box 1
HSD	Honestly significant difference
IA-2	Islet-cell antigen-2
IEQ	Islets equivalent
IFN-γ	Interferon gamma
IL-1β	Interleukin 1 beta
IPITA	International Pancreas and Islet Transplant Association
IU	International Unit
IVC	Individually ventilated cages
JNK	c-Jun N-terminal kinase
K_{ATP} channel	ATP-sensitive potassium channel
KEGG	Kyoto Encyclopedia of Genes and Genomes
LDL	Low density lipoproteins
L-glut	L-glutamine
MAPK	Mitogen-activated protein kinase
MEKK	Mitogen-activated protein kinase kinase
MEM	Minimum Essential Medium
MIN6	Mouse INsulinoma 6
mirDIP	microRNA Data Integration Portal
miRISC	Minimal miRNA-induced silencing complex

miRNA	MicroRNA
mTOR	Mechanistic target of rapamycin
NCS	Newborn calf serum
ndSTZ	non- diabetic STZ-treated
NF-κB	Nuclear factor kappa-light-chain-enhancer of activated B cells
NGS	Next-Generation Sequencing
NIH	National Institutes of Health
NKT	Natural killer T cells
NO	Nitric oxide
NOD	Non-obese diabetic
NPM1	Nucleophosmin1
nSMase2	Neutral sphingomyelinase
OGTT	Oral glucose tolerance test
OHA	Oral hypoglycemic agents
P/S	Penicillin - Streptomycin
PABP	poly(A)-binding protein
PACT	protein activator of PKR
PAN	Poly(A) Specific Ribonuclease Subunit
PBS	Phosphate-Buffered Saline
PCR	Polymerase Chain Reaction
PI3K	Phosphoinositide 3-kinase
pre-miRNA	precursor miRNA
pri-miRNAs	primary miRNAs
Ran-GTP	guanosine triphosphate-binding Ran (RAs-related Nuclear protein)
RISC	RNA-induced silencing complex
RLU	Relative light unit
RNU6	RNA, U6 small nuclear
ROC	Receiver-operating characteristic
RT-qPCR	Quantitative reverse transcription PCR
SD	Standard deviation
SEM	Standard error of the mean
SNORDs	C/D box snoRNAs
snoRNA	Small nucleolar RNA
SNP	Single-nucleotide polymorphism
STZ	Streptozotocin
TAMs	Tumor-associated macrophages
TNF-α	Tumor necrosis factor alpha

TRBP	Trans-activation response RNA-binding protein
tRNA	Transfer RNA
VGCCs	Voltage-gated calcium channels
XRN1	5’-3’ exoribonuclease 1
ZnT8	Zinc transporter 8

Abstract

Replacement of β-cells through islet transplantation is a potential therapeutic approach for individuals with type 1 diabetes that is hard-to-control with conventional approaches. β-cell stress and death, due to exposure to stressors such as inflammation and hypoxia, is a major challenge of islet transplantation. It is of utmost importance to diagnose β-cell insults before massive cell loss occurs and hence rapid intervention can be taken. Currently utilized markers often fail to detect β-cell stress and death in timely manner and only indicate massive changes in β-cell function. Thus, biomarkers reflect the actual rate of β-cell stress and death are required. Here, I set out to identify microRNAs (miRNAs) that could be reflective of β-cell stress and death. I measured circulating miRNAs in diabetic animal model established using STZ β-cell toxin and in healthy animals. I investigated miRNA induction, in response to various degrees of hypoxic and inflammatory stressors, *in vitro* in animal and human islet-stress model. Lastly, I sought to explore biological pathways targeted by cytokines- and/or hypoxia-induced miRNAs. These studies contribute to the establishment of biomarkers of β-cell stress and death in the context of islet transplantation aiming at early intervention and rescue the islet graft. Further, the findings could be useful in the development of therapies that safeguard islet against harmful stressors.

1 Introduction

1.1 Type 1 diabetes

Type 1 diabetes is a chronic autoimmune disease resulting from the selective destruction of insulin producing β-cell in the pancreatic islets by autoreactive T-cells, which leads to insulin secretion insufficiency and lifelong exogenous insulin dependency (Morran et al., 2008). The autoimmunity against β-cell is characterized by the presence of autoantibodies against autoantigens corresponding with β-cell components or products such as insulin, IA-2 and IA-2β (islet-cell antigen-2), GAD65 (glutamic acid decarboxylase 65 kDa), and ZnT8 (Zinc transporter 8).

β-cells are prime components of the pancreatic islets of Langerhans which are islands of cells grouped together in 50-500um diameter structure distributed within the pancreas and representing the hormone synthesizing part of it. Each islet has around 1000 cells, of which 60-70% are β-cells in human (Persaud et al., 2014) and the rest are comprised of glucagon-secreting α-cells, somatostatin-secreting δ-cells, and pancreatic polypeptide-secreting γ-cells (PP cells).

The main function of β-cells is insulin secretion in a well regulated process referred to as GSIS (glucose-stimulated insulin secretion). Here, insulin is secreted as a reaction to stimuli such as meals or hormones in order to keep blood glucose level tightly adjusted. Two phases of insulin secretion were identified. The GSIS starts with glucose entry to β-cells via GLUT1 (glucose transporter 1) and the following metabolism of it inside β-cells. This process results in ATP production leading to an increase of the ratio ATP/ADP, which in turn induces the shutdown of K_{ATP} channel (ATP-sensitive potassium channel). The latter causes cell membrane depolarization that leads to the induction of VGCCs (voltage-gated calcium channels) which allows the entry of Ca^{+2} inside β-cells. The quick increase of Ca^{+2} within β-cells promotes the release of insulin loaded in granules located near to the plasma membrane through exocytosis. The massive release of insulin from already synthesized granules reflects the earlier peak of insulin elevation after stimulation (first phase). The second phase represented by lower but more prolonged insulin secretion and that requires the recruitment of newly manufactured granules (Meier, 2016; Campbell and Newgard, 2021).

Given the pivotal role of β-cell in insulin secretion, their destruction by the immune system leads to the lack of such vital function of insulin secretion and the following loss of blood glucose control.

The trigger that stands behind the initiation of a β-cell attack by immune cells and, thus, the onset of type 1 diabetes is not determined yet.

Genetic predisposition plays an essential role in the development of type 1 diabetes. Certain HLA (human leukocyte antigen) class II gene loci on chromosome 6 correlated with type 1 diabetes, particularly the alleles HLA-DRB1, and HLA-DQB1/DQA1 (Noble et al., 2010). Other genomic sites have been implicated in type 1 diabetes. A number of SNPs (Single-nucleotide polymorphism) were identified that could increase type 1 diabetes prediction when used in combination with HLA genotypes (Winkler et al., 2014). Environmental factors (Forlenza and Rewers, 2011) and certain infections (Hyöty and Taylor, 2002) were investigated as potential triggers but as of today no conclusions have been reached.

The typical clinical manifestations of type 1 diabetes include frequent urination, excessive thirst, excessive appetite, weight loss and fatigue. The diagnosis of type 1 diabetes is made when fasting blood glucose is ≥126 mg/dl, random blood glucose or after 2 hours in OGTT (oral glucose tolerance test) ≥200 mg/dl or (Hemoglobin A1c) HbA1c ≥6.5% (American Diabetes Association, 2016).

The cornerstones in type 1 diabetes management are exogenous insulin replacement and close blood glucose monitoring. The aim is to keep HbA1c below 7% and blood glucose below 154 mg/dl (American Diabetes Association, 2016). The insulin replacement therapy has turned type 1 diabetes from a fatal into a relatively manageable condition and when combined with tight blood glucose control, the development of type 1 diabetes complications can be reduced in the long run. Different insulin types (e.g. rapid-, short-, intermediate-, and long-acting) in addition to the revolution in blood glucose monitoring technology (i.e. continues blood glucose monitoring) offer numerous options for individualized diabetic patient care. The insulin pump is one of these advanced technologies that allows continuous, live blood glucose monitoring and releases insulin according to the momentary needs of the patient.

Although the above-mentioned strategies offer optimal blood glucose control to many patients, such devices and compounds constitute a financial burden. Furthermore, devices have an error range, which could be problematic; for instance, if the device measures blood glucose inaccurately, this will induces the release of inaccurate dose of insulin. The establishment of a system that mimics the physiological insulin dynamics is far from being achieved.

A fraction of individuals with type 1 diabetes experience severe blood glucose control-related issues. In those individuals, it becomes difficult to control hypoglycemia/hyperglycemia, in spite of recruiting intensive conventional strategies such as insulin administration, to the extent of limiting their daily activities. Beside the life-threatening hypoglycemia unawareness; the stress, dizziness, and blurred vision could be devastating in situations such as driving. Such condition is referred to as brittle or labile type 1 diabetes. This condition raised the need for alternative management strategies.

Indeed, newer approaches for type 1 diabetes management are evolving. A huge amount of research is focused on the potential of other islet cells to replace the destructed β-cells, and the possibility of using stem cells to produce cells that are as close as possible to the insulin-producing β-cells.

Moreover, the substitution of destructed islets by healthy islets obtained from donors is showing great promise in this regard, especially for patients suffering from the brittle type 1 diabetes.

1.2 Pancreatic Islet transplantation

The principle of islet transplantation is to replace islets of a patient either by the patient's own islets (autotransplant) or by islets obtained from a deceased donor (allotransplant). Adequate quantity and quality of isolated human islets are required; therefore, several protocols were developed and shown to succeed to secure islets demand for transplantation (Paget et al., 2007). In 1967, the first method to isolate islets based on collagenase dissociation was introduced (Naftanel and Harlan, 2004), followed by the establishment of density gradient to purify islets in 1969 and the islet isolation protocol in 1981 (Horaguchi and Merrell, 1981). The eighties witnessed even more improvements in the isolation process culminating in the automated method for islet isolation described in 1988 (Ricordi et al., 1988).

The first clinical trial of islet transplantation took place in 1985 and in the beginning of 1990s the first insulin-independence cases after transplantation were reported (Scharp et al., 1990).

However, a 100% insulin independence was only reported in 2000 thanks to Edmonton protocol established by James Shapiro et al. (Shapiro et al., 2000). The protocol comprised infusing around 11500 IE/Kg (Islets equivalent/body weight) and the use of immunosuppressants (daclizumab, tacrolimus, and sirolimus) without the use of glucocorticoids. Enormous progress in the field of

islet transplantation was achieved following the initiation of Edmonton protocol. In 2016, an eight center clinical trial by the NIH (National Institutes of Health) reported HbA1c ≤7% in 87.5% and 71% of patients after 1 and 2 years post transplantation, respectively (Hering et al., 2016).

Islet allotransplantation is usually applied in the context of type 1 diabetes treatment while auto-transplantation is performed as part of pancreatitis management and will here not be discussed further (Rickels and Robertson, 2019).

In allotransplantation, tissue compatibility between the donor and the recipient needs to be tested beforehand in terms of blood group, HLA antibodies (in the recipient), and T and B lymphocyte crossmatching (to test the presence of antibodies in the recipient blood against the donor's lymphocytes). The pancreas obtained from a deceased donor is digested by collagenase injected through the pancreatic duct cannulation and by placing the pancreas into a Ricordi chamber. The digestion product is then loaded on an osmotic gradient for islets separation and purification (Rickels and Robertson, 2019). The isolated islets are then cultured for 24-72H (Shapiro et al., 2017) before transferring them to a recipient with type 1 diabetes. To do so, the portal vein of the patient is catheterized percutaneously with guidance of ultrasound and the islets are infused. After transplantation, the recipients are subjected to an immunosuppressant regimen such as daclizumab and alemtuzumab or tacrolimus to keep the islets from being destroyed by the immune system (Shapiro et al., 2017).

Not all individuals with type 1 diabetes are eligible for islet transplantation. The inclusion criteria are: type 1 diabetes for more than 5 years with non-measureable C-peptide associated with severe hypoglycemia (≥2 event/year) or one event of hypoglycemia unawareness and/or glycemic lability and that despite the use of all possible conventional insulin therapy and blood glucose monitoring utilities. The age should be more than 18 to avoid the side effects of the immunosuppressants in younger patients (Shapiro et al., 2017; Rickels and Robertson, 2019).

The outcomes of islet transplantation are promising for a number of patients, sometimes for limited time, but still, many patients that undergo transplantation relinquish the insulin injections and thus improve their quality of life. Figure 1.1. Data of 864 islet transplantation cases showed that 80% demonstrated insulin independence after ≥2 weeks and 50% after 5 years (Collaborative Islet Transplantation Registry, annual report 2014). In the Edmonton protocol, 73% of patients had HbA1c less than 6.5% after 10 years. The hypoglycemic episodes decreased significantly

as well (Shapiro et al., 2017). Some parameters, such as the number of islet infusions and the period of islet culture before infusion seem to influence the capacity of patients to reach insulin independence (Gaber et al., 2001; Markmann et al., 2003). When comparing the outcomes of islet transplantation with conventional approaches in type 1 diabetes management such as insulin therapy, it has been shown that patients with problematic hypoglycemia that underwent islet transplantation had a significant decrease in HbA1c after six months (HbA1c decreased from 8.1% to 5.6%) while no improvement in HbA1c was reported with intensive insulin therapy (HbA1c was 8.2% after six months and baseline: 8.1%) (Lablanche et al., 2018).

Although islet transplantation offers a promising option in type 1 diabetes management, the procedure faces limitations that I will discuss here.

The scarcity of islets is an important aspect since the demand is much higher than the supply; for instance, in the US there is no less than 1 million people with type 1 diabetes and hardly few thousand donors yearly (Naftanel and Harlan, 2004). Additionally, most patients will need more than one infusion to establish good blood glucose control; as required per Edmonton protocol >9000 IE/kg are needed per patient to reach insulin independency, and for that more than two donors are needed for one patient.

Poor islet engraftment is another important factor impeding full and long-term success of islet transplantation. One of the major mechanisms behind the insufficient engraftment is the inflammatory stress (Bennet et al., 2000), which eventually leads to cell death and important decrease in the number of transplanted islets and subsequent decrease in insulin secretion. The addition of antibodies against certain inflammatory cytokine receptors or the inhibition of their action during the islet transplantation protocol improve islet survival and function (Rickels et al., 2013). For example Etanercept, a TNF-α receptor antibody, and Anakinra, an IL-1β receptor antagonist, were used successfully in the protocol of islet transplantation (Hering, 2005; Matsumoto et al., 2011). Blocking the secretion of IFN-γ by NKT cells (natural killer T cells) is another way to improve islet survival, either by using an α-galactosylceramide- or HMGB1 (high-mobility group box 1) antibody (Yasunami et al., 2005; Matsuoka et al., 2010).

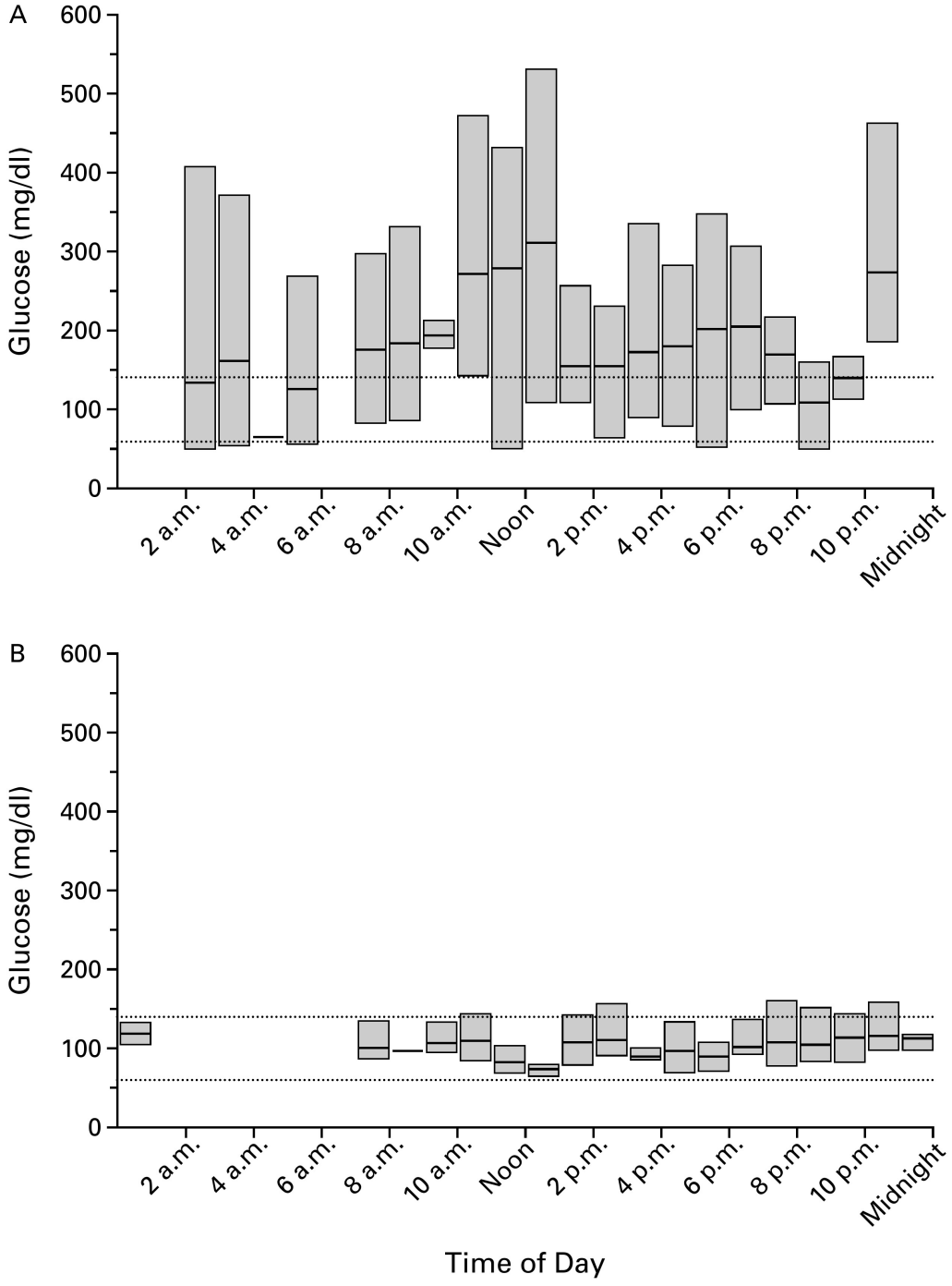

Figure 1.1: Blood glucose profile before (A) and after (B) islet transplantation. An exemplary blood glucose measurement in 24H for one patient during one month. Median values are presented. The two dotted lines indicate blood glucose range between 60 and 140 mg/dl. The figure adapted from (Shapiro et al., 2000).

Oxygen limitation is another factor leading to islet loss. In the healthy situation, islets are located in a high-oxygen supply environment due to the abundance of vascularization in the pancreas. When transferring the islets alone without its network of blood vesicles into the liver they will experience a detrimental lack of oxygen negatively affecting their viability as well as functionality, at least until new vesicles are built up around them (Komatsu et al., 2018).

Next, chronic or acute islet loss could be caused by alloimmunity, which is characterized by chronic or acute rejection of islet transplant. The use of islets from multiple donors increases the risk of formation of antibodies towards the HLA of the donor and thus risking islet survival.

And last, another reason for islet loss is recurrence of type 1 diabetes autoimmunity, and as for alloimmunity, this can occur in the short- or long-term.

The limiting factors discussed above eventually lead to islet stress and death and this clearly hinders the islets transplantation from being an optimal treatment choice particularly in the long-term. The islet stress and death results in insufficient insulin secretion and the patient will need insulin shots again, alone or with additional islet infusions. This situation demanded a tool that helps identify stress or cell death in timely manner. Such tools confer early intervention before massive loss in islets takes place. An indicator that could be characteristic of islets loss is vital in monitoring islet status after transplantation.

1.3 What is a biomarker?

A biomarker is a substance that provides valuable information about a physiological process, disease or condition. Biomarkers can serve to diagnose, classify and provide a prognosis of a disease. Biomarkers are also in use to evaluate the response to a drug or to a medical procedure (Biomarkers Definitions Working Group, 2001).

Biomarkers are used widely in daily medical routine. For instance, in the context of diabetes the measurement of blood glucose and HbA1c are the main criteria for diagnosis and are the essential parameters to monitor the response to treatment. Another example is carcinoembryonic antigen (CEA), an important biomarker used for the detection of recurrence in colorectal cancer in the absence of symptoms (Duffy, 2001).

One problem with the usage of biomarkers in the course of a disease is the possible false positivity

and/or false negativity of the biomarker measurements. Other parameters are used to determine if the measured value is indeed false positive or negative – that is, to achieve a correct evaluation of the patient‘s state. These parameters could be for instance clinical findings, or other biological measurements. An optimal laboratory test does not exist; any test can give positive outcome although the patient (sample) is negative for the tested condition or molecule and vice versa.

To which extent a test is powerful in establishing a separation between ‘normal’ and ‘abnormal,’ certain statistical measures need to be considered, namely, the specificity and sensitivity of the tested biomarker and the positive and negative predictive values, which are a function of specificity, sensitivity and the prevalence of the condition in the tested population. The sensitivity is used to assess the power of a test to identify positive ‘subjects.’ Specificity is the capability of a test to exclude a condition (identify negative subjects). However, the recent advances allow the measurement of many potential markers for example genes or proteins at once in a sample set to identify disease/condition signatures. It is well established that when the measured compounds show different patterns as a response to a disease/condition, this will enhance the specificity and sensitivity of the test (LaBaer, 2005).

Practically, the biomarker detection in a relatively easy-accessible sample such as blood or urine represents a very attractive tool in the field of disease/condition monitoring or diagnosis. One of the principles that such a procedure is based on is the notion that these markers are not present in the circulation in the “healthy” situation and once the tissue experiences distress, those markers appear in the circulation as a result of e.g. tissue damage. On the cellular level, if the cell is exposed to harmful factors (for example inflammation, infection, and metabolic stress) it tries to adapt to the new situation in order to survive. This adaptation triggers the recruitment of pathways involved in cell stress and death and the related molecules (proteins, nucleic acids, etc.). In β-cells, it was shown that inflammatory mediators can induce ER (endoplasmic reticulum) stress and NF-κB pathway, which was evidenced by pronounced changes in gene expression such as the decrease of Pdx1 and the increase of Nos2 (Tersey et al., 2012). This indicates that stressors affect molecules expressed inside β-cells and those affected molecules can break out of the cell and be therefore expressive of cell-stress. For instance, nucleic acids and proteins can find their way to extra-cellular space and their detection could be suggestive of cell stress or dysfunction. However, the exact mechanism for how the stress cascades lead to such release of molecules is not fully understood. The potential ways through which stress-indicators can leave

out to the extra-cellular space are the secretory machinery of the endoplasmic reticulum/Golgi apparatus, vesicles such as apoptotic bodies or microvesicles, and cell necrosis (Sims et al., 2018).

Through these ways some molecules have been studied as markers of β-cells stress or dysfunction and some are still being investigated. In the next chapter, I will discuss some of these molecules in more details.

1.4 Proposed markers for β-cell stress and death detection after islet transplantation

The monitoring of islet function and viability is an important aspect when it comes to establishing islet transplantation as a treatment for brittle type 1 diabetes. Such monitoring would provide a precious opportunity to rescue the islet graft on time, before a significant amount of islets are destroyed and subsequently becoming clinically overt. Several indicators are used so far and new indicators are emerging and still in development.

1.4.1 Metabolic tests

After transplantation, the monitoring of blood glucose, HbA1c, and C-peptide offers a handy way to assess islets function. Individuals with type 1 diabetes who are eligible for islet transplantation normally do not have detectable C-peptide and hence the detection of C-peptide after transplantation informs about islet function such as the conversion of C-peptide from positive to negative. Another advantage of the C-peptide monitoring is that C-peptide level is not affected when administrating exogenous insulin since it is frequent that patients who underwent islet transplantation need insulin therapy (Palmer et al., 2004).

In 2018, the IPITA (International Pancreas and Islet Transplant Association) and EPITA (European Pancreas and Islet Transplantation Association) established parameters that should be used to assess the islet graft function. Optimal graft function in patients is defined by the presence of C-peptide >0.5 ng/ml, HbA1c ≤6.5% and by the absence of severe hypoglycemia and the need of insulin therapy or OHA (oral hypoglycemic agents). Good graft function is defined by the presence of C-peptide >0.5 ng/ml, HbA1c <7%, and by the absence of severe hypoglycemia and by a >50% decrease in insulin need. Marginal graft function is defined by the presence of

C-peptide >0.5 ng/ml, HbA1c >7%, by the presence of severe hypoglycemia and by a <50% decrease in insulin need (Rickels et al., 2018).

Although these metabolic markers allow to assess the glycemic control after transplantation, they do not reflect advancing cell death of the transplanted islets and minor changes in the islet mass. C-peptide for example can be considered an important marker when massive loss of islets occurs, but does not allow to detect the gradual onset of islet stress and death (AlRashidi and Gillespie, 2018). The C-peptide level is also affected by other characteristics such as insulin sensitivity (Saisho, 2016).

1.4.2 Circulating proteins

Autoantibodies, such as antibodies against GAD65, islet antigen insulinoma-associated protein-2 (IA-2), and zinc transporter type 8 antigen (ZnT8) autoantibodies are considered potential indicators to predict islet graft status after islet transplantation. Autoantibodies are used intensively in type 1 diabetes trials and they could be useful in the context of islet transplantation as well.

If autoantibodies are negative before transplantation, and convert to positive after transplantation this conversion indicates recurrence of autoimmunity. However, if autoantibodies were positive before transplantation and a new elevation is detected after transplantation, the relation between this increase and the graft status is not clarified yet (Monti et al., 2015).

The use of multiple autoantibodies was shown to be useful for assessing the outcome of pancreas transplantation (Vendrame et al., 2010). In a study with 59 islet transplant recipients, 20.3% of patients showed autoantibodies (GADA, IA-2A, or ZnT8A) elevation which correlated with islet graft survival (Piemonti et al., 2013). Perhaps the major drawback in the use of autoantibodies to predict the graft status after transplantation is that the administration of immunosuppressants potentially highly affects the production of such autoantibodies after transplantation. Further, patients undergoing transplantation mostly already have increased type 1 diabetes specific autoantibodies. Therefore, only if a clear increase in the measured autoantibodies is detected, can one use them as a measure of poor implant status.

Some β-cell compounds, as for example GAD65, have attracted interest. Because β-cell release their content to the circulation when they die, the ability to measure β-cell proteins in the circulation should be reflective of cell death. Using highly sensitive assays, a study showed an acute

elevation of GAD65 after islet transplantation during the first 24H (Costa et al., 2015). The use of GAD65 as marker of islet death is hampered by several factors. Specificity is a concern since GAD65 is expressed predominantly in β-cell but also in the central nervous system (CNS). It might be indicative of not only autoimmunity affecting β-cells but also autoimmune disorders that affect the CNS as well. Therefore, the positivity of GAD65 should be interpreted carefully when several autoimmune disorders are present (McKeon and Tracy, 2017). Another issue is the short presence of GAD65 in the circulation since its half-life is around 180min (Darden et al., 2020), that means the need of frequent sampling to follow its detection capacity making it less attractive especially in relatively long-time interval monitoring.

1.4.3 Nucleic acid

Detecting the DNA in the circulation is a possible method to predict β-cell death since the cells release their DNA after cell death. The principle in DNA biomarkers is to investigate certain changes in the released DNA. To look for changes that are specific to β-cells that are dying, one can search for de-methylation of genes that are specifically expressed in β-cells, since the methylation is present on genes that are suppressed, while the methylation is absent in highly expressed genes.

One possible candidate for a DNA marker of β-cell death is the gene encoding for insulin (*INS*). Cytosine methylation was studied for *INS*. Since the gene is highly expressed in β-cells, one can assume that *INS* DNA that has been released from dying β-cells lacks cytosine methylation. It was therefore hypothesized that increased level of unmethylated *INS* in the circulation could be an indicator of β-cell death. Studies showed indeed an increase in unmethylated *INS* in a diabetic mouse model (diabetes induced by streptozotocin) and in non-obese diabetic mice (NOD mice) (Husseiny et al., 2014) and after islet transplantation in human (Bellin et al., 2017).

Although these findings are encouraging, tissue specificity remains an issue. Some other genes that are expressed in β-cells also showed similar pattern of unmethylation in α-cells as well (Neiman et al., 2017). Additionally, unmethylated *INS* gene was detected in other tissues (Husseiny et al., 2014) and this is problematic when it comes to tissue mass if comparing the islets mass to relatively larger tissues such as spleen. The elevation of unmethylated *INS* in the circulation could therefore not be exclusively attributed to β-cells injury but can originate as a

result of minor cell death in larger organs that express such unmethylation.

Some RNA molecules (miRNAs, circular RNAs, and small nucleolar RNAs) were proposed as markers of β-cells stress and death. MiRNAs can be accessed non-invasively as they are present in most biofluids and can be measured with relatively cost-effective methods. Adding the fact that more than 60% of the genes encoding proteins in human can be regulated by miRNAs (Friedman et al., 2008), miRNAs could mirror the status of the cell either on the physiological or on the pathological level.

The easy accessibility of miRNAs, their cost-effective quantification, implication in several physiological processes in the cell, and other characteristics (see below), created the proposition that these molecules could constitute a brand-new class of biomarkers. Some miRNAs were already extensively studied in this regard. miR-375 for example was proposed as a biomarker in the context of β-cell death and diabetes (Erener et al., 2013; Kanak et al., 2015; Latreille et al., 2015; Marchand et al., 2016; Patoulias, 2018; Sedgeman et al., 2019; Vasu et al., 2019). More miRNAs are emerging and showing promise as markers for type 1 diabetes, for example circulating miR-21, miR-25, miR-146a, and miR-181a (Liu et al., 2019).

To shed some light on these small RNA molecules I will discuss in the following chapter in detail their synthesis, biological roles and their presence in the circulation.

1.5 miRNAs

miRNAs are short (21–25 nucleotides in length) single-stranded RNA molecules, originated from a hairpin-like structure. miRNAs are considered as gene silencers post-transcriptionally.

In 1993 the first miRNA, *lin-4*, was discovered in *Caenorhabditis elegans* (Lee et al., 1993. In 2000). The door was opened widely to the miRNA research when the miRNA *let-7* was detected in *Caenorhabditis elegans* and in humans (Pasquinelli et al., 2000). Today, thanks to advances in next generation sequencing technologies numerous miRNAs have been identified and more than 1900 human miRNAs are stored in miRBase (version 22.1). Bioinformatic studies even predict 2300 miRNAs to exist in human (Alles et al., 2019).

1.5.1 Biogenesis

Starting from a miRNA gene, the transcription can be initiated by RNA polymerase II or RNA polymerase III (Pol II/ III), but in most of the cases Pol II is responsible for this process (Lee et al., 2004). The products of transcription are referred to as pri-miRNAs (primary miRNAs). pri-miRNAs have one or more hairpins and the mature miRNA sits within the double stranded structure. Fig.1.2. At the end of the hairpin structure of pri-miRNA there are two flanking segments, that, via interaction with DGCR8, guide Drosha in the cutting process of the pri-miRNA (Wahid et al., 2010).

In the nucleus, a complex comprising Drosha (RNase III enzyme) and DiGeorge critical region 8 protein (DGCR8) and termed microprocessor complex, splits the pri-miRNA into the pre-miRNA (precursor miRNA) which is around 70 nucleotide in length and still has the hairpin structure (Lee, 2002).

The pre-miRNA is then transferred from the nucleus to the cytoplasm via Exportin-5 with assistance of Ran-GTP (guanosine triphosphate-binding Ran (RAs-related Nuclear protein)) (Yi, 2003). Exportin-5 identifies the pre-miRNA by length. By exporting the pre-miRNA, Exportin-5 safeguards it from degradation in the nucleus (Zeng, 2004).

The pre-miRNA is then further processed in the cytoplasm. An RNase III enzyme, Dicer, leads the cleavage process which results in the production of the mature miRNA. Dicer acts with the help of two proteins, TRBP (trans-activation response RNA-binding protein) and PACT (protein activator of PKR) (Chendrimada et al., 2005; Lee et al., 2006). Dicer cuts the pre-miRNA loop in a miRNA duplex of around 22 nucleotides. Dicer is vital for miRNA synthesis and is an essential protein. In mouse, the knockout of Dicer leads to death in the early stages of development (Bernstein et al., 2003).

The next step is the separation of the two strands of the miRNA duplex which results in two strands. One strand is called “guide strand,” the actual effector miRNA which is loaded into RISC (RNA-induced silencing complex consisting of four types of Argonaute proteins (Ago) Ago 1-4 in human) (MacRae et al., 2008). Subsequently, the complex miRISC (minimal miRNA-induced silencing complex) is formed (Kawamata and Tomari, 2010).

The second strand is called “passenger strand” (referred to previously with an asterisk miRNA*)

which typically degrades. Some studies showed that this is not always the case and sometimes the passenger strand can act as the guide strand and can be biologically active (Guo and Lu, 2010). The nomenclature of the mature miRNA strand refers to the end of the hairpin structure from which the miRNA was produced. It is called -5p if the miRNA results from the 5′ end of the pre-miRNA and -3p if the miRNA results from the 3’ end. This new, more precise nomenclature made the asterisk used for the “passenger strand” obsolete.

The mechanism of nomination of the strand to be chosen (5p or 3p) to be incorporated with Ago proteins is not fully understood. However, it has been suggested that the thermodynamic characteristics of the miRNA duplex, the physiological and pathophysiological status of the cell and the cell type could be important determinants of this process (Khvorova et al., 2003; Meijer et al., 2014).

The pathway described above is the canonical pathway of miRNA synthesis. Non-canonical pathways were also identified. For instance, the pre-miRNAs can originate in mirtrons (short introns) without the need of the complex Drosha/DGCR8 as described above. However, they are transferred with Exportin-5 to the cytoplasm and further processed by Dicer same as for the canonical pathway (Ruby et al., 2007).

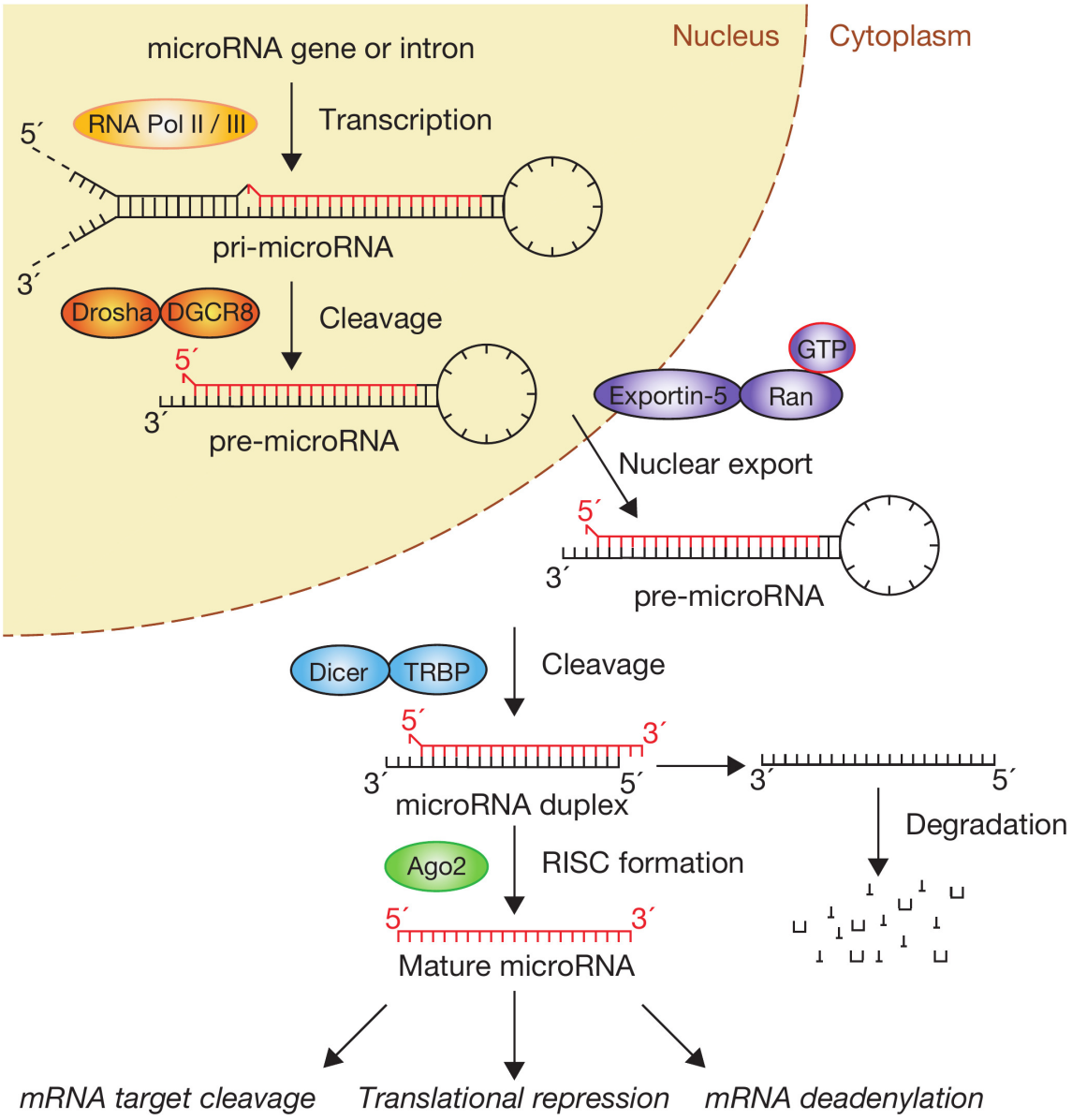

Figure 1.2: The canonical pathway of miRNA synthesis. In the nucleus, pri-miRNAs (primary miRNAS) are produced through the transcription of miRNA genes by RNA polymerase II or RNA polymerase III (Pol II/ III). The Drosha-DGCR8 complex cuts the pri-miRNA into the pre-miRNA (precursor miRNA) which is transferred to the cytoplasm by Exportin-5 where it is cleaved by Dicer-TRPB. The latter cleavage produces the guide strand (the functional mature miRNA) which is incorporated into the RISC. The other strand is degraded (referred to as passenger strand). The figure is adapted from (Winter et al., 2009).

1.5.2 Function

In general, miRNAs suppress gene expression, but some studies revealed also roles in expression induction.

In principle, miRNAs loaded within RISC associated with one of the Ago family (Ago1-4), need to bind to the mRNA (messenger RNA) target so they can exert their role. This binding occurs by means of Watson-Crick base-pairing between the miRNA seed (2-8 nucleotides), which is located at the 5′ end, and the 3'UTR (Three prime untranslated region) on the target mRNA side (Kim et al., 2017).

The extent of complementarity between the two sites (miRNA seed and 3'UTR) is essential in determining the mechanism through which the miRNA suppresses gene expression. In the case of perfect matching, the result is a cleavage of the mRNA target – and this cleavage exclusively carried out by Ago2 among the four types of Ago proteins (Kawamata and Tomari, 2010). In the case of imperfect matching, inhibition of translation is the dominant mechanism by which the gene expression is suppressed (Bartel, 2004). The inhibition of translation can occur by two mechanisms: the deadenylation and decapping of mRNA followed by mRNA degradation.

Deadenylation: The binding between miRISC and the mRNA target induces the engagement of GW182 proteins (named due to their content of glycine-tryptophan "GW" repeats and their molecular weight 182kDa (Eystathioy et al., 2002) which transact with Ago proteins of miRISC (Huntzinger and Izaurralde, 2011). The deadenylation is carried out by the interaction between GW182 and PABP C (poly(A)-binding protein). The latter engage PAN2–PAN3 and CCR4–NOT, which take over the deadenylation process (Wahle and Winkler, 2013). GW182 are 182 kDa proteins which have glycine-tryptophan repeats (GW) (Fabian and Sonenberg, 2012). It has be shown that optimal deadenylation requires interplay between the W-repeats and PABP C (Jonas and Izaurralde, 2015).

Decapping: the decapping is accomplished by DCP2 (decapping protein 2). This protein acts with the help of other proteins such as EDC3 and 4 (enhancer of decapping 3 and 4), DCP1, and DDX6 (DEAD box protein 6) (Jonas and Izaurralde, 2013). The mRNA 5' end to 3' end degradation is carried out by 5'-3' exoribonuclease 1 (XRN1) (Braun et al., 2012).

Most studies reported the downregulation effect on gene expression. However, it has been

shown that some miRNAs in particular circumstances can cause upregulation. For instance, miR-10a has been shown to promote translation of mRNA encoding ribosomal proteins in the situation of amino acid starvation (Ørom et al., 2008).

1.5.3 miRNAs in the circulation

miRNAs are measureable in the circulation in almost all bodily fluids; for example in serum (Chen et al., 2008), urine (Pospisilova et al., 2016), breast milk (Alsaweed et al., 2015), saliva (Park et al., 2009) and seminal fluid (Barceló et al., 2018). Regarding the origin of miRNAs in the cell-free space, it was proposed that miRNAs exist in the circulation as a result of cell death (Turchinovich et al., 2011). However, other studies indicated more sophisticated fashion of miRNA release. For example, a study showed that IL-4 (secreted by $CD4^+$ T cells) could induce the release of certain miRNA-loaded exosomes (miR-223) from the so-called TAMs (Tumor-associated macrophages) which in turn enhance the invading capabilities of tumor cells in breast cancer (Yang et al., 2011).

miRNAs are stable under harsh circumstances such as boiling, high (13) or low (1) pH, lengthy storage time, freeze-thaw cycles, and they survive RNase degradation. (Chen et al., 2008; Nagy and Igaz, 2015).

It is established that there are two possible ways for miRNAs to exist in the cell-free space: first, within vesicles and second, in complex with proteins. However, the actual distribution of miRNAs between the two forms is still a matter of controversy. Some studies suggested that most miRNAs are being carried within vesicles such as exosomes (Gallo et al., 2012) while others claim that most miRNAs associate with proteins such as Ago2 (Arroyo et al., 2011).

Extra-cellular vesicles that carry miRNA include microvesicles, exosomes, and membrane-bound structures such as apoptotic bodies. The loading of miRNAs into such extra-cellular vesicles relies on compounds involved in the synthesis of those vesicles such as nSMase2 (neutral sphingomyelinase) (Kosaka et al., 2010).

Interestingly, miRNA carried within extra-cellular vesicles can communicate with and target other distant cells, thus causing changes in gene expression of these cells, which could be translated to functional commands (O'Brien et al., 2020). One example is the potential role of miRNAs in the interplay between T-cells and antigen-presenting cells (APCs) in the context of antigen identification. Over immune interactions, it has been shown that T cells communicate with APCs

via specific miRNAs carried within exosomes. Moreover, those miRNAs exert their roles in the recipient cells (APCs) by targeting specific genes (Mittelbrunn et al., 2011).

The miRNA content of the extra-cellular vesicles is a determinant of the changes that occur in the cell releasing those vesicles. This can be true in physiological as well as in pathological situations (Mori et al., 2019). Therefore, the changes in miRNA content of vesicles could be an indicator of changes in the status of some cells and hereby a marker for a disease or for a condition.

There are numerous examples describing the use of miRNAs-loaded vesicles as biomarkers. For example, changes in Exosomes-loaded miRNAs were detected in breast cancer patients (Wu et al., 2020), exosomal miR-20b-5p was found to be increased in Type-2 diabetes (Katayama et al., 2019). As another example, miR-15b, miR-34a, and miR-636 were found to be increased in urine-derived exosomes in patients with type-2 diabetic kidney disease (Eissa et al., 2016).

Protein complexes allow the extracellular transportation and stabilization of miRNA. Important are lipoproteins or proteins such as NPM1 (Nucleophosmin1) and Ago2. Lipoproteins (HDL; high density lipoproteins and LDL; low density lipoproteins) were not only found to form complexes with miRNAs but also the miRNA inside them could be informative of some conditions related to the HDL kinetics and metabolism (Vickers et al., 2011; Churov et al., 2019; Scicali et al., 2019).

NPM1 and Ago2 are capable of complexing with miRNAs in the circulation. This was proven by showing that those proteins confer protection to the miRNAs and that their absence has degrading effects on the miRNAs (Cui et al., 2019). For instance, NPM1 safeguarded a synthetic miRNA in spite of the presence of RNase (Wang et al., 2010).

Although the actual role of miRNAs in the circulation is not fully understood, many studies reported alterations in miRNA profile in the circulation in various diseases. For example in cancer, miR-10b has been found in breast cancer patient's circulation, (Iorio et al., 2005), and miR-506 in ovarian cancer patient's circulation (Yang et al., 2013). Circulating miRNAs were proposed as biomarkers for autoimmune diseases (miR-551b, miR-448, and miR-124) for individuals with rheumatoid arthritis, systemic lupus erythematosus, Sjogren's syndrome and ulcerative colitis (Jin et al., 2018). In type 1 diabetes several studies revealed roles of miRNAs in the pathogenesis and reported changes in the miRNA profile of the circulation in individuals with affected by this disease (Erener et al., 2017; LaPierre and Stoffel, 2017).

1.5.4 miRNAs quantification and profiling

To investigate the potential of miRNA as biomarkers by detecting their alterations in the circulation or their profile in tissue, it is essential to quantify these molecules. Several methods have been developed that allow quantification of miRNAs in tissue samples or in the cell-free samples. Here, I will discuss two widespread methods RT-qPCR and NGS.

RT-qPCR (Real time quantitative polymerase chain reaction) is considered a very sensitive and specific method for gene expression analysis. RT-qPCR is relatively inexpensive, easy to conduct, and capable of detecting miRNA targets reliably and reproducibly. It allows quantification of large numbers of specific targets using already designed primers. There are many methods that employ RT-qPCR to quantify miRNA. An important and widely used method uses the principle of polyadenylation of the miRNA to allow reverse transcription. A poly(A) tail is added to the miRNA and reverse transcription is carried out with reverse transcriptase and with an oligonucleotide containing a poly(T) as well as a primer- binding site a; this process produces complementary DNA (cDNA). Next, using a sequence-specific primer that targets the miRNA of interest and a primer that binds the primer- binding site introduced by the reverse transcription primer, the cDNA can be quantified by RT-qPCR (Shi and Chiang, 2005).

In the RT-qPCR reaction, a DNA binding dye binds to the double stranded DNA producing a florescence signal recorded by the qPCR machine and this signal diminishes when the two strands are dissociated at the end of a PCR cycle. At the end of each PCR cycle the florescence emission is reported and plotted against the number of cycles as ΔRn (Rnf - Rnb); (the emission at any cycle – baseline emission). The quantification cycle (Cq) is the cycle number at which the ΔRn exceeds a threshold value. The Cq is conversely correlated with the target concentration in the sample (the amplicon): high Cq indicates low amount of cDNA, while low Cq indicates high amount of cDNA in the sample.

The Cq values obtained from the RT-qPCR are the core of the RT-qPCR data analysis. One of the analysis strategies is to normalize Cq values of target miRNAs to Cq of a reference miRNA, which ideally has a stable expression in the samples set, in control- and sample of interest. A ratio (or referred to as fold change) is then calculated of the target miRNA in the test sample as compared to control sample. This method is referred to as relative quantification (Pfaffl, 2001). One of the important challenges of relative quantification for miRNA analysis is the lack of

universal housekeeping miRNAs (reference genes). To overcome this issue, it was proposed to use suitable reference miRNAs in the samples and conditions of interest. This can be achieved by testing a set of reference candidates in the samples and selecting afterwards the stably expressed ones (Schwarzenbach et al., 2015; Shen et al., 2015). Additionally, the development of mathematical algorithms such as NormFinder (Andersen et al., 2004), RefFinder (Xie et al., 2012), and geNorm (Vandesompele et al., 2002), eased this process.

Data correction using external reference was also introduced. The use of exogenous miRNA is helpful when it comes to technical variation, for instance during the RNA isolation and reverse transcription. C. elegans-miR-39 (Xu et al., 2014) and C. elegans-miR-54 (Niu et al., 2016) were previously used for data normalization.

Next-generation sequencing (NGS) allows profiling of far larger number of miRNAs starting from relatively small amount of isolated RNA. In addition, it gives the opportunity to discover new miRNAs. The small size of miRNAs (21–25 nucleotides) and the existence of many miRNAs, which differ from each other by only one nucleotide, can now be tackled with high resolution and precision of the NGS techniques (Hu et al., 2017).

In the context of biomarker discovery, NGS is very attractive since it confers the possibility to profile hundreds of miRNAs at once in a set of samples from disease or pathologic conditions and to compare the profiles to control samples.

2 Scientific Aim

Replacement of β-cells via islet transplantation is a potential therapeutic approach for individuals with type 1 diabetes that is hard-to-control with conventional approaches. In this procedure, the islets are infused through the portal vein into the liver. If islets successfully engraft, they secrete insulin and glycemic control may be restored. The transplanted islets are exposed to several types of stress such as hypoxia and inflammation (Biarnes et al., 2002; Shahbazov et al., 2016) potentially negatively affecting the outcomes of the procedure. To address this issue through early medical intervention, biomarkers for monitoring β-cell function and detection of their stress and death post-transplantation are required. Such biomarkers would be highly valuable to enable early intervention before the majority of islets are destroyed. The currently utilized biomarkers such as the levels of blood glucose, haemoglobin A1C (HbA1C), stimulated C-peptide and daily insulin measurement (Piemonti, 2000), do not mirror the actual rate of β-cell loss and are only useful to monitor massive changes in β-cell function.

MicroRNAs (miRNA) are short (21–25 nucleotides in length) single-stranded RNA molecules, originated from a hairpin-like structure. miRNAs are considered as gene silencers post-transcriptionally. They have been extensively studied in the last years and proposed as very promising biomarkers for diseases such as cancer and autoimmune disorders. Studies have reported alteration in circulating miRNAs in T1D and their implication in the pathogenesis of this disease (Erener et al., 2017; LaPierre and Stoffel, 2017). Such miRNAs could serve as circulating biomarkers for β-cell stress and death. After human islet transplantation, islets exposed to stress release miRNAs potentially detectable in the circulation and reflecting the rate of islets stress or death.

The aim of my project was to identify and validate miRNAs as indicators of islets stress and death. To attain this aim I conducted extensive *in vitro* and *in vivo* studies:

1. The identification of miRNAs highly expressed in islets and validate their exclusive expression in islets as compared to the circulation.
2. The validation of identified miRNAs in an *in vivo* mouse islet stress model.
3. The validation of miRNAs identified above in an *in vitro* mouse or human islet stress model.
4. The assessment of islets viability and function and a potential relation with miRNAs release.
5. The investigation of biological relevance of validated miRNAs.

3 Materials and methods

3.1 Materials

3.1.1 Chemicals and reagents

Chemicals and reagents used for assays reconstitution, buffer preparation and mouse work are shown in table 1.

Preparation of STZ (Streptozotocin): The working solution was prepared by diluting autoclaved 0.1 M citrate buffer (0.1 M citric acid, 0.1 M sodium citrate, pH 4.4) 1:10 in PBS. Depending on the number of mice, an amount of STZ was dissolved in the working solution to obtain 30 mg/ml concentration of STZ-solution. The dose of STZ was 225 mg/kg and the volume of STZ-solution to be administrated per mouse was calculated as follows:

Volume (ul) = Dose (mg/kg) x Weight (g) / Concentration of STZ-solution (mg/ml)

For example: a mouse weighing 20 g was injected with 150 ul STZ-solution.

Table 1: Chemicals and reagents

Chemical name	Supplier
1x PBS	In house prepared by media kitchen, CRTD
DEPC-Treated Water	Life Technology
Nuclease-free water	Qiagen
Bovine serum albumin (BSA)	Sigma-Aldrich
DNAZap™ Solutions	Life Technologies
EDTA solution for molecular biology pH 8	Sigma-Aldrich
Ethanol	Carl Roth
Ethanol absolute	Carl Roth GmbH + Co.KG
Formalin (37%, acid free)	Merck
Histopaque-1077 Hybri-Max	Sigma-Aldrich
Nuclease-free water	Qiagen
RNaseZap® spray	Ambion Inc.
Trichlormethan/Chloroform, >99%, p.a.	Carl Roth GmbH + Co.KG

Table 1: Chemicals and reagents *(continued)*

Chemical name	Supplier
Tween 20	Sigma-Aldrich
Dithizone	Sigma-Aldrich
Tris, 1M, pH 8.0	Life Technology
Ketamine hydrochloride	Sigma-Aldrich
Xylazine hydrochloride	Sigma-Aldrich
Mounting medium	Vector Laboratories
Streptozocin	Sigma-Aldrich
Xylol/Xylene	Roth
Citric Acid Monohydrate	Roth
Trisodium citrate-Dihydrat	Roth
Collagenase from Clostridium Histolyticum Type 5	Sigma-Aldrich
Ficoll® 400	Sigma-Aldrich

3.1.2 Media and supplements

Media and supplements are listed in table 2. Serum supplements were filtered and stored in aliquots in -20°C and thawed in waterbath before use. Before use in mouse islet culture, RPMI was supplemented with 10% FBS or NCS, 1% P/S and 1% L-glutamine.

Table 2: Media and supplements

Name	Manufacturer
MEM 0.9 - 1.1/l glucose w/o L-Glutamine	Sigma-Aldrich
CMRL 1066, w/o: L-Glutamine, w/o: Phenol	PAN-Biotech
RPMI 1640 medium, w L-Glutamine	Sigma-Aldrich
Fetal bovine serum (FBS)	Invitrogen Ltd.
L-Glutamine 200 mM (L-Glu)	Lonza
Penicillin - Streptomycin (P/S)	Lonza

Table 2: Media and supplements *(continued)*

Name	Manufacturer
Fetal calf serum (FCS)	HyClone
Normal goat serum	Life Technology
Newborn calf serum (NCS)	Sigma-Aldrich

3.1.3 Human samples

Human islets were obtained from King's college London, KCL-Human Islet Research Tissue Bank (KCL HI-RTB); Reference 20/SW/0074 approved by South West - Central Bristol Research Ethics Committee. Human blood was collected from healthy individuals. The use of serum was approved by ethic committee and informed consent of the donors.

3.1.4 Cytokines and antibodies

Cytokines and antibodies are listed in table 3. Cytokines were reconstituted with RPMI (supplemented with 2% FBS, 1% P/S and 1% L-glutamine) and stored in aliquots in -20°C. Antibodies for immunofluorescence staining were diluted properly in antibody diluent before use.

Table 3: Cytokines and antibodies

Cytokine/Antibody	Manufacturer
recombinant murine IL-1β	Peprotech
recombinant murine TNF-α	Peprotech
recombinant murine IFN-γ	Peprotech
Anti-Insulin antibody	Abcam
Polyclonal rabbit anti-human Glucagon	Dako
Cleaved Caspase-3 Antibody	Cell Signaling
DAPI (4',6-diamidino-2-phenylindole)	Roche
Goat anti-guinea pig IgG (H+L), alexa fluor 488	Thermo Fisher Scientific
Goat anti-guinea pig IgG (H+L), alexa fluor 568	Thermo Fisher Scientific

Table 3: Cytokines and antibodies *(continued)*

Cytokine/Antibody	Manufacturer
Antibody diluent	Dako REAL

3.1.5 Kits

Commercial kits and their suppliers are listed in table 4.

Table 4: Commercial kits

Name	Catalog number	Manufacturer
miRNeasy Micro Kit	217084	Qiagen
Agilent RNA 6000 Pico Kit	5067-1513	Agilent Technologies
miRNeasy Serum/Plasma Kit	217184	Qiagen
Qubit ™ RNA HS Assay Kit	Q32852	Quant-iT ™, Qubit ™
Agilent Small RNA kit	5067-1548	Agilent Technologies
miScript II RT Kit	218160	Qiagen
TaKaRa Ex Taq® Hot start version kit	RR006B	Takara Bio
TATAA PreAmp GrandMaster® Mix	TA05-50	TATAA Biocenter
Caspase-Glo® 3/7 Assay	G8090	Promega
Insulin Mouse ELISA Kit	EMINS	Thermo Fisher Scientific

3.1.6 Consumables

Consumables and suppliers are listed in table 5.

Table 5: Consumables

Name	Supplier
Tips for Multipette	Eppendorf
Pasteur pipettes 3 ml	VWR

Table 5: Consumables *(continued)*

Name	Supplier
PCR tubes 0.2 ml	VWR
Safelock reaction tubes 0.5 ml, 1.5 ml, 2.0 ml	Eppendorf
Conical tubes 15, 50 ml	Greiner bio-one
Cell culture plates 96-well	Greiner bio-one
96 well plate seals	Thermo Fisher Scientific
Needles 23, 28, 29, 30g	BD Microlance 3
Syringes 2.5ml 5ml	Omnifix® Solo
Cell dissociation sieve	Sigma-Aldrich
Cell culture dishes 94x16 mm and 35x15 mm	Greiner bio-one
Serum-Gel 9 ml tubes	Sarstedt S-Monovette®
BD Vacutainer SST™ II Advance tubes 3.5 ml	BD Vacutainer SST™
384 Tips, Sterile, Filter 12.5µl	Integra biosciences
MicroAmp™ Optical 384-Well Reaction Plate with Barcode	Fisher
384 Well PCR Microplate for Roche Lightcycler	Axygen®
96 Well Semi-Skirted PCR Plate, Roche Style	FrameStar®
8-Strip Tubes	Sarstedt
QIAshredder (disposable cell-lysate homogenizers)	Qiagen
Micro tube 2.0ml SafeSeal	Sarstedt
Pipette tips ART 10 Reach 0,1-10ul lange Spitze	Thermo Scientific
Pipette tips Art Barrier Tips Art 20P (20ul)	Thermo Scientific
Pipette tips ART 200 1-200ul	Thermo Scientific
Pipette tips ART 1000 Reach lange Spitze	Thermo Scientific
S-Monovette 1.1 ml Z-Gel	Sarstedt
0.2-micron filter	Millipore

3.1.7 Instruments

Technical equipment used in this study are listed in table 6.

Table 6: Instruments

Device	Manufacturer
2-1000 µl Pipettes	Eppendorf
Electronic dispenser	Eppendorf
Pipetter	Thermo Fisher Scientific
Tecan Infinite® 200 PRO	Tecan Group Ltd.
Bioanalyzer	Agilent 2100 Bioanalyzer
Heating block	Eppendorf
Micro centrifuge	Eppendorf
Waterbath	LAUDA DR. R. WOBSER GmbH and Co.
Plate shaker	Barnstedt Thermo Fisher Scientific
Microscope MZ9.5	Leica
Qubit® 3.0 Fluorometer	Thermo Fisher Scientific
PCR cycler	Eppendorf
LightCycler® 480	Roche
ViiA 7	Thermo Fisher Scientific
Confocal microscope	Leica
Luminometer GloMax-96	Promega
Incubator	Binder
Centrifuge (cell culture)	Beckman Coulter
Biomark	Fluidigm

3.2 Methods

3.2.1 Preparation of mouse and human material

3.2.1.1 Preparation of islets, other tissues and serum from healthy mice

3.2.1.1.1 Isolation of Pancreata

Pancreatic islets and blood were collected from 8-weeks old C57BL/6JRj mice. The mice were purchased from Janvier (Le Genest-Saint-Isle, France) and housed at the animal facility of CRTD (Center for Regenerative Therapies TU Dresden). The mice were kept in an open cage system without IVC (individually ventilated cages) and cages were only opened under sterile conditions. The animal experiments were approved by the Landesdirektion Sachsen (Dr. Barbara Langen).

The pancreata were isolated as follows: 5 ml collagenase solution per pancreas was prepared (0.7 mg/ml collagenase in RPMI medium (5.5mM Glucose, 10% FCS, 1% P/S & 1% L-glut) and placed on ice. The mice were euthanized by cervical dislocation. 70% ethanol was sprayed on the abdomen to prevent contamination. A vertical abdominal cut starting from the lower abdomen was made to the diaphragm to reveal all abdominal organs. The liver was flipped over to reveal the hepatic duct, the cystic duct (the duct which originates from the gallbladder) and the common bile duct. The ampulla of Vater was clamped with a Bulldog clamp (the ampulla appears as a white spot where the common bile duct meets the duodenum), to prevent the collagenase solution from leaking into the small intestine and to ensure a full perfusion of the pancreas. A 5 ml syringe with a 30 gauge needle was filled with collagenase solution and under dissecting microscope, the needle was inserted gently at the point where the hepatic duct and cystic duct connect to form the common bile duct and 4-5 ml of collagenase solution were injected. After injection, the pancreas was detached from the surrounding organs with forceps and scissors and removed carefully to avoid any contamination with intestinal bacteria. The pancreata were placed in 50 ml tubes on ice until further processing.

3.2.1.1.2 Isolation of islets

The ficoll density gradient was used to isolate the islets from the collected pancreata as described previously (Borg et al., 2014).

Briefly, the pancreata were digested in water bath at 37 °C for 8.5 min. The digestion was stopped by adding RPMI medium (5.5mM Glucose, 10% FCS, 1% P/S & 1% L-glut) and shaking. The digested pancreas in RPMI was centrifuged for 2 min at 900 rpm (190 rcf) and 4 °C. The supernatant was discarded and the pellet was resuspended in RPMI and passed through a sterile metal strainer (Cell dissociation sieve CD1-1KT; Sigma). The resulting solution containing the islets was centrifuged for 2 min 900 rpm (190 rcf) at 4 °C and the pellet was resuspended gently in 23 ml of ficoll gradient with a density of 1108, and 12 ml of ficoll gradient with a density of 1096 was added slowly, followed by addition of 12 ml of ficoll gradient with a density of 1037 on top. Gradient centrifugation was performed for 18 min 1900 rpm (850 rcf) at 4 °C. The pure islets, found between the 1096 and 1037 density layers, were collected and washed with RPMI by centrifugation for 2 min 1000 rpm (230 rcf) at 4 °C. The islets were re-suspended in 10 ml RPMI, transferred into petri dishes and incubated overnight at 37 °C, 5% CO2; islets were then counted, IEQ was calculated as described below and the islets were snap-frozen after removing any remaining supernatant and stored at – 80 °C until further processing.

Islet counting:

All islets with media were transferred from the petri dishes to 50 ml tubes and spun for 2 min at 800 rpm at room temperature. The supernatant was removed and the islets were resuspended in 20 ml RPMI. 50 ul of the cell suspension was transferred to a new petri dish with gridlines and an equal volume of Dithizone (Sigma-Aldrich) was added to the sample. Under a light microscope, the islets were counted from triplicates of each sample and the absolute islet number was calculated using the formula:

Absolute islet number = Average counted islets number x Dilution factor

Where Dilution factor = total volume/sample volume (here the dilution factor was: 20ml/0.05ml = 400)

Measurement of the islet volume:

The maximal and minimal diameter of each islet in sample triplicates was measured with a ruler using a Leica microscope MZ9.5 with 5x magnification. These measurements were used to calculate the islet volume according to the formula:

Islet volume = $4/3\pi$ x maximal diameter x 2(minimal diameter) (Where $4/3\pi$ = 4.188786667)

The average islet volume was calculated in each replicate and the average of the triplicates was calculated.

Isolation index:

The isolation index was determined with the formula:

Isolation index = Average islet volume of the triplicates/the volume of an islet with a 150 um diameter

(The volume of an islet with a 150 um diameter = $4/3\pi$ x 150 x 2 x 150)

Islet equivalents:

Islet Equivalents (IEQ) were calculated as follows:

$$IEQ = \frac{\text{Isolation index}}{\text{Absolute islets number}}$$

3.2.1.1.3 Blood isolation

Before collection of the blood through cardiac puncture the mice were anesthetized using a ketamine/xylazine cocktail in PBS (at 80-100 mg/kg and 10-12.5 mg/kg, respectively). To prepare 1 ml ketamine/xylazine cocktail, 1 mg xylazine and 10 mg ketamine were dissolved in 1 ml PBS and 300-400 ul were administrated intraperitoneally with a 29G needle.

The blood was collected through cardiac puncture in Sarstedt S-Monovette® Serum-Gel 9 ml tubes containing clot activator. To allow full clotting, the tubes were left at room temperature (15–25°C) for 30 min and then centrifuged for 10 min at 3000 rpm (1900 rcf) at 4°C. The serum (upper yellow layer) was transferred to new tubes and centrifuged for 10 min at 16000 rcf to remove any remaining cell debris. After centrifugation, the supernatant was transferred to new tubes and stored in 200 ul aliquots at – 80 °C.

3.2.1.1.4 Other tissues

After euthanizing the mice as described above, an anatomical cut was made along the abdomen. The liver and the pancreas were revealed and separated from the surrounding organs with

scissors and forceps. The organs were snap-frozen in liquid nitrogen and stored at – 80 °C for later use.

3.2.1.2 miRNA extraction from mouse tissue

For miRNA extraction from purified islets and pancreas the miRNeasy Micro Kit (Qiagen) was used following the manufacturer's instructions. Briefly, 5mg of tissue was placed in 700 µl QIAzol Lysis reagent. For homogenization, the lysate was transferred to a QIAshredder spin column and centrifuged for 2 min at maximum speed at room temperature.

After centrifugation, the homogenate was left at room temperature for 5 min before adding 140 ul chloroform followed by vigorous shaking for 15 second. The tube was incubated for 3 min at room temperature and centrifuged for 15 min 12000 rcf at 4 °C. After centrifugation the upper aqueous phase (around 350 ul) was transferred to new tube containing 100% ethanol and vigorously mixed by pipetting. 700 ul of the resulted solution was transferred to RNeasy MinElute spin column in a 2 ml collection tube and centrifuged for 15 second at 12000 rpm at room temperature. The same procedure was performed with the rest of the sample.

After discarding the flow-through 700 ul buffer RWT were added, followed by centrifugation for 15 second at 12000 rpm at room temperature. The same step was repeated with 700 ul buffer RPE. After discarding the flow-through, 500 ul of 80% ethanol were added and the column was centrifuged for 2 min at 12000 rpm at room temperature. The RNeasy MinElute spin column was transferred to a new collection tube and centrifuged for 5 min at maximum speed with keeping the lid of the column open. To elute the RNA, the spin column was placed in a new tube and 14 ul of RNase-free water were added and the column was centrifuged for 1 min at maximum speed. The eluted RNA was snap-frozen and stored at – 80 °C for later use.

For miRNA extraction from serum, the miRNeasy Serum/Plasma Kit (Qiagen) was used following the provided protocol. Before starting, a working solution of the spike-In control, which is a C. elegans miR-39 miRNA mimic (Qiagen 219610), was prepared as recommended by the manufacturer to obtain a concentration of 1.6×10^8 copies/ul, by adding 300 ul RNase-free water to the spike-in vial to obtain a stock solution of 2×10^{10} copies/ul which was then further diluted with RNase-free water to obtain the working solution.

200 ul of serum were used. Frozen samples were thawed at room temperature. 1000 ul of

QIAzol Lysis Reagent were added to the samples, mixed thoroughly and left for 5 min at room temperature. 3.5 ul of the spike-In control working solution were added to each sample. 200 ul chloroform was added and the tube and was shaken vigorously for 15 seconds. From here the steps described above for the tissue miRNA extraction were followed until the end of the procedure and RNA elution and storage.

3.2.1.3 Preparation of human islets and blood

Islets

Human islets were obtained from King's college London, KCL-Human Islet Research Tissue Bank (KCL HI-RTB); Reference 20/SW/0074 approved by South West - Central Bristol Research Ethics Committee.

After arrival, the tubes containing the islets in medium were either spun for 2 min at 150 rcf at room temperature, the supernatant was removed and islets were snap-frozen and stored in aliquots at – 80 °C for later use or the tubes content was transferred into petri dishes, each 200-500 islets were handpicked in new petri dish containing 10 ml CMRL-1066 medium (PAN-Biotech P04-84600) and incubated at 37 °C for next day use.

Blood

Blood samples were collected in BD Vacutainer SST™ II Advance tubes. The blood was left to clot at room temperature for 30 min and then centrifuged for 10 min at 3000 rpm (1900 rcf) at 4°C. The serum (upper yellow layer) was transferred to new tubes and centrifuged for 10 min at 16000 rcf to remove any remaining cell debris. After centrifugation, the supernatant was transferred to new tubes and stored in 200 ul aliquots at – 80 °C.

3.2.1.4 miRNA extraction from human tissue

For miRNA extraction from islets, an input of 1000 IEQ was used as a starting material. The steps described in 3.2.1.2 for miRNA extraction from mouse islets were followed here. For miRNA extraction from human serum, the steps described in 3.2.1.2 for miRNA extraction from mouse serum were followed.

3.2.1.5 Quantitative and qualitative RNA analysis

Qubit

To determine the total RNA concentration in the samples, the Qubit® RNA HS Assay was used according to the manufacturer recommendations. Briefly, before starting, the Qubit® RNA HS Reagent was diluted 1:200 in Qubit® RNA HS Buffer to obtain the Qubit® working solution. To calibrate the Qubit® Fluorometer, the standards were prepared by adding 10 ul of each Qubit® standard to 190 ul of the working solution. The samples were prepared by adding 1 ul of 1:10 diluted samples (or of a higher dilution for samples which is expected to contain very high RNA concentration) to 199 ul working solution. The standard and sample tubes were left at room temperature for 2 min.

The Qubit® 3.0 Fluorometer instrument was used. To calibrate the instrument, the standards were run first. After running the standards, the samples were run and the RNA concentration was determined after multiplying the resulting concentration determined by the Fluorometer by the dilution factor.

Bioanalyzer

To quantitatively analyze the miRNAs in the cell free samples, the small RNA kit (Agilent) for the 2100 Bioanalyzer System was used according to the manufacturer recommendations. Before starting, the reagents were prepared as follows: the small RNA ladder was heated for 2 min at 70 °C and stored in aliquots at – 80 °C. The small RNA gel matrix was filtered using a spin column filter and centrifugation for 15 min at 10000 rcf and stored at 4 °C. The gel-dye mix was prepared by adding 40 ul of filtered gel to 2 ul of small RNA dye, mixing the solution and with centrifugation for 10 min 13000 rcf at room temperature.

All reagents were brought to room temperature 30 min before starting the procedure. While the small RNA chip was placed on the priming station, the gel-dye mix was pipetted into the relevant well. The priming station was closed by pulling out the plunger 1 ml for 60 seconds and then releasing it, and allowing it to set back to 0.3 ml. After opening the priming station, 9.0 µl of the gel-dye mix were pipetted into the wells marked G. 9 ul of the conditioning solution was pipetted into the corresponding well and 5 ul of the small RNA marker was added to all sample wells and to the ladder well. The RNA samples were heated for 2 min at 70 °C and 1 ul was pipetted into the sample wells. 1 ul of thawed ladder was pipetted into the ladder well. The chip was vortexed for 60 seconds at 2400 rpm and placed into Agilent 2100 Bioanalyzer for analysis.

3.2.2 miRNA quantification by RT-qPCR

3.2.2.1 Reverse transcription and multiplex pre-amplification

Reverse transcription

The miScript II RT Kit (Qiagen) was used for the cDNA synthesis according the manufacturer's recommendations. Briefly, the reaction master mix was prepared by mixing 4 ul miScript HiSpec buffer, 2 ul miScript nucleics mix, 2 ul miScript reverse transcriptase mix and 7 ul RNase-free water. 1 ug RNA, in a volume of 5 ul, isolated from islets or pancreatic tissue was added to the reaction mix. For cell free samples, 5 ul of the total RNA volume was used. The reaction components were mixed by short spinning and incubated in a thermal cycler for 60 min at 37 °C followed by 5 min at 95 °C. cDNA was stored at 4 °C for short term or – 20 °C for later use.

Multiplex pre-amplification

The TaKaRa Ex Taq® Hot start version kit (Takara Bio) was used to amplify the panel of miRNA targets. Briefly, the reaction mixture was comprised of 1X (2 mM) Ex Taq Buffer (Mg^{2+}plus), 5 U/µl TaKaRa Ex Taq HS and a final concentration of 0.2 uM universal primer (backward primer) and 200 uM of dATP, dGTP, and dCTP. Equal volumes and concentrations of the target primers (forward primers) were mixed to obtain a primer pool which was added to the 20 ul reaction to obtain a final concentration of 0.2 uM for each primer. The cDNA template was diluted 1:5 in distilled water and 3 ul were added to 20 ul reaction mixture.

The reaction mixture was incubated in a thermal cycler for 1 min at 94 °C, 40 seconds at 55 °C and 30 seconds at 72 °C for 16 cycles. After the final cycle the tubes were incubated for 6 min at 72 °C and stored at 4 °C or – 20 °C for later use.

3.2.2.2 qPCR

qPCR master mix contained 1X TB Green Premix Ex Taq II (Takara Bio), 0.5 uM miScript primer assay (for each miRNA target of interest) and 0.5 uM universal primer final concentration. 20 ul master mix was prelaid into 384- or 96-well plates and 1.2 ul of 1:10 diluted cDNA template were added in triplicates. The plate was sealed and spun for 1 min at 1000 rpm. The qPCR was carried out in LightCycler® 480 (Roche) or ViiA 7 (Thermo Fisher Scientific). The adapted qPCR conditions for LightCycler are described in table 7 and for ViiA 7 in table 8. When using the ViiA

7 instrument, ROX reference dye was added to the master mix to constitute 1/250 of reaction volume.

Table 7: Cycling conditions used for qPCR with miScript assays (LightCycler)

Step	Time	Temperature °C	Ramp rate °C/s
Initial incubation	30 sec	95°C	4.40
Amplification (x40)	5 sec	95°C	4.40
	30 sec	55°C	2.20
	20 sec	72°C	4.40
Melting curve	5 sec	95°C	4.40
	1 min	60°C	2.20
	-	95°C	0.11
Cooling	30 sec	50°C	2.20

Table 8: Cycling conditions used for qPCR with miscript assays (ViiA 7)

Step	Time	Temperature °C	Ramp rate °C/s
Hold stage	30 sec	95°C	1.60
PCR stage (x40)	5 sec	95°C	1.60
	34 sec	60°C	1.60
Melt curve stage	15 sec	95°C	1.60
	1 min	60°C	1.60
	15 sec	95°C	0.11

After the run was complete, the primer melting temperature (Tm) and the quantification cycle (Cq) values were extracted for analysis.

3.2.2.3 qPCR Assays

3.2.2.3.1 Design

miScript primer assays that target miRNA of interest were purchased from Qiagen. The name and sequence of the mature miRNA targets were retrieved from the microRNA database (miRBase version 22.1) and are listed in table 9 and 10. The miScript primer assays were reconstituted in 550 ul TE buffer (1 mM EDTA, 10 mM Tris/HCL, pH 8) by vortexing and were stored in aliquots at – 20 °C. The universal primer (GAATCGAGCACCAGTTACGC) was purchased from Metabion and was reconstituted to obtain a final concentration of 10 uM. The housekeeping genes for tissue and cell-free samples in human and mouse are listed in table 11.

Table 9: Mouse assays

miRNA	Sequence	Reference
mmu-miR-98-5p	UGAGGUAGUAAGUUGUAUUGUU	(Bunt et al., 2013; Tattikota et al., 2013; Tattikota et al., 2014)
mmu-miR-200b-3p	UAAUACUGCCUGGUAAUGAUGA	(Bunt et al., 2013; Tattikota et al., 2013; Tattikota et al., 2014)
mmu-miR-30c-5p	UGUAAACAUCCUACACUCUCAGC	(Bunt et al., 2013; Tattikota et al., 2013; Tattikota et al., 2014)
mmu-miR-23b-3p	AUCACAUUGCCAGGGAUUACC	(Bunt et al., 2013; Tattikota et al., 2013; Tattikota et al., 2014)
mmu-miR-182-5p	UUUGGCAAUGGUAGAACUCACACCG	(Bunt et al., 2013; Tattikota et al., 2013; Tattikota et al., 2014)

Table 9: Mouse assays *(continued)*

miRNA	Sequence	Reference
mmu-miR-411-5p	UAGUAGACCGUAUAGCGUACG	(Bunt et al., 2013; Tattikota et al., 2013; Tattikota et al., 2014)
mmu-miR-183-5p	UAUGGCACUGGUAGAAUUCACU	(Bunt et al., 2013; Tattikota et al., 2013; Tattikota et al., 2014)
mmu-miR-141-3p	UAACACUGUCUGGUAAAGAUGG	(Bunt et al., 2013; Tattikota et al., 2013; Tattikota et al., 2014)
mmu-miR-27b-3p	UUCACAGUGGCUAAGUUCUGC	(Bunt et al., 2013; Tattikota et al., 2013; Tattikota et al., 2014)
mmu-miR-148a-3p	UCAGUGCACUACAGAACUUUGU	(Bunt et al., 2013; Tattikota et al., 2013; Tattikota et al., 2014)
mmu-miR-30a-5p	UGUAAACAUCCUCGACUGGAAG	(Bunt et al., 2013; Tattikota et al., 2013; Tattikota et al., 2014)
mmu-miR-200c-3p	UAAUACUGCCGGGUAAUGAUGGA	(Bunt et al., 2013; Tattikota et al., 2013; Tattikota et al., 2014)
mmu-miR-143-3p	UGAGAUGAAGCACUGUAGCUC	(Bunt et al., 2013; Tattikota et al., 2013; Tattikota et al., 2014)
mmu-miR-29a-3p	UAGCACCAUCUGAAAUCGGUUA	(Bunt et al., 2013; Tattikota et al., 2013; Tattikota et al., 2014)

Table 9: Mouse assays *(continued)*

miRNA	Sequence	Reference
mmu-miR-30e-5p	UGUAAACAUCCUUGACUGGAAG	(Bunt et al., 2013; Tattikota et al., 2013; Tattikota et al., 2014)
mmu-miR-30d-5p	UGUAAACAUCCCCGACUGGAAG	(Bunt et al., 2013; Tattikota et al., 2013; Tattikota et al., 2014)
mmu-miR-99b-5p	CACCCGUAGAACCGACCUUGCG	(Bunt et al., 2013; Tattikota et al., 2013; Tattikota et al., 2014)
mmu-miR-26a-5p	UUCAAGUAAUCCAGGAUAGGCU	(Bunt et al., 2013; Tattikota et al., 2013; Tattikota et al., 2014)
mmu-let-7f-5p	UGAGGUAGUAGAUUGUAUAGUU	(Bunt et al., 2013; Tattikota et al., 2013; Tattikota et al., 2014)
mmu-miR-22-3p	AAGCUGCCAGUUGAAGAACUGU	(Bunt et al., 2013; Tattikota et al., 2013; Tattikota et al., 2014)
mmu-miR-191-5p	CAACGGAAUCCCAAAAGCAGCUG	(Bunt et al., 2013; Tattikota et al., 2013; Tattikota et al., 2014)
mmu-let-7b-5p	UGAGGUAGUAGGUUGUGUGGUU	(Bunt et al., 2013; Tattikota et al., 2013; Tattikota et al., 2014)
mmu-let-7a-5p	UGAGGUAGUAGGUUGUAUAGUU	(Bunt et al., 2013; Tattikota et al., 2013; Tattikota et al., 2014)

Table 9: Mouse assays *(continued)*

miRNA	Sequence	Reference
mmu-miR-151-3p	CUAGACUGAGGCUCCUUGAGG	(Tattikota et al., 2013; Tattikota et al., 2014)
mmu-miR-434-3p	UUUGAACCAUCACUCGACUCCU	(Tattikota et al., 2013; Tattikota et al., 2014)
mmu-miR-434-5p	GCUCGACUCAUGGUUUGAACCA	(Tattikota et al., 2013; Tattikota et al., 2014)
mmu-miR-423-5p	UGAGGGGCAGAGAGCGAGACUUU	(Tattikota et al., 2013; Tattikota et al., 2014)
mmu-miR-375-3p	UUUGUUCGUUCGGCUCGCGUGA	(Tattikota et al., 2013; Tattikota et al., 2014)
mmu-miR-7a-5p	UGGAAGACUAGUGAUUUUGUUGU	(Tattikota et al., 2013; Tattikota et al., 2014)
mmu-miR-184-3p	UGGAAGACUAGUGAUUUUGUUGU	(Tattikota et al., 2013; Tattikota et al., 2014)
mmu-miR-127-3p	UCGGAUCCGUCUGAGCUUGGCU	(Tattikota et al., 2013; Tattikota et al., 2014)
mmu-miR-101a-3p	UACAGUACUGUGAUAACUGAA	(Tattikota et al., 2013; Tattikota et al., 2014)
mmu-miR-30b-5p	UGUAAACAUCCUACACUCAGCU	(Tattikota et al., 2013; Tattikota et al., 2014)
mmu-let-7c-5p	UGAGGUAGUAGGUUGUAUGGUU	(Tattikota et al., 2013; Tattikota et al., 2014)
mmu-miR-132-3p	UAACAGUCUACAGCCAUGGUCG	(Bunt et al., 2013)
mmu-miR-222-3p	AGCUACAUCUGGCUACUGGGU	(Bunt et al., 2013)
mmu-miR-200a-5p	CAUCUUACCGGACAGUGCUGGA	(Bunt et al., 2013)
mmu-miR-29c-3p	UAGCACCAUUUGAAAUCGGUUA	(Bunt et al., 2013)
mmu-miR-127-5p	CUGAAGCUCAGAGGGCUCUGAU	(Bunt et al., 2013)

Table 9: Mouse assays *(continued)*

miRNA	Sequence	Reference
mmu-miR-212-3p	UAACAGUCUCCAGUCACGGCCA	(Bunt et al., 2013)
mmu-miR-125b-1-3p	ACGGGUUAGGCUCUUGGGAGCU	(Bunt et al., 2013)
mmu-miR-582-5p	AUACAGUUGUUCAACCAGUUAC	(Bunt et al., 2013)
mmu-miR-141-5p	CAUCUUCCAGUGCAGUGUUGGA	(Bunt et al., 2013)
mmu-miR-493-3p	UGAAGGUCCUACUGUGUGCCAGG	(Bunt et al., 2013)
mmu-miR-668-3p	UGUCACUCGGCUCGGCCCACUACC	(Bunt et al., 2013)
mmu-miR-216a-3p	CACAGUGGUCUCUGGGAUUAUG	(Bunt et al., 2013)
mmu-miR-652-3p	AAUGGCGCCACUAGGGUUGUG	(Tattikota et al., 2014)
mmu-miR-320-3p	AAAAGCUGGGUUGAGAGGGCGA	(Tattikota et al., 2014)
mmu-miR-382-5p	GAAGUUGUUCGUGGUGGAUUCG	(Tattikota et al., 2014)
mmu-miR-152-3p	UCAGUGCAUGACAGAACUUGG	(Tattikota et al., 2014)
mmu-let-7d-5p	AGAGGUAGUAGGUUGCAUAGUU	(Bunt et al., 2013; Tattikota et al., 2013; Tattikota et al., 2014)
mmu-miR-129-5p	CUUUUUGCGGUCUGGGCUUGC	(Bunt et al., 2013; Tattikota et al., 2013; Tattikota et al., 2014)
mmu-miR-24-3p	UGGCUCAGUUCAGCAGGAACAG	(Bunt et al., 2013; Tattikota et al., 2013; Tattikota et al., 2014)
mmu-miR-204-5p	UUCCCUUUGUCAUCCUAUGCCU	(Bunt et al., 2013; Tattikota et al., 2013)
mmu-miR-148a-5p	AAAGUUCUGAGACACUCCGACU	(Bunt et al., 2013; Tattikota et al., 2013)
mmu-miR-181c-5p	AACAUUCAACCUGUCGGUGAGU	(Bunt et al., 2013; Tattikota et al., 2013)
mmu-miR-410-3p	AAUAUAACACAGAUGGCCUGU	(Tattikota et al., 2013)

Table 9: Mouse assays *(continued)*

miRNA	Sequence	Reference
mmu-miR-409-3p	GAAUGUUGCUCGGUGAACCCCU	(Tattikota et al., 2013)
mmu-miR-25-3p	CAUUGCACUUGUCUCGGUCUGA	(Tattikota et al., 2013)
mmu-miR-379-5p	UGGUAGACUAUGGAACGUAGG	(Bunt et al., 2013; Tattikota et al., 2014)
mmu-miR-7b-5p	UGGAAGACUUGUGAUUUUGUUGU	(Tattikota et al., 2013; Tattikota et al., 2014)
mmu-miR-153-5p	UUUGUGACGUUGCAGCU	(Zhao et al., 2009)
mmu-miR-29b-3p	UAGCACCAUUUGAAAUCAGUGUU	(Zhao et al., 2009)
mmu-miR-211-5p	UUCCCUUUGUCAUCCUUUGCCU	(Zhao et al., 2009)
mmu-miR-136-5p	ACUCCAUUUGUUUUGAUGAUGG	(Zhao et al., 2009)
mmu-miR-423-3p	AGCUCGGUCUGAGGCCCCUCAGU	(Kameswaran et al., 2014)
mmu-miR-184-5p	CCUUAUCACUUUUCCAGCCAGC	(Bunt et al., 2013; Kameswaran et al., 2014)
mmu-miR-381-5p	AGCGAGGUUGCCCUUUGUAUAUU	(Bunt et al., 2013; Nesca et al., 2013)
mmu-miR-323-3p	CACAUUACACGGUCGACCUCU	(Vasu et al., 2019)
mmu-miR-543-3p	AAACAUUCGCGGUGCACUUCUU	(Kim and Zhang, 2019)
mmu-miR-770-3p	CGUGGGCCUGACGUGGAGCUGG	(NGS)
mmu-let-7k	UGAGGUAGGAGGUUGUGUG	(NGS)
mmu-miR-487b-3p	AAUCGUACAGGGUCAUCCACUU	(NGS)
mmu-miR-5099	UUAGAUCGAUGUGGUGCUCC	(NGS)

Table 10: Human assays

miRNA	Sequence	Reference
hsa-miR-4454	GGAUCCGAGUCACGGCACCA	(Roat et al., 2017)
hsa-miR-125b-5p	UCCCUGAGACCCUAACUUGUGA	(Roat et al., 2017)
hsa-let-7g-5p	UGAGGUAGUAGUUUGUACAGUU	(Roat et al., 2017)
hsa-miR-29b-3p	UAGCACCAUUUGAAAUCAGUGUU	(Roat et al., 2017)
hsa-miR-720	UCUCGCUGGGGCCUCCA	(Roat et al., 2017)
hsa-miR-200c-3p	UAAUACUGCCGGGUAAUGAUGGA	(Roat et al., 2017)
hsa-miR-23b-3p	AUCACAUUGCCAGGGAUUACC	(Roat et al., 2017)
hsa-miR-199a-5p	CCCAGUGUUCAGACUACCUGUUC	(Roat et al., 2017)
hsa-let-7b-5p	UGAGGUAGUAGGUUGUGUGGUU	(Bunt et al., 2013; Roat et al., 2017)
hsa-miR-148a-3p	UCAGUGCACUACAGAACUUUGU	(Bunt et al., 2013; Roat et al., 2017)
hsa-miR-7-5p	UGGAAGACUAGUGAUUUUGUUGU	(Bunt et al., 2013; Roat et al., 2017)
hsa-let-7a-5p	UGAGGUAGUAGGUUGUAUAGUU	(Bunt et al., 2013; Roat et al., 2017)
hsa-miR-375	UUUGUUCGUUCGGCUCGCGUGA	(Bunt et al., 2013; Bunt et al., 2013; Roat et al., 2017)
hsa-miR-184	UGGACGGAGAACUGAUAAGGGU	(Bunt et al., 2013)
hsa-miR-409-5p	AGGUUACCCGAGCAACUUUGCAU	(Bunt et al., 2013)
hsa-miR-182-5p	UUUGGCAAUGGUAGAACUCACACU	(Bunt et al., 2013)
hsa-miR-1468-5p	CUCCGUUUGCCUGUUUCGCUG	(Bunt et al., 2013)
hsa-miR-183-5p	UAUGGCACUGGUAGAAUUCACU	(Bunt et al., 2013)
hsa-miR-136-3p	CAUCAUCGUCUCAAAUGAGUCU	(Bunt et al., 2013)
hsa-miR-127-5p	CUGAAGCUCAGAGGGCUCUGAU	(Bunt et al., 2013)
hsa-miR-153-3p	UUGCAUAGUCACAAAAGUGAUC	(Bunt et al., 2013)

Table 10: Human assays *(continued)*

miRNA	Sequence	Reference
hsa-miR-143-3p	UGAGAUGAAGCACUGUAGCUC	(Bunt et al., 2013)
hsa-let-7f-5p	UGAGGUAGUAGAUUGUAUAGUU	(Bunt et al., 2013)
hsa-miR-27b-3p	UUCACAGUGGCUAAGUUCUGC	(Bunt et al., 2013)
hsa-miR-192-5p	CUGACCUAUGAAUUGACAGCC	(Bunt et al., 2013)
hsa-miR-30a-5p	UGUAAACAUCCUCGACUGGAAG	(Bunt et al., 2013)
hsa-miR-30d-5p	UGUAAACAUCCCCGACUGGAAG	(Bunt et al., 2013)
hsa-miR-26a-5p	UUCAAGUAAUCCAGGAUAGGCU	(Bunt et al., 2013)
hsa-miR-21-5p	UAGCUUAUCAGACUGAUGUUGA	(Bunt et al., 2013)
hsa-miR-370-3p	GCCUGCUGGGGUGGAACCUGGU	(Bunt et al., 2013)

Table 11: Housekeeping genes

miRNA	Sequence	Reference
hsa-miR-23a-3p	AUCACAUUGCCAGGGAUUUCC	(Blondal et al., 2013),Qiagen
hsa-miR-146a-5p	UGAGAACUGAAUUCCAUGGGUU	(Blondal et al., 2013),Qiagen
hsa-miR-145-5p	GUCCAGUUUUCCCAGGAAUCCCU	(Blondal et al., 2013),Qiagen
hsa-miR-126-3p	UCGUACCGUGAGUAAUAAUGCG	(Blondal et al., 2013),Qiagen
hsa-miR-26b-5p	UUCAAGUAAUUCAGGAUAGGU	(Blondal et al., 2013),Qiagen
hsa-miR-22-3p	AAGCUGCCAGUUGAAGAACUGU	(Blondal et al., 2013),Qiagen

Table 11: Housekeeping genes *(continued)*

miRNA	Sequence	Reference
hsa-miR-103a-3p	AGCAGCAUUGUACAGGGCUAUGA	(Blondal et al., 2013; Gharbi et al., 2018),Qiagen
hsa-let-7a-5p	UGAGGUAGUAGGUUGUAUAGUU	(Wang et al., 2012; Blondal et al., 2013),Qiagen
hsa-miR-92a-3p	UAUUGCACUUGUCCCGGCCUGU	(Wang et al., 2012; Blondal et al., 2013),Qiagen
hsa-miR-26a-5p	UUCAAGUAAUCCAGGAUAGGCU	(Donati et al., 2019),Qiagen
hsa-miR-423-5p	UGAGGGGCAGAGAGCGAGACUUU	(Blondal et al., 2013; Donati et al., 2019),Qiagen
hsa-miR-21-5p	UAGCUUAUCAGACUGAUGUUGA	(Blondal et al., 2013; Donati et al., 2019),Qiagen
hsa-miR-191-5p	CAACGGAAUCCCAAAAGCAGCUG	(Blondal et al., 2013; Donati et al., 2019),Qiagen
hsa-miR-222-3p	AGCUACAUCUGGCUACUGGGU	(Blondal et al., 2013; Tay et al., 2017),Qiagen
hsa-miR-24-3p	UGGCUCAGUUCAGCAGGAACAG	(Blondal et al., 2013; Tan et al., 2014),Qiagen
hsa-miR-93-5p	CAAAGUGCUGUUCGUGCAGGUAG	(Blondal et al., 2013; Niu et al., 2016),Qiagen

Table 11: Housekeeping genes *(continued)*

miRNA	Sequence	Reference
hsa-miR-25-3p	CAUUGCACUUGUCUCGGUCUGA	(Blondal et al., 2013; Niu et al., 2016),Qiagen
mmu-miR-16-5p	UAGCAGCACGUAAAUAUUGGCG	(Mi et al., 2012)
mmu-miR-195a-5p	UAGCAGCACAGAAAUAUUGGC	(Mi et al., 2012)
mmu-miR-146a-5p	UGAGAACUGAAUUCCAUGGGUU	(Mi et al., 2012)
cel-miR-39-3p	UCACCGGGUGUAAAUCAGCUUG	(Schwarzenbach et al., 2015; Chen et al., 2018; Fauth et al., 2019)
hsa-let-7c-5p	UGAGGUAGUAGGUUGUAUGGUU	Qiagen
SNORD68	CGCGTGATGACATTCTCCG-GAATCGCTGTACGGCCTTGATGAAAG-CACATTTGAACCCTTTTCCATCTGATT	Qiagen
SNORD95	GCGGTGATGACCCCAACATGCCATCT-GAGTGTCGGTGCTGAAATCCAGAG-GCTGTTTCTGAGC	Qiagen
SNORD72	AGCTTATCAGTGATGTTG-TAAAAATAAATGTCTGAACATATGAAT-GCAGTATTGATTTCAGCATTTAACTGA-GATAAGCG	Qiagen
SNORD61	GCTATGATGAATTTGATTG-CATTGATCGTCTGACATGATAATG-TATTTTTGTCCTCTAAGAAGTTCT-GAGCTT	Qiagen
SNORD96A	CCTGGTGATGACAGATG-GCATTGTCAGCCAATCCC-CAAGTGGGAGTGAGGACATGTCCTG-CAATTCTGAAGG	Qiagen

Table 11: Housekeeping genes *(continued)*

miRNA	Sequence	Reference
RNU6-6P	GTGCTCGCTTCGGCAGCACATATAC-TAAAATTGGAACGATACAGAGAA-GATTAGCATGGCCCCTGCGCAAGGAT-GACACGCAAATTCGTGAAGCGTTC-CATATTTTT	Qiagen

3.2.2.3.2 Efficiency

The amplification efficiency of each miScript assay was calculated by generating a standard curve of the Cq values obtained by qPCR from a dilution series containing the target sequence. The slope of the regression line was calculated and the amplification efficiency was determined: $E = -1 + 10^{-1/Slope}$. To evaluate the efficiency of each miscript qPCR assay, human or mouse RNA was reverse transcribed into cDNA, preamplified in order to obtain sufficient amounts of template to be detected, and then serially diluted and measured by qPCR.

Reverse transcription and Multiplex pre-amplification The cDNA synthesis and multiplex pre-amplification were performed as described in 3.2.2.1.

qPCR The qPCR master mix was prepared as described in 3.2.2.2.

Preparation of dilution series: starting from a 1:1 diluted cDNA, 6 dilutions were prepared to obtain $2x10^{-1}$, $4x10^{-2}$, $8x10^{-3}$, $16x10^{-4}$, $32x10^{-5}$ and $64x10^{-6}$ dilutions , respectively, in dilution buffer (1 mM EDTA, 0.05% Tween 20, 10 mM Tris HCl, pH 8.0). 1.2 ul of the 6 cDNA dilutions were added to the qPCR master mix and the qPCR was performed in triplicates for each dilution step.

The mean Cq values for the triplicates were calculated. A standard curve for each primer assay was generated by plotting the average Cq values against the log base 10 of the concentrations of the dilution series. The slope of the linear regression was determined and the amplification efficiency was calculated using the equation:

$$E = -1 + 10^{-1/Slope}$$

3.2.2.3.3 Inhibition

For each experiment involving the quantification of a set of numerous miRNA targets in parallel (multiplex PCR), an inhibition test was performed, to ensure that the multiplexed miScript assays were not inhibiting each other. cDNA synthesis and pre-amplification for 12 cycles were conducted as described in section in 3.2.2.1, with some differences in the pre-amplification (another kit was used (TATAA PreAmp GrandMaster® Mix) with final concentrations of 0.025 uM universal primer, 0.025 uM of each of the primer assays and 1X ul TATAA PreAmp GrandMaster® Mix. 5 ul cDNA template was added to make up a 50 ul reaction volume and triplicates for each sample were prepared. The cycling conditions were: 60 seconds at 95 °C, followed by 12 cycles of 15 seconds at 95 °C, 2 min at 60 °C, 1 min at 72 °C and a final elongation phase at 72 °C for 1 min. The pre-amplified cDNA was then used as a template cDNA in the qPCR directly (non-pre-amplified sample) or underwent an additional pre-amplification step before qPCR (pre-amplified sample). The pre-amplified samples (obtained in the 1st PCR) were run in duplicates and the none-pre-amplified samples were diluted 1:10 and run in quadruplicates. The qPCR was performed as described in 3.2.2.2. To evaluate whether the assays were inhibiting each other's amplification, the difference in Cq (ΔCq) between each sample of the pre-amplified samples and the non-pre-amplified samples was determined, and the resulting values were averaged (mean ΔCq). In theory, for an uninhibited assay, the mean ΔCq = cycle number. The absolute Cq value of 80% of the cycle numbers preformed in the 1st PCR was determined as follows:

80% of the cycle numbers = (Cycles number x 0.8 x E)/100

Where E: primer amplification efficiency

An assay was considered uninhibited when mean ΔCq ≥ 80% of the cycle numbers.

3.2.3 Animal experiments

3.2.3.1 Establishment of STZ-treatment protocol in mouse

14 of C57BL/6JRj 7-weeks old mice were purchased from Janvier (Le Genest-Saint-Isle, France) and housed at the animal facility of the CRTD. All procedures were performed in sterile conditions. At 10-weeks age, 10 mice were injected with STZ using a 29G needle intraperitoneally and 4 control mice were injected with PBS. Body weight and blood glucose were monitored 14 days before the day of the STZ treatment, at the day of STZ treatment and daily after the treatment over 7 days experimental time course. The weight loss and blood glucose level measurements were given points based on their daily observations and scoring points were calculated. A loss of body weight of <5% was given 1 point, 5-10%: 5 points, 11-20%: 10 points, and >20%: 20 points. A blood glucose level between 151-300mg/dl was given 1 point, 301-500mg/dl: 10 points, and >500mg/dl: 15 points. The STZ-treated mice were sacrificed when a total score of ≥20 points was reached, otherwise all mice were sacrificed at day 7. Diabetes was diagnosed if the blood glucose level exceeds 300mg/dl. The blood glucose level was measured by puncturing the tail vein with a 30G needle and allowing around 5 ul blood to spill onto a test strip (Breeze 2, Bayer Vital GmbH, Leverkusen) and inserting the strip in blood glucose monitoring device (Breeze 2, Bayer).

Blood samples were collected before the STZ treatment (-14 day) from the leg vein from which around 70 ul blood were obtained. The blood was collected before sacrificing the animal through cardiac puncture after anesthesia, around 600 – 700 ul were obtained. The blood collection and serum separation and storage were performed as described in 3.2.1.1.3. After sacrificing the animals, the pancreata were isolated and placed in formaldehyde overnight. The pancreata were embedded in paraffin blocks and kept at room temperature for later use. The liver, spleen, one kidney, brain, one lung, heart, and one leg muscle were isolated from the mice, snap-frozen in liquid nitrogen and stored at - 80 °C.

3.2.3.2 Diabetic mouse model

Type 1 diabetes was induced in 10-weeks age C57BL/6JRj mice using Streptozotocin (STZ). The mice were purchased from Janvier (Le Genest-Saint-Isle, France) and housed at the animal facility of the CRTD. The animal experiments were approved by the Landesdirektion Sachsen

(TVV 6/2018, Dr. Barbara Langen). The STZ solution was prepared as described in 3.1.1 and placed on ice. In sterile conditions and using a 29G needle and insulin syringes, 57 mice were injected with STZ and 45 control mice were injected with the same volume of PBS (Phosphate-Buffered Saline) intraperitoneally. The body weight and blood glucose of the mice were measured 14 days before the treatment, before the injection at the day of the treatment, and daily after the treatment until day 4. Except the day of the treatment the experiment lasted for 4 days and all animals where sacrificed at day 4 through cervical dislocation. Blood samples were collected before the STZ treatment (-14 day), day 1, day 3, and day 4. The sampling was performed from the retro-orbital plexus except at day 4 through cardiac puncture after the mice were anesthetized with ketamine/xylazine cocktail as described in 3.2.1.1.3. Around 70 ul blood were collected day-14, day 1 and day 3. At day 4 600-700 ul were collected. The blood was collected in S-Monovette 1.1 ml Z-Gel (Sarstedt) and serum was immediately separated as described in 3.2.1.1.3.

Due to the relatively small volume of serum obtained from each mouse at day -14, day 1 or day 3, serum samples from several animals from the same group were pooled to make up a total of 200 ul sample suitable for miRNA isolation. This produced 3 samples from PBS-treated animals (control), 3 sample from diabetic STZ-treated and 2 samples from non-diabetic STZ-treated animals at each time point. Table 12 illustrates the number of mice used for each sample pool.

Table 12: Number of mice used in sample preparation at day -14, day 1, day 3, and day 4.

Animal group	Sample 1	Sample 2	Sample 3	Total animals
Control	15	15	15	45
Diabetic STZ-treated	19	12	10	57
Non-diabetic STZ-treated	0	7	9	

3.2.3.3 Immunofluorescence staining to assess β-cell death

Tissue slices were obtained from the paraffin embedded pancreata and placed onto histology slides for staining. The slides were kept in suitable boxes at room temperature for later use. Two sections were prepared on each slide.

Preparing buffer, Xylene and ethanol gradient

10 mM citrate buffer (0.1 M citric acid + 0.1 M sodium citrate, pH 6) was freshly prepared. Two chambers filled with 200 ml Xylene each were prepared. Two chambers for 100% and two chambers for 96% ethanol were prepared. One chamber for 80%, 70% ethanol and water were prepared.

Deparaffinization and staining

The slides were placed into a slide holder and soaked in each of the Xylene chamber for 10 min. The slides were placed shortly into each of the ethanol chambers starting from 100%, 96%, 80%, and 70% and at the end into the water chamber. The slides were placed into a cuvette filled with citrate buffer and the cuvette was placed in already heated steamer for 10 min. The cuvette was taken out and allowed to cool down for 20 min. The buffer was discarded and the slides were washed by filling the cuvette with water and discarding it 3 times. The sections were washed with PBS + 0.1% Tween. Antibody diluent solution was prepared (antibody diluent + 10% goat serum). Each section was incubated in 50 ul of the antibody diluent solution for 30 min in the dark. The sections were washed 2 times with PBS + 0.1% Tween. The primary antibody for insulin (Abcam-ab7842) was diluted 1:200 in antibody diluent and 50 ul was pipetted onto each section. The sections were incubated at 4 °C overnight in the dark, and then washed 3 times with PBS + 0.1% Tween. The secondary antibody (Goat anti-guinea pig IgG (H+L), alexa fluor 488 Thermo Fisher Scientific A-11073) was diluted 1:600 in antibody diluent and 50 ul were added to each section and incubated for 30 min at room temperature. The sections were washed 3 times with PBS + 0.1% Tween. The primary antibody for glucagon (Dako-A0565) and cleaved caspase-3 (Cell Signaling-9661L) were diluted 1:100 and 1:300 in antibody diluent, respectively. On the same slide, 50 ul glucagon antibody was added to one section, 50 ul cleaved caspase-3 antibody was added to the other section and the slides were incubated at room temperature for 1 hour in the dark, and then washed 3 times with PBS + 0.1% Tween. The secondary antibody (Goat anti-guinea pig IgG (H+L), alexa fluor 568 Thermo Fisher Scientific A-11075) was mixed with DAPI (4′,6-diamidino-2-phenylindole, Roche 10236276001) in antibody diluent to obtain dilutions of 1:600 and 1:6 respectively, and the sections were incubated with the mixture for 30 min at room temperature in the dark and then washed 3 times with PBS + 0.1% Tween. The slides were placed in a chamber filled with distilled water for 5 min. A drop of mounting solution

(VECTASHIELD H-1000) was added to each section and covered with a coverslip. The slides were kept at 4 °C for later examination under florescence microscope. The images were captured using HCX APO U-V-I 40.0x0.75 Dry UV or HCX PL APO lambda blue 63.0x1.20 Water UV objectives on a SP5 I laser scanning confocal microscope (Leica microsystems) provided with a transmission channel and 5 spectral detectors.

3.2.4 *In vitro* mouse islets stress model

3.2.4.1 Mouse islets isolation for *in vitro* islets stress model

Pancreata were from 6- to 8-weeks old male CD-1 mice. The mice were purchased from Charles River Laboratories and bred in-house as a core colony at the BSU (biological service unit) at King's college London, Guy's campus. The animal experiments were approved (PBCFBE464). The pancreata were isolated as described in 3.2.1.1.1 and placed in 50 ml tubes on ice. The tubes were then incubated in a water bath at 37 °C for 10 min. 25 ml MEM (Minimum essential medium, Sigma-M2279, 10% NCS (Newborn calf serum), 1% P/S and 1% L-glut) were added and the tubes were shaken vigorously and spun for 1.5 min 1400 rpm at 10 °C. The supernatant was discarded and 25 ml MEM were added. The tubes were vortexed and spun for 1.5 min 1400 rpm at 10 °C and washing was repeated 3 times. After the last wash the supernatant was discarded and 25 ml MEM were added and vortexed. The tubes' content was poured through a sterile metal strainer into new 50 ml tubes. 25-35 ml MEM were added to the new tubes and spun for 1.5 min 1500 rpm at 10°C. The supernatant was discarded and tubes were inverted on a paper towel to dry out. The pellet of islets was resuspended in 15 ml Histopaque®-1077 (Sigma-H8889) and vortexed. 10 ml MEM were added slowly so that an interface is created between the Histopaque and the MEM. The tubes were centrifuged for 24 min 3510 rpm at 10 °C. After centrifugation the islets were floating between the Histopaque and MEM. The islets were collected by aspirating the islets and transferring them to new 50 ml tubes. The tubes were filled with MEM and spun for 1.5 min 1500 rpm at 10 °C. The islets were washed 3 times with MEM and the supernatant was kept each time to be examined by microscopy and to collect any present islets. After the last wash the islets were suspended in 10 ml MEM and transferred into petri dishes. The dishes were examined under light microscope. The islets were hand picked with a 50 ul pipette to new petri dishes containing 10 ml RPMI (Sigma-R8758, added 10% FCS, 1% P/S and 1% L-glut). Around 200-500 islets were transferred into each dish. The islets were

kept overnight in a cell culture incubator at 37 °C, 5% CO2, and 20% O2.

3.2.4.2 Cytokine cocktail and hypoxia conditions

Proinflammatory cytokines cocktails of recombinant murine IL-1β, TNF-α, and IFN-γ (Peprotech 211-11B, 315-01A, 315-05) were prepared. Mild cytokine cocktail contained 1 ng/ml IL-1β, 5 ng/ml TNF-α and 5 ng/ml IFN-γ and aggressive cytokine cocktail 20 ng/ml IL-1β, 100 ng/ml TNF-α and 100 ng/ml IFN-γ. For Hypoxia conditions, the cell culture incubators were adjusted at 1% O2, 5% CO2 and 94% N2.

3.2.4.3 Islets culture

After an overnight culture, the petri dishes containing the islets were taken out of the incubator. RPMI medium (10% FBS, 1% P/S & 1% L-glut) containing mild cytokine cocktail, aggressive cytokine cocktail or without cytokines was prepared. For each condition, 120 islets were hand picked under light microscope and under islet culture hood in sterile conditions and placed into petri dish (ø x h = 35 x 15 mm) containing 2.5 ml RPMI medium. The non-hypoxic condition were 5% CO2, and 20% O2 and the hypoxic condition 1% O2, 5% CO2 and 94% N2. The islets were cultured in the presence of aggressive cytokines cocktail with or without hypoxic condition, mild cytokines cocktail with or without hypoxic condition, hypoxic condition only, and without cytokines cocktail in non-hypoxic condition as a control. The incubation time for each condition was 3, 6, 24, 48, or 72 H. Each condition was at least in duplicates. After incubation, the petri dishes were taken out of the incubators and placed under the microscope in the islets culture hood. The supernatant (culture medium) was aspirated with a 23G needle connected to 2.5 ml syringe. The aspiration was performed carefully so none of the islets were allowed to be aspirated. Around 1.5 ml supernatant were transferred to 2 ml tubes (Eppendorf). The tubes were centrifuged for 10 min full speed at 4 °C. The supernatant was transferred to 2.5 ml syringe and filtered with 0.2-micron filter in new tubes. The samples were snap-frozen and stored at – 80 °C for later use. The islets were transferred with the remaining medium to 1.5 ml tubes and centrifuged for 2 min 150 rcf at room temperature. The islets were snap-frozen and stored at – 80 °C for later use.

3.2.4.4 Assessment of miRNA content in supernatant

The supernatant samples were thawed and the miRNA isolation was performed. The quality of the RNA samples was analyzed using small RNA Bioanalyzer kit.

3.2.4.5 Apoptosis assay

Islets were isolated and incubated over night at 37 °C, 5% CO2, and 20% O2. The islets were transferred to cell culture plates (Greiner Bio-One 655083). 3 islets in 50 ul RPMI (containing mild, aggressive or no cytokines cocktail) were pipetted into each well. The plates were incubated in hypoxic or non-hypoxic conditions for 3, 6, and 24H. At least 12 replicates were performed for each condition and incubation time. At the end of an incubation time, the Caspase-Glo® 3/7 assay (Promega) was used to quantify the caspase activity in the wells according to the manufacturer recommendations. Briefly, the reagents were brought to room temperature 2 hours before use. The Caspase-Glo® 3/7 buffer was added to the Caspase-Glo® 3/7 Substrate and mixed. 50 ul of the Caspase-Glo® 3/7 Reagent were added to each well. The plate was covered with a lid, shaken on a plate shaker for 30 seconds 400 rpm and incubated for 1.5H in the dark at room temperature. The plate was analyzed in a luminometer (GloMax-96 Promega) and the data were extracted for analysis.

3.2.4.6 Glucose stimulated insulin secretion assay

After each treatment condition the islets were washed with 2 uM glucose solution by aspirating the culture media with 23G needle connected to 5 ml syringe, the washing repeated 3 times. After the final wash, the glucose solution was kept and the islets were incubated at 37 °C, 5% CO2 and 20% O2 for 1-2H. After incubation, 5 islets were transferred into one 1.5 ml tubes containing 500 ul of 2 uM or 20 uM glucose. The tubes were incubated at 37 °C for 1H and centrifuged for 2 min 2000 rpm at 4 °C. 200-300 ul of the supernatant were transferred to new 1.5 ml tubes, snap-frozen and stored at – 80 °C for later processing.

Secreted insulin was quantified in the samples using a mouse insulin ELISA kit (Thermo scientific) according to the manufacturer recommendations. Briefly, a dilution series of inulin was prepared to obtain 400, 200, 100, 50, 25, 12.5, 6.25 uIU/ml concentrations. 100 ul of each sample (diluted 1:10 when high insulin content is expected) and 100 ul standards were pipetted into a 96-well plate coated with an anti-insulin AB (provided). The plate was covered and incubated at room temperature for 2.5H with shaking. The solution was discarded and the wells were washed 4

times with 1X wash buffer. 100 ul biotinylated antibody was added to each well and the plate was incubated for 1H at room temperature with shaking. After washing 4 times, 100 ul Streptavidin-HRP solution were added and the plate was incubated for 45 min and the washing repeated 4 times. 100 ul TMB substrate were added and incubated 30 min in the dark. The plate was analyzed in ELISA plate reader (Infinite® 200 PRO, TECAN) at 450 nm and 550 nm.

3.2.5 miRNA profiling using Next generation sequencing

50 ng total RNA of tissue samples or 10.5 ul total RNA of cell free samples were used for small RNA sequencing at the NGS facility of the CRTD (Dr. Andreas Dahl). Library preparation was done with the NEXTflex Small RNA-Seq kit V3 (Bioo Scientific/PerkinElmer) and sequencing was conducted on Illumina NextSeq 550. The raw data (fastq files) were obtained from the NGS facility and the analysis was carried out in cooperation with Virag Sharma.

3.2.6 Data Analysis

All analysis was done in R (version 3.6.3) or Spyder (version 4.1.1).

The ΔΔ Cq method (Pfaffl, 2001) was used for RT-qPCR data analysis with the use of endogenous or exogenous reference miRNAs for data normalization. The following miRNAs were used as normalizers; mmu-miR-195a-5p and mmu-miR-16-5p for mouse serum, hsa-miR-22-3p, hsa-miR-93-5p, hsa-miR-191-5p, and hsa-miR-146a-5p and hsa-miR-23a-3p for human serum, SNORD61, SNORD68, SNORD72, SNORD95, and SNORD96A and RNU6B for human and mouse islets, and cel-miR-39 (synthetic miRNA) for supernatant samples in the in vitro islet stress model.

Statistical analysis was performed with one- or two-way ANOVA method and statistical significance was established at a *p*-value of 0.05. Multiple comparisons tested by Tukey's HSD (honestly significant difference) post-hoc test. Student's t-test was used when analyzing two groups. Pearson correlation coefficient (Pearson's *r*) was used to determine the association between miRNA level and blood glucose level in mice and apoptosis activation in the in cultured islets. Receiver-operating characteristic (ROC) curves were established, and the areas under the ROC curves (AUC) were calculated using the plotROC package.

Next generation sequencing data analysis: The raw reads were trimmed using Cutadapt (Kechin et al., 2017) and the primer specific for smRNAseq "TGGAATTCTCGGGTGCCAAGG"

was removed. Only reads with a minimum length of 15 bp were kept for downstream analysis (quality-cutoff set to 20). Subsequent analysis was performed using the QuickMIRSeq pipeline (Zhao et al., 2017).

Briefly, the QuickMIRSeq pipeline first created a database of small RNA molecules for the species of interest (mouse). The second step involved the mapping of the raw reads to the database of interest. Identical reads were collapsed into unique reads within and across samples, thereby reducing computational time. Reads that were mapped to miRNA molecules with mismatches were remapped to the reference genome to remove spurious hits to miRNA molecules and thereby reducing false positive matches. Lastly, the strand information was also taken into account. QuickMIRSeq pipeline was used for expression quantification and the resulting count matrix was then used to identify differentially expressed miRNAs using the DESeq2 (Love et al., 2014).

GSIS data analysis: The absorbance difference between 450 nm and 550 nm was determined for each concentration of the insulin dilution series. Afterwards, the difference was plotted against insulin concentrations to create a standard curve. Figure 3.1 shows an example of such curve obtained in one of the plates. Using the absorbance data obtained from ELISA plate reader and based on the generated standard curve, the insulin concentration was calculated in the samples using Dose-Response Analysis package (Ritz et al., 2015). The insulin concentrations in the diluted samples were multiplied by the dilution factor.

Pathway analysis: In mouse, target genes of miRNAs were identified using miRNAtap and org.Mm.eg.db packages. In human, target genes were identified from mirDIP (microRNA Data Integration Portal) (Tokar et al., 2018). KEGG analysis was performed on the identified targets of each miRNA using clusterProfiler package (Yu et al., 2012). The enriched pathways were filtered with a cut-off p value 0.05.

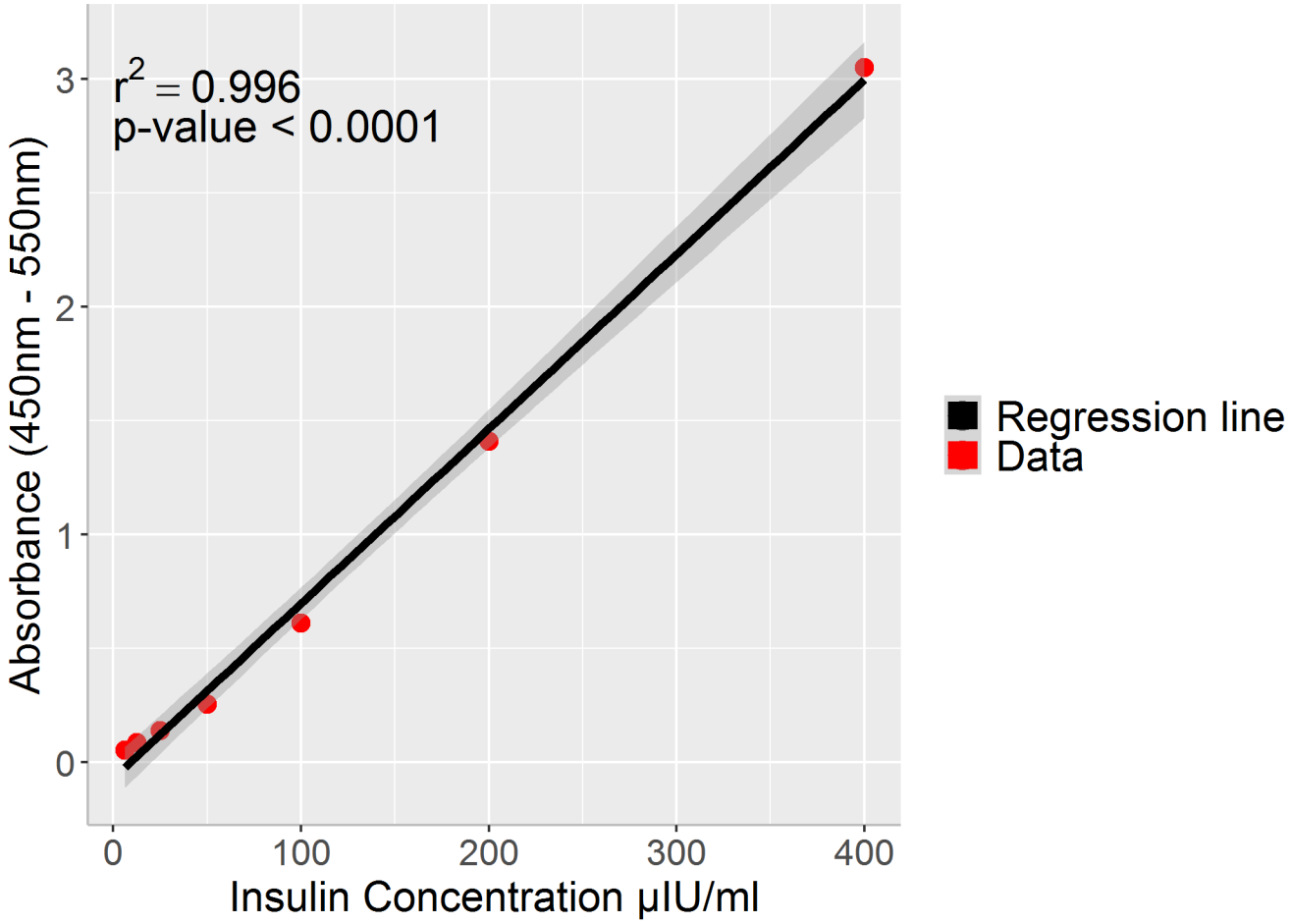

Figure 3.1: An exemplary standard curve generated in one of the analyzed ELISA plates. Fitting linear model was conducted. Reported are adjusted R-squared (r^2) and *p*-value .

3.2.7 Panels selection

The flowchart (Figure 3.2) describes the panel selection and generation of miRNA panels. The initial analysis of NGS data evolved and resulted in analysis 2 (Panel B). Through literature review, a panel of 70 miRNAs was identified. This panel was extended up to 74 by adding 4 miRNAs from the NGS data (Analysis 1). All miRNA panels mentioned in the flowchart are listed below.

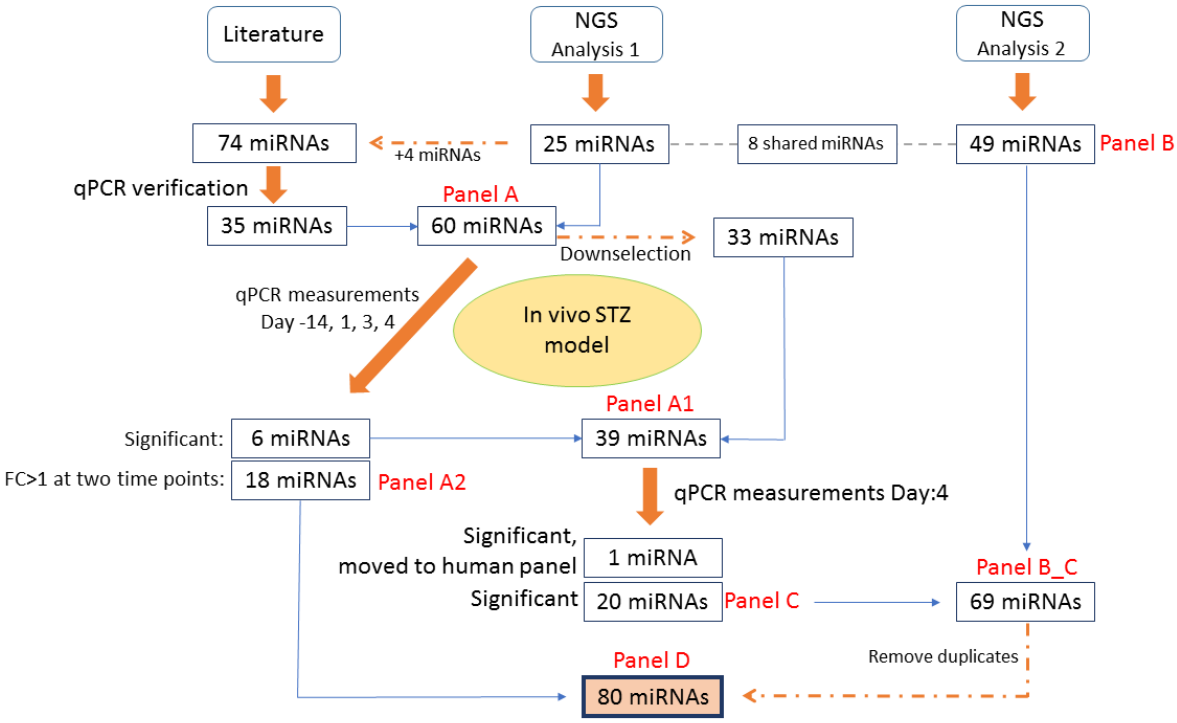

Figure 3.2: Panels selection.

Panel A comprised of 60 miRNAs (Table 13); from NGS data: 25 miRNAs top upregulated in islets as compared to serum, from qPCR: 29 miRNA significant (Figure 4.1B) + 6 miRNAs not significant, selected based on fold change or Cq values (Figure 3.3).

Table 13: Panel A (60 miRNAs). Tm: Melting Temperature, E: Amplification Efficiency

miRNA	Sequence	Tm	E
mmu-miR-770-3p	CGUGGGCCUGACGUGGAGCUGG	79.9	1.95
mmu-let-7k	UGAGGUAGGAGGUUGUGUG	79.3	1.98
mmu-miR-323-3p	CACAUUACACGGUCGACCUCU	78.3	1.63
mmu-miR-98-5p	UGAGGUAGUAAGUUGUAUUGUU	79.1	2.00
mmu-miR-487b-3p	AAUCGUACAGGGUCAUCCACUU	79.6	1.97
mmu-miR-434-3p	UUUGAACCAUCACUCGACUCCU	79.4	1.98
mmu-miR-434-5p	GCUCGACUCAUGGUUUGAACCA	79.6	2.00
mmu-miR-200b-3p	UAAUACUGCCUGGUAAUGAUGA	78.9	1.91

Table 13: *(continued)*

miRNA	Sequence	Tm	E
mmu-miR-132-3p	UAACAGUCUACAGCCAUGGUCG	79.6	1.96
mmu-miR-652-3p	AAUGGCGCCACUAGGGUUGUG	79.4	1.93
mmu-miR-30c-5p	UGUAAACAUCCUACACUCUCAGC	79.2	1.88
mmu-miR-23b-3p	AUCACAUUGCCAGGGAUUACC	79.3	1.93
mmu-miR-423-3p	AGCUCGGUCUGAGGCCCCUCAGU	80.0	1.99
mmu-miR-320-3p	AAAAGCUGGGUUGAGAGGGCGA	80.5	1.91
mmu-let-7d-5p	AGAGGUAGUAGGUUGCAUAGUU	79.3	1.98
mmu-miR-543-3p	AAACAUUCGCGGUGCACUUCUU	79.3	1.97
mmu-miR-375-3p	UUUGUUCGUUCGGCUCGCGUGA	81.1	1.98
mmu-miR-7a-5p	UGGAAGACUAGUGAUUUUGUUGU	79.4	1.94
mmu-miR-411-5p	UAGUAGACCGUAUAGCGUACG	80.0	1.91
mmu-miR-141-3p	UAACACUGUCUGGUAAAGAUGG	79.5	1.99
mmu-miR-148a-3p	UCAGUGCACUACAGAACUUUGU	79.5	1.91
mmu-miR-200c-3p	UAAUACUGCCGGGUAAUGAUGGA	79.7	1.92
mmu-miR-379-5p	UGGUAGACUAUGGAACGUAGG	79.2	1.90
mmu-miR-101a-3p	UACAGUACUGUGAUAACUGAA	79.3	1.92
mmu-miR-29b-3p	UAGCACCAUUUGAAAUCAGUGUU	79.2	1.90
mmu-miR-26a-5p	UUCAAGUAAUCCAGGAUAGGCU	79.3	1.97
mmu-let-7f-5p	UGAGGUAGUAGAUUGUAUAGUU	79.3	1.92
mmu-miR-136-5p	ACUCCAUUUGUUUUGAUGAUGG	79.4	1.97
mmu-miR-7b-5p	UGGAAGACUUGUGAUUUUGUUGU	79.5	1.95
mmu-miR-129-5p	CUUUUUGCGGUCUGGGCUUGC	80.0	1.98
mmu-miR-184-3p	UGGAAGACUAGUGAUUUUGUUGU	79.4	1.92
mmu-miR-141-5p	CAUCUUCCAGUGCAGUGUUGGA	80.9	2.00
mmu-miR-127-3p	UCGGAUCCGUCUGAGCUUGGCU	80.2	1.94
mmu-let-7c-5p	UGAGGUAGUAGGUUGUAUGGUU	79.4	1.95
mmu-miR-99b-5p	CACCCGUAGAACCGACCUUGCG	80.5	1.90

Table 13: *(continued)*

miRNA	Sequence	Tm	E
mmu-let-7b-5p	UGAGGUAGUAGGUUGUGUGGUU	79.5	1.96
mmu-miR-668-3p	UGUCACUCGGCUCGGCCCACUACC	80.7	1.98
mmu-miR-770-5p	AGCACCACGUGUCUGGGCCACG	81.1	1.94
mmu-miR-151-3p	CUAGACUGAGGCUCCUUGAGG	79.5	1.95
mmu-miR-5099	UUAGAUCGAUGUGGUGCUCC	79.6	1.92
mmu-miR-222-3p	AGCUACAUCUGGCUACUGGGU	79.2	1.99
mmu-miR-423-5p	UGAGGGGCAGAGAGCGAGACUUU	79.4	1.89
mmu-miR-125a-5p	UCCCUGAGACCCUUUAACCUGUGA	79.3	1.99
mmu-miR-541-5p	AAGGGAUUCUGAUGUUGGUCACACU	80.0	1.99
mmu-miR-485-5p	AGAGGCUGGCCGUGAUGAAUUC	80.2	1.92
mmu-miR-384-3p	AUUCCUAGAAAUUGUUCACAAU	78.5	1.90
mmu-miR-598-3p	UACGUCAUCGUCGUCAUCGUUA	79.2	1.86
mmu-miR-340-3p	UCCGUCUCAGUUACUUUAUAGC	78.8	1.99
mmu-miR-433-3p	AUCAUGAUGGGCUCCUCGGUGU	81.4	1.93
mmu-miR-92b-3p	UAUUGCACUCGUCCCGGCCUCC	81.4	1.92
mmu-miR-369-3p	AAUAAUACAUGGUUGAUCUUU	79.3	1.91
mmu-miR-369-5p	AGAUCGACCGUGUUAUAUUCGC	79.1	1.83
mmu-miR-26b-5p	UUCAAGUAAUUCAGGAUAGGU	79.0	1.88
mmu-miR-429-3p	UAAUACUGUCUGGUAAUGCCGU	79.3	1.92
mmu-miR-204-5p	UUCCCUUUGUCAUCCUAUGCCU	79.9	1.99
mmu-miR-127-5p	CUGAAGCUCAGAGGGCUCUGAU	79.7	1.88
mmu-miR-381-5p	AGCGAGGUUGCCCUUUGUAUAUU	79.9	1.91
mmu-miR-582-5p	AUACAGUUGUUCAACCAGUUAC	79.5	1.90
mmu-miR-409-3p	GAAUGUUGCUCGGUGAACCCCU	80.0	1.99
mmu-miR-27b-3p	UUCACAGUGGCUAAGUUCUGC	80.1	1.97

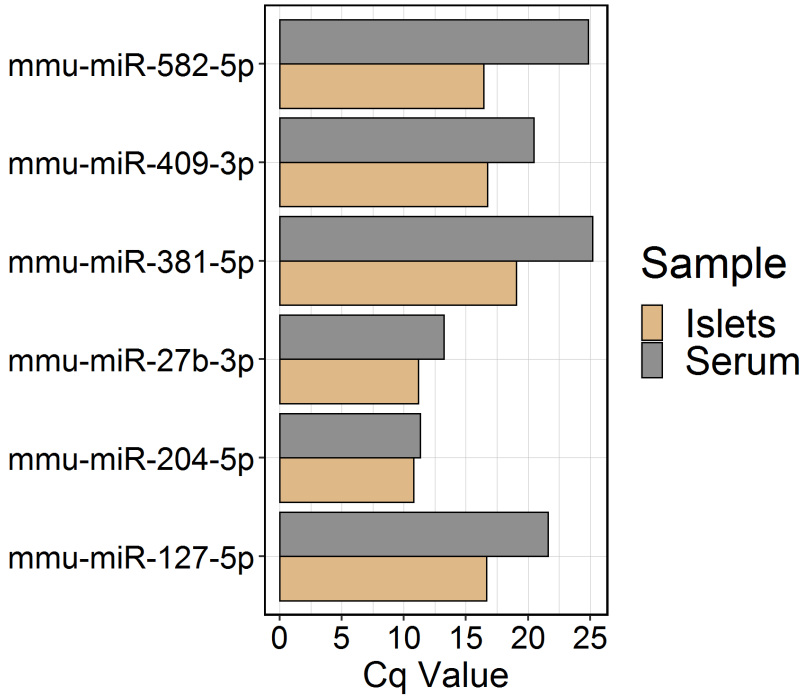

Figure 3.3: 6 miRNAs added to Panel A. Presented their Cq values in islets and serum

miRNAs of Panel A1 are listed in table 14.

Table 14: Panel A2 (39 miRNAs). Tm: Melting Temperature, E: Amplification Efficiency

miRNA	Sequence	Tm	E
mmu-miR-375-3p	UUUGUUCGUUCGGCUCGCGUGA	81.1	1.98
mmu-miR-132-3p	UAACAGUCUACAGCCAUGGUCG	79.6	1.96
mmu-let-7c-5p	UGAGGUAGUAGGUUGUAUGGUU	79.4	1.95
mmu-miR-184-3p	UGGAAGACUAGUGAUUUUGUUGU	79.4	1.92
mmu-miR-141-3p	UAACACUGUCUGGUAAAGAUGG	79.5	1.99
mmu-let-7b-5p	UGAGGUAGUAGGUUGUGUGGUU	79.5	1.96
mmu-miR-136-5p	ACUCCAUUUGUUUUGAUGAUGG	79.4	1.97
mmu-miR-652-3p	AAUGGCGCCACUAGGGUUGUG	79.4	1.93
mmu-miR-148a-3p	UCAGUGCACUACAGAACUUUGU	79.5	1.91
mmu-miR-30c-5p	UGUAAACAUCCUACACUCUCAGC	79.2	1.88
mmu-miR-127-5p	CUGAAGCUCAGAGGGCUCUGAU	79.7	1.88

Table 14: *(continued)*

miRNA	Sequence	Tm	E
mmu-miR-543-3p	AAACAUUCGCGGUGCACUUCUU	79.3	1.97
mmu-miR-222-3p	AGCUACAUCUGGCUACUGGGU	79.2	1.99
mmu-miR-200c-3p	UAAUACUGCCGGGUAAUGAUGGA	79.7	1.92
mmu-miR-770-3p	CGUGGGCCUGACGUGGAGCUGG	79.9	1.95
mmu-miR-23b-3p	AUCACAUUGCCAGGGAUUACC	79.3	1.93
mmu-miR-770-5p	AGCACCACGUGUCUGGGCCACG	81.1	1.94
mmu-miR-320-3p	AAAAGCUGGGUUGAGAGGGCGA	80.5	1.91
mmu-miR-127-3p	UCGGAUCCGUCUGAGCUUGGCU	80.2	1.94
mmu-miR-423-3p	AGCUCGGUCUGAGGCCCCUCAGU	80.0	1.99
mmu-miR-379-5p	UGGUAGACUAUGGAACGUAGG	79.2	1.90
mmu-miR-423-5p	UGAGGGGCAGAGAGCGAGACUUU	79.4	1.89
mmu-let-7k	UGAGGUAGGAGGUUGUGUG	79.3	1.98
mmu-let-7d-5p	AGAGGUAGUAGGUUGCAUAGUU	79.3	1.98
mmu-miR-323-3p	CACAUUACACGGUCGACCUCU	78.3	1.63
mmu-miR-99b-5p	CACCCGUAGAACCGACCUUGCG	80.5	1.90
mmu-miR-98-5p	UGAGGUAGUAAGUUGUAUUGUU	79.1	2.00
mmu-miR-487b-3p	AAUCGUACAGGGUCAUCCACUU	79.6	1.97
mmu-miR-151-3p	CUAGACUGAGGCUCCUUGAGG	79.5	1.95
mmu-miR-29b-3p	UAGCACCAUUUGAAAUCAGUGUU	79.2	1.90
mmu-miR-434-3p	UUUGAACCAUCACUCGACUCCU	79.4	1.98
mmu-miR-411-5p	UAGUAGACCGUAUAGCGUACG	80.0	1.91
mmu-miR-434-5p	GCUCGACUCAUGGUUUGAACCA	79.6	2.00
mmu-miR-200b-3p	UAAUACUGCCUGGUAAUGAUGA	78.9	1.91
mmu-miR-141-5p	CAUCUUCCAGUGCAGUGUUGGA	80.9	2.00
mmu-miR-129-5p	CUUUUUGCGGUCUGGGCUUGC	80.0	1.98
mmu-miR-5099	UUAGAUCGAUGUGGUGCUCC	79.6	1.92
mmu-miR-204-5p	UUCCCUUUGUCAUCCUAUGCCU	79.9	1.99

Table 14: *(continued)*

miRNA	Sequence	Tm	E
mmu-miR-101a-3p	UACAGUACUGUGAUAACUGAA	79.3	1.92

Table 15: Panel B. NGS reads of 49 miRNAs in 3 islet samples and 3 serum samples.

	Islets			Serum		
miRNA	**1**	**2**	**3**	**1**	**2**	**3**
mmu-miR-375-3p	2529539	2195561	2508657	130	288	184
mmu-miR-7a-5p	763042	680781	702778	141	282	565
mmu-miR-7b-5p	184333	147563	149353	2	17	14
mmu-miR-200c-3p	122089	113165	98767	27	47	87
mmu-let-7e-5p	67221	53005	92333	43	72	58
mmu-miR-541-5p	43687	34272	38119	69	35	42
mmu-miR-129-5p	15383	16758	13081	2	3	3
mmu-miR-129-2-3p	12254	9551	4692	0	0	0
mmu-miR-129-1-3p	12038	8744	4299	0	3	1
mmu-miR-3968	11247	5219	18697	11	11	11
mmu-miR-433-3p	7278	6478	6190	2	1	5
mmu-miR-7a-2-3p	6443	4992	5607	1	0	1
mmu-miR-129b-3p	6329	7280	5479	0	1	0
mmu-miR-487b-3p	4856	5109	4449	13	2	11
mmu-miR-485-5p	3167	2705	3552	1	2	0
mmu-miR-384-5p	2735	3376	1693	0	0	3
mmu-miR-200b-5p	2667	2575	2685	3	9	3
mmu-miR-668-3p	2491	2087	1945	4	1	0
mmu-miR-485-3p	2397	1212	2676	3	0	1
mmu-miR-340-3p	2106	1501	1812	1	3	1
mmu-miR-323-3p	2008	1596	1194	0	0	0

Table 15: *(continued)*

	Islets			Serum		
miRNA	**1**	**2**	**3**	**1**	**2**	**3**
mmu-miR-409-5p	1442	960	771	0	0	5
mmu-miR-667-3p	1379	1173	1094	1	4	2
mmu-miR-543-3p	1308	1322	1465	1	0	0
mmu-miR-383-5p	1052	844	738	0	0	0
mmu-miR-673-5p	919	810	618	0	0	0
mmu-miR-3099-3p	817	1441	826	0	0	0
mmu-miR-666-5p	774	812	614	0	1	1
mmu-miR-1224-5p	596	968	973	0	0	0
mmu-miR-384-3p	577	687	446	0	0	0
mmu-miR-770-5p	543	637	558	0	0	0
mmu-miR-325-3p	535	435	182	0	0	0
mmu-miR-370-3p	531	391	410	0	0	0
mmu-miR-130b-5p	524	335	759	1	0	2
mmu-miR-325-5p	313	249	102	0	0	0
mmu-miR-34c-3p	302	279	118	1	0	0
mmu-miR-23b-5p	283	277	380	0	0	0
mmu-miR-770-3p	267	329	184	0	0	0
mmu-miR-666-3p	238	191	197	0	0	0
mmu-miR-412-5p	232	155	144	1	0	0
mmu-miR-141-5p	197	277	136	0	0	0
mmu-miR-3072-3p	193	325	111	0	0	1
mmu-miR-153-3p	190	296	198	0	0	0
mmu-miR-154-3p	154	149	143	0	0	0
mmu-miR-1193-3p	143	126	106	0	0	0
mmu-miR-3547-3p	134	132	50	0	0	0
mmu-miR-370-5p	131	59	71	0	0	0

Table 15: *(continued)*

	Islets			Serum		
miRNA	**1**	**2**	**3**	**1**	**2**	**3**
mmu-miR-216b-5p	54	238	12	0	0	0
mmu-miR-6238	43	33	194	0	0	0

Table 16: Panel BC

miRNA	**Panel**	**miRNA**	**Panel**
mmu-miR-375-3p	B	mmu-miR-130b-5p	B
mmu-miR-7a-5p	B	mmu-miR-325-5p	B
mmu-miR-7b-5p	B	mmu-miR-34c-3p	B
mmu-miR-200c-3p	B	mmu-miR-23b-5p	B
mmu-let-7e-5p	B	mmu-miR-666-3p	B
mmu-miR-541-5p	B	mmu-miR-412-5p	B
mmu-miR-129-5p	B	mmu-miR-3072-3p	B
mmu-miR-433-3p	B	mmu-miR-153-3p	B
mmu-miR-487b-3p	B	mmu-miR-154-3p	B
mmu-miR-485-5p	B	mmu-miR-1193-3p	B
mmu-miR-340-3p	B	mmu-miR-3547-3p	B
mmu-miR-323-3p	B	mmu-miR-370-5p	B
mmu-miR-543-3p	B	mmu-miR-216b-5p	B
mmu-miR-384-3p	B	mmu-miR-6238	B
mmu-miR-770-5p	B	mmu-miR-375-3p	C
mmu-miR-770-3p	B	mmu-miR-129-5p	C
mmu-miR-141-5p	B	mmu-miR-487b-3p	C
mmu-miR-129-2-3p	B	mmu-miR-323-3p	C
mmu-miR-129-1-3p	B	mmu-miR-543-3p	C
mmu-miR-3968	B	mmu-miR-770-5p	C

Table 16: Panel BC *(continued)*

miRNA	Panel	miRNA	Panel
mmu-miR-7a-2-3p	B	mmu-miR-770-3p	C
mmu-miR-129b-3p	B	mmu-miR-127-5p	C
mmu-miR-384-5p	B	mmu-let-7d-5p	C
mmu-miR-200b-5p	B	mmu-miR-132-3p	C
mmu-miR-668-3p	B	mmu-miR-411-5p	C
mmu-miR-485-3p	B	mmu-miR-434-3p	C
mmu-miR-409-5p	B	mmu-miR-222-3p	C
mmu-miR-667-3p	B	mmu-miR-320-3p	C
mmu-miR-383-5p	B	mmu-miR-423-3p	C
mmu-miR-673-5p	B	mmu-miR-423-5p	C
mmu-miR-3099-3p	B	mmu-miR-99b-5p	C
mmu-miR-666-5p	B	mmu-miR-101a-3p	C
mmu-miR-1224-5p	B	mmu-miR-29b-3p	C
mmu-miR-325-3p	B	mmu-miR-5099	C
mmu-miR-370-3p	B		

Panel A2 comprised of 18 miRNAs which had FC>1 at least at two time points after STZ treatment (Figure 3.4).

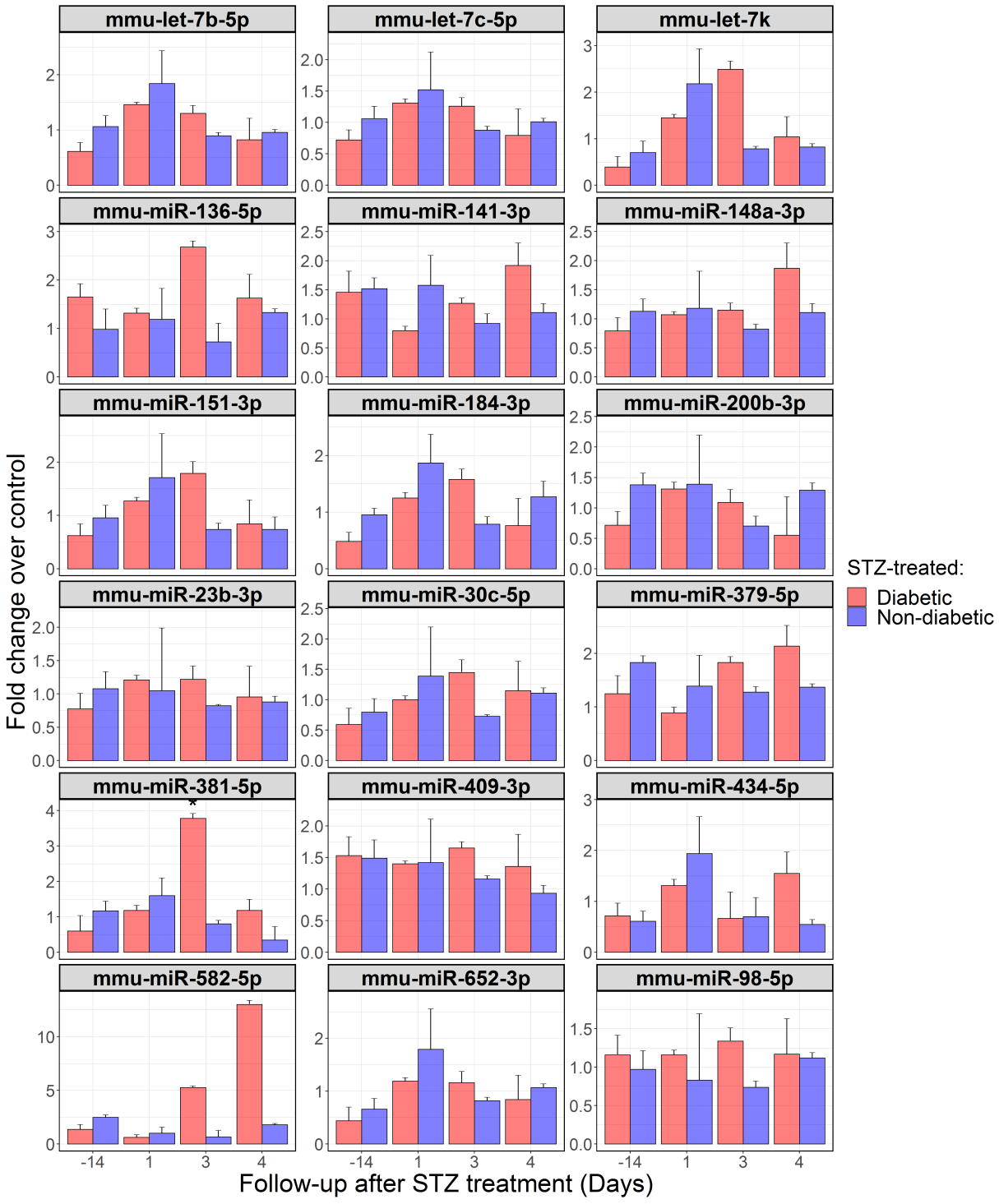

Figure 3.4: Panel A2

Table 17: Panel D (80 miRNAs). Tm: Melting Temperature, E: Amplification Efficiency

miRNA	Sequence	Tm	E
mmu-miR-375-3p	UUUGUUCGUUCGGCUCGCGUGA	80.4	1.97
mmu-miR-7a-5p	UGGAAGACUAGUGAUUUUGUUGU	78.0	1.93
mmu-miR-7b-5p	UGGAAGACUUGUGAUUUUGUUGUU	78.0	1.93
mmu-miR-200c-3p	UAAUACUGCCGGGUAAUGAUGGA	78.8	1.90
mmu-let-7e-5p	UGAGGUAGGAGGUUGUAUAGUU	78.2	1.99
mmu-miR-541-5p	AAGGGAUUCUGAUGUUGGUCACACU	80.0	1.95
mmu-miR-129-5p	CUUUUUGCGGUCUGGGCUUGC	77.7	1.96
mmu-miR-433-3p	AUCAUGAUGGGCUCCUCGGUGU	77.6	1.95
mmu-miR-487b-3p	AAUCGUACAGGGUCAUCCACUU	79.4	1.98
mmu-miR-485-5p	AGAGGCUGGCCGUGAUGAAUUC	80.3	2.00
mmu-miR-340-3p	UCCGUCUCAGUUACUUUAUAGC	77.6	1.94
mmu-miR-323-3p	CACAUUACACGGUCGACCUCU	76.6	1.70
mmu-miR-543-3p	AAACAUUCGCGGUGCACUUCUU	78.3	1.98
mmu-miR-384-3p	AUUCCUAGAAAUUGUUCACAAU	77.7	1.82
mmu-miR-770-5p	AGCACCACGUGUCUGGGCCACG	81.1	1.92
mmu-miR-770-3p	CGUGGGCCUGACGUGGAGCUGG	79.2	1.97
mmu-miR-141-5p	CAUCUUCCAGUGCAGUGUUGGA	80.3	1.91
mmu-miR-141-3p	UAACACUGUCUGGUAAAGAUGG	78.1	1.86
mmu-miR-582-5p	AUACAGUUGUUCAACCAGUUAC	77.9	1.91
mmu-miR-200b-3p	UAAUACUGCCUGGUAAUGAUGA	78.2	1.98
mmu-miR-98-5p	UGAGGUAGUAAGUUGUAUUGUU	77.6	1.95
mmu-miR-184-3p	UGGACGGAGAACUGAUAAGGGU	78.4	1.96
mmu-miR-381-5p	AGCGAGGUUGCCCUUUGUAUAUU	78.8	1.92
mmu-miR-434-5p	GCUCGACUCAUGGUUUGAACCA	79.8	1.97
mmu-miR-23b-3p	AUCACAUUGCCAGGGAUUACC	78.8	1.97
mmu-miR-127-5p	CUGAAGCUCAGAGGGCUCUGAU	78.3	2.00
mmu-let-7d-5p	AGAGGUAGUAGGUUGCAUAGUU	77.9	1.96

Table 17: *(continued)*

miRNA	Sequence	Tm	E
mmu-miR-136-5p	ACUCCAUUUGUUUUGAUGAUGG	77.7	1.94
mmu-miR-132-3p	UAACAGUCUACAGCCAUGGUCG	79.4	1.99
mmu-miR-411-5p	UAGUAGACCGUAUAGCGUACG	79.1	1.94
mmu-let-7k	UGAGGUAGGAGGUUGUGUG	78.4	1.93
mmu-miR-409-3p	GAAUGUUGCUCGGUGAACCCCU	78.7	1.96
mmu-miR-652-3p	AAUGGCGCCACUAGGGUUGUG	79.1	1.95
mmu-miR-434-3p	UUUGAACCAUCACUCGACUCCU	79.3	1.91
mmu-miR-379-5p	UGGUAGACUAUGGAACGUAGG	78.1	1.93
mmu-miR-148a-3p	UCAGUGCACUACAGAACUUUGU	78.0	1.95
mmu-miR-30c-5p	UGUAAACAUCCUACACUCUCAGC	78.4	1.89
mmu-miR-222-3p	AGCUACAUCUGGCUACUGGGUCU	84.2	1.94
mmu-miR-320-3p	AAAAGCUGGGUUGAGAGGGCGA	80.0	1.94
mmu-miR-423-3p	AGCUCGGUCUGAGGCCCCUCAGU	79.2	1.99
mmu-miR-423-5p	UGAGGGGCAGAGAGCGAGACUUU	78.3	1.99
mmu-miR-99b-5p	CACCCGUAGAACCGACCUUGCG	80.0	1.97
mmu-miR-101a-3p	UACAGUACUGUGAUAACUGAA	77.6	1.99
mmu-miR-29b-3p	UAGCACCAUUUGAAAUCAGUGUU	78.2	1.97
mmu-miR-5099	UUAGAUCGAUGUGGUGCUCC	79.1	1.91
mmu-let-7c-5p	UGAGGUAGUAGGUUGUAUGGUU	77.8	2.00
mmu-let-7b-5p	UGAGGUAGUAGGUUGUGUGGUU	78.0	1.97
mmu-miR-151-3p	CUAGACUGAGGCUCCUUGAGG	79.5	1.98
mmu-miR-129-2-3p	AAGCCCUUACCCCAAAAAGCAU	78.5	1.96
mmu-miR-129-1-3p	AAGCCCUUACCCCAAAAAGUAU	78.2	1.99
mmu-miR-3968	CGAAUCCCACUCCAGACACCA	79.3	1.98
mmu-miR-7a-2-3p	CAACAAGUCCCAGUCUGCCACA	80.2	1.95
mmu-miR-129b-3p	CAAGCCCAGACCGCAAAAAGAUU	80.2	1.99
mmu-miR-384-5p	UGUAAACAAUUCCUAGGCAAUGU	78.3	1.75

Table 17: *(continued)*

miRNA	Sequence	Tm	E
mmu-miR-200b-5p	CAUCUUACUGGGCAGCAUUGGA	79.0	1.98
mmu-miR-668-3p	UGUCACUCGGCUCGGCCCACUACC	80.5	1.91
mmu-miR-485-3p	AGUCAUACACGGCUCUCCUCUC	79.2	1.99
mmu-miR-409-5p	AGGUUACCCGAGCAACUUUGCAU	79.2	1.92
mmu-miR-667-3p	UGACACCUGCCACCCAGCCCAAG	81.4	1.92
mmu-miR-383-5p	AGAUCAGAAGGUGACUGUGGCU	77.6	1.96
mmu-miR-673-5p	CUCACAGCUCUGGUCCUUGGAG	79.1	1.96
mmu-miR-3099-3p	UAGGCUAGAGAGAGGUUGGGGA	78.3	1.97
mmu-miR-666-5p	AGCGGGCACAGCUGUGAGAGCC	79.0	1.98
mmu-miR-1224-5p	GUGAGGACUGGGGAGGUGGAG	78.5	1.97
mmu-miR-325-3p	UUUAUUGAGCACCUCCUAUCAA	78.7	1.93
mmu-miR-370-3p	GCCUGCUGGGGUGGAACCUGGU	79.4	1.99
mmu-miR-130b-5p	ACUCUUUCCCUGUUGCACUACU	78.5	1.92
mmu-miR-325-5p	CCUAGUAGGUGCUCAGUAAGUGU	79.8	1.99
mmu-miR-34c-3p	AAUCACUAACCACACAGCCAGG	79.7	2.00
mmu-miR-23b-5p	GGGUUCCUGGCAUGCUGAUUU	78.4	1.89
mmu-miR-666-3p	GGCUGCAGCGUGAUCGCCUGCU	80.0	1.97
mmu-miR-412-5p	UGGUCGACCAGCUGGAAAGUAAU	79.0	2.00
mmu-miR-3072-3p	UGCCCCCUCCAGGAAGCCUUCU	78.5	1.98
mmu-miR-153-3p	UUGCAUAGUCACAAAAGUGAUC	77.8	1.95
mmu-miR-154-3p	AAUCAUACACGGUUGACCUAUU	79.3	1.96
mmu-miR-1193-3p	UAGGUCACCCGUUUUACUAUC	78.1	1.94
mmu-miR-3547-3p	UGAGCACCACCCCUCUCUCAG	79.8	1.99
mmu-miR-370-5p	CAGGUCACGUCUCUGCAGUU	78.0	2.00
mmu-miR-216b-5p	AAAUCUCUGCAGGCAAAUGUGA	78.7	1.93
mmu-miR-6238	UUAUUAGUCAGUGGAGGAAAUG	78.2	1.98

Panel P: miRNAs selected to be tested in the pilot experiment of *in vitro* mouse islet stress. The panel P contains 15 miRNAs, selected from Panel B (7 miRNAs), Panel A2 (4 miRNAs), and Panel C (4 miRNAs). Table 18.

The human miRNAs with identical sequence to their peers in mouse species were tested in *in vitro* human islet stress model. The miRNA ID and sequence obtained from miRbase version 22.1.

Table 18: Panel P

Panel	Mouse ID	Human ID	Sequence homology
A2	mmu-miR-141-3p	hsa-miR-141-3p	Identical
A2	mmu-miR-30c-5p	hsa-miR-30c-5p	Identical
A2	mmu-miR-148a-3p	hsa-miR-148a-3p	Identical
A2	mmu-miR-582-5p	NA	NA
B	mmu-miR-129-5p	hsa-miR-129-5p	Identical
B	mmu-let-7e-5p	hsa-let-7e-5p	Identical
B	mmu-miR-200c-3p	hsa-miR-200c-3p	Identical
B	mmu-miR-7a-5p	NA	NA
B	mmu-miR-7b-5p	NA	NA
B	mmu-miR-375-3p	hsa-miR-375-3p	Identical
B	mmu-miR-541-5p	NA	NA
C	mmu-miR-127-5p	hsa-miR-127-5p	Identical
C	mmu-miR-132-3p	hsa-miR-132-3p	Identical
C	mmu-miR-543-3p	NA	NA
C	mmu-miR-770-5p	NA	NA

4 Results

4.1 Identification of islet specific miRNAs

4.1.1 Identification of mouse islet specific miRNAs

To identify miRNAs that are highly expressed in islets, I reviewed profiling studies from the literature and collected miRNAs that have been reported to be highly expressed in β-cells or in islets. The thus selected 74 miRNAs (Table 9 in methods) were filtered by measuring their expression levels in islets and serum isolated from three BL6 mice by RT-qPCR. Only miRNAs with significantly higher expression in islets relative to serum were selected. A panel comprising 29 miRNAs was thus established (Figure 4.1A and B).

Next-generation sequencing to identify mouse islets specific miRNAs

To expand the panel of potentially islets specific miRNA, small RNA sequencing was performed on 3 islet- and 3 serum-samples isolated from 3 BL6 mice. 345 miRNAs were differentially expressed, with 194 upregulated and 151 downregulated in islets as compared to serum (Figure 4.2A). The top 50 upregulated miRNAs are presented in the heatmap (Figure 4.2B).

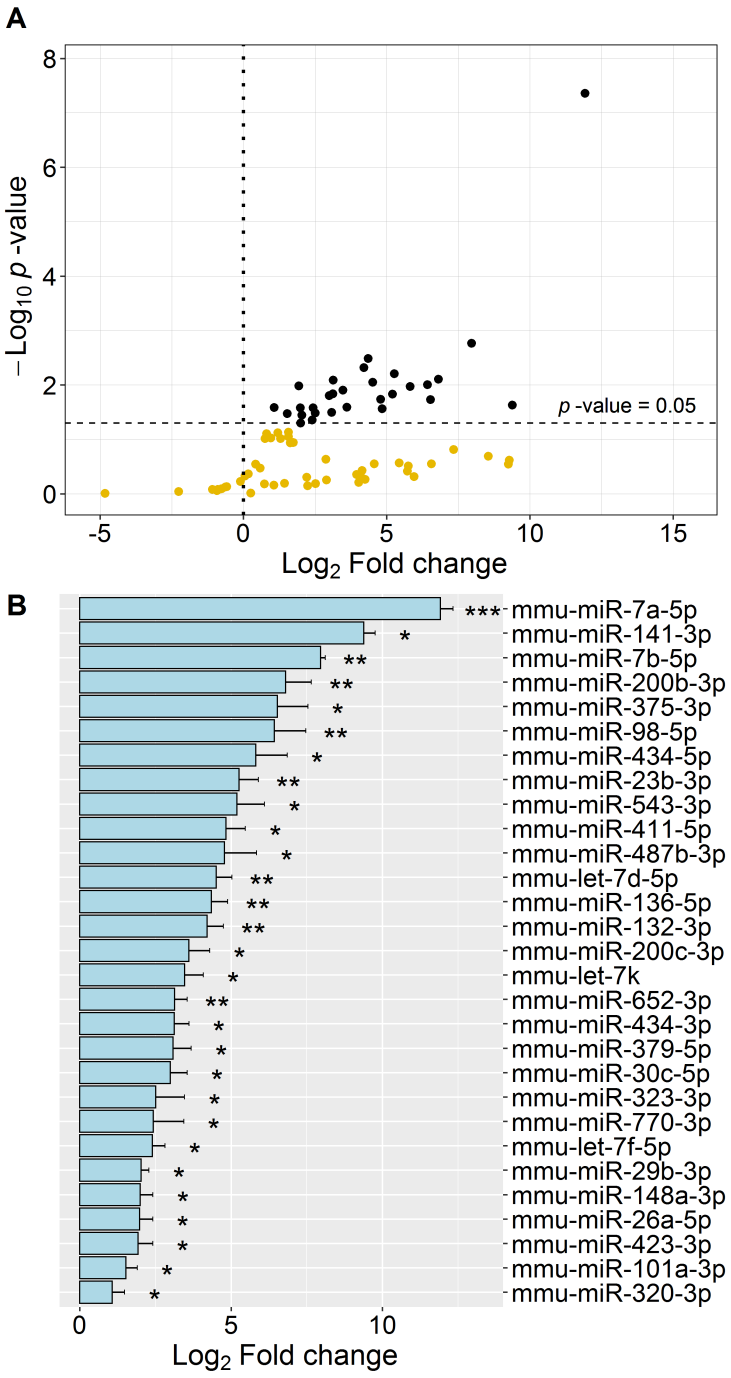

Figure 4.1: Identification of mouse miRNAs with higher expression in islets as compared to serum. A: Volcano plot shows the 74 tested miRNAs. Their significance as -$\log_{10}$ *p*-value is presented against their expression level, as $\log_2$ fold change, in islets (N=3) relative to serum (N=3). Each sample was tested in triplicate. The vertical line indicates a fold change of 1 and the horizontal line a *p*-vale of 0.05. The black dots represent 29 miRNA with fold change >1 and *p*-value <0.05, also presented in the bar plot (**B**) which shows the $\log_2$ fold change of their expression level in islets relative to serum and their significance. *t*-test was performed on ΔCq values (Cq_{Target} - $Cq_{Reference}$).**p < 0.05, **p < 0.01, ***p < 0.001 and ****p < 0.0001*

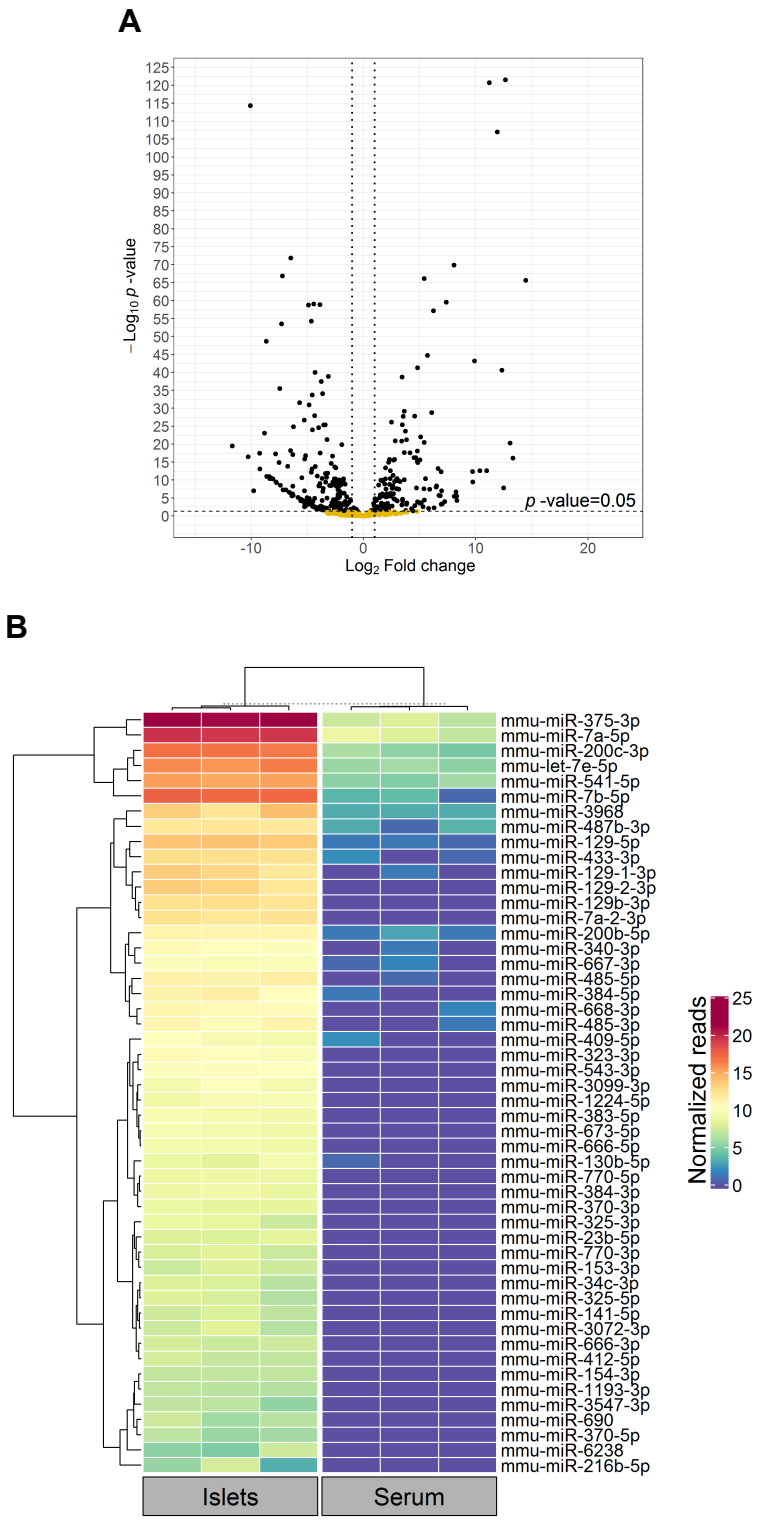

Figure 4.2: Small RNA-seq on serum and islets in BL6 mice. A: Volcano plot shows 571 miRNAs identified in total with 194 upregulated and 151 downregulated ones in islets as compared to serum. The $\log_2$ fold change is presented against the $-\log_{10}$ *p*-value. **B:** Heatmap shows the top 50 upregulated miRNAs in islets in comparison to serum. Log_2 of the normalized reads is presented. Each column indicates an islet or serum sample. The heatmap is clustered by euclidean distance and scaled by rows.

A panel of 60 miRNA (Figure 4.3) were selected from the NGS panel (25 miRNAs) and the PCR panel (35 miRNAs) to be tested in the *in vivo* animal model. (Table 13 in methods).

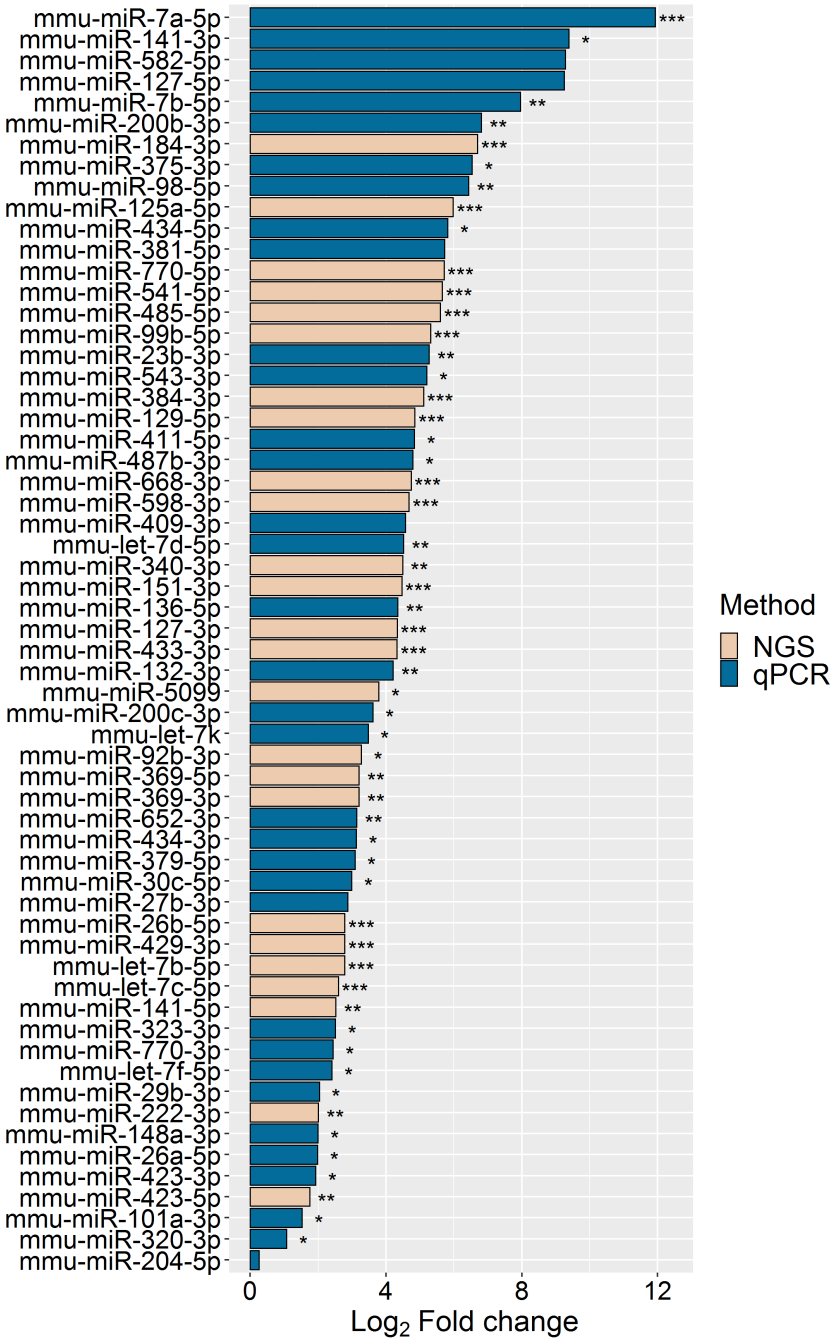

Figure 4.3: Panel of 60 miRNAs selected from NGS- and qPCR data for testing in the *in vivo* mouse model. Log_2 fold change (enrichment in islets as compared to serum) is presented.*$p < 0.05$, **$p < 0.01$, ***$p < 0.001$ and ****$p < 0.0001$.

4.1.2 Identification of human islet specific miRNAs

A panel of 30 human and potentially islet specific miRNAs (Table 10 in methods) was established by reviewing miRNA profiling data from the literature (Bunt et al., 2013; Roat et al., 2017). Using RT-qPCR, islet-specific expression of the miRNAs of this panel were measured in five human islets samples obtained from deceased donors and six human serum samples obtained from six healthy individuals. 15 miRNAs had significantly higher concentrations in islets as compared to serum and were therefore selected as islet specific (Figure 4.4).

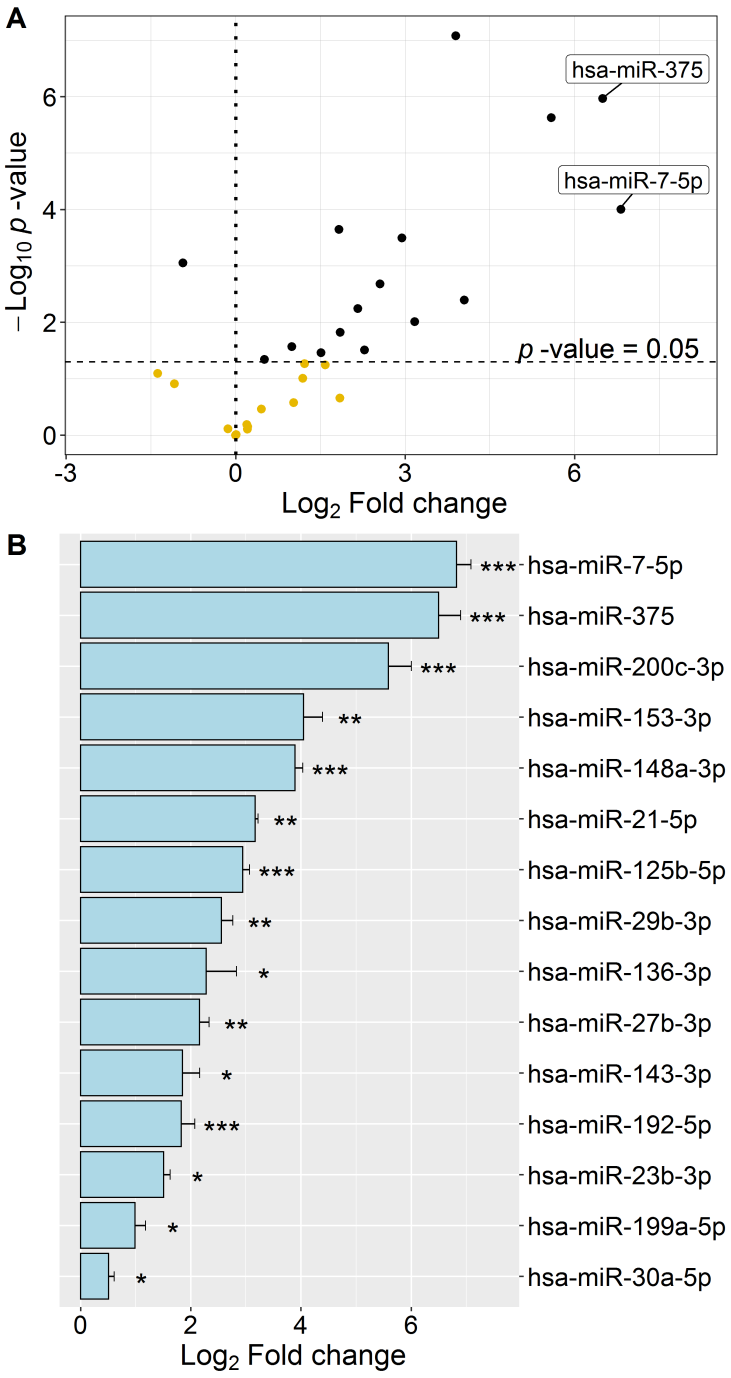

Figure 4.4: Identification of human miRNAs with significantly higher expression in islets as compared to serum. A: Volcano plot shows the 30 tested miRNAs. Their significance as $-\log_{10}$ *p*-value is presented against their expression level as $\log_2$ fold change in islets (N=5) relative to serum (N=6). The vertical line indicates a fold change of 1 and the horizontal line a *p*-vale of 0.05. The black dots in the right upper quarter represent miRNA with fold change >1 and *p*-vale <0.05 that are presented in the bar plot (**B**) which shows the $\log_2$ fold of their expression level in islets relative to serum and their significance. *t*-test was performed on ΔCq values (Cq_{Target} - $Cq_{Reference}$).**p < 0.05, **p < 0.01, ***p < 0.001 and ****p < 0.0001.*

4.2 Identification of reference miRNAs

As qPCR and relative quantification were the main methods used in this study to quantify target miRNAs in serum and tissue, housekeeping- or reference genes needed to be selected for normalization. Reference genes should be stably expressed across the samples of interest and their expression should not be affected by a treatment or a condition and, ideally, they should have high expression levels (Schwarzenbach et al., 2015).

To normalize the measurements of human and mouse islet miRNAs, a commercially available panel of small nucleolar RNAs (snoRNAs) (SNORD61, SNORD68, SNORD72, SNORD95, and SNORD96A and the small nuclear RNA (snRNA) RNU6B) was used for data normalization, as recommended to be used for tissue material by Qiagen. References to normalize serum miRNA expression needed to be selected for human as well as for mouse samples.

4.2.1 Reference miRNAs for mouse serum

As we planned to use STZ (Streptozotocin) to induce diabetes in mice, I aimed to pick miRNAs with a stable expression in mouse serum after STZ treatment. Using RT-qPCR and serum samples I therefore assessed, in STZ treated- and control- mice, the stability of three endogenous miRNAs, miR-195a-5p, miR-16-5p and miR-146a-5p that had been previously used as references (Mi et al., 2012).

The candidate miRNAs were measured on serum collected in the context of the establishment of the STZ-treatment protocol in mouse (see 3.2.3.1 for more details). Seven serum samples from the STZ-treated mice and 4 control samples were chosen for the reference miRNAs assessment. The raw Cq values of the four candidate reference genes are presented in (Figure 4.5A). The analysis in Normfinder (Andersen et al., 2004) revealed that the best combination of reference genes to be used in the two tested groups (STZ- and control mice) was miR-195a-5p with miR-16-5p (Figure 4.5B).

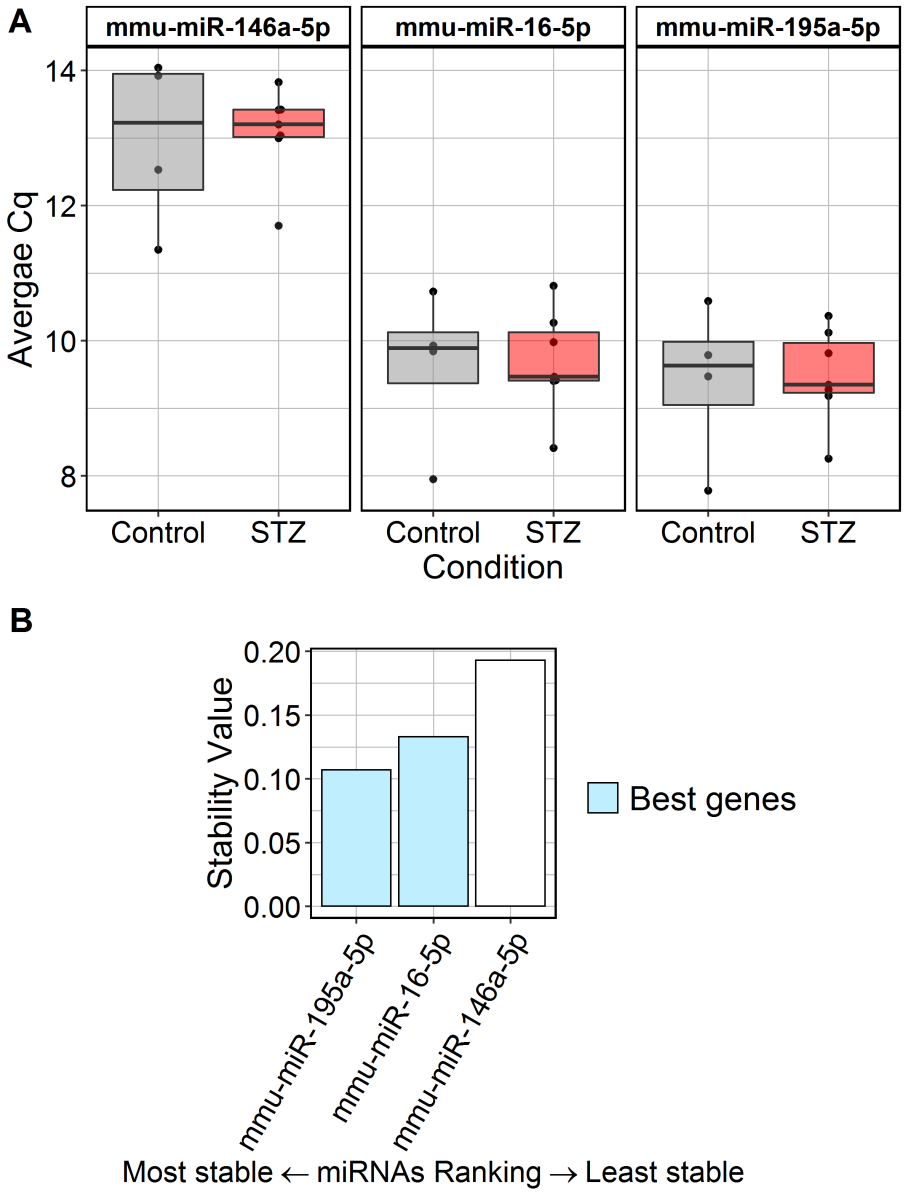

Figure 4.5: Stability in the expression levels of candidate reference mouse miRNAs in STZ- treated and control-mice. A: Boxplots of raw Cq values of 3 candidate reference miRNAs tested in healthy and STZ- treated mouse sera. Each dot represents the average of triplicate qPCR measurements of one serum sample from a mouse. N=4 for control and N=7 for STZ. **B**: Ranking according to NormFinder; the smaller the value, the higher the stability. miR-195a-5p and miR-16-5p were found to be the most stably expressed miRNA in STZ treated- and control mice (highlighted in blue).

4.2.2 Reference miRNAs for human serum

The stability of expression of 18 candidate human reference miRNAs (hsa-miR-22-3p, hsa-miR-93-5p, hsa-miR-191-5p, hsa-miR-21-5p, hsa-miR-146a-5p, hsa-miR-222-3p, hsa-miR-23a-3p, hsa-miR-103a-3p, hsa-miR-126-3p, hsa-let-7c-5p, hsa-miR-24-3p, hsa-miR-26b-5p, hsa-let-7a-5p, hsa-miR-26a-5p, hsa-miR-423-5p, hsa-miR-92a-3p, hsa-miR-25-3p, and hsa-miR-145-5p), selected by literature search, was tested using RT-qPCR in six human serum samples collected in triplicate from healthy individuals. The Cq values are shown in (Figure 4.6A). The NormFinder algorithm and the RefFinder web-based tool (Xie et al., 2012) were used and the reference miRNAs were ranked according to their stability values. The lower the value the higher the stability of the reference gene (Figure 4.6B). Based on NormFinder and RefFinder ranking, 5 miRNAs (hsa-miR-23a-3p, hsa-miR-191-5p, hsa-miR-146a-5p, hsa-miR-93-5p, hsa-miR-22-3p) were selected to be used for data normalization. This selection based on the five most stable reference miRNA candidates (top lowest stability value) in each method (NormFinder and RefFinder). Shared miRNAs and unique ones in each selection were considered for use as reference miRNAs. miR-21-5p was excluded because it had significantly higher expression in islets as compared to serum (Figure 4.4).

Table 19 shows miRNAs selected in NormFinder and RefFinder (in bold). Shared miRNAs: hsa-miR-22-3p, hsa-miR-93-5p, hsa-miR-191-5p, and hsa-miR-146a-5p and unique in each selection: hsa-miR-21-5p (Ranked 4 in Normfinder) and hsa-miR-23a-3p (Ranked 5 in RefFinder) were selected.

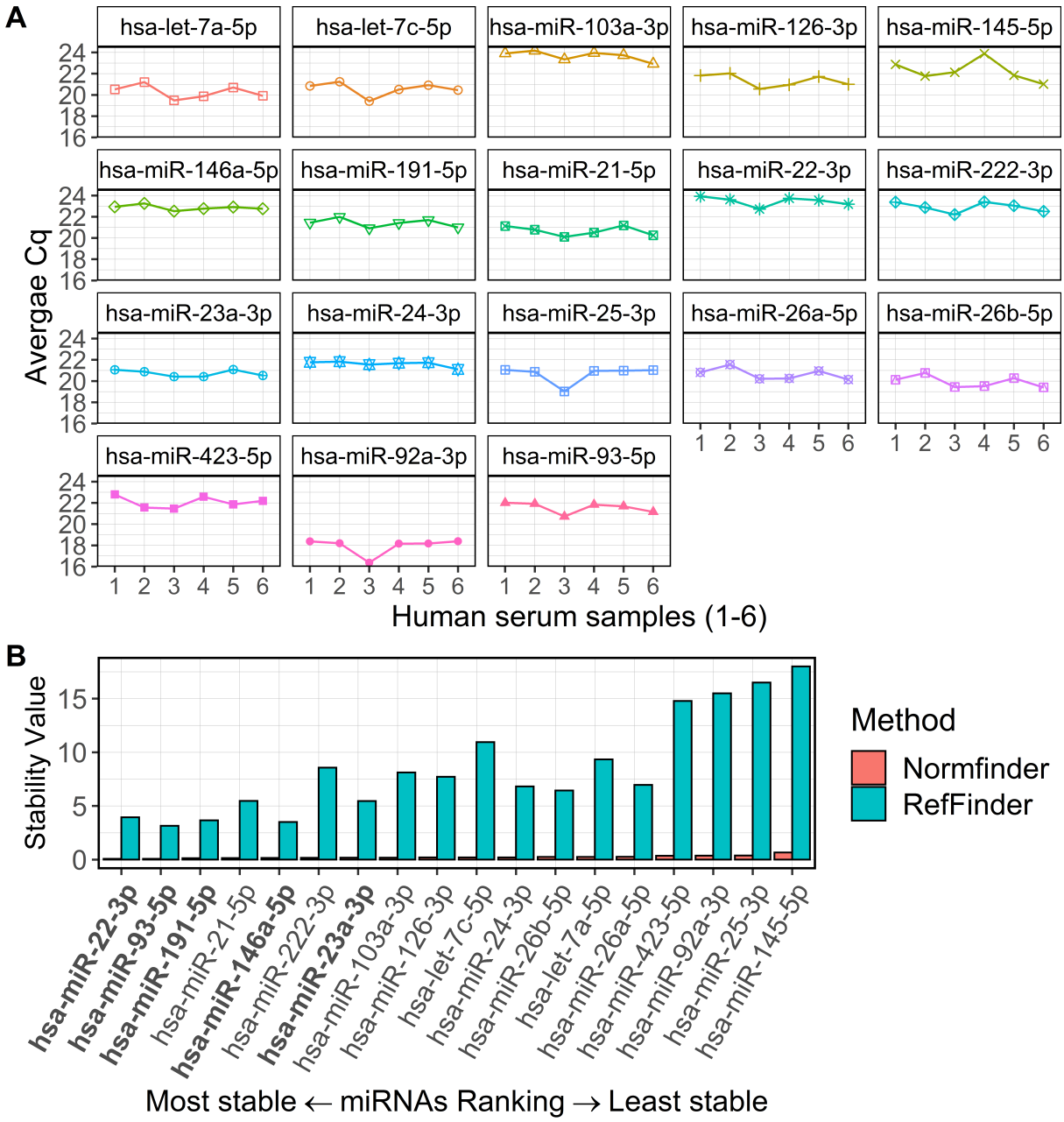

Figure 4.6: Expression levels of candidate reference miRNAs and their stability values. **A**: 18 human miRNAs were measured by RT-qPCR; the average Cq values for each putative reference miRNA across 6 healthy individuals from triplicate samples are shown. **B**: The reference miRNAs ranked according to their stability as found by NormFinder and RefFinder. The lower the stability value, the higher the stability. 5 miRNAs (in bold) were selected.

Table 19: Ranking of candidate reference miRNAs in human serum

Ranking	NormFinder	Stability value	RefFinder	Stability value
1	**hsa-miR-22-3p**	**0.067**	**hsa-miR-93-5p**	**3.15**
2	**hsa-miR-93-5p**	**0.068**	**hsa-miR-146a-5p**	**3.50**
3	**hsa-miR-191-5p**	**0.128**	**hsa-miR-191-5p**	**3.66**
4	**hsa-miR-21-5p**	**0.145**	**hsa-miR-22-3p**	**3.94**
5	**hsa-miR-146a-5p**	**0.154**	**hsa-miR-23a-3p**	**5.45**
6	hsa-miR-222-3p	0.161	hsa-miR-21-5p	5.47
7	hsa-miR-23a-3p	0.176	hsa-miR-26b-5p	6.44
8	hsa-miR-103a-3p	0.182	hsa-miR-24-3p	6.82
9	hsa-miR-126-3p	0.195	hsa-miR-26a-5p	6.96
10	hsa-let-7c-5p	0.199	hsa-miR-126-3p	7.71
11	hsa-miR-24-3p	0.201	hsa-miR-103a-3p	8.11
12	hsa-miR-26b-5p	0.242	hsa-miR-222-3p	8.56
13	hsa-let-7a-5p	0.242	hsa-let-7a-5p	9.34
14	hsa-miR-26a-5p	0.259	hsa-let-7c-5p	10.94
15	hsa-miR-423-5p	0.357	hsa-miR-423-5p	14.78
16	hsa-miR-92a-3p	0.366	hsa-miR-92a-3p	15.49
17	hsa-miR-25-3p	0.380	hsa-miR-25-3p	16.49
18	hsa-miR-145-5p	0.667	hsa-miR-145-5p	18.00

4.2.3 Reference for *in vitro* islet stress model

As I planned to treat the islets *in vitro* with cytokines and hypoxia and collect the supernatant to analyze miRNAs level at 3 time points, I added spike-in control (cel-miR-39 mimic) to the supernatant samples for data normalization. An exemplary analysis of cel-miR-39 in *in vitro* mouse islets stress model is shown in figure 4.7.

The presence of the spike-in was analyzed to ensure that the measured quantity did not vary over the time points. There was no significant difference in the detected quantity of the spike-in between the time points.

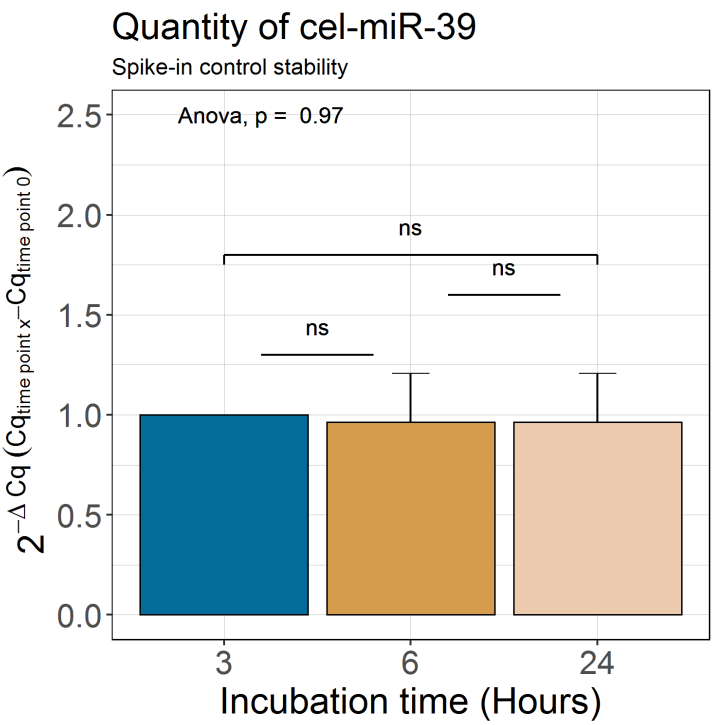

Figure 4.7: Quantity of the spike-in control in supernatant samples. The cel-miR-39 mimic was added to the supernatant samples and used as normalizer. The quantity relative to the first time point was presented as $2^{-\Delta Cq}$ (where $\Delta Cq = Cq_{\text{time point x}} - Cq_{\text{time point 0}}$). Two-way ANOVA followed by Tukey's HSD multiple comparison test was performed for statistical analysis.

4.3 *In vivo* islet stress model

4.3.1 Diabetes induction in mice using STZ

STZ was used to induce the destruction of insulin-secreting β-cells in BL6 mice. In a pilot experiment, I tested a protocol for the STZ- treatment and the monitoring of diabetes development. A small cohort of mice was used in the pilot experiment: 10 mice were treated with STZ and 4 mice were treated with PBS as controls. Blood glucose and body weight of the mice were monitored 14 days before the treatment, at the day of the treatment, and daily after the treatment until day 7 (Figure 4.8A and B). Using the blood glucose and body weight measurements, scoring points were calculated and the mice were sacrificed when a score of ≥20 points was reached (3.2.3.1). According to this criterion, 60% of STZ-treated mice (6 mice) developed diabetes (blood glucose >16.7 mmol/L with 5-10% weight loss) between day 3 and 7. The remaining 4 STZ-treated mice remained euglycemic and had no significant change in their body weight and

were sacrificed at day 7. As most of the diabetic STZ-treated mice (4 mice out of 6; 66.6%) developed diabetes by day 4, I selected this time point as the final time point, when mice would be sacrificed in the subsequent experiment.

After successful completion of the pilot study and after consultation with Konrad Schubert (Institut für Medizinische Informatik und Biometrie), the number of BL6 mice to be treated with STZ and PBS was determined to be 57 and 45, respectively. The blood glucose and body weight were monitored 14 days before treatment, at the day of the treatment and daily over 4 days (Figure 4.9A and B). By day four, 71.9% (41) of the STZ-treated mice had developed diabetes (blood glucose >16.7 mmol/L with 5-10% weight loss) and 28.1% (16 mice) remained euglycemic (blood glucose <16.7 mmol/L without significant change in body weight).

The diabetic STZ-treated mice showed significant elevation of blood glucose at the first day after treatment (12.43 mmol/L ± 4.0) as compared to day 0 (8.94 mmol/L ± 1.3), the PBS-treated mice (8.55 mmol/L ± 1.2) and to the non-diabetic STZ-treated mice (7.63 mmol/L ± 1.6; median ± SD) ANOVA p = 7.9e-11, and their blood glucose continued to increase significantly until day 4 after treatment (33.30 mmol/L ± 6.3) versus 10.60 mmol/L ± 1.7 and 9.52 mmol/L ± 1.4 (median ± SD) for the control- and non-diabetic STZ-treated mice, respectively, (ANOVA p = 6.4e-41). Figure 4.9A.

The body weight of the diabetic STZ-treated mice started to decrease significantly at the second day after the treatment (23.3 ± 1.3 g versus 25.2 ± 1.3 g at day 0) and continued to decline gradually until day 4 (21.8 G ± 1.5). Figure 4.9B.

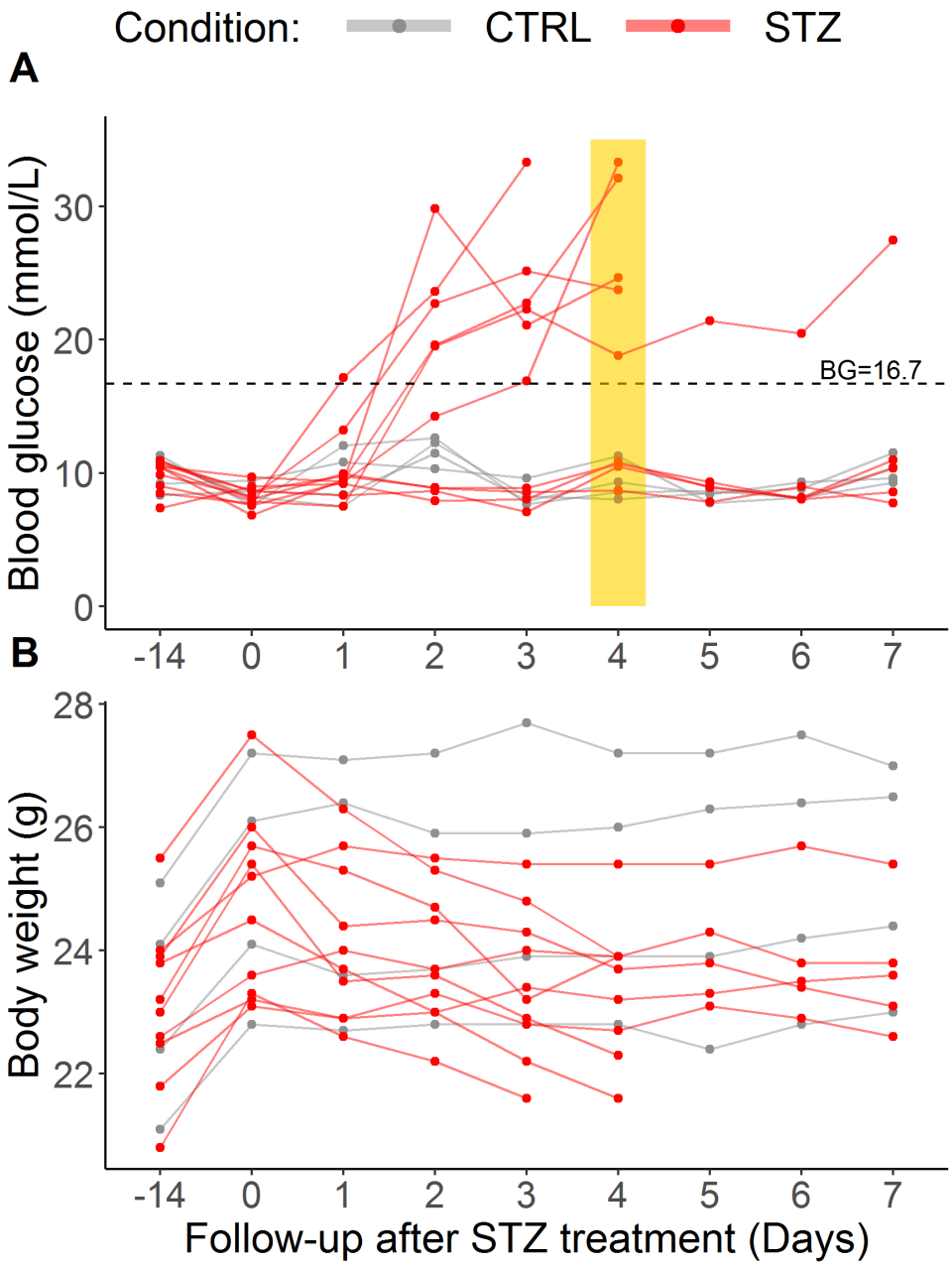

Figure 4.8: Line plots illustrate the blood glucose- and body weight measurements of STZ-treated and control mice. A: Blood glucose values (mmol/L) in STZ- (N=10) and PBS-treated (N=4) mice observed over maximally 7 days after treatment and 14 days before. Each line represents the measurements in one mouse, the last point of a line indicates the day at which the mouse was sacrificed. The yellow shaded vertical area indicates the time point at which most STZ-treated mice developed diabetes. The dotted horizontal line indicates the threshold for diabetes (16.7 mmol/L). **B**: Body weight values (g) in the STZ- (N=10) and PBS-treated (N=4) mice.

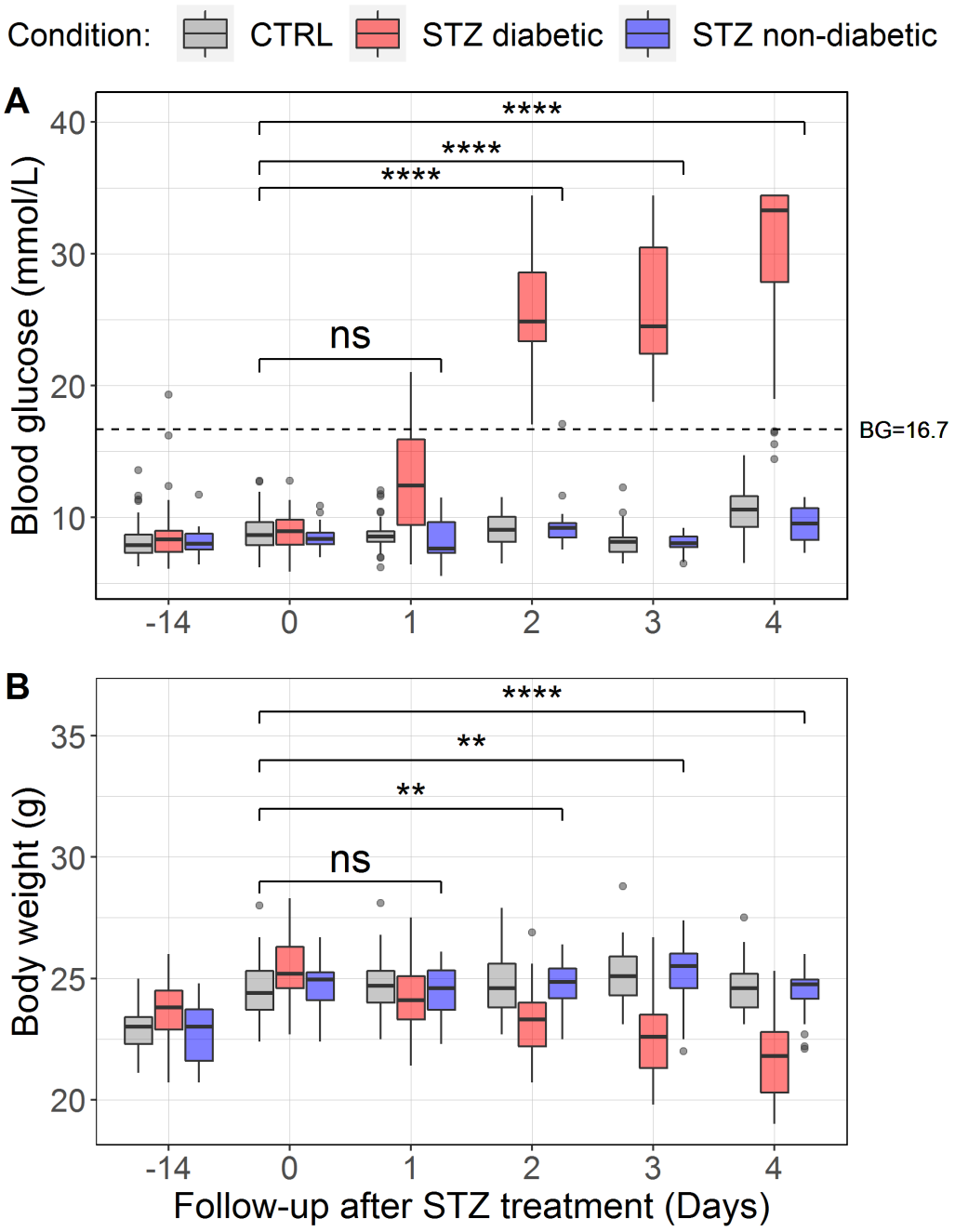

Figure 4.9: Induction of diabetes in BL6 mice. Boxplots show **A**: blood glucose- and **B** body weight measurements of 102 BL6 mice at Day -14, at the treatment day and daily over 4 days after STZ/PBS treatment. Three groups of mice are presented: PBS-treated mice (Control) (N=45; in grey), diabetic STZ-treated mice (N=41; in red), and non-diabetic STZ-treated mice (N=16; in blue). One-way ANOVA at each time point was performed (*$p < 0.05$, **$p < 0.01$, ***$p < 0.001$ and ****$p < 0.0001$.) The dotted line represents the diabetic threshold (16.7 mmol/L).

4.3.2 Serum miRNAs after STZ treatment

60 selected islet specific miRNAs (Panel A Figure 4.3) were quantified by qPCR in the serum of all mice before STZ/PBS treatment (day -14) and after STZ/PBS treatment at day 1, 3, and 4.

Due to the relatively small amount of serum obtained by venous puncture at the tail at day -14, 1 and 3 from the living mice, I pooled samples from each treatment group (STZ- and PBS-treated animals) to obtain 3 sample pools for each of these time points and for each condition (Table 12).

Six miRNAs were significantly increased in at least one time point after STZ-treatment in mice that developed diabetes (Figure 4.10). Four miRNAs thereof (mmu-miR-99b-5p, mmu-miR-381-5p, mmu-miR-127-3p, and mmu-miR-411-5p) increased significantly only in the diabetic STZ-treated mice at day 3 as compared to the control mice (STZ-treated non diabetic- and PBS control mice). mmu-miR-375-3p increased significantly in the diabetic STZ-treated mice at day 1 after treatment, its level declined at day 3 but remained significantly higher as compared to the control mice (ANOVA p=0.0046). The dynamic pattern of mmu-miR-101a-3p in serum over the four day time course was significantly different in diabetic mice as compared to controls (ANOVA p=0.0098). mmu-miR-381-5p was not further tested in the *in vivo* model and was moved to be tested in the *in vitro* model.

At day 4, when the mice were sacrificed, blood was collected through cardiac puncture instead of tail-vein blood draw as done at the time points before. Therefore, sufficient material for miRNA measurement by qPCR was available from each mouse. After excluding mice with insufficient volume of serum or serum with haemolysis, the quantity of the 39 selected miRNAs (Figure 3.2) could be analyzed at day 4 from 30 diabetic, 11 non-diabetic and 28 control mice. The sensitivity and specificity of the measured miRNAs to classify STZ-treated-diabetic, non-diabetic and control mice were then analyzed by generating receiver-operating characteristic (ROC) curves. The area under the ROC curve (AUC) was determined against the control mice for the diabetic STZ-treated (AUC-dSTZ) and non-diabetic STZ-treated mice (AUC-ndSTZ). An AUC of more than 0.5 indicates a separation between tested groups.

I found 18 miRNAs (miRNAs in bold in table 20) with significant increases in the STZ-treated (diabetic- and non-diabetic) mice as compared to the control mice, including 15 miRNAs (highlighted in yellow in table 20) increased significantly in the diabetic STZ-treated mice only as compared to control mice and three miRNAs in both, diabetic- and non-diabetic STZ-treated

mice (highlighted in green in table 20).

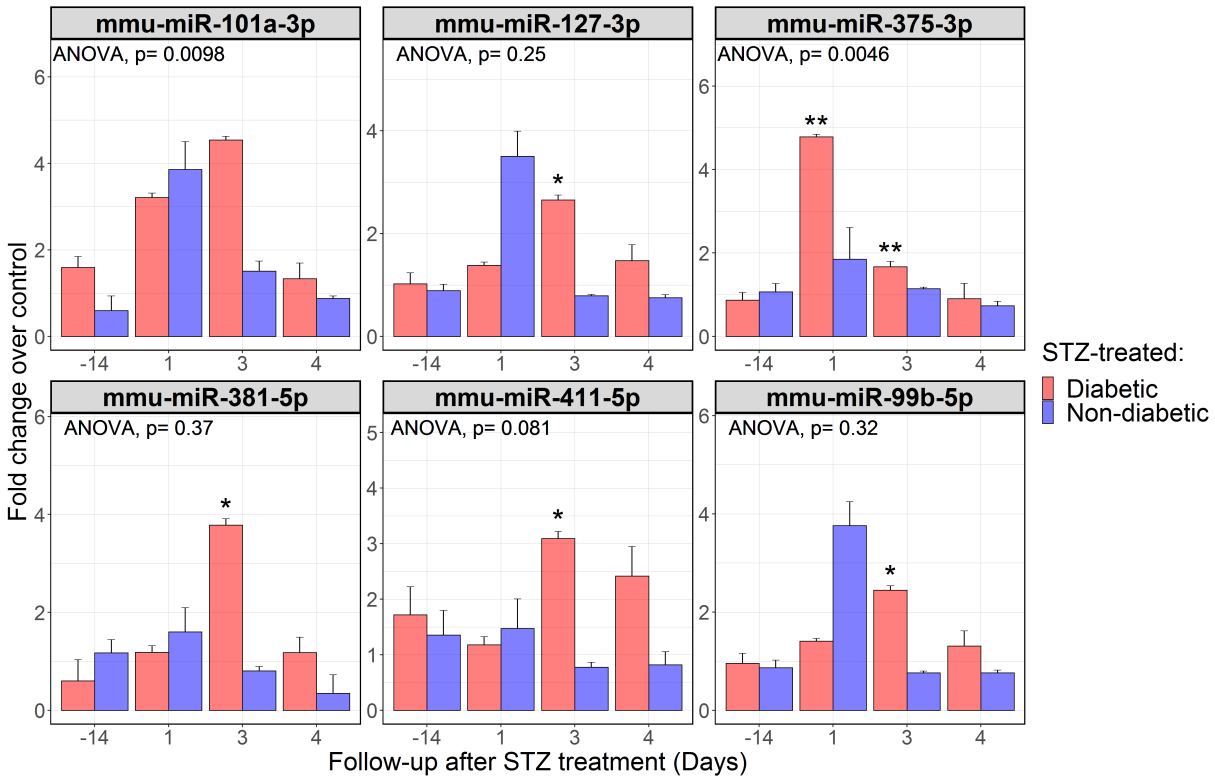

Figure 4.10: Measurements of miRNAs after STZ treatment over 4 days after treatment from the pooled samples. The serum level of mmu-miR-101a-3p, mmu-miR-127-3p, mmu-miR-375-3p, mmu-miR-381-5p, mmu-miR-411-5p, and mmu-miR-99b-5p in diabetic and non-diabetic STZ-treated mice. Presented is fold change as compared to control mice at each time point. Data are presented as mean ± SEM (N=3 per condition). Two-way ANOVA followed by Tukey's HSD multiple comparison test was performed for statistical analysis. (**p < 0.05, **p < 0.01, ***p < 0.001 and ****p < 0.0001.*) Diabetic mice are in red and non–diabetic in blue.

Table 20: miRNA measurement at day 4 (Individual mice)

	Fold change		***p*-valaue**		**AUC**	
miRNA	**dSTZ**	**ndSTZ**	**dSTZ vs CTRL**	**ndSTZ vs CTRL**	**dSTZ**	**ndSTZ**
mmu-miR-487b-3p	1.75	0.74	2.4e-03	3.6e-01	0.73	0.34
mmu-miR-222-3p	1.44	1.10	9.2e-05	6.4e-01	0.80	0.60
mmu-miR-411-5p	3.76	2.75	2.5e-04	5.4e-02	0.75	0.74
mmu-miR-127-5p	1.90	1.00	9.6e-04	1.0e+00	0.74	0.51

Table 20: miRNA measurement at day 4 (Individual mice) *(continued)*

	Fold change		*p*-valaue		AUC	
miRNA	**dSTZ**	**ndSTZ**	**dSTZ vs CTRL**	**ndSTZ vs CTRL**	**dSTZ**	**ndSTZ**
mmu-miR-434-3p	2.37	2.07	7.9e-04	5.1e-02	0.76	0.73
mmu-miR-29b-3p	1.38	0.75	3.5e-02	2.4e-01	0.68	0.31
mmu-miR-99b-5p	1.68	1.07	8.3e-03	9.6e-01	0.72	0.51
mmu-miR-770-3p	1.79	1.35	5.5e-03	4.3e-01	0.74	0.67
mmu-miR-423-5p	1.51	0.89	2.3e-02	8.5e-01	0.69	0.43
mmu-miR-5099	1.80	1.00	2.1e-02	1.0e+00	0.71	0.47
mmu-miR-543-3p	1.94	1.53	1.9e-02	4.1e-01	0.71	0.65
mmu-miR-129-5p	1.67	1.18	2.1e-02	8.0e-01	0.70	0.58
mmu-miR-132-3p	1.31	1.12	2.4e-02	6.9e-01	0.70	0.58
mmu-miR-320-3p	1.39	1.25	3.0e-02	3.9e-01	0.69	0.63
mmu-miR-30c-5p	1.21	1.17	5.0e-02	3.3e-01	0.69	0.65
mmu-miR-423-3p	2.29	2.37	2.5e-04	5.6e-03	0.82	0.82
mmu-miR-770-5p	2.49	2.31	4.8e-04	2.3e-02	0.81	0.78
mmu-miR-101a-3p	2.35	2.76	1.3e-02	3.4e-02	0.75	0.68
mmu-let-7d-5p	1.18	0.63	4.3e-01	3.2e-02	0.59	0.28
mmu-miR-375-3p	1.51	0.43	3.0e-01	6.9e-02	0.62	0.29
mmu-miR-323-3p	1.24	0.36	7.7e-01	4.5e-02	0.55	0.31
mmu-miR-204-5p	1.79	0.69	1.6e-01	6.5e-01	0.64	0.47
mmu-miR-127-3p	1.38	0.70	3.4e-01	4.6e-01	0.60	0.36
mmu-miR-200b-3p	0.69	1.02	9.1e-02	9.9e-01	0.34	0.56
mmu-miR-23b-3p	1.29	1.12	5.6e-02	7.2e-01	0.70	0.56
mmu-miR-379-5p	1.68	1.09	8.6e-02	9.7e-01	0.72	0.54
mmu-miR-98-5p	1.20	0.71	5.5e-01	3.4e-01	0.57	0.33
mmu-miR-200c-3p	0.77	0.91	1.6e-01	8.8e-01	0.39	0.55
mmu-miR-136-5p	1.57	0.91	3.1e-01	9.6e-01	0.74	0.43
mmu-miR-434-5p	1.45	1.71	3.4e-01	2.9e-01	0.63	0.69

Table 20: miRNA measurement at day 4 (Individual mice) *(continued)*

	Fold change		*p*-valaue		AUC	
miRNA	**dSTZ**	**ndSTZ**	**dSTZ vs CTRL**	**ndSTZ vs CTRL**	**dSTZ**	**ndSTZ**
mmu-miR-141-5p	1.54	1.01	2.4e-01	1.0e+00	0.62	0.53
mmu-let-7b-5p	0.86	0.82	3.6e-01	3.5e-01	0.39	0.33
mmu-miR-148a-3p	1.39	1.23	2.3e-01	7.3e-01	0.65	0.51
mmu-miR-151-3p	1.16	0.97	4.7e-01	9.8e-01	0.57	0.50
mmu-let-7c-5p	0.89	0.86	4.7e-01	5.2e-01	0.40	0.37
mmu-let-7k	1.04	0.87	9.2e-01	6.2e-01	0.52	0.37
mmu-miR-184-3p	1.00	0.78	1.0e+00	6.6e-01	0.49	0.35
mmu-miR-141-3p	1.27	0.95	7.0e-01	9.9e-01	0.52	0.40
mmu-miR-652-3p	0.98	1.04	9.8e-01	9.5e-01	0.46	0.47

Abbreviations:

AUC: Area under the curve; **dSTZ:** Diabetic STZ-treated; **ndSTZ:** Non-diabetic STZ-treated

AUC-dSTZ value for the 15 miRNAs, which increased only in the diabetic STZ-treated mice, ranged from 0.68 for mmu-miR-29b-3p to 0.8 for mmu-miR-222-3p (Figure 4.11A). miR-770-5p, miR-423-3p (Figure 4.11B) and miR-101a-3p allowed to discriminate STZ-treated from non- STZ-treated mice as they showed significant increase in their level after STZ-treatment (AUC-ndSTZ: 0.78, 0.82, and 0.68 respectively, and for diabetic STZ-treated mice (AUC-dSTZ: 0.81, 0.82, and 0.75 respectively). The analysis of all measured miRNAs is summarized in a heatmap (Figure 4.12).

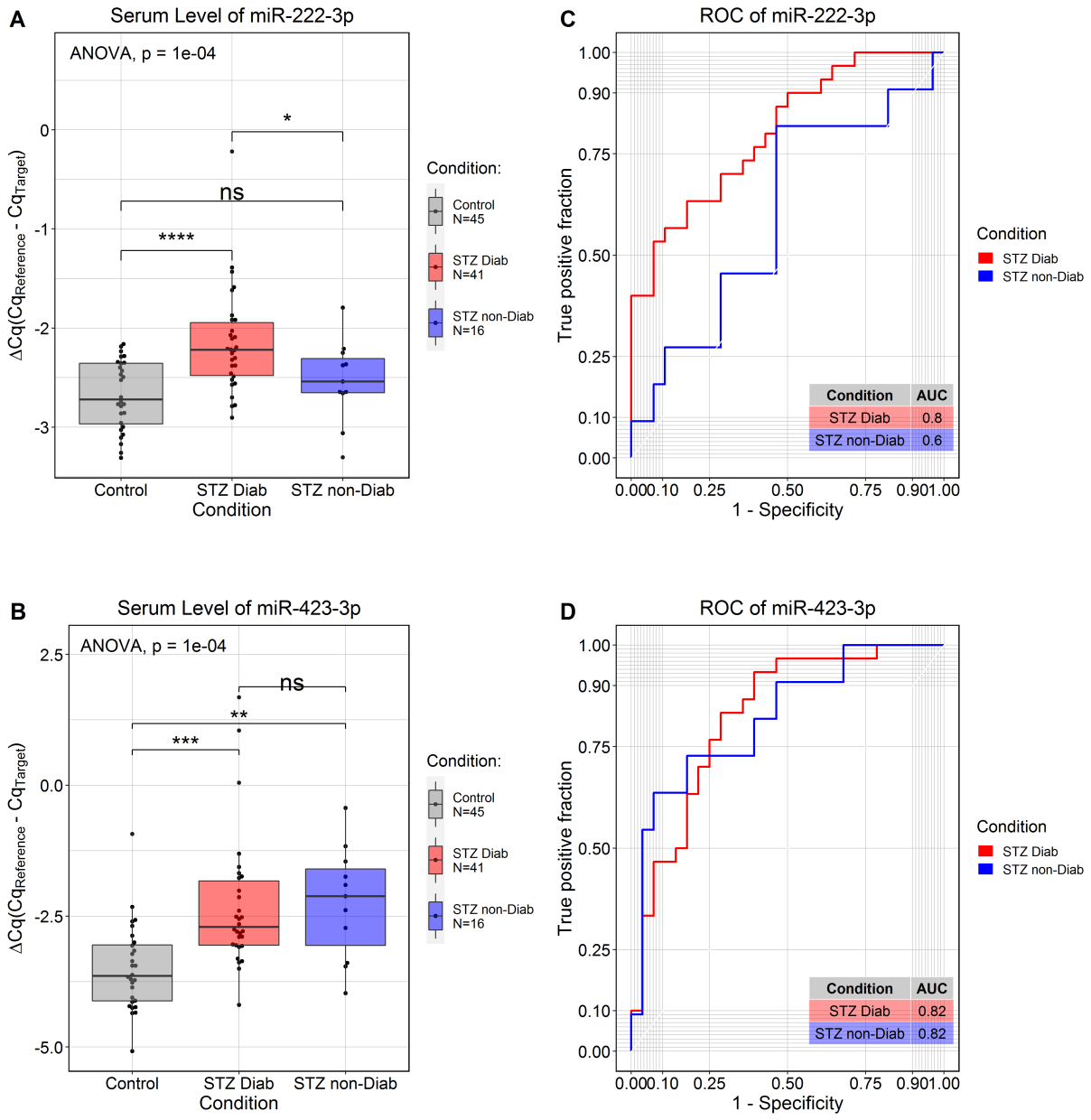

Figure 4.11: Representative miRNA measurements at day 4. The level of two representative miRNAs **A:** miR-222-3p and **B:** miR-423-3p quantified at the end of the study in STZ-treated diabetic (red), STZ-treated non-diabetic (blue) and control mice (grey). miR-423-3p is an exemplary miRNA that increases upon STZ-treatment (in treated diabetic and non-diabetic mice) and miR-222-3p is an exemplary miRNA that can be measured upon diabetes after STZ-treatment. Receiver-operating characteristic curves for discriminatory performance of **C:** miR-222-3p and **D:** miR-434-3p in distinguishing diabetic STZ- and non-diabetic STZ-treated from control mice. One-way ANOVA followed by Tukey's HSD multiple comparison test was performed for statistical analysis **p < 0.05, **p < 0.01, ***p < 0.001 and ****p < 0.0001.*

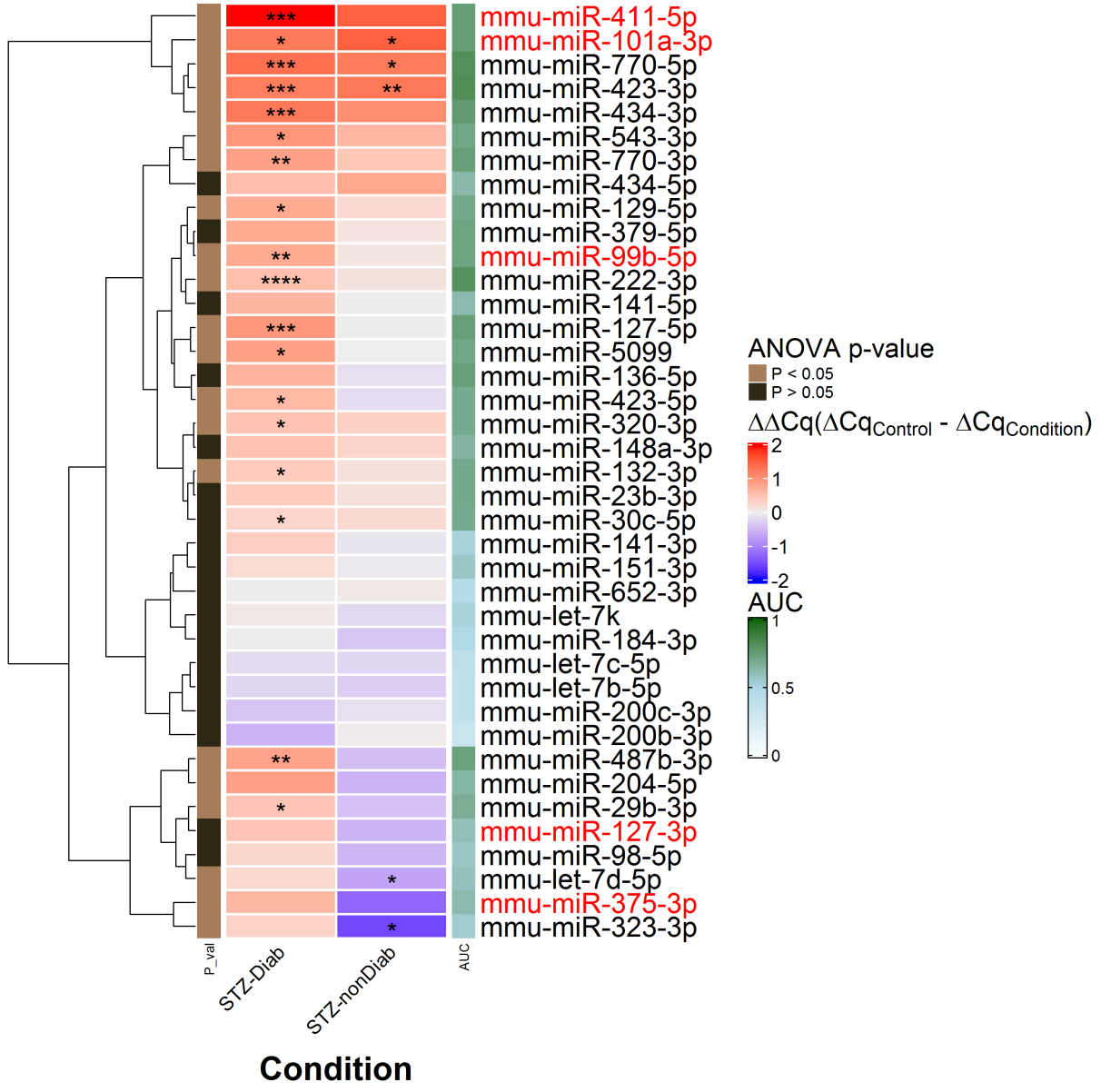

Figure 4.12: Profile of 39 miRNAs measured in serum after 4 days of STZ-treatment. Presented are $\Delta\Delta$Cq values (ΔCq $_{control}$ - ΔCq $_{condition}$). N=30 diabetic STZ, N=11 non-diabetic STZ, and N=28 control. One-way ANOVA followed by Tukey's HSD multiple comparison test was performed for statistical analysis. ANOVA *p*-value is presented in the left column annotation (black: $p>0.05$, brown: $p<0.05$). *p*-values of multiple comparisons against control are indicated inside cells (*$p < 0.05$, **$p < 0.01$, ***$p < 0.001$ and ****$p < 0.0001$.) Area under the curve (AUC) is presented in the right column annotation (green). The heatmap is clustered by Euclidean distance and scaled by rows. Highlighted in red are 5 of the miRNAs presented in figure 4.10 and found significant in the earlier time points.

Comparing the miRNA measurements obtained from pooling samples of figure 4.10 with the day 4 measurements from individual mice (miRNAs highlighted in red in the heatmap Figure 4.12), revealed that mmu-miR-101a-3p, mmu-miR-99b-5p, and mmu-miR-411-5p showed a significant increase in the diabetic STZ-treated mice as compared to the control at day 4 (AUC-dSTZ: 0.75, 0.72, 0.75 respectively), while those miRNAs didn't show significant changes at day 4 in the time points measurements using pooled samples (Figure 4.10).

Interestingly, mmu-miR-127-3p, picked up from the pooled samples, did not show any significant changes at day 4 and mmu-miR-375-3p showed significant global One-way ANOVA $p<0.05$ but didn't pass the multiple comparisons (AUC-dSTZ=0.62).

4.3.3 Assessment of β-cell destruction using Immunofluorescence staining

At the end of the time course after STZ treatment (day 4), we stained pancreatic sections of STZ- and PBS-treated mice for insulin, glucagon (Figure 4.13), and cleaved caspase-3 (Figure 4.14) to assess islets destruction.

Image analysis showed that in the diabetic STZ-treated mice (6 mice), there was a significant loss of insulin positive cells (Percentage of insulin positive cells: 30% ± 5.8; mean ± SEM) as compared to both, the PBS-treated (8 mice) and non-diabetic STZ-treated mice (10 mice) (Percentage of insulin positive cells: 89 ± 3.5% and 83 ± 4.4%, respectively). Figure 4.15A.

In the diabetic STZ-treated mice (3 mice), there was a pronounced apoptosis activity, revealed by staining for cleaved caspase-3. The difference between cells with apoptosis activity in these mice (percentage of cleaved caspase-3 positive cells 59 ± 2.0%) and the cells with apoptosis activity in PBS- treated (3 mice) and non-diabetic STZ-treated mice (4 mice) was significant (4 ± 3.6% and 12 ± 4.4% respectively, mean ± SEM). Figure 4.15B.

We noticed that the percentage of glucagon-secreting α-cells was significantly higher in diabetic STZ-treated mice (3 mice, 80 ± 7.5%) as compared to the PBS-treated (4 mice, 14 ± 4.7%) and non-diabetic STZ-treated mice (6 mice, 20 ± 6.7% mean ± SEM). Figure 4.15C.

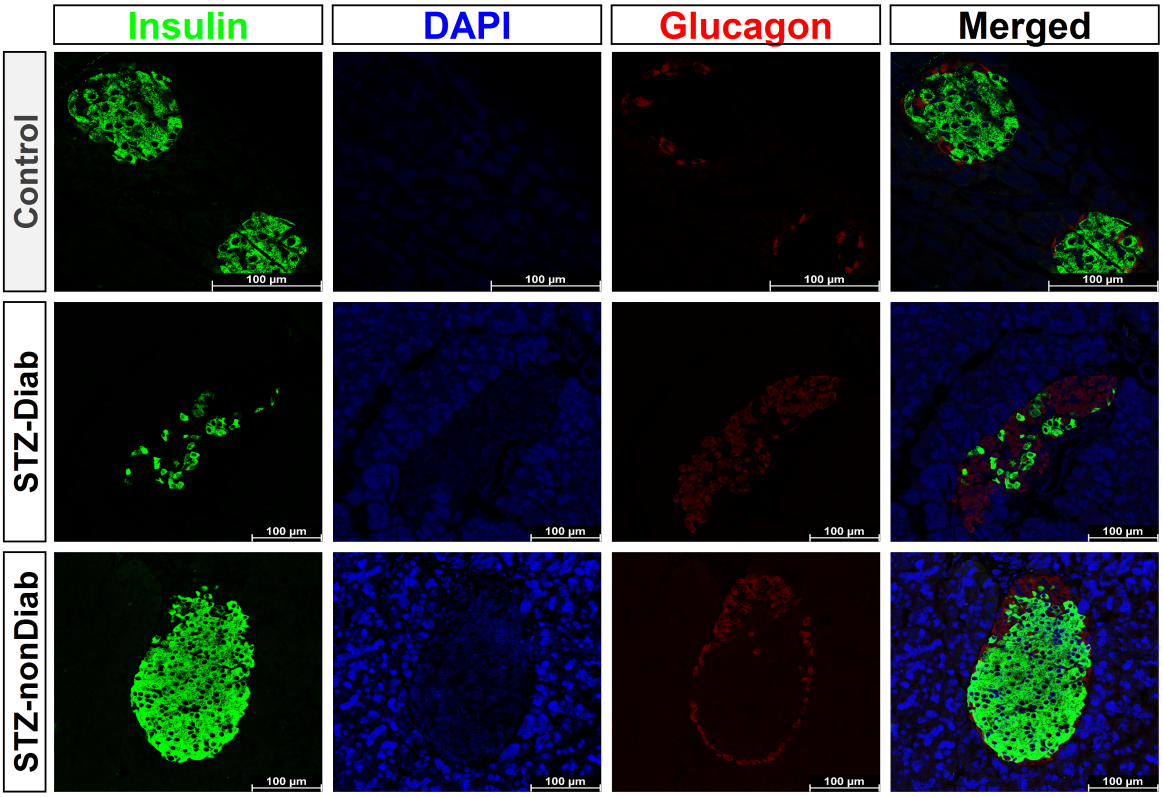

Figure 4.13: Assessment of β-cell death after STZ-treatment. Exemplary immunofluorescence staining of β-cells in the PBS-treated (control; top row) and STZ-treated mice (diabetic: middle row, non-diabetic: bottom row) after 4 days of PBS- and STZ treatment. Images in each row are taken for one pancreatic section of one mouse. Insulin (green), DAPI (blue), glucagon (red). (Scale bar: 100 um). DAPI; 4´,6-diamidino-2-phenylindole.

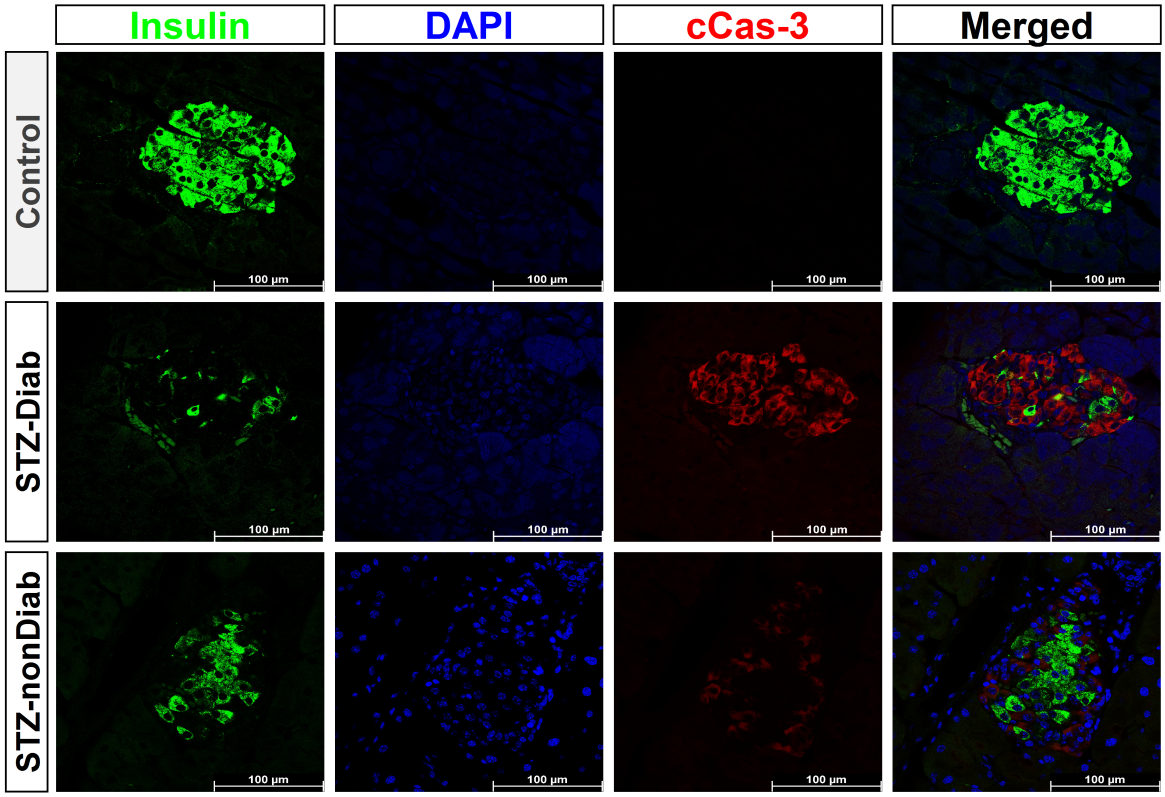

Figure 4.14: Assessment of β-cell death after STZ-treatment. Exemplary immunofluorescence staining of β-cells in the PBS-treated mice (control: top row) and STZ-treated mice (diabetic: middle row, non-diabetic: bottom row) after 4 days of PBS- and STZ-treatment. Images in each row are taken for one pancreatic section from one mouse. Insulin (green), DAPI (blue), cleaved caspase-3 (red). (Scale bar: 100 um). cCas-3; cleaved caspase-3.

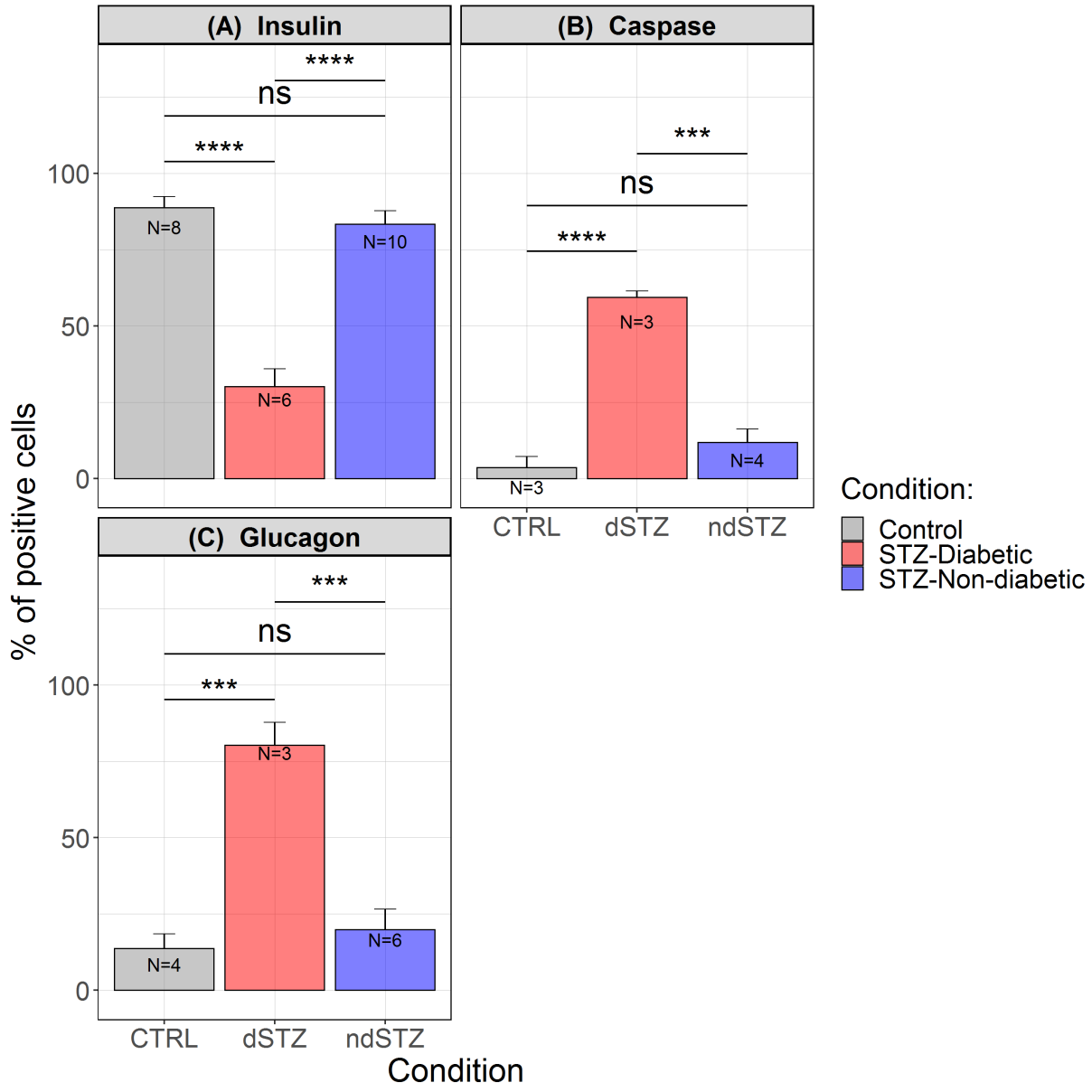

Figure 4.15: Analysis of immunofluorescent images after STZ treatment. The percentage of **A**: insulin positive β-cells in the PBS-treated (N=8), diabetic (N=6), and non-diabetic STZ-treated mice (N= 10) **B**: Glucagon positive α-cells in the PBS-treated (N=4), diabetic (N=3), and non-diabetic STZ-treated mice (N= 6) and **C**: Cleaved caspase-3 positive cells in the PBS-treated (N=3), diabetic (N=3), and non-diabetic STZ-treated mice (N= 4). Control (grey), diabetic (red), and non-diabetic STZ-treated mice (blue). Data are presented as mean ± SEM. One-way ANOVA followed by Tukey's HSD multiple comparison test was performed for statistical analysis. (*$p < 0.05$, **$p < 0.01$, ***$p < 0.001$ and ****$p < 0.0001$.)

In conclusion, upon β-cells death islet specific miRNAs increased in the circulation of STZ-treated mice. Some miRNAs increased rapidly after STZ treatment and some increased at later time points. 18 miRNAs increased in the diabetic STZ-treated animals and 3 miRNAs were persistent in diabetic- and non-diabetic STZ-treated animals.

4.4 *In vitro* islet stress model

4.4.1 Mouse islets

To confirm our findings from the *in vivo* STZ-mouse model by an *in vitro* model, I exposed *in vitro* cultured islets to hypoxic and inflammatory stress to assess whether these treatments induce the release of selected miRNA into the culture medium in a measurable way. Simultaneously, I wanted to assess islet viability after these treatments by quantifying the apoptosis activity in the islets as well as their capability to secrete insulin and correlate these measures with miRNA release.

I isolated the islets from 6- to 8-weeks old CD-1 mice and incubated them under hypoxic condition and/or with the addition of mild cytokine (a mix of recombinant mouse TNF-α, IFN-γ, and IL-1β) or aggressive cytokine addition (20 times the concentration of the mild cytokine addition). A panel of 80 miRNAs was assembled to be tested in the *in vitro* model. This panel comprised 49 miRNAs found to be significantly enriched in islets by NGS (top 49 upregulated in islets as compared to serum in NGS) and 38 miRNAs found to be significant in the *in vivo* model (20 miRNAs found be significant at day 4 measurements and 18 miRNAs that were selected from the day 1 and 3 measurements. 7 miRNAs were found in both pools and therefore the final poll comprised 80 miRNAs (Flowchart 3.2 in methods).

4.4.1.1 Inflammatory- and hypoxic stress induces the release of different miRNAs

In a small pilot experiment, I first aimed to assess the whole miRNA content of the supernatant after exposure to hypoxia and inflammatory cytokines and to determine the optimal time points of treatment before planning a larger experiment. Islets were isolated from 6 CD-1 mice and treated with aggressive cytokine mix and hypoxia for 6, 24, 48, and 72 hours. For each time point and for each condition (non-treated islets: control; treated islets: hypoxia + aggressive cytokine), I hand-picked 120 islets to be assembled into a sample and cultivated them in a small size petri

dish.

After treatment, the supernatant was collected, RNA isolated and analyzed using the bioanalyzer. Figure 4.16 shows exemplary electropherograms where the small RNA (RNA sized <200nt) and miRNA (4 - 40 nt) fractions are revealed. The large, flat peaks in the miRNA area observed in the supernatant of treated islets indicate the abundance of miRNA molecules found at each time point after treatment. The concentrations of small RNA and miRNA and the fraction of miRNA fraction in each sample were also determined (Figure 4.17). The maximum miRNA concentration was measured at 6H time point (1509.1 pg/ul) and the miRNA concentration declined after 24H (1398.5 pg/ul) of treatment until 48H (533.1 pg/ul). The miRNA concentrations in the supernatant of non-treated islets remained stable over time.

After confirming that whole miRNA could be measured and quantified in supernatant of islets in culture, a small panel of 15 miRNA (Panel P; Table 18 in methods) was quantified in the supernatant samples of treated and non-treated islets. The measured miRNAs revealed variable patterns over the time course. Some miRNAs, such as mmu-let-7e-5p, mmu-miR-132-3p, and mmu-miR-200c-3p, showed a maximum concentration at 6H and 24H and declined thereafter. Other miRNAs, such as mmu-miR-30c-5p, mmu-miR-375-3p, and mmu-miR-770-5p showed maximum a concentration only at 24H and declined afterwards (Figure 4.18).

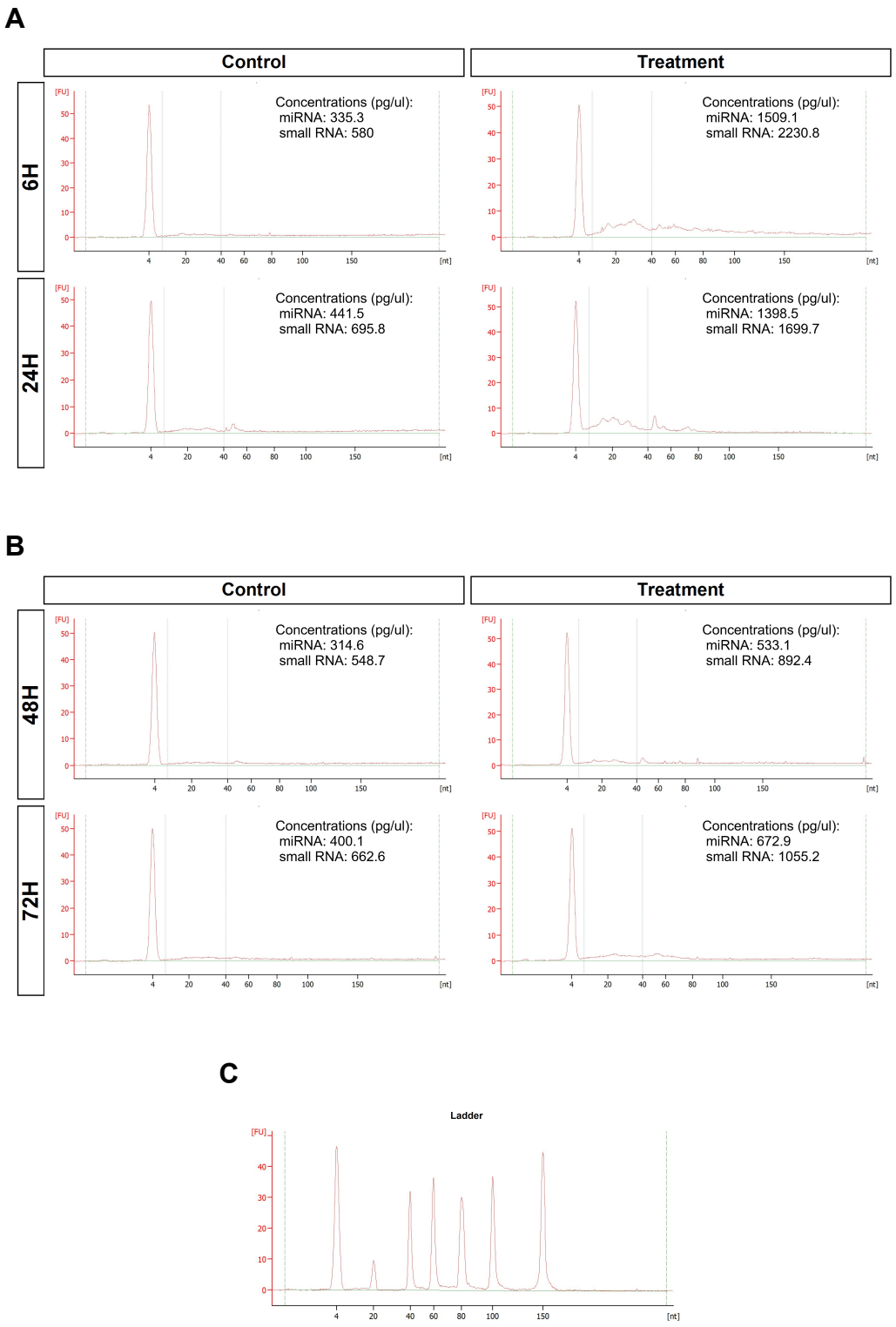

Figure 4.16: Electrophergram of the small RNA/miRNA distribution in the supernatant of islets treated with aggressive cytokine mix and hypoxia. One replicate was performed per condition at each time point **A**: 6, 24H; **B**: 48, 72H. The electropherograms were generated by Agilent 2100 RNA bioanalyzer. The condition, time point, and concentrations of miRNA/small RNA are indicated. **C**: The ladder illustrates the size distribution of RNA fragments.

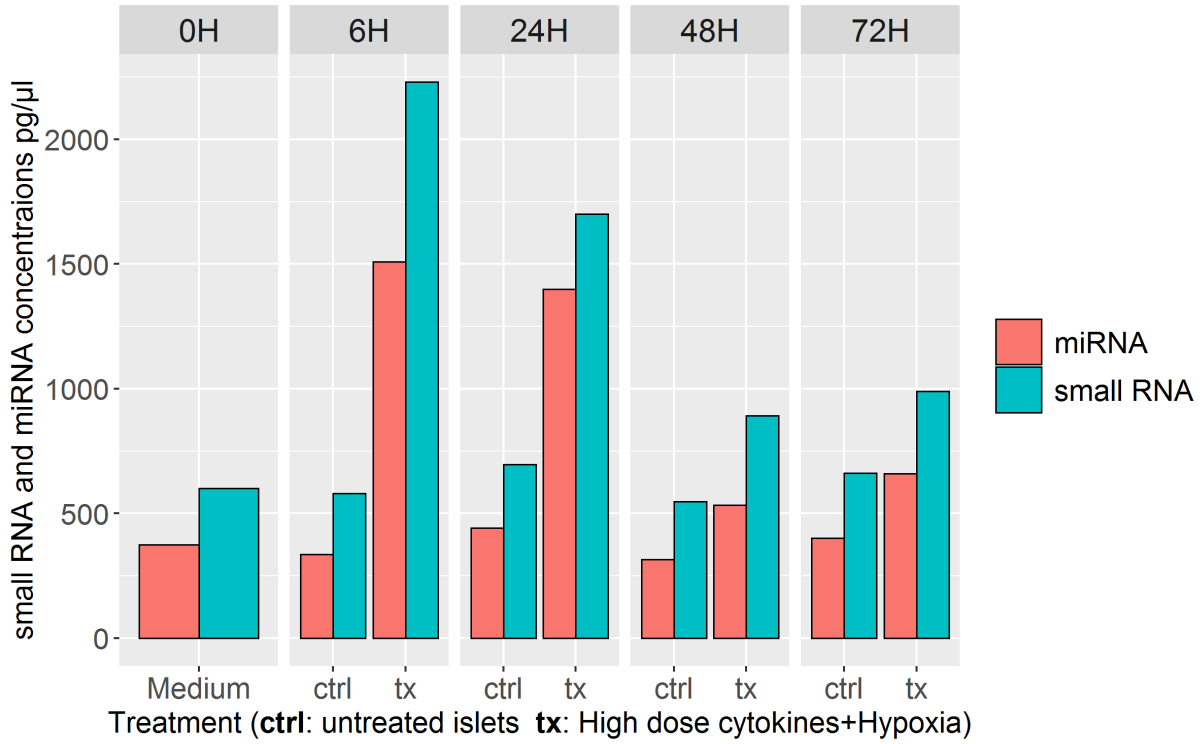

Figure 4.17: small RNA (turquoise) and miRNA (red) concentrations in the supernatant of control (ctrl) and treated islets (tx). The islets were treated with aggressive cytokine mix and hypoxia (1% O2) and supernatants collected after 6, 24, 48, and 72H for bioanalyzer analysis. At each time point one sample per condition was analyzed.

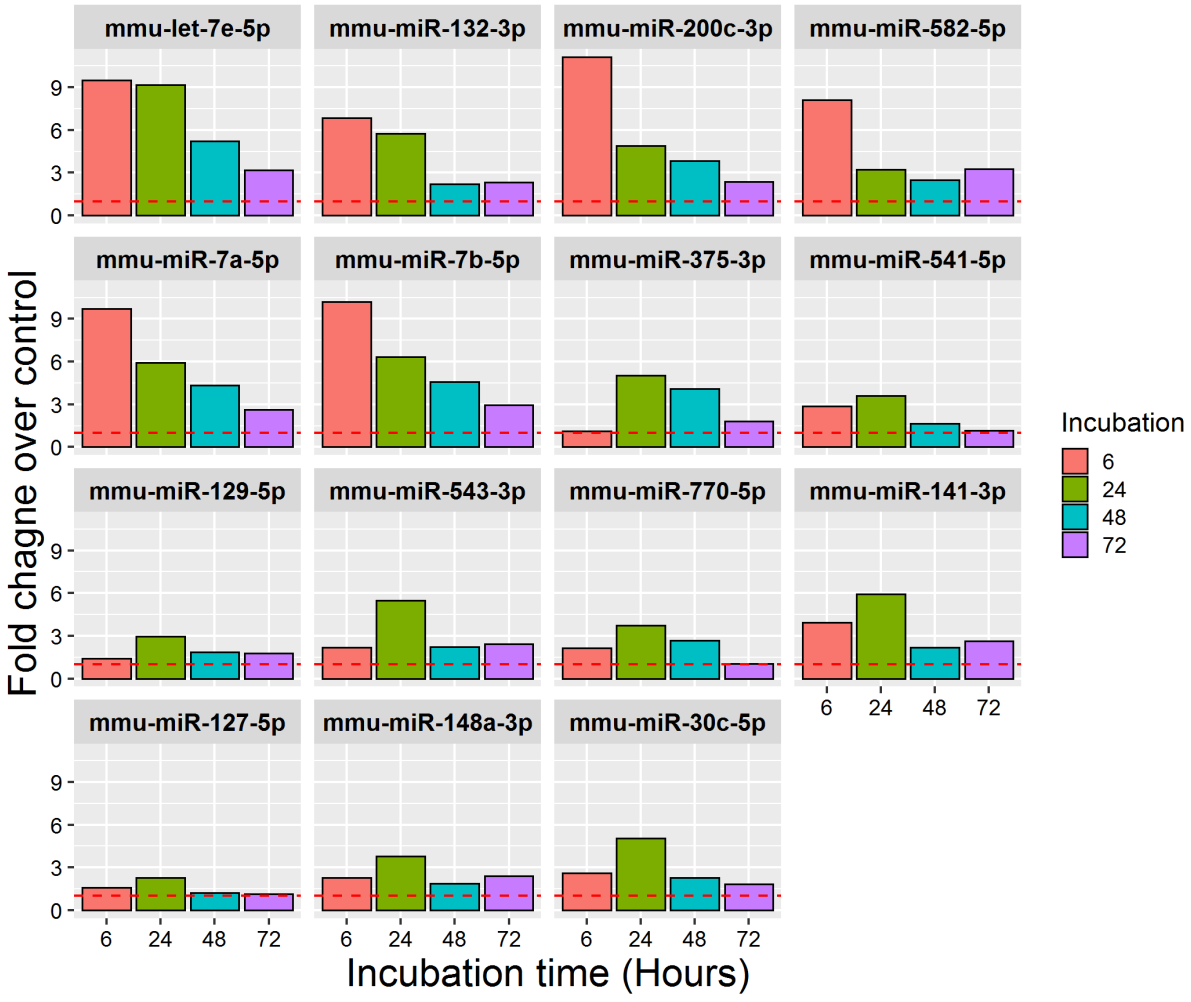

Figure 4.18: miRNA measurements in the supernatant as part of the pilot experiment. 15 miRNAs were measured in the supernatant from control- versus treated islet cultures. The islets were treated with aggressive cytokine mix and incubated under hypoxic condition for 6, 24, 48, and 72H. One sample per condition at each time point was analyzed. Data is presented as fold change over control. The horizontal broken line indicates a fold change of 1.

Based on these measurements and on the whole miRNA concentrations detected by Bioanalyzer, both suggesting that the abundance of miRNA was at its highest at the earlier time points, I added an even earlier time point (3H) for the measurement of miRNA in a larger scale experiment.

In order to mimic different scenarios of stress exposure, I planned five treatment conditions: aggressive cytokine mix with and without hypoxia, mild cytokine mix with and without hypoxia, and hypoxic condition alone. Untreated islets were used as control. The islets were cultured under the above-mentioned conditions for 3, 6, and 24H and quadruplicate samples were collected at

each time point. qPCR to measure 80 miRNAs was then run in triplicates.

The miRNA measurements showed various patterns after exposure to the various stressors. For example, mmu-miR-7a-5p showed the highest significant increase at 6H and 24H induced by hypoxia and mild cytokines. At 6H, hypoxia alone or with aggressive cytokine mix, and mild or aggressive cytokine mix alone induced a significant increase as well. The level of this miRNA was also highly affected by hypoxia alone at 24H. The level of mmu-miR-375-3p showed a similar pattern (Figure 4.19). miR-7a-2-3p and miR-99b-5p increased significantly in response to the aggressive cytokine mix at 24H and 6H respectively (Figure 4.19).

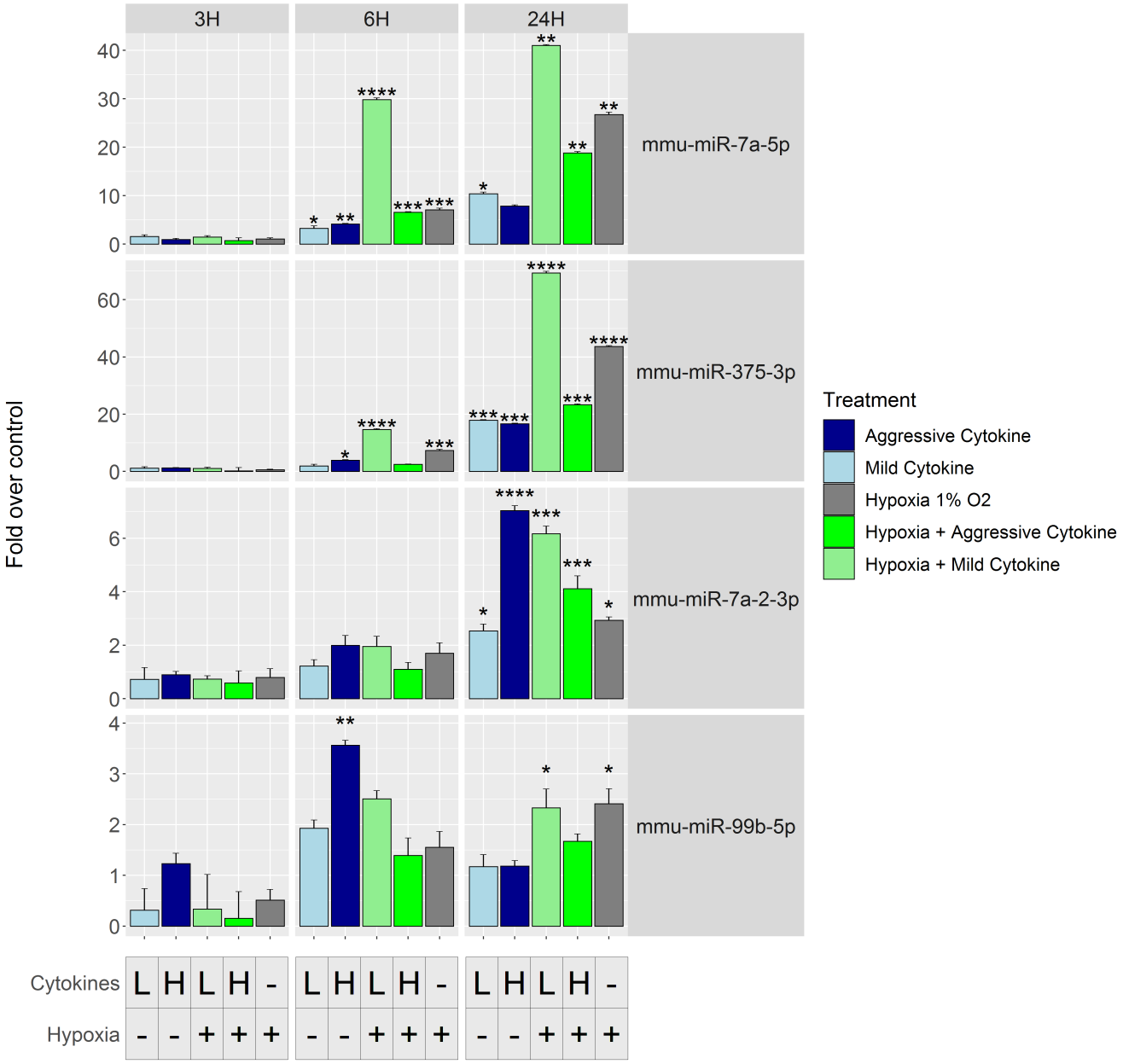

Figure 4.19: Exemplary measurements of miRNA levels in supernatant of treated islets. The islets were treated with aggressive or mild cytokine mix and/or hypoxia (1% O2) and supernatant was collected after 3, 6, and 24H. Data are presented as fold change in treated islets as compared to control (untreated islets). Quadruplicates for each sample at each time point were collected and triplicates in qPCR were performed. One-way ANOVA followed by Tukey's HSD multiple comparison test was performed for statistical analysis. (**p < 0.05, **p < 0.01, ***p < 0.001 and ****p < 0.0001*.) Mild cytokines: light blue; aggressive cytokines: dark blue; Hypoxia + mild cytokines: light green; Hypoxia + aggressive cytokines: dark green; Hypoxia alone: grey. L: low and H: high.

The 80 miRNAs were quantified in the supernatant of treated and untreated islets using the Biomark. After data pre-processing and analysis, several assays revealed the amplification of unspecific products leading to the exclusion of 16 miRNAs, with 64 miRNAs left for the final analysis. The analysis of 64 miRNAs is summarized in a heatmap (Figure 4.20).

At 3H, 6H, or 24H; 45 miRNAs had significant increase in the supernatant of treated islets as compared to untreated islets, as indicated by One-way ANOVA (p<0.05) (Figure 4.21). The 45 miRNAs were plotted using a Venn diagram to find shared miRNAs between treatment conditions, cytokines, hypoxia, and the combination of hypoxia and cytokines (Figure 4.22).

At 3H time point, 9 miRNAs were found to be uniquely measureable after cytokine treatment and 3 miRNAs were found after cytokine- and the combination treatment (Figure 4.22A).

At 6H, 3 miRNAs were found to be unique for cytokine treatment, 4 miRNAs shared between cytokine- and the combination treatment, and 18 miRNAs were measurable after all treatment conditions (Figure 4.22B).

At 24H, 3 miRNAs were found to be shared between hypoxia and the combination treatment and 38 miRNAs were measurable after all treatment conditions (Figure 4.22C).

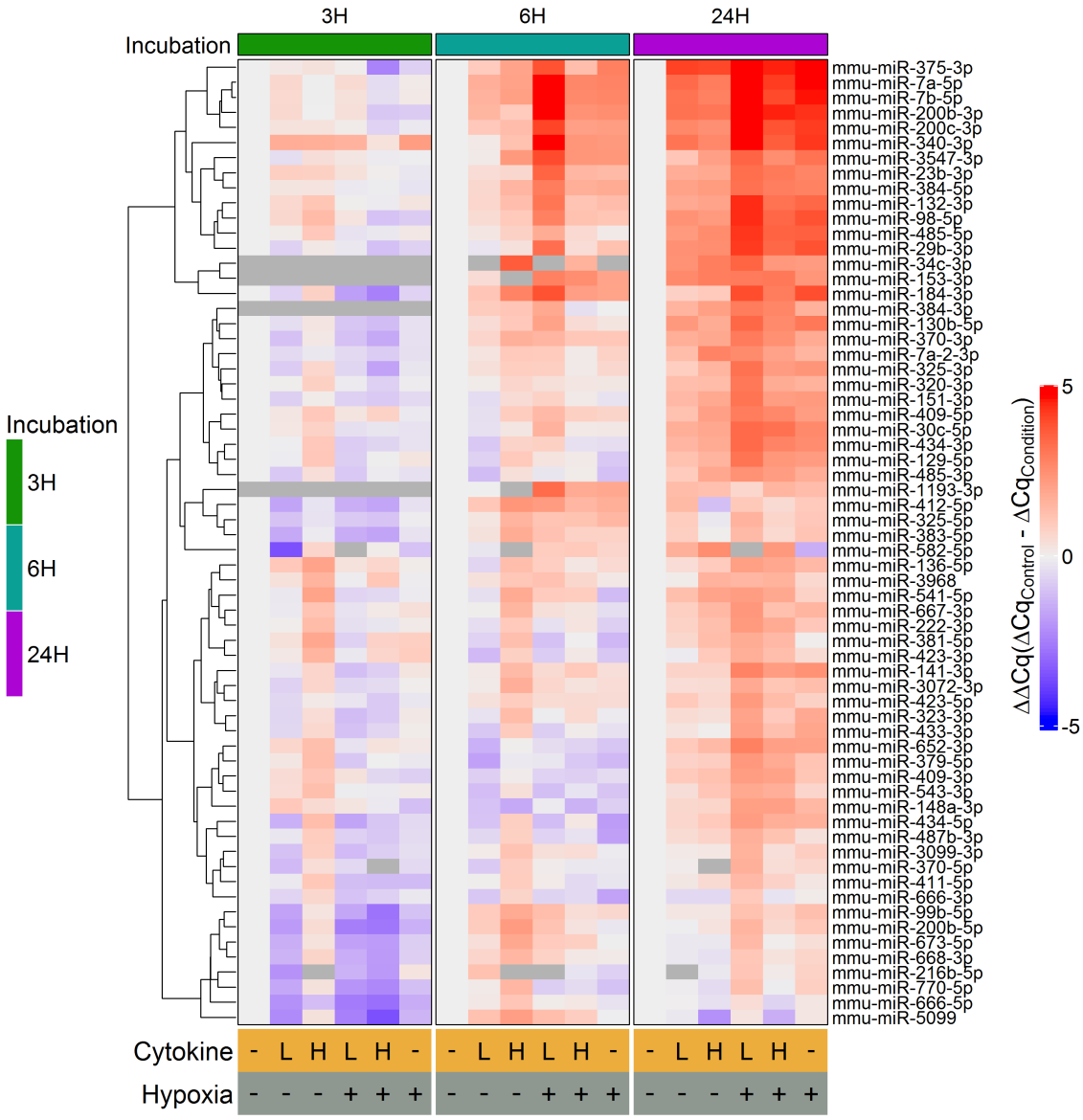

Figure 4.20: miRNA analysis in supernatant of treated and untreated islets. The level of 64 miRNAs in the supernatant of treated islets relative to untreated islets is presented as $\Delta\Delta$Cq values (ΔCq $_{control}$ - ΔCq $_{condition}$) at 3H, 6H, and 24H. At each time point four replicate samples were collected (N=4 petri dishes) and triplicates in qPCR were performed. The heatmap is clustered by Euclidean distance and scaled by rows. Grey cells indicate not available value (NA). Symbols: L: low cytokines concentration, H: high cytokines concentration, (-) and (+): indicate eliminating or the addition of the specified treatment respectively.

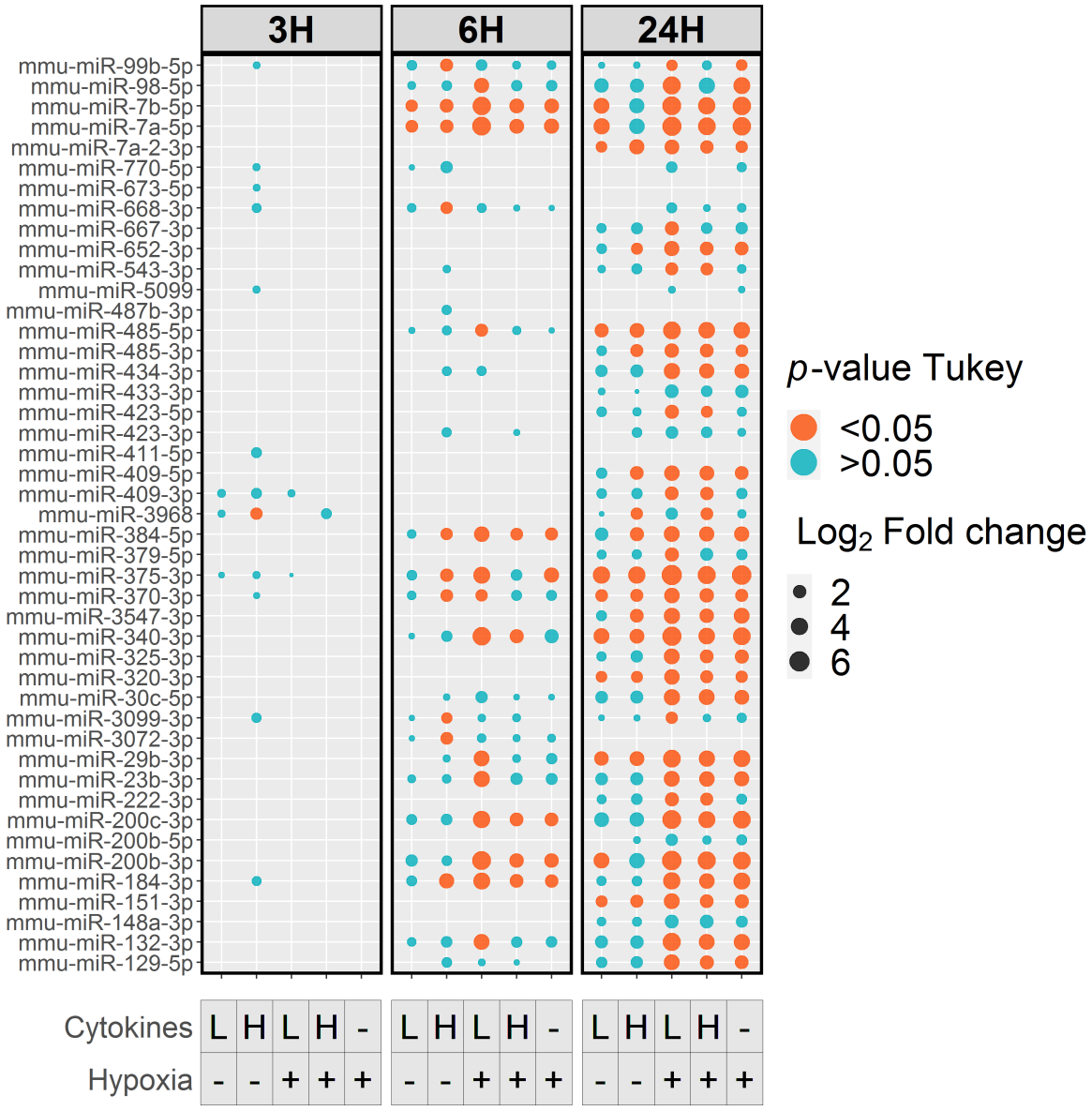

Figure 4.21: Significant 45 miRNAs measured in the supernatant of treated islets. The level of 45 miRNAs presented as Log_2 fold change in supernatants of treated islets as compared to untreated islets. The dot size scaled by Log_2FC values and miRNAs filtered based on FC>1. *p*-value Tukey: the *p* values of multiple comparisons testing conducted by Tukey HSD (Blue: $p>0.05$, Red: $p<0.05$). All presented miRNAs showed significance by One-way ANOVA testing ($p<0.05$) across all time points 3H, 6H, and 24H. One-way ANOVA followed by Tukey's HSD multiple comparison test was performed for statistical analysis.

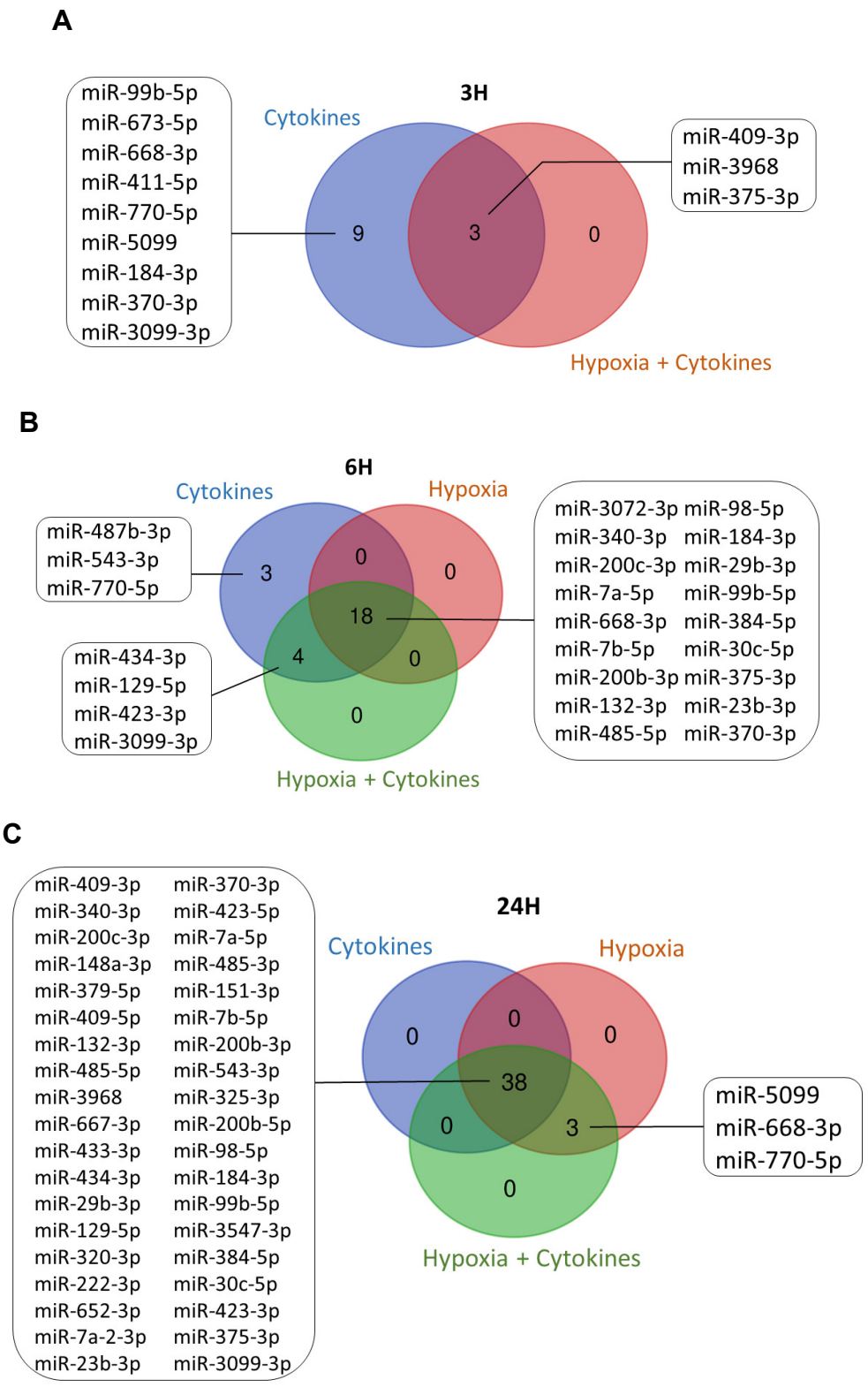

Figure 4.22: Venn diagrams of 45 miRNAs between treatment conditions. The analyzed miRNAs in figure 4.21 are plotted in Venn diagrams at **A**: 3H, **B**: 6H, and **C**: 24H. The shared miRNAs and their number are indicated on the figure. The miRNAs affected by aggressive and mild cytokines are merged under one condition indicated as cytokines in the figure.

4.4.1.2 Quantification of apoptosis in stressed islets

In a separate experiment, the islets were treated with mild and/or aggressive cytokines mix with or without hypoxia for 3, 6, and 24H. After treatment an apoptosis assay was performed to quantify cleaved caspase-3 activity in the islets.

The mild or aggressive cytokines mix did not cause significant increase in cleaved caspase-3 activity at 3H or 6H, but at 24H both cytokine concentrations caused significant increase as compared to control (Figure 4.23). There was no significant difference in cleaved caspase-3 activity between aggressive and mild cytokines in the three time points.

The combination of cytokines and hypoxia led to significant increase in cleaved caspase-3 at 3H as compared to control when the aggressive cytokines mix was used and the aggressive mix showed significant higher effect when compared to the mild mix at 3H (Figure 4.24A).

At 6H and 24H the combination treatment led to significant increase in cleaved caspase-3 as compared to control without significant difference when comparing the aggressive to mild mix at those two time points (Figure 4.24B and C).

The islets exposed to hypoxic stress alone and the untreated islets did not show significant changes in cleaved caspase-3 activity at 3H, 6H, and 24H (Figure 4.23).

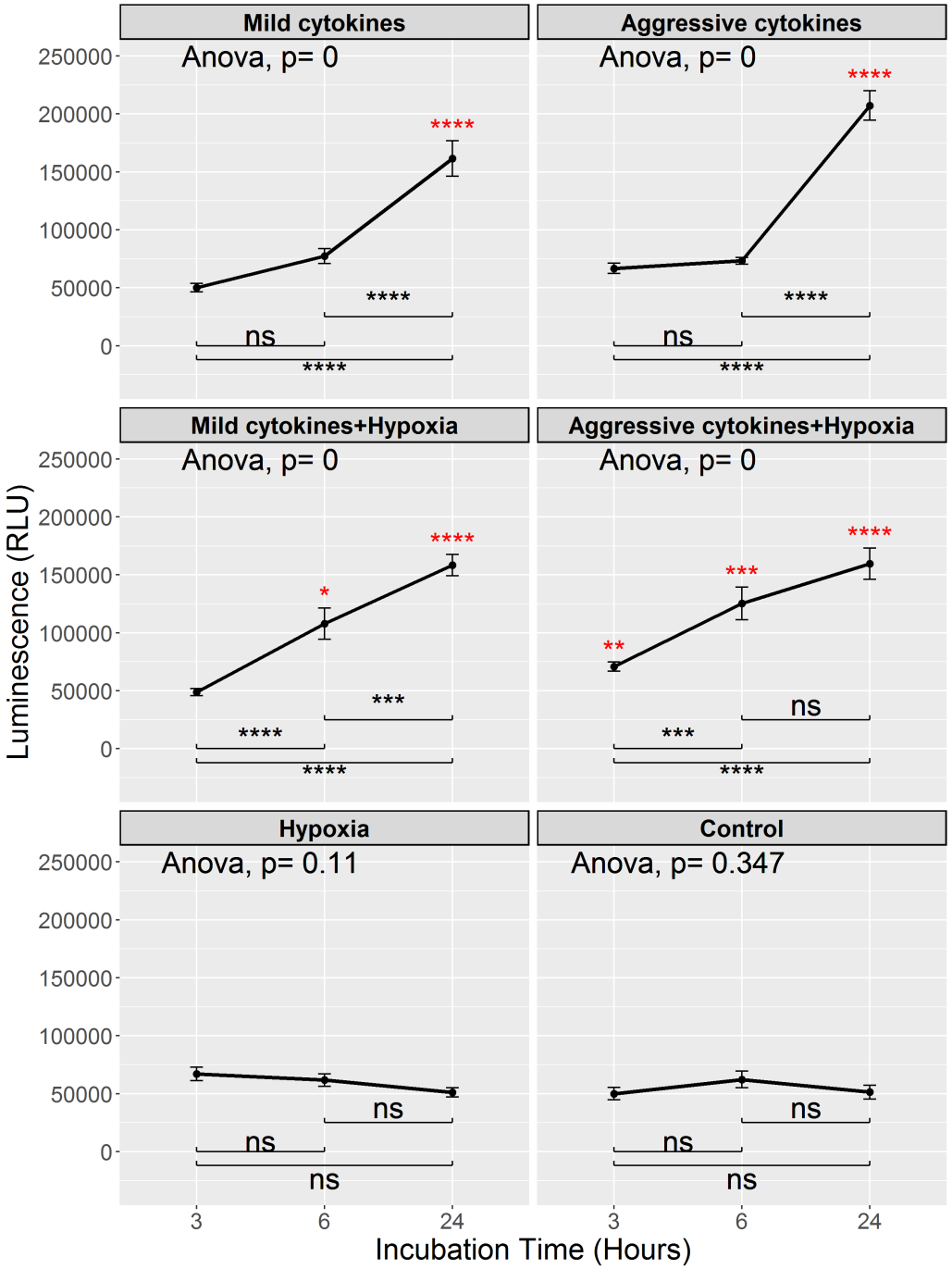

Figure 4.23: Apoptosis assay in the *in vitro* islet stress model. Mouse islets were incubated in mild and/or aggressive cytokine mix with or without hypoxia for 3, 6, and 24H. Three islets per well were used for apoptosis assay. At least 12 replicates for each condition were performed. The plates were analyzed in a luminometer and the obtained readings presented as relative light units (RLU). One-way ANOVA followed by Tukey's HSD multiple comparison test was performed for statistical analysis. The multiple comparisons between time points in each treatment condition presented below each line, and the ANOVA *p* value indicated on top. Asterisks in red represent the significance as compared to control (untreated islets) at the specified time point. (**p < 0.05, **p < 0.01, ***p < 0.001 and ****p < 0.0001*.)

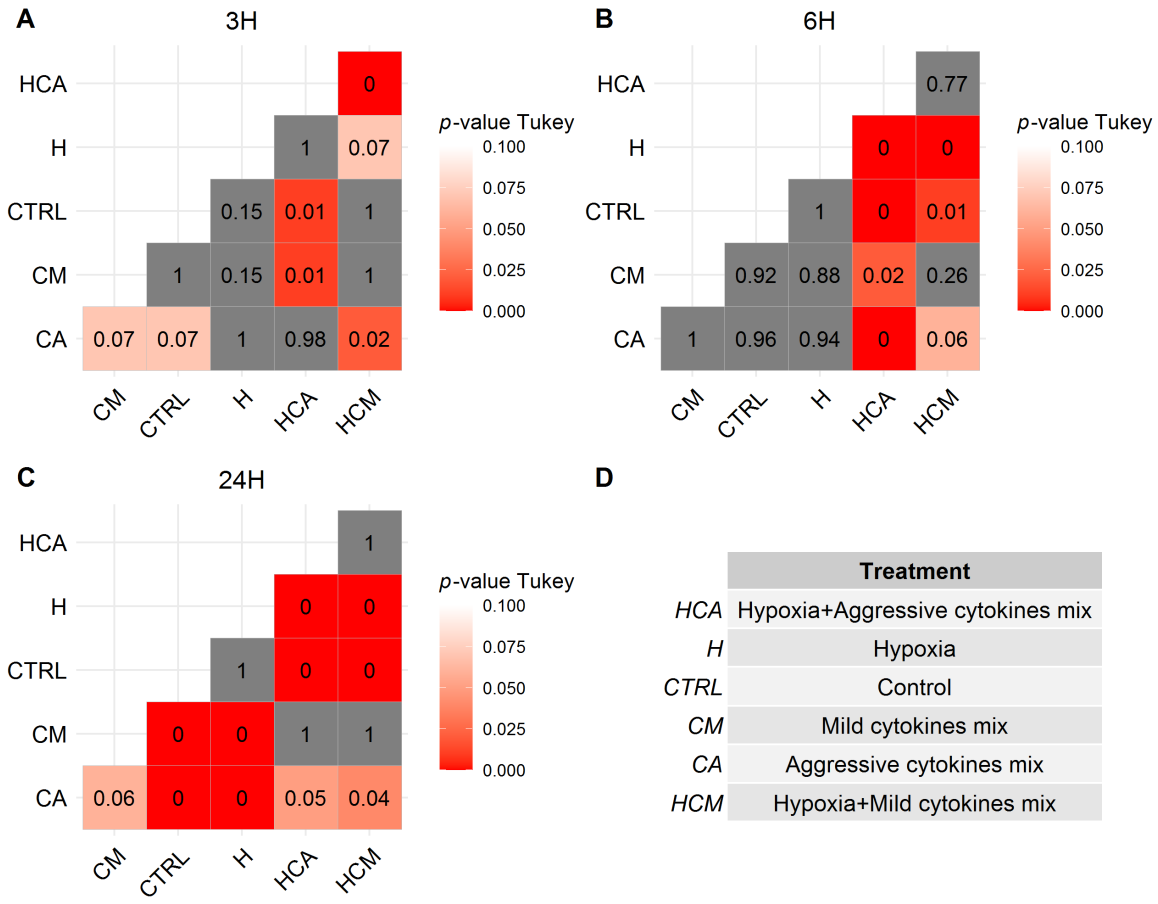

Figure 4.24: Multiple comparisons test between treatment conditions at (A): 3H, (B): 6H, and (C): 24H. One-way ANOVA followed by Tukey's HSD multiple comparison test was performed for statistical analysis. Presented are *p*-values by Tukey's HSD multiple comparison test between treatment conditions at each time point. Symbols are indicated in the table (**D**). Grey colour indicates values higher than the scale limit (0.1).

To investigate a potential relation between the measurable level of miRNAs (64 miRNAs Figure 4.20) in the supernatant and the stress-induced cleaved caspase-3 activity in islets, pearson's correlation analysis was performed between miRNA level at each time point and the caspase-3 level. The pearson's *r* was determined for each miRNA and presented in heatmap (Figure 4.25).

Three miRNAs (mmu-miR-541-5p, mmu-miR-582-5p, and mmu-miR-381-5p) showed positive significant correlation with caspase-3 at 24H (*r*: 0.88, 0.94, and 0.83 respectively). One miRNA (mmu-miR-423-3p) correlated significantly at 3H (*r*: 0.83). mmu-miR-200b-3p showed negative significant correlation with caspase-3 at 3H (*r*: -0.85). Figure 4.26 and highlighted in bold in heatmap (Figure 4.25).

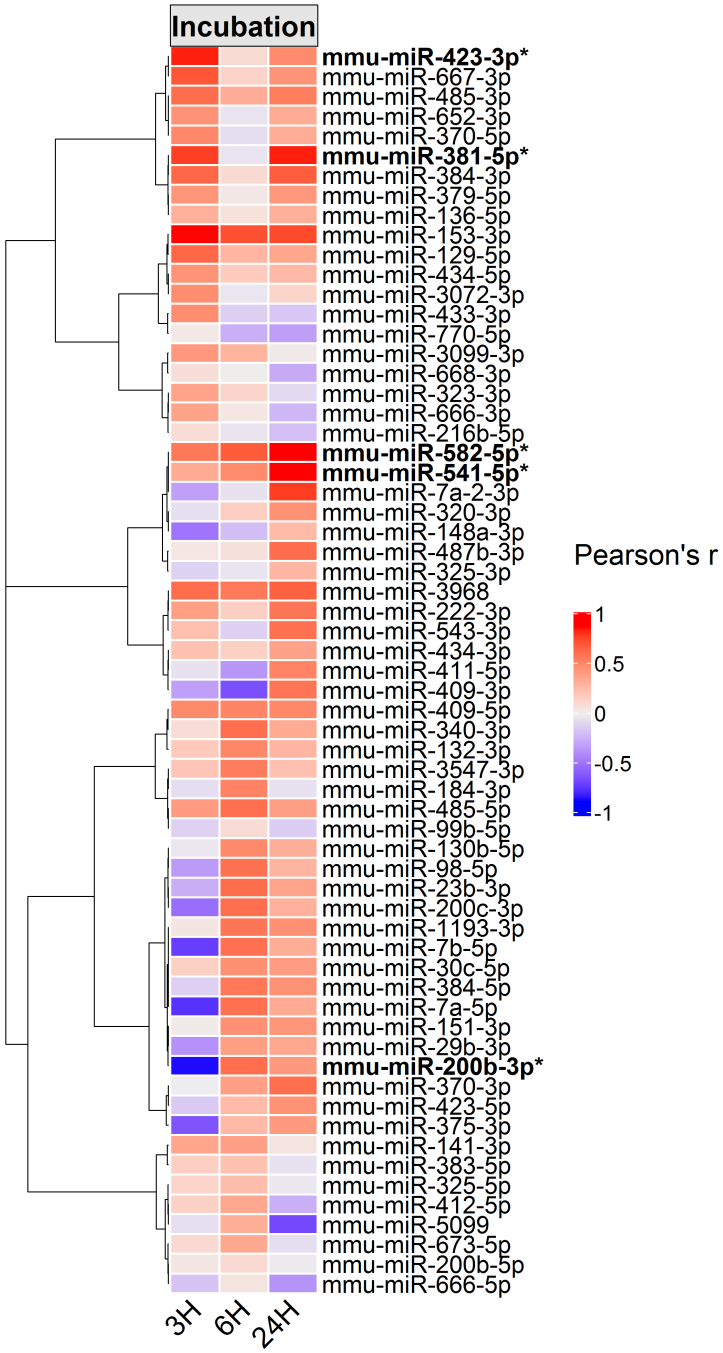

Figure 4.25: Correlation analysis between miRNA level and apoptosis. The correlation between the presence of 64 miRNAs and islet cell apoptosis was analyzed at 3H, 6H, and 24H. The pearson's *r* values was used in the heatmap. Presented are 63 miRNAs (mmu-miR-34c-3p was excluded because of insufficient values for correlation at 3H; *r* at 6H, and 24H: 0.09 and 0.71 respectively). The heatmap is clustered by pearson's distance and scaled by rows. miRNAs labelled in bold with an asterisk indicate showed significant correlation ($p<0.05$) with apoptosis in at least one time point.

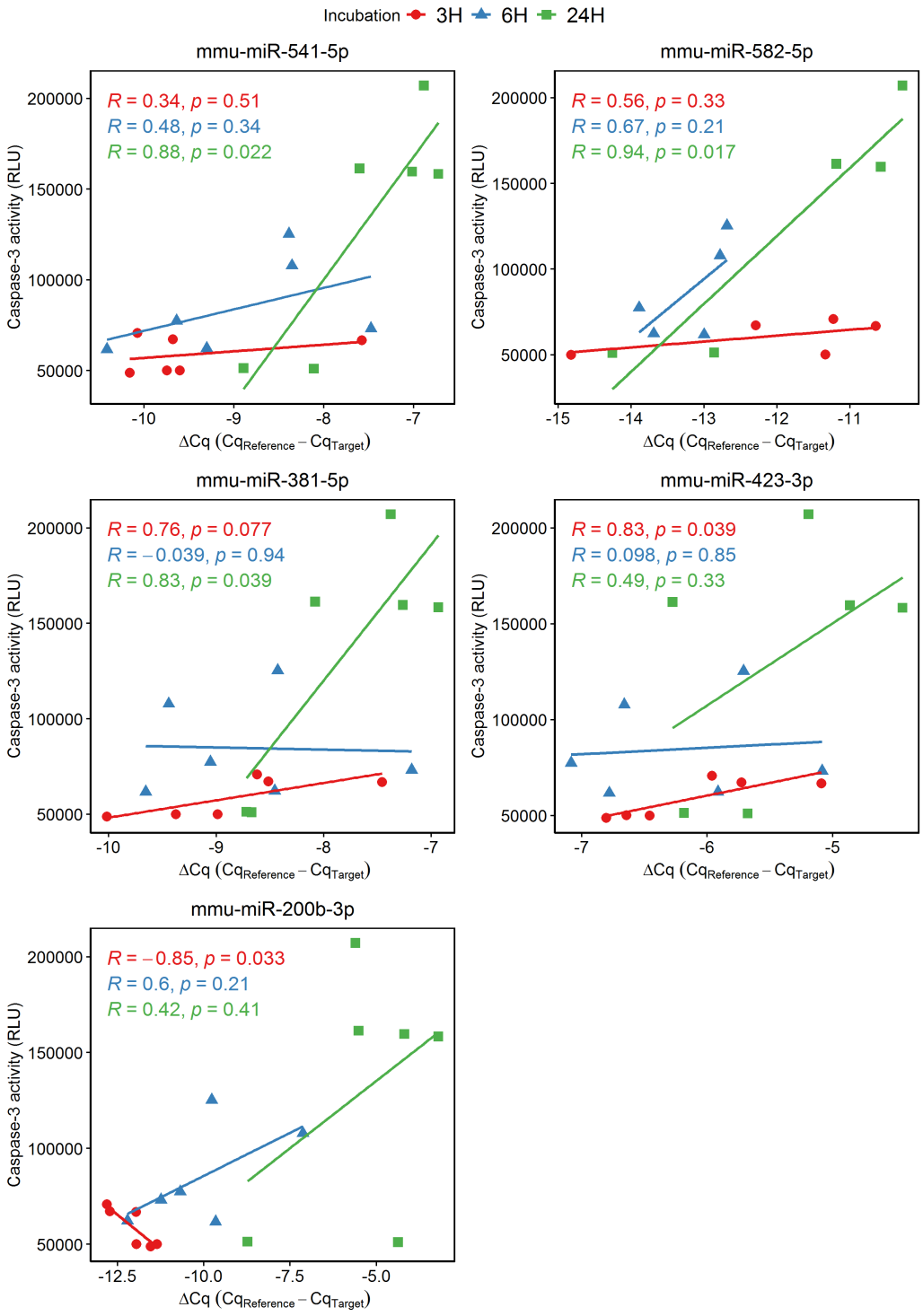

Figure 4.26: miRNAs correlated significantly with apoptosis. mmu-miR-541-5p, mmu-miR-582-5p, and mmu-miR-381-5p showed positive significant correlation with caspase-3 at 24H, mmu-miR-423-3p showed positive significant correlation with caspase-3 at 3H. mmu-miR-200b-3p showed negative significant correlation with caspase-3 at 3H. Presented on Y axis: caspase-3 activity as measured by luminometer relative light units (RLU); X axis: miRNA level (ΔCq= Cq $_{\text{Reference}}$ - Cq $_{\text{Target}}$). The *p* values and pearson's *r* indicated on the figures.

4.4.1.3 Impairment of Insulin secretion in stressed islets

To assess the islet's ability to secrete insulin after stress exposure, the glucose-stimulated insulin secretion (GSIS) assay was performed. The insulin secretion from stressed islets was quantified after exposure to mild and/or aggressive cytokines mix with or without hypoxia after 3, 6, and 24H, in response to two glucose concentrations, 2mM and 20mM.

After 3H of cytokine- or hypoxia only treatment, the islets maintained a pronounced glucose-stimulated insulin secretion indicated by the significant difference between the basal (2mM) and stimulated (20mM) glucose concentration. The combination of hypoxia and cytokines (at either concentration) has led to elevated basal (2mM) secretion and no further response to 20mM glucose.

At 6h, after treatment with low dose of cytokines, the islets remained responsive to 20mM glucose with significant difference to 2mM. High dose of cytokines, hypoxia alone, and the combination treatment increased the basal secretion and there was no further response to 20mM concentration.

At 24H, the basal rates of secretion increased generally after treatment with any of the stressors, and there was no further increase in the stimulated (20mM) insulin secretion indicating major impairment in GSIS at this time point (Figure 4.27).

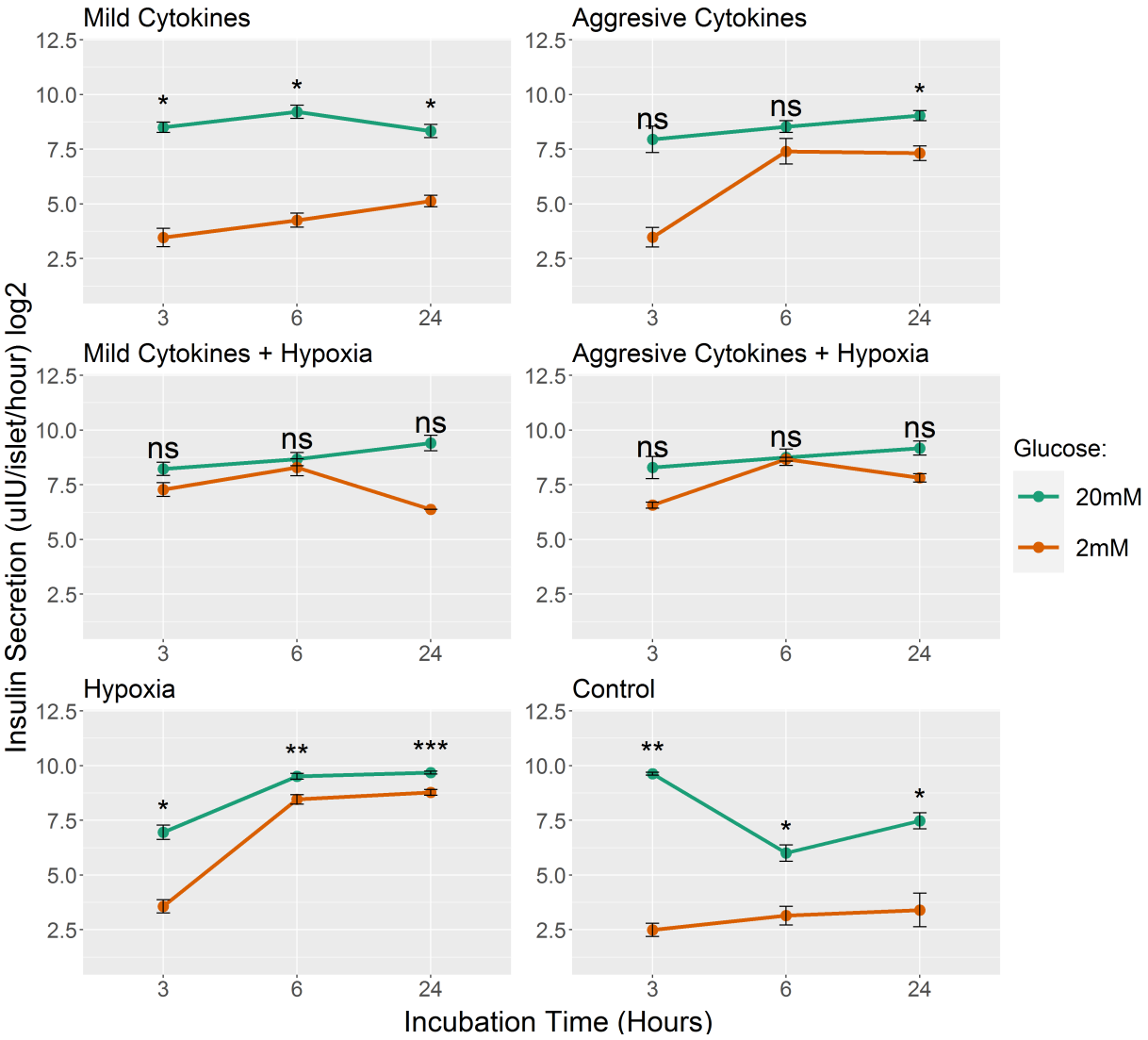

Figure 4.27: Glucose-stimulated insulin secretion assay (GSIS) in the *in vitro* islets stress model. The islets were incubated in mild and/or aggressive cytokines mix with or without hypoxia for 3, 6, and 24H. After treatment, the islets were incubated in 2mM or 20mM for 1H at 37°C. The supernatant was collected and secreted insulin was measure by ELISA secretion. Presented is the insulin concentration (uIU) per islet per hour. Student's *t*-test was performed for statistical analysis between 2mM and 20mM at each time point. **p < 0.05, **p < 0.01 ***p < 0.001.*

4.4.1.4 Pathway analysis

KEGG pathway enrichment analysis was performed to find pathways affected by the miRNAs (shown in figure 4.22) induced by treatment with cytokines (at either concentration) or with the combination. To do so, the targets of the miRNAs were identified *in silico* and KEGG enrichment analysis was performed.

The cytokines-induced miRNAs comprised 11 miRNAs (induced after 3H and/or 6H) that had 2559 mRNA targets in total. (number of targets: mmu-miR-99b-5p: 80, mmu-miR-673-5p: 679, mmu-miR-668-3p: 186, mmu-miR-411-5p: 244, mmu-miR-770-5p: 421, mmu-miR-5099: 22, mmu-miR-184-3p: 51, mmu-miR-370-3p: 285, mmu-miR-3099-3p: 115, mmu-miR-487b-3p: 15, and for mmu-miR-543-3p: 461 targets). After KEGG analysis on the identified targets and filtering the enriched pathways with a *p* value 0.05, seven miRNAs and their targets remained, presented in (Figure 4.28). The top significant enriched pathways, the number of the targets involved in each pathway, and the number of involved miRNAs found here are shown in (Figure 4.29). The highest number of target genes are involved in the MAPK signalling pathway (65 genes; *p*= 5.43e-07) targeted by three miRNAs found in our analysis (mmu-miR-411-5p, mmu-miR-370-3p, and mmu-miR-487b-3p).

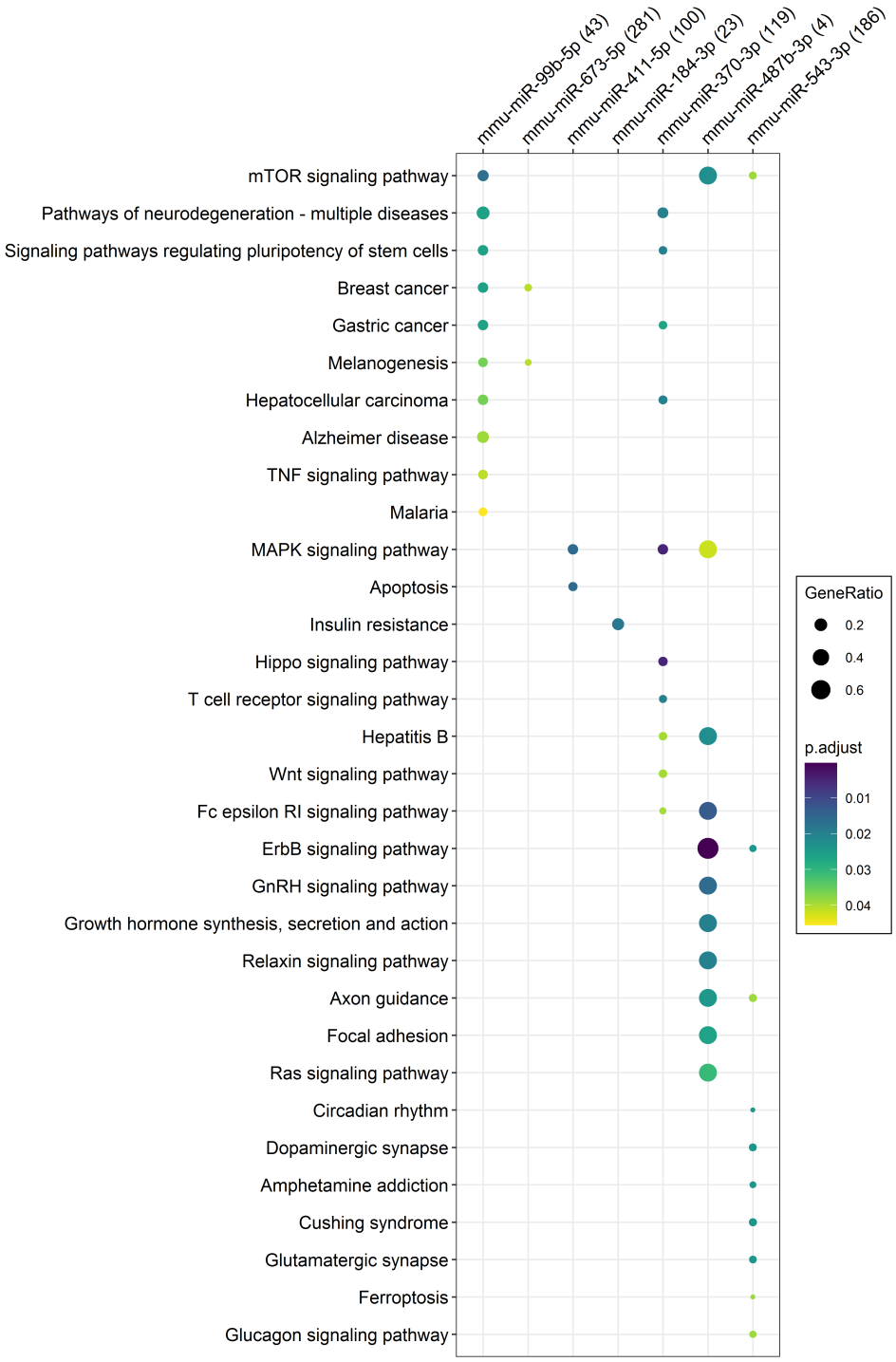

Figure 4.28: KEGG enrichment analysis for cytokines-induced miRNAs. The significant pathways are presented (p<0.05). The number of target genes significantly involved in a pathway is indicated between brackets beside each miRNA name. The dot size indicates the gene ratio: the ratio of the genes from the pathway to the input target of genes.

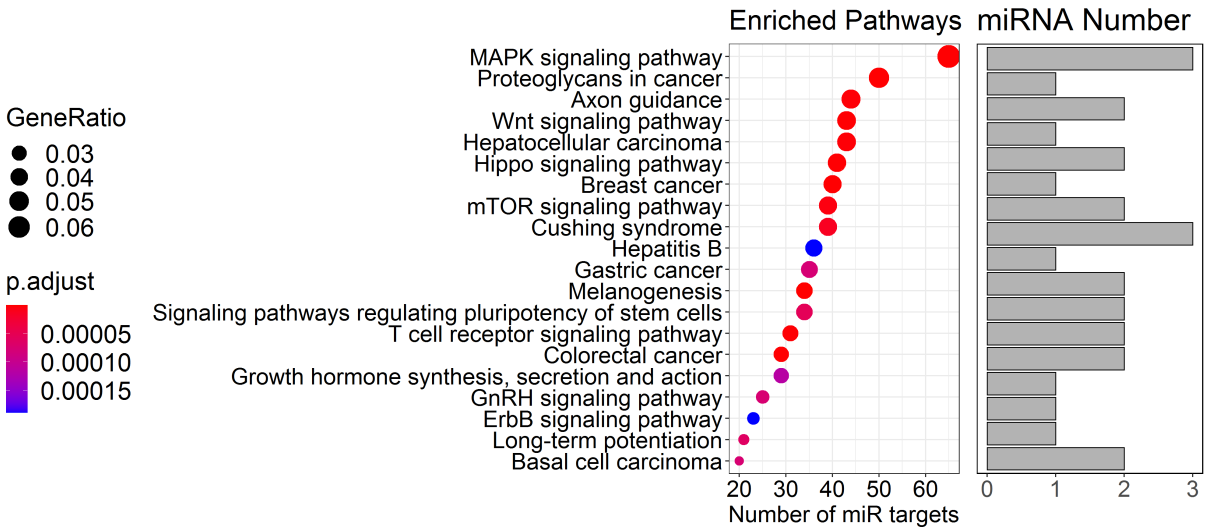

Figure 4.29: The top significant pathways targeted by cytokines-induced miRNAs. The number of target genes and the number of involved miRNAs found here for each pathway are indicated. The target genes of the analyzed miRNAs were pooled and only the unique targets were further analyzed to identify enriched pathways. The dot size indicates the gene ratio: the ratio of the genes from the pathway to the input target genes. The dot color shows the *p* value.

The 40 combination-treatment-induced miRNAs found after 3, 6 and 24H targeted 15017 genes (7092 after excluding shared targets between miRNAs). Table 21.

KEGG analysis was performed on the identified targets of each miRNA and the enriched pathways were filtered with a *p* value 0.05. 26 miRNAs and their targets survived the cut-off for significance and are presented in figure 4.30. The top 20 most significant pathways are shown in figure 4.31. 173 target genes significantly targeted (*p*= 8.85e-10) PI3K-Akt signalling pathway with 7 miRNAs involved (mmu-miR-200c-3p, mmu-miR-200b-3p, mmu-miR-29b-3p, mmu-miR-384-5p, mmu-miR-148a-3p, mmu-miR-320-3p, and mmu-miR-222-3p). 164 genes significantly targeted MAPK signalling pathway (*p*= 9.42e-16) with 13 miRNAs involved (mmu-miR-200c-3p, mmu-miR-200b-3p, mmu-miR-132-3p, mmu-miR-98-5p, mmu-miR-29b-3p, mmu-miR-384-5p, mmu-miR-30c-5p, mmu-miR-370-3p, mmu-miR-148a-3p, mmu-miR-320-3p, mmu-miR-222-3p, mmu-miR-423-5p, and mmu-miR-325-3p). PI3K-Akt signalling pathway and MAPK signalling pathway are pointed to with arrows in figure 4.30.

Table 21: Number of target genes

miRNA	Target genes No.	miRNA	Target genes No.
mmu-miR-3072-3p	137	mmu-miR-379-5p	234
mmu-miR-340-3p	88	mmu-miR-409-5p	158
mmu-miR-200c-3p	736	mmu-miR-3968	95
mmu-miR-7a-5p	552	mmu-miR-667-3p	120
mmu-miR-668-3p	186	mmu-miR-433-3p	221
mmu-miR-7b-5p	548	mmu-miR-434-3p	127
mmu-miR-200b-3p	739	mmu-miR-129-5p	257
mmu-miR-132-3p	360	mmu-miR-320-3p	448
mmu-miR-485-5p	517	mmu-miR-222-3p	270
mmu-miR-98-5p	848	mmu-miR-652-3p	12
mmu-miR-184-3p	51	mmu-miR-7a-2-3p	184
mmu-miR-29b-3p	814	mmu-miR-423-5p	592
mmu-miR-99b-5p	80	mmu-miR-485-3p	78
mmu-miR-384-5p	1097	mmu-miR-151-3p	187
mmu-miR-30c-5p	1094	mmu-miR-543-3p	461
mmu-miR-375-3p	210	mmu-miR-325-3p	1354
mmu-miR-23b-3p	654	mmu-miR-200b-5p	158
mmu-miR-370-3p	285	mmu-miR-3547-3p	153
mmu-miR-409-3p	126	mmu-miR-423-3p	84
mmu-miR-148a-3p	587	mmu-miR-3099-3p	115

Figure 4.30: KEGG enrichment analysis of miRNAs effected by the combination treatment. The significant pathways are presented (p<0.05). The number of target genes significantly involved in a pathway is indicated between brackets beside each miRNA name. The dot size indicates the gene ratio: the ratio of the genes from the pathway to the input target genes. The dot color shows the p value.

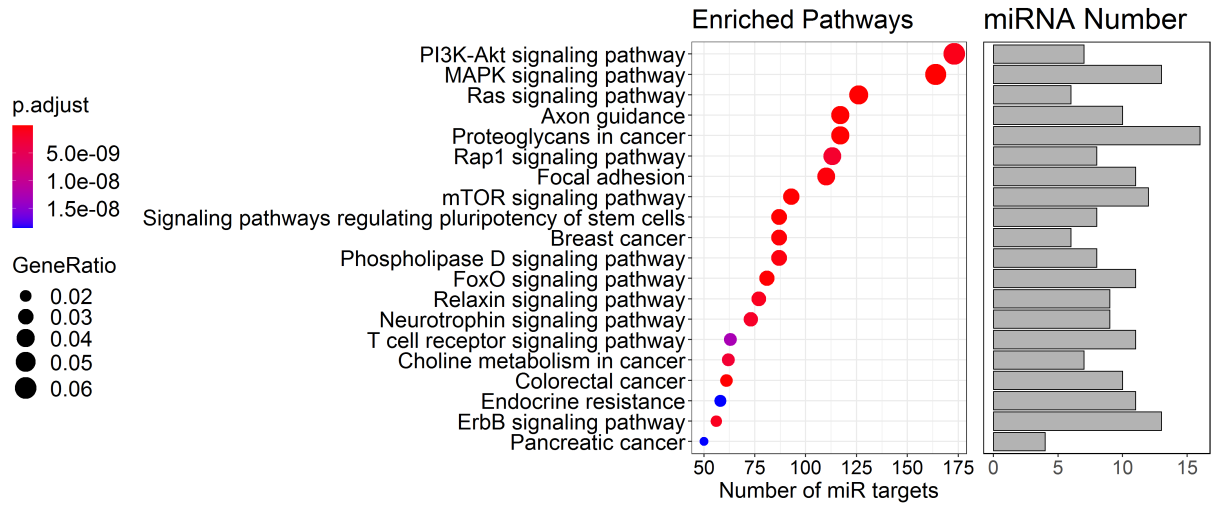

Figure 4.31: The top significant pathways targeted by combination treatment-induced miRNAs. The number of target genes and number of involved miRNAs for each pathway are indicated. The target genes of the analyzed miRNAs were pooled and only the unique targets were further analyzed to identify enriched pathways. The dot size indicates the gene ratio: the ratio of the genes from the pathway to the input target genes. The dot color shows the *p* value.

The top 20 most significant pathways targeted by the combination treatment-induced miRNAs and cytokines-induced miRNAs were combined and shared pathways were identified: Axon guidance, MAPK signalling pathway, Proteoglycans in cancer, Signalling pathways regulating pluripotency of stem cells, Colorectal cancer, mTOR signalling pathway, Breast cancer, ErbB signalling pathway, and T cell receptor signalling pathway (Figure 4.32).

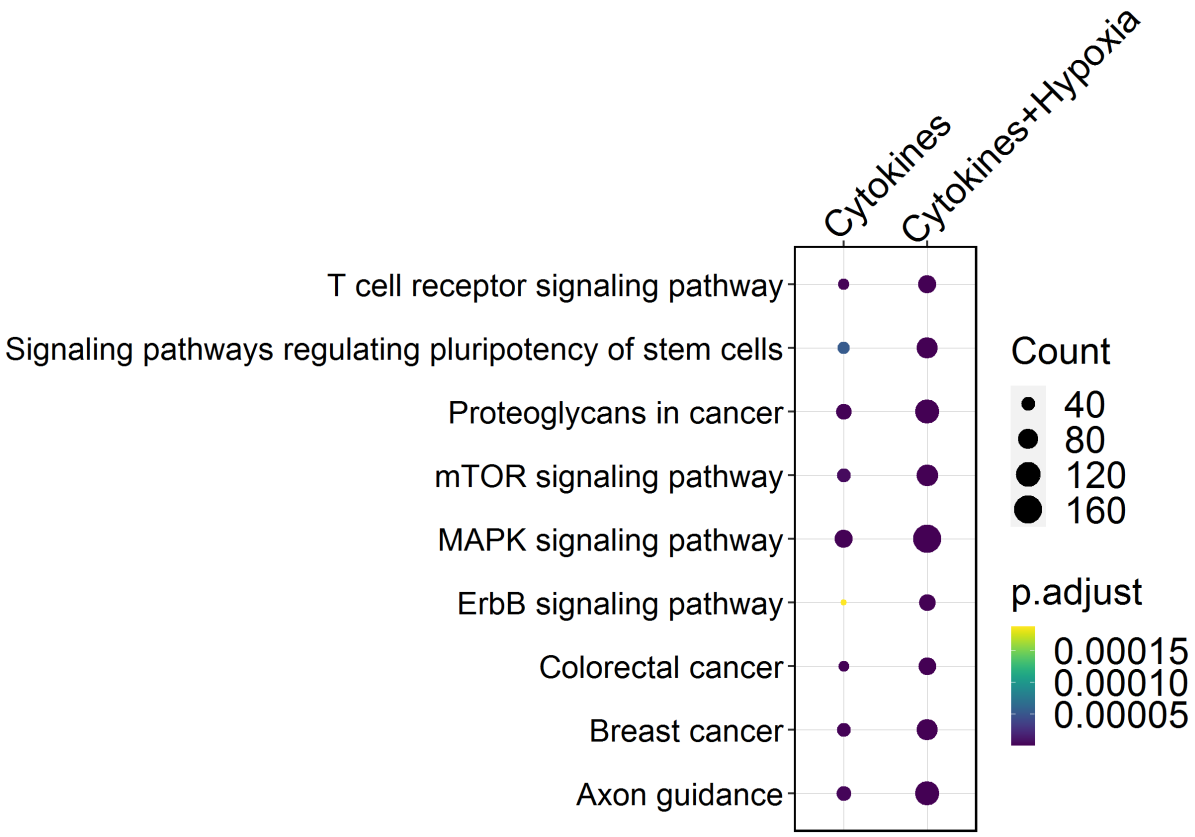

Figure 4.32: Shared pathways. Nine pathways were found in common between the combination treatment-induced miRNAs and cytokines-induced miRNAs. Top 20 pathways were selected from each treatment. Count: target genes number.

4.4.2 Human islets

To test whether some miRNAs that were induced in the *in vitro* mouse model could also be induced in a comparable human *in vitro* model, and to compare their dynamics between mouse and human, I treated human islets with aggressive cytokines mix and hypoxia. The same procedure that was used in the *in vitro* mouse islet model was performed using human islet. The supernatant of treated human islet was assessed for miRNA content as compared to untreated islet. miRNAs were quantified in the supernatant of treated human islets and untreated islets.

4.4.2.1 miRNA content in the supernatant of stressed islets

Human islets were treated with aggressive cytokines mix and hypoxia and their supernatant was collected after 24H and 48H. RNA was isolated from the supernatant samples and analyzed

using bioanalyzer to assess the miRNA content, as described for the mouse islets. The large peak in the miRNA area (4-40nt) (Figure 4.33) indicated high miRNA content in the supernatant of treated islets as compared to control (untreated islets). At 24H, the miRNA concentration in the supernatant of treated islets was 194771.8 ± 21413 pg/ul as compared to 2260.833 ± 585.7 pg/ul in the supernatant of untreated islets. The miRNA concentrations declined after 24H in the supernatant of treated islets to 56879.967 ± 54037.1 pg/ul as well as in the supernatant of untreated islets 719.367 ± 205.4 pg/ul (mean ± SEM) (Figure 4.34).

4.4.2.2 Inflammatory- and hypoxic stress induces the release of miRNAs from human islets

Nine miRNAs (Panel P; Table 18 in methods) were quantified in the supernatant of islets treated with aggressive cytokines mix and hypoxia after 24H and 48H. Five miRNAs (hsa-let-7e-5p, hsa-miR-141-3p, hsa-miR-148a-3p, hsa-miR-200c-3p and hsa-miR-30c-5p) increased significantly in the supernatant of treated islets as compared to control after both, 24H and 48H. hsa-miR-127-5p, hsa-miR-129-5p, and hsa-miR-375-3p showed significant increase in the supernatant of treated islets at 24H only. hsa-miR-132-3p did not significantly changed after 24H or 48H of treatment (Figure 4.35).

Pathway analysis was performed on the miRNAs that were significantly induced by treatment (all 9 except hsa-miR-132-3p). Figure 4.36. A total of 11496 target genes (thereof 6407 unique ones) were identified (Table 22).

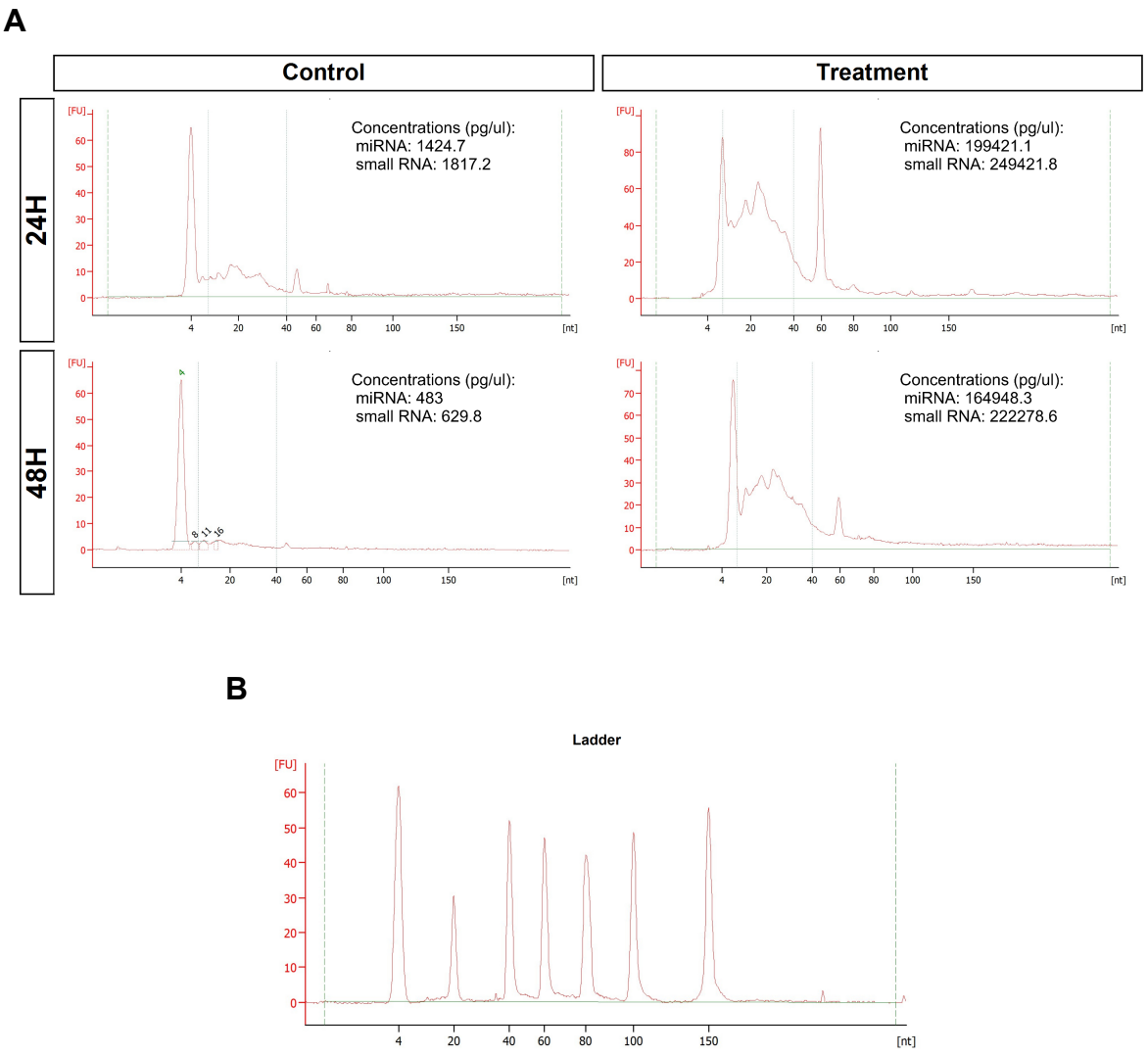

Figure 4.33: Exemplary electropherograms of the small RNA/miRNA distribution in the supernatant of islets treated with aggressive cytokine mix and hypoxia (1% O2) or untreated. Triplicates of each sample at each time point (**A**: 24H and 48H) were performed. The electropherograms were generated by Agilent 2100 RNA bioanalyzer. The condition and time point as indicated. **B**: The ladder illustrates the size distribution of RNA fragments.

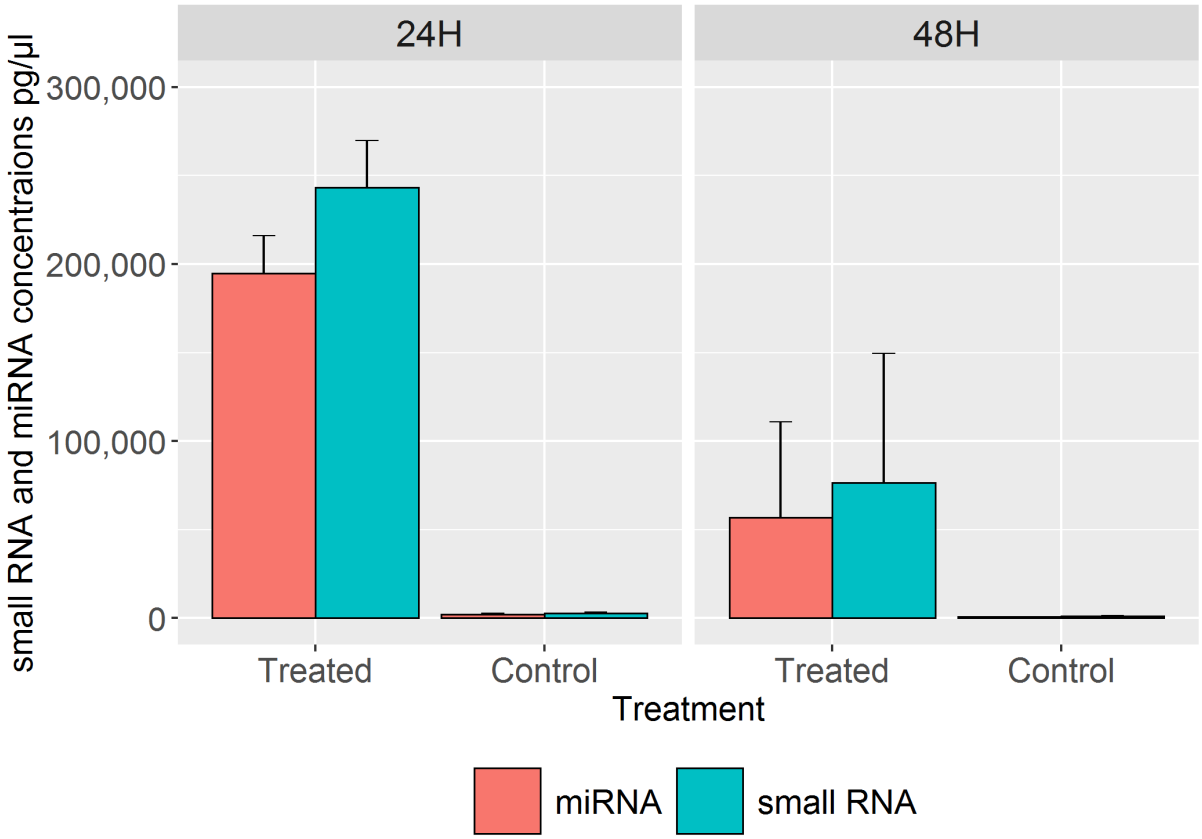

Figure 4.34: Small RNA- and miRNA concentrations in the supernatant of control and treated islets. The islets were treated with aggressive cytokine mix and hypoxia (1% O2) and the supernatant collected after 24, 48H and used in bioanalyzer analysis. Triplicates were performed for each sample at each time point. Shown is the concentration in pg/ul. Data are presented as mean ± SEM. Small RNA concentration (blue), miRNA concentration (red).

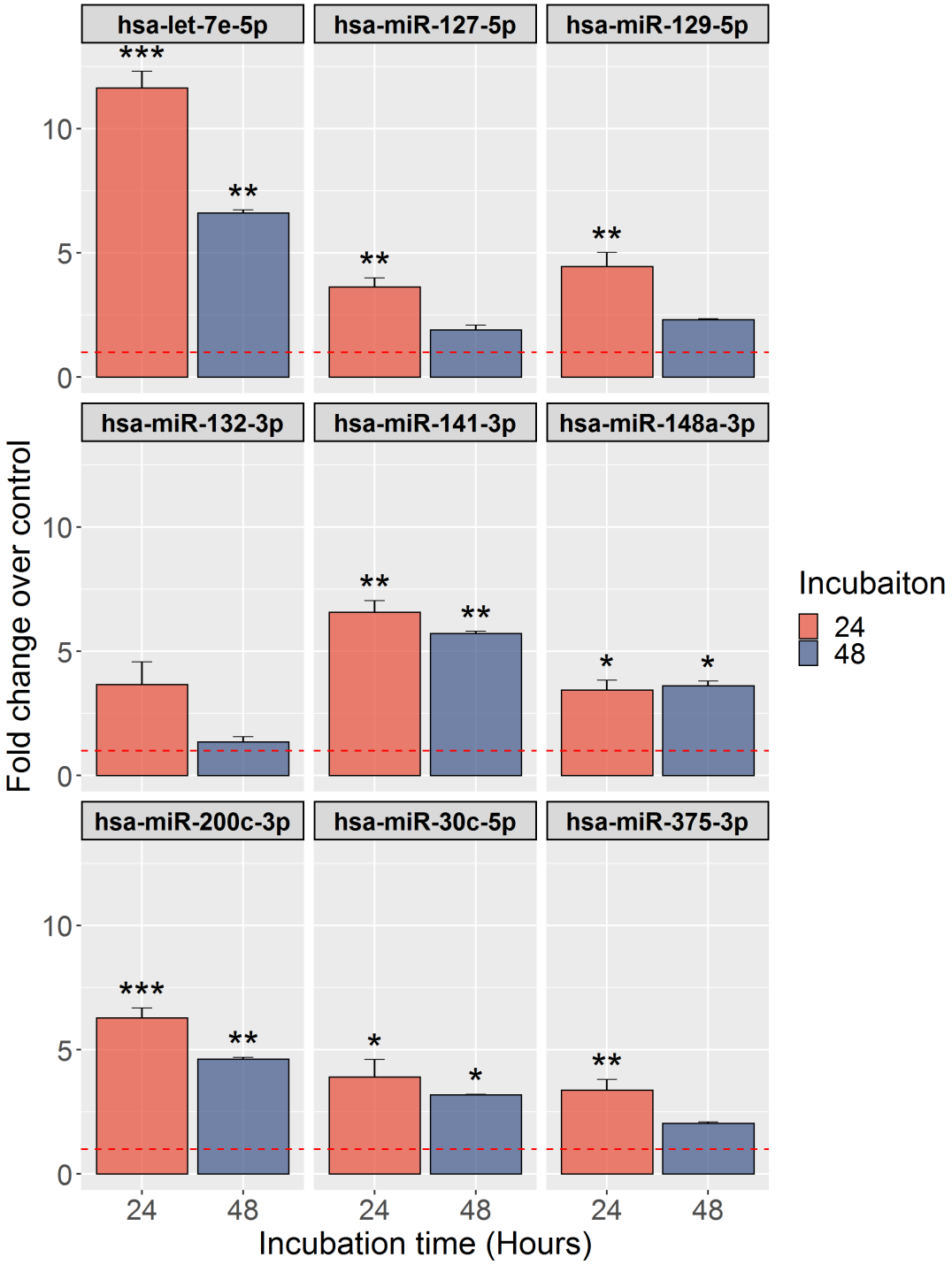

Figure 4.35: miRNA measurements in supernatant of treated human islets. Nine miRNAs were quantified in the supernatant of human islets treated with aggressive cytokine mix and hypoxia after 24H (red) and 48H (blue). Presented is fold change (± SEM) relative to supernatant of untreated islets (control). Two-way ANOVA followed by Tukey's HSD multiple comparison test was performed for statistical analysis. **p < 0.05, **p < 0.01, and ***p < 0.001* . Each sample =120 islets; control: N=3, treated islets: N=3. Triplicates were performed in qPCR. The red broken line indicates fold change of 1.

Figure 4.36: KEGG enrichment analysis of human miRNAs affected by aggressive cytokines and hypoxia. KEGG enrichment analysis of human miRNAs affected by aggressive cytokines and hypoxia. The target genes were identified using mirDIP database (microRNA Data Integration Portal (Tokar et al., 2018)) and then analyzed using KEGG enrichment analysis. The significant pathways are presented (p<0.05). The number of target genes significantly involved in a pathway is indicated between brackets beside each miRNA name. The dot size indicates the gene ratio: the ratio of the genes pathway to input target genes. The dot colour scaled by p value.

Table 22: Number of target genes

miRNA	Target genes No.
hsa-miR-30c-5p	1629
hsa-miR-200c-3p	1702
hsa-let-7e-5p	1387
hsa-miR-148a-3p	1279
hsa-miR-141-3p	1891
hsa-miR-129-5p	2475
hsa-miR-375	645
hsa-miR-127-5p	488

Two of the main pathways discovered to be targeted by miRNAs released upon cytokine- and /or Hypoxia treatment in the mouse islet assays were also found to be targeted by miRNAs released in the human assays. The MAPK signalling pathway contained 150 genes targeted by 6 miRNAs (hsa-miR-375, hsa-miR-200c-3p, hsa-let-7e-5p, hsa-miR-129-5p, hsa-miR-141-3p, hsa-miR-148a-3p) and the PI3K-Akt signalling pathway contained 177 genes targeted by 5 miRNAs (hsa-miR-200c-3p, hsa-let-7e-5p, hsa-miR-129-5p, hsa-miR-141-3p, hsa-miR-148a-3p). Figure 4.37.

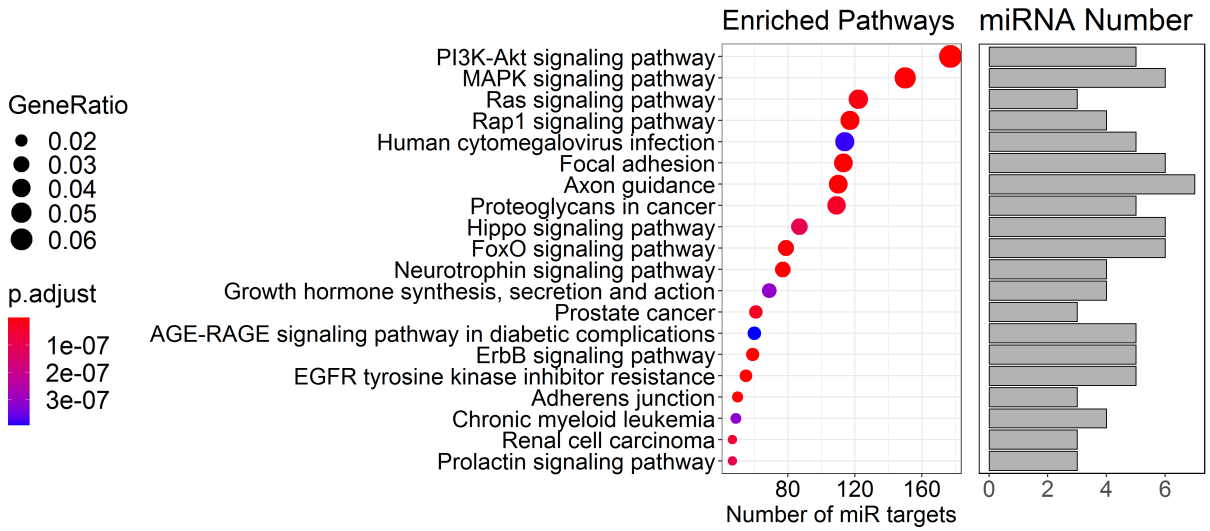

Figure 4.37: The top significant pathways targeted by 8 human miRNAs induced by aggressive cytokines mix and hypoxia. The number of target genes and number of involved miRNAs for each pathway are indicated. The target genes of the analyzed miRNAs were pooled and only the unique targets were further analyzed to identify enriched pathways. The dot size indicates the gene ratio: the ratio of the genes from the pathway to the input target genes. The dot color shows the *p* value.

4.4.3 Comparing miRNAs induced in human and mouse islet stress model

From the nine human miRNA measured in the *in vitro* model, miR-375-3p, miR-30c-5p, miR-200c-3p, and miR-129-5p, that showed significant increase in the supernatant, had also been found significantly increased in mouse islets treated with aggressive cytokines mix and hypoxia after 24H (Figure 4.38A). miR-148a-3p and miR-141-3p showed significant increase only in the supernatant of treated human islets and not in mouse islets (Figure 4.38B). miR-132-3p showed significant increase only in the supernatant of treated mouse islets and not in human islets (Figure 4.38B). let-7e-5p and miR-127-5p were also measured in the human and the mouse model, but they were excluded during data analysis and processing in the mouse model.

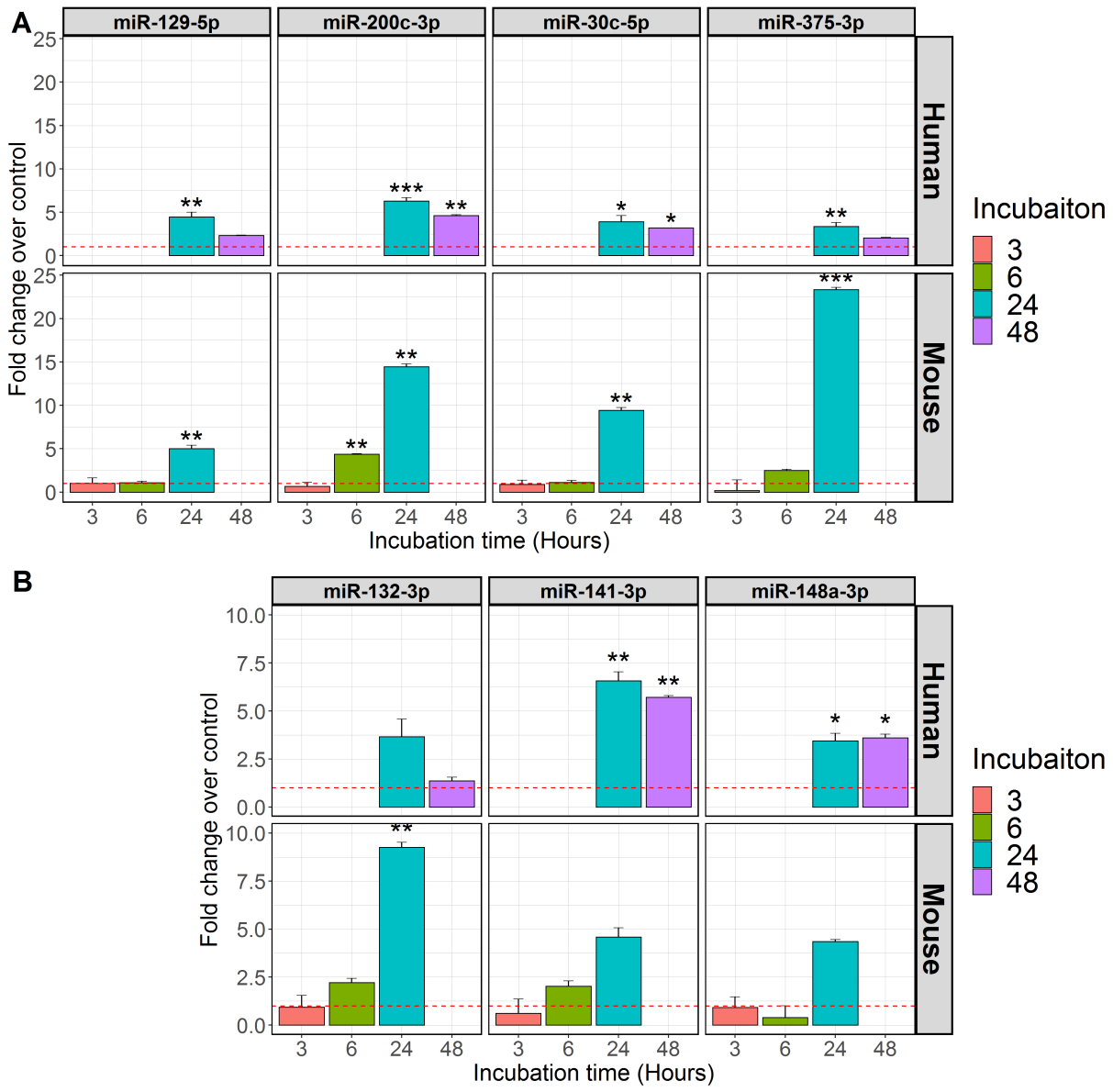

Figure 4.38: The measurements of 7 miRNAs in human and mouse islet stress model. A: miR-375-3p, miR-30c-5p, miR-200c-3p, and miR-129-5p showed significant increase in both species or **B**: only in one; miR-148a-3p and miR-141-3p (human), miR-132-3p (mouse). Human and mouse islets were treated with aggressive cytokines mix and hypoxia for 24H, and 48H for human islets, 3H, 6H, and 24H for mouse islets. The data are presented as fold change relative to untreated islets (control) in each model (FC ± SEM). For human: control: N=3, treated islets: N=3. For mouse: control: N=4, treated islets: N=4. Triplicates were performed in qPCR. Horizontal dotted line in red indicates FC=1. The sequence of presented miRNAs is identical between human and mouse. Two-way ANOVA followed by Tukey's HSD multiple comparison test was performed for statistical analysis. *$p < 0.05$, **$p < 0.01$ and ***$p < 0.001$.

4.4.4 Human Panel

A Final human miRNA panel which contains potential human miRNA biomarkers was assembled as follows (Figure 4.39):

From 64 Mouse miRNAs presented in figure 4.20, peers in human species were searched for in miRBase version 22.1 by mature ID or by sequence (Table 23). 51 miRNAs were identified and selected for the human panel. 31 with and 20 without identical sequence. One miRNA (miR-204-5p) was added from the day 4 measurements (Panel A1) to this panel.

The 16 mouse miRNAs excluded during the data analysis and processing were re-considered for further testing and included in the human panel if a human homolog was found (as described above). (Table 24). 9 were included with and 3 without identical sequence.

2 additional human miRNAs, recently described as potential islet specific miRNAs, were added to the panel (Table 25).

15 miRNAs (Figure 4.4B), initially discovered by literature search and confirmed by qPCR were added to the human panel (Table 26).

18 miRNAs were tested and confirmed previously (Figure 4.6) as reference miRNAs in healthy human serum and were added to the human panel to be tested and selected in the context of islet transplantation and hence can be used as reference genes for data normalization (Table 27).

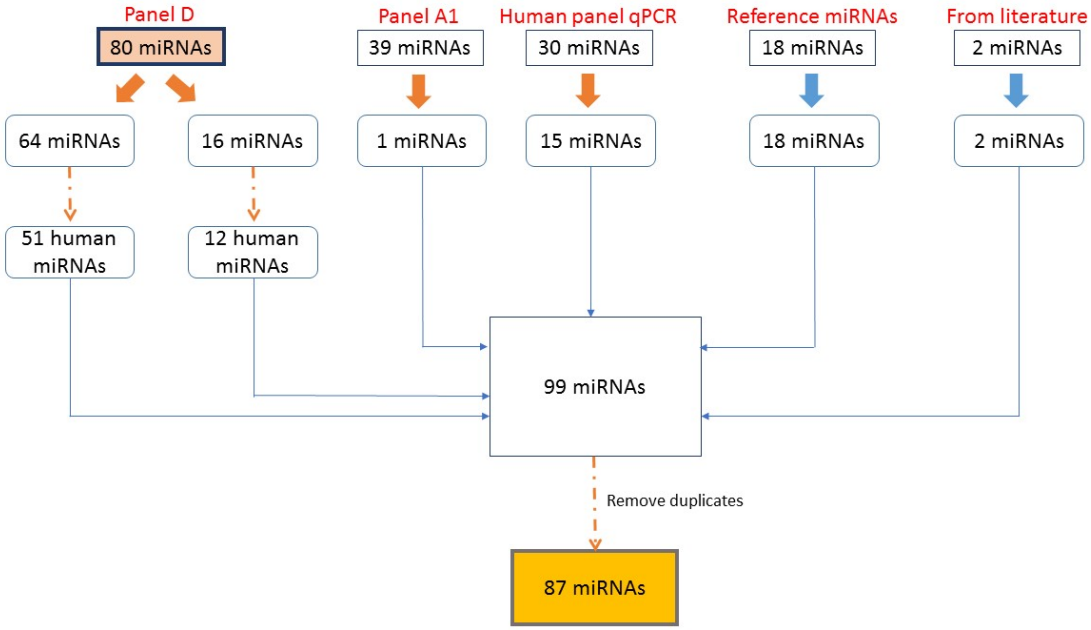

Figure 4.39: Illustration of human panel selection

Table 23: 64 Mouse miRNAs of which 51 miRNAs found in human. Last column indicates whether the sequence of a miRNA is identical between the two species or not. The ID in mouse and human is presented.

Mouse ID	Human ID	Human seq	Seq homology
mmu-miR-541-5p	hsa-miR-541-5p	AAAGGAUUCUGCUGUCGGUCCCACU	no
mmu-miR-384-3p	hsa-miR-384	AUUCCUAGAAAUUGUUCAUA	no
mmu-miR-770-5p	hsa-miR-770-5p	UCCAGUACCACGUGUCAGGGCCA	no
mmu-miR-582-5p	hsa-miR-582-5p	UUACAGUUGUUCAACCAGUUACU	no
mmu-miR-381-5p	hsa-miR-381-5p	AGCGAGGUUGCCCUUUGUAUAU	no
mmu-miR-136-5p	hsa-miR-136-5p	ACUCCAUUUGUUUUGAUGAUGGA	no
mmu-miR-222-3p	hsa-miR-222-3p	AGCUACAUCUGGCUACUGGGU	no
mmu-miR-151-3p	hsa-miR-151a-3p	CUAGACUGAAGCUCCUUGAGG	no
mmu-miR-7a-2-3p	hsa-miR-7-1-3p	CAACAAAUCACAGUCUGCCAUA	no
mmu-miR-7a-2-3p	hsa-miR-7-2-3p	CAACAAAUCCCAGUCUACCUAA	no
mmu-miR-384-5p	hsa-miR-384	AUUCCUAGAAAUUGUUCAUA	no
mmu-miR-668-3p	hsa-miR-668-3p	UGUCACUCGGCUCGGCCCACUAC	no
mmu-miR-485-3p	hsa-miR-485-3p	GUCAUACACGGCUCUCCUCUCU	no

Table 23: *(continued)*

Mouse ID	Human ID	Human seq	Seq homology
mmu-miR-383-5p	hsa-miR-383-5p	AGAUCAGAAGGUGAUUGUGGCU	no
mmu-miR-325-3p	hsa-miR-325	CCUAGUAGGUGUCCAGUAAGUGU	no
mmu-miR-130b-5p	hsa-miR-130b-5p	ACUCUUUCCCUGUUGCACUAC	no
mmu-miR-34c-3p	hsa-miR-34c-3p	AAUCACUAACCACACGGCCAGG	no
mmu-miR-412-5p	hsa-miR-412-5p	UGGUCGACCAGUUGGAAAGUAAU	no
mmu-miR-1193-3p	hsa-miR-1193	GGGAUGGUAGACCGGUGACGUGC	no
mmu-miR-370-5p	hsa-miR-370-5p	CAGGUCACGUCUCUGCAGUUAC	no
mmu-miR-375-3p	hsa-miR-375	UUUGUUCGUUCGGCUCGCGUGA	yes
mmu-miR-7a-5p	hsa-miR-7-5p	UGGAAGACUAGUGAUUUUGUUGU	yes
mmu-miR-200c-3p	hsa-miR-200c-3p	UAAUACUGCCGGGUAAUGAUGGA	yes
mmu-miR-129-5p	hsa-miR-129-5p	CUUUUUGCGGUCUGGGCUUGC	yes
mmu-miR-433-3p	hsa-miR-433-3p	AUCAUGAUGGGCUCCUCGGUGU	yes
mmu-miR-487b-3p	hsa-miR-487b-3p	AAUCGUACAGGGUCAUCCACUU	yes
mmu-miR-485-5p	hsa-miR-485-5p	AGAGGCUGGCCGUGAUGAAUUC	yes
mmu-miR-340-3p	hsa-miR-340-3p	UCCGUCUCAGUUACUUUAUAGC	yes
mmu-miR-323-3p	hsa-miR-323a-3p	CACAUUACACGGUCGACCUCU	yes
mmu-miR-543-3p	hsa-miR-543	AAACAUUCGCGGUGCACUUCUU	yes
mmu-miR-141-3p	hsa-miR-141-3p	UAACACUGUCUGGUAAAGAUGG	yes
mmu-miR-200b-3p	hsa-miR-200b-3p	UAAUACUGCCUGGUAAUGAUGA	yes
mmu-miR-98-5p	hsa-miR-98-5p	UGAGGUAGUAAGUUGUAUUGUU	yes
mmu-miR-184-3p	hsa-miR-184	UGGACGGAGAACUGAUAAGGGU	yes
mmu-miR-23b-3p	hsa-miR-23b-3p	AUCACAUUGCCAGGGAUUACC	yes
mmu-miR-132-3p	hsa-miR-132-3p	UAACAGUCUACAGCCAUGGUCG	yes
mmu-miR-411-5p	hsa-miR-411-5p	UAGUAGACCGUAUAGCGUACG	yes
mmu-miR-409-3p	hsa-miR-409-3p	GAAUGUUGCUCGGUGAACCCCU	yes
mmu-miR-652-3p	hsa-miR-652-3p	AAUGGCGCCACUAGGGUUGUG	yes
mmu-miR-379-5p	hsa-miR-379-5p	UGGUAGACUAUGGAACGUAGG	yes
mmu-miR-148a-3p	hsa-miR-148a-3p	UCAGUGCACUACAGAACUUUGU	yes
mmu-miR-30c-5p	hsa-miR-30c-5p	UGUAAACAUCCUACACUCUCAGC	yes
mmu-miR-423-3p	hsa-miR-423-3p	AGCUCGGUCUGAGGCCCCUCAGU	yes
mmu-miR-423-5p	hsa-miR-423-5p	UGAGGGGCAGAGAGCGAGACUUU	yes

Table 23: *(continued)*

Mouse ID	Human ID	Human seq	Seq homology
mmu-miR-99b-5p	hsa-miR-99b-5p	CACCCGUAGAACCGACCUUGCG	yes
mmu-miR-29b-3p	hsa-miR-29b-3p	UAGCACCAUUUGAAAUCAGUGUU	yes
mmu-miR-200b-5p	hsa-miR-200b-5p	CAUCUUACUGGGCAGCAUUGGA	yes
mmu-miR-409-5p	hsa-miR-409-5p	AGGUUACCCGAGCAACUUUGCAU	yes
mmu-miR-370-3p	hsa-miR-370-3p	GCCUGCUGGGGUGGAACCUGGU	yes
mmu-miR-153-3p	hsa-miR-153-3p	UUGCAUAGUCACAAAAGUGAUC	yes
mmu-miR-216b-5p	hsa-miR-216b-5p	AAAUCUCUGCAGGCAAAUGUGA	yes
mmu-miR-7b-5p	NA	NA	NA
mmu-miR-434-5p	NA	NA	NA
mmu-miR-434-3p	NA	NA	NA
mmu-miR-320-3p	NA	NA	NA
mmu-miR-5099	NA	NA	NA
mmu-miR-3968	NA	NA	NA
mmu-miR-667-3p	NA	NA	NA
mmu-miR-673-5p	NA	NA	NA
mmu-miR-3099-3p	NA	NA	NA
mmu-miR-666-5p	NA	NA	NA
mmu-miR-325-5p	NA	NA	NA
mmu-miR-666-3p	NA	NA	NA
mmu-miR-3072-3p	NA	NA	NA
mmu-miR-3547-3p	NA	NA	NA
mmu-miR-204-5p	hsa-miR-204-5p	UUCCCUUUGUCAUCCUAUGCCU	yes

Table 24: 16 mouse miRNAs of which 12 found in human (9 with- and 3 without identical sequence). The ID in human and mouse is presented.

Mouse ID	Human ID	Human seq	Seq homology
mmu-let-7e-5p	hsa-let-7e-5p	UGAGGUAGGAGGUUGUAUAGUU	yes
mmu-miR-141-5p	hsa-miR-141-5p	CAUCUUCCAGUACAGUGUUGGA	no
mmu-miR-127-5p	hsa-miR-127-5p	CUGAAGCUCAGAGGGCUCUGAU	yes
mmu-let-7d-5p	hsa-let-7d-5p	AGAGGUAGUAGGUUGCAUAGUU	yes

Table 24: *(continued)*

Mouse ID	Human ID	Human seq	Seq homology
mmu-let-7c-5p	hsa-let-7c-5p	UGAGGUAGUAGGUUGUAUGGUU	yes
mmu-let-7b-5p	hsa-let-7b-5p	UGAGGUAGUAGGUUGUGUGGUU	yes
mmu-miR-129-2-3p	hsa-miR-129-2-3p	AAGCCCUUACCCCAAAAAGCAU	yes
mmu-miR-129-1-3p	hsa-miR-129-1-3p	AAGCCCUUACCCCAAAAAGUAU	yes
mmu-miR-1224-5p	hsa-miR-1224-5p	GUGAGGACUCGGGAGGUGG	no
mmu-miR-23b-5p	hsa-miR-23b-5p	UGGGUUCCUGGCAUGCUGAUUU	no
mmu-miR-101a-3p	hsa-miR-101-3p	UACAGUACUGUGAUAACUGAA	yes
mmu-miR-154-3p	hsa-miR-154-3p	AAUCAUACACGGUUGACCUAUU	yes
mmu-miR-770-3p	NA	NA	NA
mmu-let-7k	NA	NA	NA
mmu-miR-129b-3p	NA	NA	NA
mmu-miR-6238	NA	NA	NA

Table 25: 2 human miRNAs were added to the human panel from literature.

Mouse ID	Human ID	Human seq	Reference
Not tested	hsa-miR-181a-5p	AACAUUCAACGCUGUCGGUGAGU	(Liu et al., 2019)
Not tested	hsa-miR-216a-5p	UAAUCUCAGCUGGCAACUGUGA	(Saravanan et al., 2019)

Table 26: 15 miRNAs initially discovered by literature search and confirmed by qPCR. The ID, sequence, Tm (melting temperature) and E (primer amplification efficiency) are indicated.

miRNA	Sequence	Tm	E
hsa-miR-21-5p	UAGCUUAUCAGACUGAUGUUGA	79.42	1.96
hsa-miR-125b-5p	UCCCUGAGACCCUAACUUGUGA	79.29	1.91
hsa-miR-29b-3p	UAGCACCAUUUGAAAUCAGUGUU	78.97	1.93
hsa-miR-148a-3p	UCAGUGCACUACAGAACUUUGU	79.14	1.92
hsa-miR-7-5p	UGGAAGACUAGUGAUUUUGUUGU	79.08	1.92
hsa-miR-375	UUUGUUCGUUCGGCUCGCGUGA	80.81	1.95

Table 26: *(continued)*

miRNA	Sequence	Tm	E
hsa-miR-200c-3p	UAAUACUGCCGGGUAAUGAUGGA	79.48	1.90
hsa-miR-23b-3p	AUCACAUUGCCAGGGAUUACC	79.22	1.94
hsa-miR-199a-5p	CCCAGUGUUCAGACUACCUGUUC	79.18	1.93
hsa-miR-136-3p	CAUCAUCGUCUCAAAUGAGUCU	78.92	1.94
hsa-miR-153-3p	UUGCAUAGUCACAAAAGUGAUC	78.70	1.93
hsa-miR-143-3p	UGAGAUGAAGCACUGUAGCUC	79.08	1.95
hsa-miR-27b-3p	UUCACAGUGGCUAAGUUCUGC	79.20	1.93
hsa-miR-192-5p	CUGACCUAUGAAUUGACAGCC	79.30	1.93
hsa-miR-30a-5p	UGUAAACAUCCUCGACUGGAAG	79.55	1.93

Table 27: 18 miRNAs were added to the human panel to be tested and selected in the context of islet transplantation and hence can be used as reference genes for data normalization. The ID, sequence, Tm (melting temperature) and E (primer amplification efficiency) are indicated.

miRNA	Sequence	Tm	E
hsa-miR-23a-3p	AUCACAUUGCCAGGGAUUUCC	79.50	1.91
hsa-miR-103a-3p	AGCAGCAUUGUACAGGGCUAUGA	79.67	1.94
hsa-let-7a-5p	UGAGGUAGUAGGUUGUAUAGUU	79.18	1.90
hsa-miR-26a-5p	UUCAAGUAAUCCAGGAUAGGCU	79.22	1.94
hsa-miR-423-5p	UGAGGGGCAGAGAGCGAGACUUU	79.51	1.92
hsa-miR-21-5p	UAGCUUAUCAGACUGAUGUUGA	79.42	1.96
hsa-miR-222-3p	AGCUACAUCUGGCUACUGGGU	79.61	1.93
hsa-miR-92a-3p	UAUUGCACUUGUCCCGGCCUGU	80.17	1.93
hsa-miR-24-3p	UGGCUCAGUUCAGCAGGAACAG	79.97	1.94
hsa-miR-191-5p	CAACGGAAUCCCAAAAGCAGCUG	79.58	1.93
hsa-miR-146a-5p	UGAGAACUGAAUUCCAUGGGUU	79.33	1.95
hsa-miR-145-5p	GUCCAGUUUUCCCAGGAAUCCCU	80.02	1.94
hsa-miR-126-3p	UCGUACCGUGAGUAAUAAUGCG	79.17	1.93

Table 27: *(continued)*

miRNA	Sequence	Tm	E
hsa-miR-93-5p	CAAAGUGCUGUUCGUGCAGGUAG	80.05	1.95
hsa-miR-26b-5p	UUCAAGUAAUUCAGGAUAGGU	79.18	1.94
hsa-miR-25-3p	CAUUGCACUUGUCUCGGUCUGA	79.85	1.95
hsa-miR-22-3p	AAGCUGCCAGUUGAAGAACUGU	79.71	1.94
hsa-let-7c-5p	UGAGGUAGUAGGUUGUAUGGUU	79.40	1.93

5 Discussion

Islet transplantation is a promising strategy to manage difficult-to-control type 1 diabetes patients. It confers the opportunity to relinquish insulin injections and improve quality of life. The procedure is hindered by islet loss which is triggered by harmful stressors such as hypoxia and inflammation. The detection of islet loss is of great importance to improve the transplantation outcomes. Current tools do not detect islet destruction before massive loss already occurred. Therefore, an indicator that can detect early islet loss could facilitate early intervention before a great mass of islets is destroyed. Many efforts have been given to research the potential of miRNAs as biomarkers of various diseases, among them type 1 diabetes. Their roles as markers of islet stress and death in the context of islet transplantation are emerging. Here, I identified miRNAs, which are released from islets in response to stressors or after cell death and therefore are reflective of islets stress and death. My *in vitro* and *in vivo* experiments demonstrated a direct relation between miRNA release and the stressor types as indicated by the pathway analysis of miRNA target genes. My results indicate that miRNAs could be detected after stress exposure before gross islet dysfunction takes place *in vitro*. Lastly, my experiments on mouse- and human islets showed that transferring findings from a mouse to a human model is possible.

In theory, miRNAs which are highly expressed in islets and are absent in the circulation, appear in the circulation after islet destruction or injury due to exposure to stressors or after cell death. Therefore, they represent potential candidate biomarkers indicating that islets are subjected to stressors. In line with this theory, I established a panel of miRNAs with high expression in islets as compared to serum. In the process of assembling the panel, I identified limitations and advantages to my approach. A considerable number of miRNAs were identified through literature search. Many of them were confirmed to have high expression in islets as compared to serum but some were not confirmed. MiRNA profiling using small RNA sequencing revealed a large number of miRNAs significantly differed between islets and serum. The profiling data on one hand showed that the top highly expressed miRNAs in islets were consistent with previously reported studies (Tattikota et al., 2014), and on the other hand extended the available data of the islet-miRNome. In the mouse, I showed that the measurement of miRNAs in islets and serum could be greatly exploited to identify miRNAs with higher expression in islets as compared to serum since I obtained samples from both tissues from the same animal. However, in human,

it was not possible to obtain islets and blood samples from the same donor. The islets were obtained from healthy deceased donors while the blood samples stemmed from other, healthy living donors and this could be a limitation since it is not clear whether the miRNome in islets as compared to serum could differ significantly between individuals.

To quantify a target miRNA, a reference miRNA is required for the normalization of RT-qPCR data. Unfortunately, reference miRNA that is stably expressed in all tissue types does not exist yet. Therefore, I needed to assess the stability of potential reference miRNAs in my various sample types, respecting the treatment conditions I applied. The use of multiple reference miRNAs is a gold standard ensuring the robustness of the analysis. The utility of stable endogenous miRNA corrects for variations related to the samples such as sampling and samples quality and reveals true alterations in target miRNA level. I found reference miRNAs for my RT-qPCR analysis in mouse and human.

My data revealed miRNAs, which could be stably expressed in serum of mice treated with STZ as well as in untreated animals. STZ created a hyperglycemic milieu and induced islet destruction. Stable miRNAs in such conditions are essential to detect real alterations in circulating miRNAs. I confirmed the stable expression patterns of the tested miRNAs using NormFinder algorithm. The algorithm takes Cq values as input data and it is capable of analyzing more than one treatment condition. The output of such algorithm is stability values; lower values indicate higher stability. Using these tools, I identified miRNAs stably expressed in the circulation of control-mice that therefore could be used to normalize target miRNAs level in the presence of STZ.

My findings were supported by another study done in similar conditions which showed stable expression patterns of the tested miRNAs in NOD mice (Mi et al., 2012). However, another study showed unstable patterns, but it was done using a different disease model (Chen et al., 2016). This supports the notion that individualized assessment of miRNAs in each experimental condition of interest is needed.

I also tested the stability of a group of miRNAs in healthy human serum samples. Here I used RefFinder in addition to NormFinder and both methods revealed comparable stability of the tested miRNAs. The advantage of using RefFinder is that the algorithm incorporates the other known algorithms (comparative Delta-Ct method, BestKeeper, geNorm, and NormFinder) to generate a comprehensive ranking of reference genes. Nevertheless, NormFinder is superior to RefFinder

because it offers the possibility to assess genes' stability in different sample groups (treated or untreated), the reason why I chose to use it in the STZ- model. The limitation of those algorithms is that they are not capable of identifying a cut-off stability value of the tested reference genes. However, the ranking provided by those algorithms gives valuable information that guided me in my selection of the most stable genes. Of note, two highly stable miRNAs I found in human serum had been reported previously to be stably expressed in human plasma in health and disease condition (Barry et al., 2015; Korma et al., 2020).

Because the supernatant of cultured islets is an artificial environment and does not contain miRNA profiles of body fluids such as serum, a search for miRNAs stably expressed in the supernatant is obsolete. I showed that the addition of a synthetic miRNA to the supernatant samples could be an alternative to the missing endogenous miRNAs. My results showed that the concentration of the spike-in miRNA did not vary across supernatant samples and thus can be used for miRNA normalization in the supernatant samples. The disadvantage of the use of a spike-in is that it does not correct for variations occurring before the RNA isolation process such as sample collection. However, the normalization to a synthetic miRNA is still used in the literature (Turchinovich et al., 2011; Geekiyanage et al., 2020). In our *in vitro* model, miRNAs released from islets were measured. Therefore, ideally, miRNA normalization should be performed using a stably released miRNA. However, the identification of such miRNA released from islets into the supernatant in a stable manner, without being affected by treatment conditions, would require further investigation.

To assemble my miRNA panels and to select normalizers, I analyzed the release of hypothetically islet specific miRNA during islet stress and after islet death. I showed that miRNAs could be detected, *in vivo*, in the circulation following the administration of STZ to the mice. The experimental design allowed me to explore the dynamics of miRNAs release throughout 4 days after treatment. In my experiment, the monitoring of blood glucose and body weight before and after STZ injection showed that the majority of the mice were diabetic by day 4 and only a fraction of the animals did not develop diabetes by day 4. The development of severe diabetes in STZ-treated mice is time dependent and it is known that more than 90% of mice develop diabetes eventually, after more than 5 days of treatment (Deeds et al., 2011). This implies that even most euglycemic STZ-treated mice could have a degree of islet stress/death after 4 days of treatment. Therefore, I exploited these animals to serve as a model of minimally injured islets. All samples from diabetic and non-diabetic STZ-treated animals were therefore used for miRNA

quantification.

The data obtained one day after treatment demonstrated that all STZ-treated animals were still euglycemic. MiR-375 increased immediately at the first day after acute islet destruction caused by STZ and remained detectable after 72H of treatment. This suggests that miR-375 could be an indicator of early islet loss without overt hyperglycemia. A study found a comparable pattern of this miRNA, an elevation after 2H and after 1 day of STZ treatment was detected as well as at day 7 (Erener et al., 2013). No other miRNA showed an elevation until 3 days after treatment. I can speculate that a higher mass of islets needs to be destroyed for those miRNAs to be detected in the circulation. The correlation between islets mass and the level of detected miRNAs requires further study. Unfortunately, little is known about miRNA kinetics *in vivo*. A study proposed that the miRNA stability and thus their half-life in the circulation relies on their GC content. It showed that for some miRNAs the half-life varies from few- up to 12 hours (Coenen-Stass et al., 2019). This sequence-dependent stability could contribute to the heterogeneous patterns I observed for various miRNAs in the STZ mouse model.

STZ induces DNA damage and β-cell necrosis (Lenzen, 2008). The release of miRNAs after cell death caused by necrosis was proposed to be in the shape of free nucleic acid (naked miRNA) (Sims et al., 2018). While the striking stability of miRNAs is well established, whether this stability is attributed to the fact that the major fraction of circulating miRNAs is loaded into vesicles for export or bound to Ago proteins is still controversial. It could be speculated that even non-binding miRNAs (not loaded within vesicles and not bound to Ago) are resistant to degradation in the harsh environment of the serum and thus could explain the stability of STZ-induced miRNAs.

A limitation of using the STZ model is that the compound is not completely specific to β-cell. STZ acts by entering a cell through GLUT2 which is also present in liver, kidney, and intestine cells (Thorens, 2015). It remains unclear to which degree those tissues are affected by STZ in our model. The measurement of tissue-injury markers (for example AST/ALT for the liver) could provide a tool to assess STZ effect to other tissues.

The day 4 analysis revealed 15 miRNAs significantly elevated in diabetic, STZ-treated animals and 3 miRNAs in diabetic and non- diabetic STZ-treated animals. Importantly, those miRNAs were detected after relatively long time of islet injury broadening the detection-window of such potential markers. The longer life-span of those miRNAs could be explained by a study which showed that

miRNAs could be divided into two major groups, one short-living with a half-life up to 14H and another with half-life more than 24H (Marzi et al., 2016). Simultaneously, I showed that significant loss of β-cells had occurred already by day 4 after treatment. The immunofluorescence analysis of the pancreatic sections from diabetic mice indicated a significant decrease in insulin-positive cells compared to control animals. These findings, together with the presence of apoptotic β-cells, as indicated by the cleaved caspase 3 staining, provided evidence that the miRNAs detected in the circulation at this time point or before could be indicators of β-cell death. These markers were either accumulating in the circulation over time and their measurement became possible at day 4 and was only a snapshot, or they were indeed released only at day 4. Such hypotheses require further investigations in longer time course experiments.

Some miRNAs increased in the circulation of non-diabetic STZ-treated animals. These miRNAs could have the potential of detecting early islet death since they were elevated in euglycemic mice that had minimally destructed islets as indicated by immunofluorescence staining. The image analysis showed that the islets of this group of mice had no apoptosis activity and that there was no significant loss of insulin-positive cells in these animals. Mmu-miR-423-3p was particularly striking; it had high AUC values in diabetic STZ-treated and non-diabetic STZ-treated mice (0.82 in both). This miRNA increased significantly in diabetic- and non-diabetic STZ-treated mice after 4 days of treatment. This indicates that this miRNA could be sensitive to minor changes in β-cell mass rather than to β-cell dysfunction as it was increased in euglycemic animals as well as in hyperglycemic ones. This miRNA was also reported to be correlated with type 1 diabetes onset in humans (Garavelli et al., 2020).

Contrary to what I have found, a report showed that STZ was acting more on islet function rather than on mass since it shed more light on the STZ effects on the cellular- and whole pancreas level. It was shown that the β-cell mass was not hugely affected due to STZ treatment as indicated by the whole organ imaging. It was proposed that the deterioration in β-cell function holds more responsibility for hyperglycemia in the STZ-treated animals than the loss in their overall mass. The β-cell dysfunction was indicated by downregulation of GLUT2 and other important genes for β-cell function such as *Ins1* and *Ins2* (Hahn et al., 2020). Applied to our findings, we could speculate that the STZ-induced stress led to responses on the cellular level and that these responses could represent an attempt of β-cells to escape stress. The induction of these mechanisms could implicate several molecules, including miRNAs. Such molecules could be

upregulated in the earlier stages of stress response and then released passively when cells die. Further studies are needed to elucidate the mechanisms of STZ effect on β-cells prior to cell death.

I aimed to further investigate the release of miRNAs (panel D) from islets in response to clearly defined stressors. Inflammatory mediators and hypoxia were reported to be implicated in islet stress and death in the context of type 1 diabetes and islet transplantation (Maedler et al., 2002; Kim et al., 2007; Donath et al., 2010; Olsson et al., 2011; Yoshimatsu et al., 2017; Komatsu et al., 2018). I showed that indeed, miRNAs could be detected in the supernatant of cultured islets exposed to low oxygen culture environment (hypoxia) and/or cytokine cocktail (TNF-α, IFN-γ, and IL-1β). The results revealed that miRNA dynamics are stressor- and time-dependent. The stressors induced apoptosis in islets and impaired their ability to secrete insulin as indicated by cleaved-caspase-3 and GSIS assays.

Prior to miRNA measurements, it was not clear to which extent the stressed/destroyed islets would release RNA molecules such as miRNAs into their surrounding culture medium and therefore I first studied the small RNA quantity and size distribution in the supernatant of the samples after exposure to stress. In mouse, after the treatment with high dose cytokines and hypoxia, I showed that the small RNA/miRNA quantities in the culture medium were high early after exposure (6H) and started to decline over 24H and 48H (with a slight increase at 72H as compared to 48H). I hypothesized and showed that the decline in miRNA concentrations was due to their degradation.

The analysis of miRNA quantity and distribution in the supernatant of islet culture was not previously reported. The decline in miRNA concentration over time could be attributed to limited half-lives of miRNAs released from stressed islets. It was proposed that miRNA half-life *in vitro* varies for different miRNA-species, as some miRNAs showed less stability than others (Bail et al., 2010). In contrast, the authors of another study suggested that most miRNAs are complexed with Ago2 when released from cells and thus confer them high stability (Turchinovich et al., 2011).

Similarly, in human islets treated with high dose cytokines and hypoxia, I measured lower supernatant-miRNA concentration after 48H than after 24H. The concentrations of miRNA released from human islets to the culture medium were strikingly higher than those observed in the mouse. The distribution of supernatant-small RNA from human islet cultures showed a peak at 60nt after treatment which was absent without treatment. This peak was more pronounced at

24H than at 48H. It is not clear whether the 60nt-peak represents other RNA species released in response to stressors. Two small RNA families, transfer RNA (tRNA) and small nucleolar RNA (snoRNA) could be the species observed. However, tRNA are 73–90nt (Arroyo et al., 2021) and snoRNA are 60–300nt length (Malik et al., 2019). Further electrophoresis studies are needed to investigate the nature of this peak. I exposed mouse islets to five different treatment conditions to simulate different stress-exposure situations (Hypoxia +/- aggressive cytokines, Hypoxia +/- mild cytokines, and hypoxia alone). 80 miRNAs were quantified in the supernatant of treated islets after 3H, 6H, and 24H. The results revealed again that miRNA release occurred in various patterns. A series of miRNAs seemed to be affected by high dose cytokines earlier, after 3H. Another series was strikingly high after 6H in response to low dose cytokines and hypoxia. At 24H, more miRNAs were measured in response to all treatment conditions (Figure 4.20).

Some miRNAs showed comparable dynamics. For instance, cytokines induced the release both miR-7a-5p and miR-375 in a dose-dependent manner at 6H. However, this was not the case at 24H where low dose cytokines had stronger effect than the high dose. The measurements at all time points showed that the combination treatment with low dose cytokines and hypoxia led to higher miRNA release compared to high dose cytokines and hypoxia. Other miRNAs, such as miR-7a-2-3p and miR-99b-5p, showed high association with a high-dose cytokine treatment.

Cytokines and hypoxia were shown previously to induce miRNA release *in vitro* (Erener et al., 2013; Saravanan et al., 2019). My data showed that low-dose cytokines combined with hypoxia had a more pronounced effect on miRNA release quantitatively and qualitatively as compared to high-dose cytokines combined with hypoxia. After 6H, for example, 14 miRNAs were induced in the presence of low-dose cytokines combined with hypoxia while only 7 in the presence of high-dose cytokines combined with hypoxia, and at 24H, 33 and 29 miRNAs were induced, respectively. It seems that the cytokines alone had a dose-dependent effect, while in the combination treatment this was not present. The immense heterogeneity of miRNA release observed after the various treatment conditions suggests that miRNA release from stressed islets is a regulated process and not only a result of end-stage cell death. If miRNAs were released uniquely because of cell death, their levels and their nature would be comparable between all treatment conditions.

If miRNA release was indeed a regulated process, it could explain why a low dose of cytokines

induced a higher release of miRNAs as compared to a high dose of cytokines, in combination with hypoxia. High doses could be damaging to the islets to the extent of impairing mechanisms important for the regulated miRNA release while the low dose cytokines combined with hypoxia allowed the maintenance of such mechanisms. The induction of apoptosis starting after 3H of high dose cytokines combined with hypoxia and not of low dose cytokines combined with hypoxia would be consistent with a higher detrimental effect of the high dose cytokine/hypoxia combination. However, the regulated release of miRNA would be circumvented at the later time points (24H) because of cell death as indicated the elevation of caspase-3 activity. Thus, the high number of miRNAs detected here could rather be attributed to cell death and passive release of miRNAs.

Importantly, some miRNAs were detected even before the onset of apoptosis. These include, for example, the increase of miR-3968 at 3H and miR-184-3p at 6H in response to high dose cytokines. This observation suggests again, that these miRNAs are secreted in a regulated fashion. These miRNAs could serve as markers of early β-cell stress.

My data showed that cleaved caspase-3 was activated in the course of cytokine treatment but was absent in hypoxia treatment regardless of the time of exposure. There is controversy about this: a study found an elevation of cleaved caspase-3 protein in MIN6 cells (Bensellam et al., 2016) while another study reported a decrease in cleaved caspase-3 expression in response to hypoxia (Sato et al., 2014).

It was shown previously that apoptosis of β-cells induced by inflammatory cytokines occurs through a cascade of events. One of those events is the activation of caspase-3 which I was able to detect after the treatment with both doses. This activation was time-dependent and this was also observed in other studies (Demine et al., 2020). Interestingly, it seems that the dose of cytokines could determine the mechanism of β-cell death. High doses of cytokines promoted β-cell death through NO (nitric oxide) (Collier et al., 2006) while lower doses of cytokines acted through Bad (Bcl-2-associated death promoter (Phospho-Ser136)), caspases activation and others (Grunnet et al., 2009). This dose-dependent induction of β-cell death mechanisms could also explain the heterogeneous miRNA profiles found in this study. It is established that gene expression dysregulation in β-cells occurs in the context of cytokine exposure (Cardozo et al., 2001). Since miRNA are prime gene regulators, they could contribute to this dysregulation caused

by inflammatory cytokines. Some miRNAs elevated in islets in response to cytokine treatment and their blockage led to protection against apoptosis (Roggli et al., 2010).

Gene expression alterations after hypoxia treatment of islet cells were reported previously. It was proposed that hypoxic stress promotes apoptosis in islets cell by inducing expression of the transcription factor NFκB and the subsequent upregulation of genes implicated in apoptosis (Lai et al., 2009). However, other genes were downregulated (Sato et al., 2014). The downregulation effect could be regulated by the induction of certain miRNAs in response to hypoxia.

The combination between hypoxia and cytokines led to the detection of more miRNAs in the culture medium as compared to the single treatments. There are several points that require more attention and some additional experiments. First, it is not clear whether cross-talk between components of biological pathways induced by each treatment occur and contribute to the involvement of other miRNAs. The cytokine dose-effect I observe on miRNA release also requires further studies to be understood. Exposing the islets to a dilution series of cytokines and/or different O2 concentrations and analyzing the miRNA profiles in the culture supernatant could provide more information in this regard. To also better understand the relationship between miRNA secretion and a certain stressor, it could be useful to quantify miRNAs in islets and supernatant simultaneously. And last, exposure to strong stressors such as aggressive cytokines and hypoxia induced massive morphological changes in the islets and sometimes the islets were even completely destroyed, as shown by microscopy. Such islets were technically difficult to collect for miRNA quantification and this is a limitation to this study.

In parallel with quantification of miRNA in the culture supernatant, I studied the effect of the various treatment conditions on islet function. A major indicator of β-cell function is the ability to react to glucose concentration changes by secreting insulin. The glucose-stimulated insulin secretion assay (GSIS) is widely used to assess responsiveness to glucose. I assessed GSIS of the treated islets in the presence of two different glucose concentrations (2uM and 20uM) to document conditions that impair this function and synchronously identify miRNAs released. I showed that some miRNAs can be detected in the supernatant of treated islets before major changes in GSIS take place. The data show that the number of induced miRNAs increased drastically in parallel with the impairment of GSIS over time.

After 3H, cytokine or hypoxia treatment alone did not appear to be very damaging to the islet

function, with a minor increase in basal secretion and a slightly decreased stimulated secretion. However, the combination of hypoxia and cytokines (at either concentration was very damaging to islet function, with greatly elevated basal (2mM) secretion and no further response to 20mM glucose, suggestive of non-specific leakage of insulin, rather than regulated exocytosis. The findings at 6H were largely consistent with those at 3H but more pronounced, in accordance with the more prolonged incubation time. Low dose cytokines did not seem to be very damaging to the islets, with a small increase in basal secretion. However, high dose cytokines was clearly detrimental, as was hypoxia alone or in combination. With a combinational treatment, the secretory function appeared to be equally compromised at both time points (3H and 6H). The 24h data were consistent with the 3H and 6H data with basal rates of secretion increasing with time of exposure to the stressors.

It is well established that hypoxia induces Hypoxia-inducible factor-1α (HIF-1α), a transcription factor that regulates genes implicated in glucose metabolism and insulin secretion. For example, GLUT1 is up- and GLUT2 is downregulated in response to HIF-1α (Cantley et al., 2010).

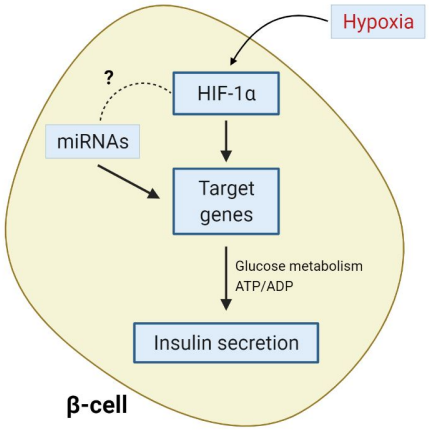

It has been proposed that these hypoxia-induced changes result in impairment of glucose control and GSIS *in vivo* and *in vitro* (Cantley et al., 2013). An interaction between miRNAs and HIF-1α was previously reported in several cells types (Spinello et al., 2015; Wang et al., 2016; Serocki et al., 2018). However, after 13 days, decreased levels of HIF-1α and elevated levels of miRNAs were detected in an islet transplantation model (Pileggi et al., 2013). Thus, the relation between HIF-1α and miRNA expression in β-cells is not fully understood. The investigation of roles of those miRNAs in the axis linking hypoxia to HIF-1α and to GSIS could potentially reveal therapeutic avenues.

Similar to hypoxic stress, cytokines are known to impair insulin secretion. IL-1β for example was found to reduce the presence of important proteins such as insulin in β-cells, proposedly through the induction of NF-κB (Papaccio et al., 2005). Upon exposure to cytokines, NF-κB was induced and a changed expression of several genes could be detected (Sarkar et al., 2009). It

was proposed that during GSIS, NF-κB plays a role in transferring the Ca^{+2} signal to the nucleus and so maintains GSIS (Norlin et al., 2005). NF-κB could be a target of several miRNAs and conversely, NF-κB could promote or inhibit the expression of miRNAs (Ma et al., 2011). Based on these findings, cytokine-induced impairment of GSIS could be a result of interactions between miRNAs and NF-κB. Our data demonstrated that apoptosis occurred particularly in later time points after cytokine treatment and thus GSIS could be simply affected due to cell death at these time points. Therefore, miRNAs detected earlier could be more reflective of islet dysfunction.

Collectively, the information obtained through GSIS, the apoptosis dynamics and the miRNA release changes I measured allowed to build a model of stress. As an example, insulin secretion and caspase-3 activity in the presence of low dose cytokines revealed the following: after 3H islet function was maintained, islets did not show cell death and the secretion of miRNAs was unchanged. After 6H, islet function and viability remained unchanged, but the release of 2 miRNAs was induced. After 24H islet function was moderately compromised, cell death could be measured and the number of secreted miRNA increased simultaneously (Figure 5.1).

Motivated by the data obtained with the mouse model, I performed similar experiment using human islets. In the mouse experiments, islets were cultured for 3H, 6H and 24H, while in human experiments for 24H and 48H. Seven conserved miRNAs (with identical sequence in mouse and human; panel P) were measured in the supernatant of human islets treated with high dose cytokines with hypoxia. I compared the measurements of those miRNAs with their peers in the mouse experiment and found that four miRNAs showed a comparable induction in the mouse and human islet stress model. Two others were induced only in human and one was induced only in the mouse. These findings are encouraging and suggest that we can transfer the data gained in the *in vitro* mouse study to human.

The magnitude of miRNA release induction in the mouse was relatively higher than the one in human (Figure 4.38A). I found higher fold change of miRNA measurement in the islet culture supernatant induced by treatment in mouse than in human. However, it was reported previously that mouse islets are more vulnerable to stressors such as cytokines than human islets (Kawahara and Kenney, 1991) and our findings could well reflect this.

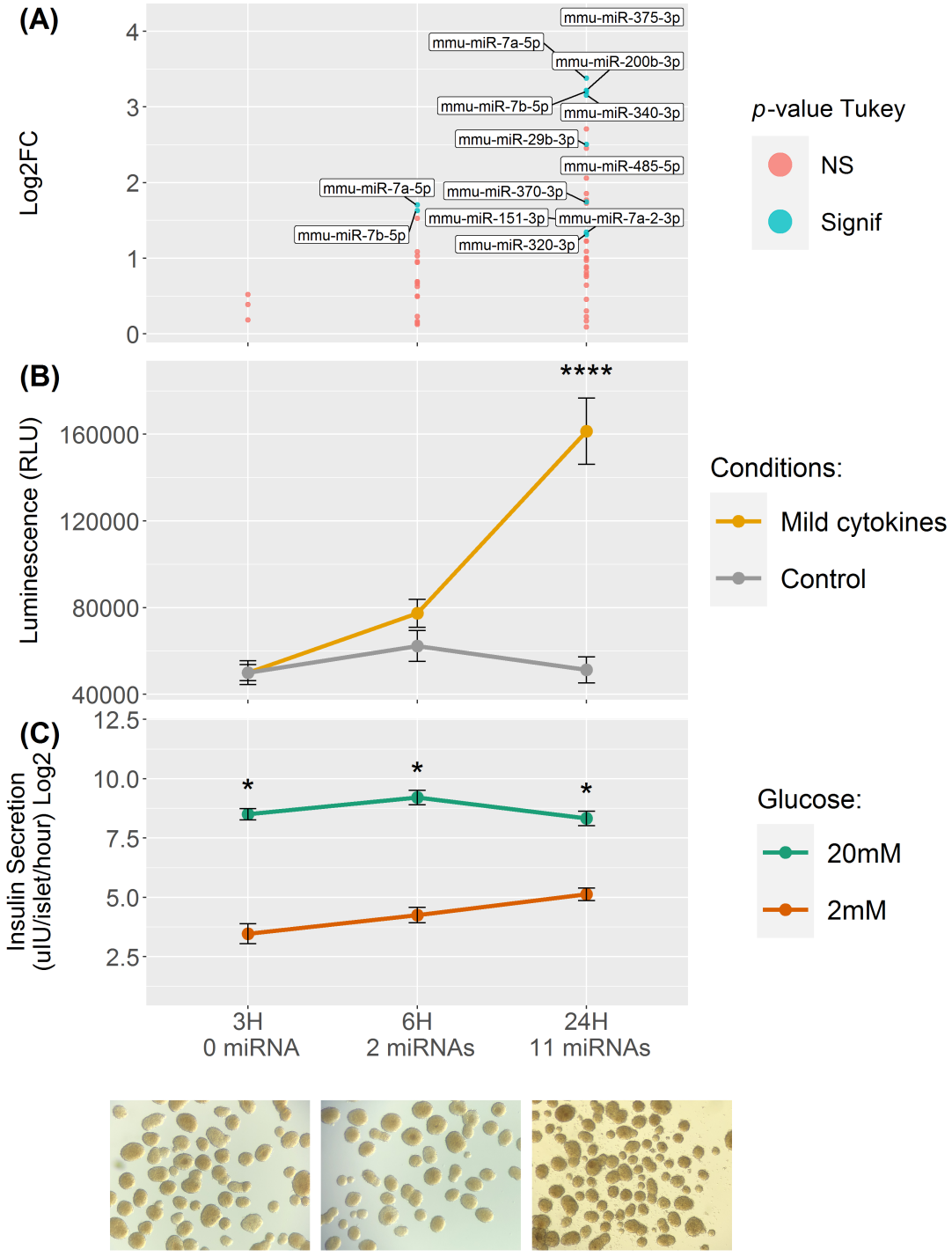

Figure 5.1: Schematic figure showing mild cytokine effects on mouse islets viability, function, and the presence in the culture supernatant of miRNAs after 3H, 6H, and 24H. A: miRNAs released into the supernatant of islets treated with mild cytokines (red: non-significant, blue: significant as indicated by Tukey HSD multiple comparisons to control untreated islets). **B**: Caspase activity in treated and untreated islets. **C**: GSIS assay in response to basic (2mM) and stimulated (20mM) glucose concentrations. Bottom annotation: exemplary images showing morphological changes in islets.

Performing a larger scale experiment in human islets, as performed in mouse with different treatment conditions and time points, was limited by some factors. First, human islets are not easily accessible particularly as compared to mouse islets due to scarcity of donors. Second, human islets function and quality differ between preparations (Kayton et al., 2015) and this could result in heterogeneity in response to stressors and thus has an impact on the measured miRNA dynamics.

The *in vitro* islet stress model allowed me to identify 64 potential miRNA biomarkers, which were induced by inflammatory and/or hypoxic stress over 3 time points. I aimed to find biological functions for the induced miRNAs. I therefore performed pathway analysis of mRNA targeted by those miRNAs. To do so I first identified the target genes of the miRNAs *in silico*.

In mouse, 3 cytokine-induced miRNAs were targeting genes primarily involved in MAPK signaling pathway while 7 and 13 miRNAs induced by the combinational treatment were targeting genes primarily involved in the PI3K-Akt signaling pathway and the MAPK signaling pathway, respectively.

The implication of the MAPK signaling pathway in islet cell death has been reported previously.

The stimulation of MAPKs (mitogen-activated protein kinases) has been reported in the context of cytokine-induced stress in β-cells and consecutive cell death (Abdelli et al., 2004). However, the mechanism by which MAPK are stimulated is not fully understood. A study suggested an important role for MEKK-1 (mitogen-activated protein kinase kinase-1) in the phosphorylation of JNK (c-Jun N-terminal kinase), which is a MAPK and induces the events leading to cell death by apoptosis (Mokhtari et al., 2008).

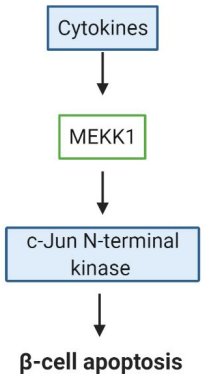

PI3K (Phosphatidylinositol 3-Kinase) has been found to be implicated in β-cell function (Eto et al., 2002) and dysfunction as a response to stress (Chen et al., 2006). I found that the addition of hypoxia to cytokine treatment triggered the release of miRNAs controlling the PI3K pathway. Indeed, the interaction between miRNAs and components of PI3K-Akt signaling pathway in the course of islet damage caused by hypoxic conditions was also reported previously (Zhang et al., 2017).

Interestingly, the two main pathways targeted by combination treatment-induced mouse miRNAs were also found to be the targets of miRNA induced under the same conditions in human islets. Here the PI3K-Akt signaling pathway (177 genes) is targeted by 5 miRNAs, while the MAPK signaling pathway (150 genes) is targeted by 6 miRNAs. It remains to be investigated whether those miRNAs have regulatory roles in vital β-cell function and in β-cell death and whether, therefore, they were upregulated in the presence of cell death and dysfunction, or whether they are final products of pathway/s cascade. It was suggested that the induction of a pathway network by a stimulus could control miRNA level through targeting their biogenesis. This control aims to execute or suppress biological functions of those miRNAs (Nikolov, 2013).

Importantly, our data show that the detection of certain miRNAs could allow us to retrospectively identify the initial stimulus that leads to β-cell defects or death (i.e. hypoxia or cytokines) through the identification of the targeted pathways. This could be of great value to monitor islet graft after transplantation. It would allow to select the appropriate medical intervention, reacting either to inflammatory or hypoxic stress.

In summary, I assembled a final panel of potential 87 miRNA candidate biomarkers, based on extensive *in vitro* and *in vivo* models. This panel is largely composed of miRNAs discovered in the *in vitro* and *in vivo* mouse model, but some human miRNAs were also added. Reference miRNAs for human serum miRNA quantification and normalization are also present in the panel.

The human panel will be validated in the context of clinical islet transplantation in the future. miRNAs will be measured in samples from patients, collected before and after transplantation. The metabolic data of the patients will be analyzed as well, allowing to find potential association with miRNAs level.

Future Outlook

The identified islet specific miRNAs that are released after β-cell death or stress could represent a very valuable clinical tool to detect islet stress and death at a very early stage, before a great mass of islets is lost. In this study, I found miRNAs increased in the circulation or the outer milieu during the earlier stages of stress. The advantage of using these miRNAs as biomarkers is that they potentially provide a timely alarm of ongoing islet stress.

In clinical settings, combining the detection potential of miRNA biomarkers, metabolites, and pathway analysis could be a cornerstone of close monitoring of islet graft. The flow chart (Figure 5.2) summarizes a strategy to be followed after islet transplantation. The presence of some miRNAs in the circulation could predict future or onset islet graft dysfunction. The correlation between miRNA level in the circulation and metabolites could provide even more information. Pathway analysis has allowed us to uncover mechanisms induced by the stressors and hence potentially will allow to plan interventions for example using compounds protecting the engrafted islets against hypoxic and/or inflammatory stress. These compounds could target components of the vital pathways identified, inducing or inhibiting them in a way that potentially modifies cell response to a stressor from dysfunction/death into adaptation. The development of miRNA-based therapeutics is emerging. It is of utmost importance to elucidate the interaction between miRNAs and molecules involved in stress pathways for miRNA targeting to be studied in this regard.

This thesis could be seen as a working pipeline to identify and validate multi-miRNA biomarkers that could finally find their way into clinical applications, not only in the context of islet transplantation but also in type 1 diabetes early-onset prediction.

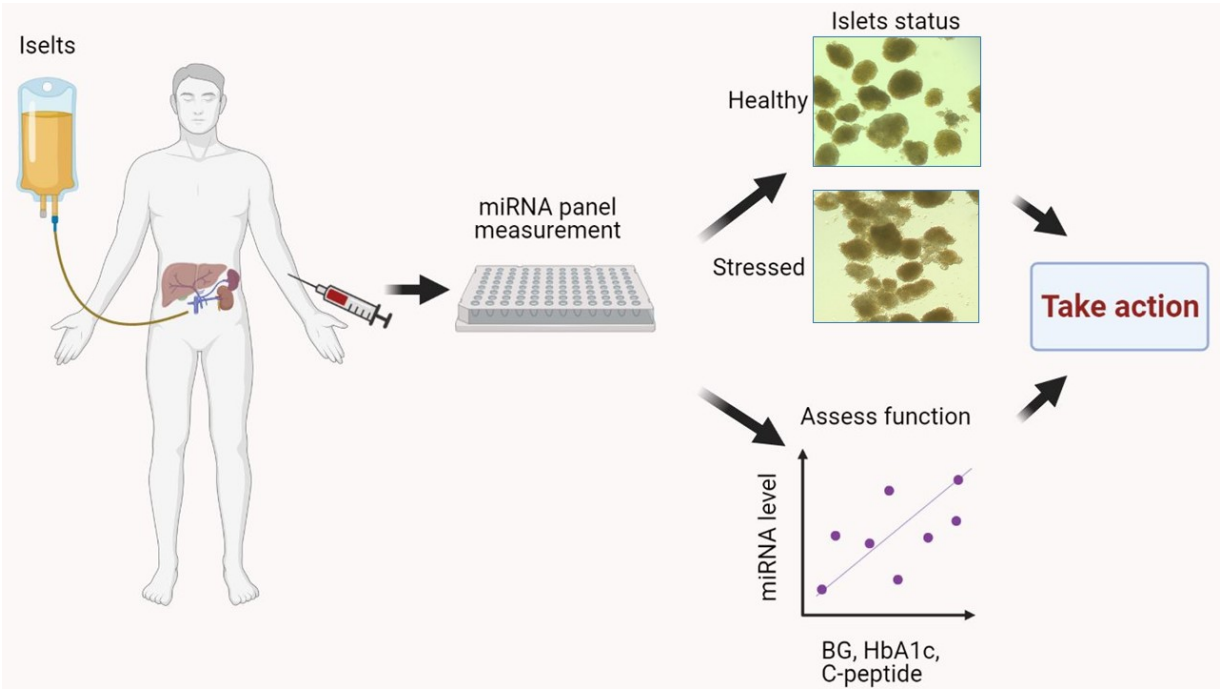

Figure 5.2: Future prospects of multi-miRNA biomarkers utility. After islet transplantation, quantification of a miRNA-biomarker set could provide precious information on “live” islet cell state as shown in images: healthy or damaged islets. The analysis of the relation between measured miRNAs and metabolites (conventional metabolites such as BG, HbA1c or stimulation tests such as MTT) would be valuable in sooner prediction of islet function deterioration. Jointly, the information provided would help to establish an intervention strategy. Human islets images were captured under light microscope.

6 Summary

Background

Replacement of β-cells via islet transplantation is a potential therapeutic approach for individuals with type 1 diabetes that is hard-to-control with conventional approaches. Post-transplantation, islets are prone to stress such as hypoxia and inflammation (Biarnes et al., 2002; Shahbazov et al., 2016). It is of utmost importance to diagnose β-cell insults before massive cell loss occur and hence rapid intervention can be taken. Currently utilized markers often fail to detect β-cell stress and death in timely manner and only indicate massive changes in β-cell function. Thus, biomarkers reflecting the actual rate of β-cell stress and death are required.

MiRNAs are short (21–25 nucleotides in length) single-stranded RNA molecules, originated from a hairpin-like structure. miRNAs are considered as post-transcriptional gene silencers. Studies have reported alteration in circulating miRNAs in type 1 diabetes and their implication in the pathogenesis of this disease (Erener et al., 2017; LaPierre and Stoffel, 2017). Such miRNAs could serve as circulating biomarkers for β-cell stress and death. After human islet transplantation, islets exposed to stresses release miRNAs potentially detectable in the circulation and reflecting the rate of islets stress or death.

Scientific aim

I aimed to identify circulating miRNAs that could be reflective of β-cell stress and death. To achieve this, I analyzed potential miRNA biomarkers in the circulation of diabetic animal model as well as in the context *in vitro* islet stress model.

Material and methods

To establish a panel of potential islet specific miRNAs I reviewed profiling studies in the literature and validated them using RT-qPCR on human/mouse islets and serum. For miRNA profiling, I used small RNA sequencing in mouse islets and serum. Previously used circulating reference miRNAs were identified through the literature and tested in healthy human serum samples as well as in control- and STZ-treated mice. Reference miRNAs were analyzed using NormFinder and/or RefFinder algorithms to identify stably expressed miRNAs.

For diabetes induction *in vivo*, BL6 mice were treated with STZ. MiRNAs were quantified in the

circulation before and after STZ treatment using RT-qPCR.

In the *in vitro* islet stress model, human or mouse islets were treated with a cocktail of recombinant IL-1β, TNF-α, and IFN-γ and/or hypoxia (1% O2). MiRNAs were quantified in the supernatant 3H, 6H, and 24H after cytokine and/or hypoxia treatment. Caspase-3 activity was measured in the islets to assess apoptosis in parallel with miRNA induction. Basal (2mM) and stimulated insulin secretion was quantified using ELISA in the supernatant of islets treated as described above.

KEGG enrichment analysis was performed on significantly induced miRNAs in order to identify targeted pathways.

Results

In mouse, a panel of 60 miRNAs was established through the validation of literature-selected miRNAs and NGS. Reference miRNAs for RT-qPCR data normalization of circulating miRNAs were analyzed and 2 miRNAs were selected as normalizers using NormFinder. In human 15 miRNAs were identified after validation of literature- selected miRNAs. 5 miRNAs were identified as reference miRNAs after confirmation of RefFinder and NormFinder analysis.

STZ treatment of mice led to increased serum concentrations of 24 of the 60 islet enriched miRNAs between 1 and 4 days post-treatment. Of these, 3 were also increased in treated mice that did not develop diabetes. Using this information, a panel of 80 miRNAs was assembled and used to measure miRNA release in relation to apoptosis and glucose stimulated insulin release in mouse and human islets exposed to cytokine and/or hypoxia induced stress *in vitro*. In total, 64 of the miRNAs increased in the supernatant of islets, treated with high or low dose cytokines and/or hypoxia, as compared to untreated islets over 3H, 6H, and 24H. A pathway analysis revealed that cytokine-induced miRNAs targeted genes primarily involved in MAPK signaling pathway, and that the cytokine plus hypoxia-induced miRNAs targeted genes primarily involved in PI3K-Akt and MAPK signaling pathway. Based on all the findings, a panel of 87 miRNAs was finally established and an assay to screen for these miRNAs was developed that can now be used for further validation in pre- and post-transplantation samples.

Conclusion

The work in the *in vivo* and *in vitro* models allowed the identification of potential miRNA biomarkers of islet stress and death that reflect the mode of induced stress. Those miRNAs could be used

to monitor islet graft post-transplantation. Further validation of those miRNAs is required in the context of islet transplantation in human samples.

7 Zusammenfassung

Hintergrund

β-Zell-Ersatz durch eine Inselzell-Transplantation ist ein potentieller Ansatz, um Typ 1 Diabetes Patienten zu behandeln, welche mit konventioneller Therapie schwierig zu kontrollieren sind. Nach einer Transplantation sind Inselzellen aber oft Hypoxie- und Entzündungs-Stress ausgesetzt (Biarnes et al., 2002; Shahbazov et al., 2016). Es ist sehr wichtig, solche Stressfaktoren so früh wie möglich zu erkennen, um noch klinisch intervenieren zu können, bevor die Inselzellen Schaden nehmen und massiver Zellverlust einsetzt. Die zurzeit bekannten Marker erlauben es aber nicht, β-Zell–Stress rechtzeitig zu erkennen, lediglich schon massive Veränderungen der β-Zell-Funktion können detektiert werden. Deshalb sind Biomarker nötig, welche eine frühzeitige Erkennung von β-Zell-Stress und Zerstörung erlauben.

miRNA sind kurze, einzel-strängige RNAs, welche aus einer Haarnadelstruktur entstehen und als post-transkriptionelle „Gen-Silencer“ bekannt sind. Studien berichten, dass im Serum von Typ 1 Diabetes Patienten Veränderungen in der Konzentration einiger miRNAs gemessen wurden; man vermutet daher, dass diese miRNAs an der Pathogenese der Krankheit beteiligt sind (Erener et al., 2017; LaPierre and Stoffel, 2017). Diese miRNAs könnten auch als zirkulierende Biomarker für Inselzell-Stress dienen. Nach einer Inselzell–Transplantation setzen Inselzellen miRNAs frei, welche man potentiell in der Zirkulation detektieren kann, und welche voranschreitenden β-Zell-Stress und Zerstörung reflektieren könnten.

Wissenschaftliche Zielstellung

Mein Ziel war es, zirkulierende miRNAs zu finden, welche β-Zell-Stress und Zerstörung reflektieren, und potentiell bei einer Insellzell-Transplantation zum Einsatz kommen könnten. Um dies zu erreichen, habe ich in einem Mausmodell und in einem *in vitro* Inselzell-Stress Modell Inselzell-spezifische, potentielle Biomarker untersucht.

Materialien und Methoden

Um eine Sammlung von Inselzell-spezifischen miRNAs zusammenzustellen, habe ich die Literatur durchsucht und zur Validierung der ausgewählten miRNAs habe ich qPCR und humanes- und Maus-Serum sowie Inselzellmaterial verwendet. Um weitere Inselzell-spezifische miRNAs zu entdecken, habe ich „small RNA Sequencing“ von Maus-Serum- und Inselzellmaterial angewen-

det. Zirkulierende Referenz-miRNAs habe ich in der Literatur entdeckt, und mittels qPCR mit humanem Serum und mit Serum von STZ-behandelten Mäusen und entsprechenden Kontrollen validiert. Um die stabilsten Referenz miRNAs zu finden, habe ich die Algorithmen „NormFinder und RefFinder“ benutzt.

Um Diabetes *in vivo* zu induzieren, habe ich BL6 Mäuse mit STZ behandelt. miRNAs in der Zirkulation wurden vor und nach der Behandlung mittels qPCR quantifiziert.

Im *in vitro* Stress-Modell wurden humane oder Maus-Inselzellen mit einem Cocktail aus rekombinantem IL-1β, TNF-α und IFN-γ und/oder mit Hypoxia (1% O2) behandelt. miRNAs wurden 3H, 6H und 24H nach der Behandlung im Kulturüberstand gemessen.

Um Apoptose zu messen, wurde parallel zu der miRNA-Induktion die Caspase-3 Aktivität in den Inselzellen gemessen. Basale- und stimulierte Insulin-Sekretion wurde mittels ELISA aus dem Kulturüberstand der behandelten Inselzellen gemessen. Um relevante Signalwege zu finden, wurden die signifikant induzierten miRNAs mittels „KEGG enrichment“ analysiert.

Resultate

Ich habe 60 potentielle Inselzell-spezifische Maus-miRNAs validiert, indem ich eine Literatur-Recherche sowie „small RNA Sequencing“ durchgeführt habe. Ich habe zirkulierende Referenz-miRNAs für die qPCR Analyse identifiziert und 2 davon wurden mit „NormFinder und RefFinder“ als die am besten geeigneten Referenzen ausgewählt. 15 humane, in der Literatur gefundene und potentielle Inselzell-spezifische miRNAs, sowie 5 Referenz-miRNAs für die qPCR Analyse wurden experimentell validiert.

Die STZ-Behandlung der Mäuse führte zu einer im Serum messbaren Erhöhung von 24 der 60 ausgewählten miRNAs, von Tag 1 auf Tag 4 nach der Behandlung. 3 dieser miRNAs waren auch im Serum von Mäusen, welche nach der Behandlung nicht diabetisch wurden, erhöht. Die aus der Literatur-Recherche und den *in vivo* Experimenten gewonnene Information wurde genutzt, um eine Sammlung von 80 miRNAs zusammen zu stellen, welche *in vitro* eingesetzt wurde. miRNA-Freisetzung wurde dazu im Zusammenhang mit Apoptose und stimulierter Insulin-Sekretion in humanen- und Maus-Inselzellen, welche Zytokin- und/oder Hypoxia-induziertem Stress ausgesetzt waren, gemessen. Im Ganzen konnte eine Anreicherung von 64 der getesteten miRNAs im Überstand von mit Zytokinen oder mit Hypoxia behandelten Inselzellen im Vergleich

zu unbehandelten Inselzellen nach 3H, 6H und 12H gemessen werden. Eine Signalweg Analyse zeigte, dass die Zytokin-induzierten miRNAs primär solche Gene, welche im MAPK-Signalweg involviert sind, und die Zytokin- und Hypoxia-induzierten miRNAs Gene des PI3K- und MAPK-Signalweges anvisieren.

Aufgrund all dieser Erkenntnisse konnte schlussendlich eine Sammlung von 87 potentiellen Biomarkern zusammengestellt und qPCR-„Assays“, um sie zu messen, etabliert werden. Diese können nun auf prä- und post-Transplantations-Serumproben validiert werden.

Schlussfolgerung

Meine Arbeit mit den *in vivo* und *in vitro* Modellen erlaubte mir, potentielle Biomarker für Inselzell-Stress und Tod zu identifizieren. Diese Biomarker erlauben auch Rückschlüsse auf den Stress, welcher auf die Inselzellen einwirkte. Diese Biomarker könnte man nun einsetzten, um Inselzell-Transplantate zu überwachen. Davor werden aber weitere Validierungsexperimente benötigt, welche diese Biomarker im Kontext einer Inselzell-Transplantation untersuchen.

References

Abdelli S, Ansite J, Roduit R, Borsello T, Matsumoto I, Sawada T, Allaman-Pillet N, Henry H, Beckmann JS, Hering BJ, Bonny C. 2004. Intracellular stress signaling pathways activated during human islet preparation and following acute cytokine exposure. Diabetes, 53(11):2815–2823 DOI: 10.2337/diabetes.53.11.2815.

Alles J, Fehlmann T, Fischer U, Backes C, Galata V, Minet M, Hart M, Abu-Halima M, Grässer FA, Lenhof H-P, Keller A, Meese E. 2019. An estimate of the total number of true human miRNAs. Nucleic Acids Res, 47(7):3353–3364 DOI: 10.1093/nar/gkz097.

AlRashidi FT, Gillespie KM. 2018. Biomarkers in islet cell transplantation for type 1 diabetes. Curr Diab Rep, 18(10):94 DOI: 10.1007/s11892-018-1059-4.

Alsaweed M, Hartmann P, Geddes D, Kakulas F. 2015. MicroRNAs in breastmilk and the lactating breast: Potential immunoprotectors and developmental regulators for the infant and the mother. IJERPH, 12(11):13981–14020 DOI: 10.3390/ijerph121113981.

American Diabetes Association. 2016. Classification and diagnosis of diabetes. Sec. 2. In standards of medical care in diabetes. Dia Care, 39(Supplement 1):S13–S22 DOI: 10.2337/dc16-S005.

Andersen CL, Jensen JL, Ørntoft TF. 2004. Normalization of real-time quantitative reverse transcription-PCR data: A model-based variance estimation approach to identify genes suited for normalization, applied to bladder and colon cancer data sets. Cancer Res, 64(15):5245–5250 DOI: 10.1158/0008-5472.CAN-04-0496.

Arroyo JD, Chevillet JR, Kroh EM, Ruf IK, Pritchard CC, Gibson DF, Mitchell PS, Bennett CF, Pogosova-Agadjanyan EL, Stirewalt DL, Tait JF, Tewari M. 2011. Argonaute2 complexes carry a population of circulating microRNAs independent of vesicles in human plasma. Proc Natl Acad Sci, 108(12):5003–5008 DOI: 10.1073/pnas.1019055108.

Arroyo MN, Green JA, Cnop M, Igoillo-Esteve M. 2021. tRNA biology in the pathogenesis of diabetes: Role of genetic and environmental factors. IJMS, 22(2):496 DOI: 10.3390/ijms22020496.

Bail S, Swerdel M, Liu H, Jiao X, Goff LA, Hart RP, Kiledjian M. 2010. Differential regulation of

microRNA stability. RNA, 16(5):1032–1039 DOI: 10.1261/rna.1851510.

Barceló M, Mata A, Bassas L, Larriba S. 2018. Exosomal microRNAs in seminal plasma are markers of the origin of azoospermia and can predict the presence of sperm in testicular tissue. Hum Reprod, 33(6):1087–1098 DOI: 10.1093/humrep/dey072.

Barry SE, Chan B, Ellis M, Yang Y, Plit ML, Guan G, Wang X, Britton WJ, Saunders BM. 2015. Identification of miR-93 as a suitable miR for normalizing miRNA in plasma of tuberculosis patients. J Cell Mol Med, 19(7):1606–1613 DOI: 10.1111/jcmm.12535.

Bartel DP. 2004. MicroRNAs. Cell, 116(2):281–297 DOI: 10.1016/S0092-8674(04)00045-5.

Bellin MD, Clark P, Usmani-Brown S, Dunn TB, Beilman GJ, Chinnakotla S, Pruett TL, Ptacek P, Hering BJ, Wang Z, Gilmore T, Wilhelm JJ, Hodges JS, Moran A, Herold KC. 2017. Unmethylated insulin DNA is elevated after total pancreatectomy with islet autotransplantation: Assessment of a novel beta cell marker. Am J Transplant, 17(4):1112–1118 DOI: 10.1111/ajt.14054.

Bennet W, Groth C-G, Larsson R, Nilsson B, Korsgren O. 2000. Isolated human islets trigger an instant blood mediated inflammatory reaction: Implications for intraportal islet transplantation as a treatment for patients with type 1 diabetes. Ups J Med Sci, 105(2):125–133 DOI: 10.1517/03009734000000059.

Bensellam M, Maxwell EL, Chan JY, Luzuriaga J, West PK, Jonas J-C, Gunton JE, Laybutt DR. 2016. Hypoxia reduces ER-to-Golgi protein trafficking and increases cell death by inhibiting the adaptive unfolded protein response in mouse beta cells. Diabetologia, 59(7):1492–1502 DOI: 10.1007/s00125-016-3947-y.

Bernstein E, Kim SY, Carmell MA, Murchison EP, Alcorn H, Li MZ, Mills AA, Elledge SJ, Anderson KV, Hannon GJ. 2003. Dicer is essential for mouse development. Nat Genet, 35(3):215–217 DOI: 10.1038/ng1253.

Biarnes M, Montolio M, Nacher V, Raurell M, Soler J, Montanya E. 2002. β-cell death and mass in syngeneically transplanted islets exposed to short- and long-term hyperglycemia. Diabetes, 51(1):66–72 DOI: 10.2337/diabetes.51.1.66.

Biomarkers Definitions Working Group. 2001. Biomarkers and surrogate endpoints: Preferred definitions and conceptual framework. Clin Pharmacol Ther, 69(3):89–95 DOI:

10.1067/mcp.2001.113989.

Blondal T, Jensby Nielsen S, Baker A, Andreasen D, Mouritzen P, Wrang Teilum M, Dahlsveen IK. 2013. Assessing sample and miRNA profile quality in serum and plasma or other biofluids. Methods, 59(1):S1–S6 DOI: 10.1016/j.ymeth.2012.09.015.

Borg DJ, Weigelt M, Wilhelm C, Gerlach M, Bickle M, Speier S, Bonifacio E, Hommel A. 2014. Mesenchymal stromal cells improve transplanted islet survival and islet function in a syngeneic mouse model. Diabetologia, 57(3):522–531 DOI: 10.1007/s00125-013-3109-4.

Braun JE, Truffault V, Boland A, Huntzinger E, Chang C-T, Haas G, Weichenrieder O, Coles M, Izaurralde E. 2012. A direct interaction between DCP1 and XRN1 couples mRNA decapping to 5′ exonucleolytic degradation. Nat Struct Mol Biol, 19(12):1324–1331 DOI: 10.1038/nsmb.2413.

Bunt M van de, Gaulton KJ, Parts L, Moran I, Johnson PR, Lindgren CM, Ferrer J, Gloyn AL, McCarthy MI. 2013. The miRNA profile of human pancreatic islets and beta-cells and relationship to type 2 diabetes pathogenesis. In: Wilusz CJ (ed) PLoS ONE, 8(1):e55272 DOI: 10.1371/journal.pone.0055272.

Campbell JE, Newgard CB. 2021. Mechanisms controlling pancreatic islet cell function in insulin secretion. Nat Rev Mol Cell Biol, 22(2):142–158 DOI: 10.1038/s41580-020-00317-7.

Cantley J, Grey ST, Maxwell PH, Withers DJ. 2010. The hypoxia response pathway and β-cell function. Diabetes Obes Metab, 12:159–167 DOI: 10.1111/j.1463-1326.2010.01276.x.

Cantley J, Walters SN, Jung M-H, Weinberg A, Cowley MJ, Whitworth PT, Kaplan W, Hawthorne WJ, O'connell PJ, Weir G, Grey ST. 2013. A preexistent hypoxic gene signature predicts impaired islet graft function and glucose homeostasis. Cell Transplant, 22(11):2147–2159 DOI: 10.3727/096368912X658728.

Cardozo AK, Kruhoffer M, Leeman R, Orntoft T, Eizirik DL. 2001. Identification of novel cytokine-induced genes in pancreatic β-cells by high-density oligonucleotide arrays. Diabetes, 50(5):909–920 DOI: 10.2337/diabetes.50.5.909.

Chen J, Li K, Pang Q, Yang C, Zhang H, Wu F, Cao H, Liu H, Wan Y, Xia W, Wang J, Dai Z, Li Y. 2016. Identification of suitable reference gene and biomarkers of serum miRNAs for osteoporosis. Sci Rep, 6(1):36347 DOI: 10.1038/srep36347.

Chen X, Ba Y, Ma L, Cai X, Yin Y, Wang K, Guo J, Zhang Y, Chen J, Guo X, Li Q, Li X, Wang W, Zhang Y, Wang J, Jiang X, Xiang Y, Xu C, Zheng P, Zhang J, Li R, Zhang H, Shang X, Gong T, Ning G, Wang J, Zen K, Zhang J, Zhang C-Y. 2008. Characterization of microRNAs in serum: A novel class of biomarkers for diagnosis of cancer and other diseases. Cell Res, 18(10):997–1006 DOI: 10.1038/cr.2008.282.

Chen X, Lou N, Ruan A, Qiu B, Yan Y, Wang X, Du Q, Ruan H, Han W, Wei H, Yang H, Zhang X. 2018. miR-224/miR-141 ratio as a novel diagnostic biomarker in renal cell carcinoma. Oncol Lett, 16(2):1666–1674 DOI: 10.3892/ol.2018.8874.

Chen YW, Huang CF, Tsai KS, Yang RS, Yen CC, Yang CY, Lin-Shiau SY, Liu SH. 2006. The role of phosphoinositide 3-kinase/akt signaling in low-dose mercury-induced mouse pancreatic β-cell dysfunction in vitro and in vivo. Diabetes, 55(6):1614–1624 DOI: 10.2337/db06-0029.

Chendrimada TP, Gregory RI, Kumaraswamy E, Norman J, Cooch N, Nishikura K, Shiekhattar R. 2005. TRBP recruits the dicer complex to Ago2 for microRNA processing and gene silencing. Nature, 436(7051):740–744 DOI: 10.1038/nature03868.

Churov A, Summerhill V, Grechko A, Orekhova V, Orekhov A. 2019. MicroRNAs as potential biomarkers in atherosclerosis. IJMS, 20(22):5547 DOI: 10.3390/ijms20225547.

Coenen-Stass AML, Pauwels MJ, Hanson B, Martin Perez C, Conceição M, Wood MJA, Mäger I, Roberts TC. 2019. Extracellular microRNAs exhibit sequence-dependent stability and cellular release kinetics. RNA Biol, 16(5):696–706 DOI: 10.1080/15476286.2019.1582956.

Collier JJ, Fueger PT, Hohmeier HE, Newgard CB. 2006. Pro- and antiapoptotic proteins regulate apoptosis but do not protect against cytokine-mediated cytotoxicity in rat islets and β-cell lines. Diabetes, 55(5):1398–1406 DOI: 10.2337/db05-1000.

Costa OR, Stangé G, Verhaeghen K, Brackeva B, Nonneman E, Hampe CS, Ling Z, Pipeleers D, Gorus FK, Martens GA. 2015. Development of an enhanced sensitivity bead-based immunoassay for real-time in vivo detection of pancreatic β-cell death. Endocrinology, 156(12):4755–4760 DOI: 10.1210/en.2015-1636.

Cui M, Wang H, Yao X, Zhang D, Xie Y, Cui R, Zhang X. 2019. Circulating MicroRNAs in cancer: Potential and challenge. Front Genet, 10:626 DOI: 10.3389/fgene.2019.00626.

Darden CM, Farrow AE, Rajan SK, Lakhani M, Lawrence MC, Naziruddin B. 2020. Predicting the function of islets after transplantation. In: Transplantation, bioengineering, and regeneration of the endocrine pancreas. Elsevier, pp. 547–561 DOI: 10.1016/B978-0-12-814833-4.00044-7.

Deeds MC, Anderson JM, Armstrong AS, Gastineau DA, Hiddinga HJ, Jahangir A, Eberhardt NL, Kudva YC. 2011. Single dose streptozotocin-induced diabetes: Considerations for study design in islet transplantation models. Lab Anim, 45(3):131–140 DOI: 10.1258/la.2010.010090.

Demine S, Schiavo AA, Marín-Cañas S, Marchetti P, Cnop M, Eizirik DL. 2020. Pro-inflammatory cytokines induce cell death, inflammatory responses, and endoplasmic reticulum stress in human iPSC-derived beta cells. Stem Cell Res Ther, 11(1):7 DOI: 10.1186/s13287-019-1523-3.

Donath MY, Böni-Schnetzler M, Ellingsgaard H, Halban PA, Ehses JA. 2010. Cytokine production by islets in health and diabetes: Cellular origin, regulation and function. Trends Endocrinol Metab, 21(5):261–267 DOI: 10.1016/j.tem.2009.12.010.

Donati S, Ciuffi S, Brandi ML. 2019. Human circulating miRNAs real-time qRT-PCR-based analysis: An overview of endogenous reference genes used for data normalization. IJMS, 20(18):4353 DOI: 10.3390/ijms20184353.

Duffy MJ. 2001. Carcinoembryonic antigen as a marker for colorectal cancer: Is it clinically useful? Clin Chem, 47(4):624–630 DOI: 10.1093/clinchem/47.4.624.

Eissa S, Matboli M, Aboushahba R, Bekhet MM, Soliman Y. 2016. Urinary exosomal microRNA panel unravels novel biomarkers for diagnosis of type 2 diabetic kidney disease. J Diabetes Complications, 30(8):1585–1592 DOI: 10.1016/j.jdiacomp.2016.07.012.

Erener S, Marwaha A, Tan R, Panagiotopoulos C, Kieffer TJ. 2017. Profiling of circulating microRNAs in children with recent onset of type 1 diabetes. JCI Insight, 2(4) DOI: 10.1172/jci.insight.89656.

Erener S, Mojibian M, Fox JK, Denroche HC, Kieffer TJ. 2013. Circulating miR-375 as a biomarker of β-cell death and diabetes in mice. Endocrinology, 154(2):603–608 DOI: 10.1210/en.2012-1744.

Eto K, Yamashita T, Tsubamoto Y, Terauchi Y, Hirose K, Kubota N, Yamashita S, Taka J, Satoh

S, Sekihara H, Tobe K, Iino M, Noda M, Kimura S, Kadowaki T. 2002. Phosphatidylinositol 3-Kinase suppresses glucose-stimulated insulin secretion by affecting post-cytosolic [$Ca2^{+}$] elevation signals. Diabetes, 51(1):87–97 DOI: 10.2337/diabetes.51.1.87.

Eystathioy T, Chan EKL, Tenenbaum SA, Keene JD, Griffith K, Fritzler MJ. 2002. A phosphorylated cytoplasmic autoantigen, GW182, associates with a unique population of human mRNAs within novel cytoplasmic speckles. In: Gall J (ed) MBoC, 13(4):1338–1351 DOI: 10.1091/mbc.01-11-0544.

Fabian MR, Sonenberg N. 2012. The mechanics of miRNA-mediated gene silencing: A look under the hood of miRISC. Nat Struct Mol Biol, 19(6):586–593 DOI: 10.1038/nsmb.2296.

Fauth M, Hegewald AB, Schmitz L, Krone DJ, Saul MJ. 2019. Validation of extracellular miRNA quantification in blood samples using RT-qPCR. FASEB BioAdvances, 1(8):481–492 DOI: 10.1096/fba.2019-00018.

Forlenza GP, Rewers M. 2011. The epidemic of type 1 diabetes: What is it telling us? Curr Opin Endocrinol Diabetes Obes, 18(4):248–251 DOI: 10.1097/MED.0b013e32834872ce.

Friedman RC, Farh KK-H, Burge CB, Bartel DP. 2008. Most mammalian mRNAs are conserved targets of microRNAs. Genome Res, 19(1):92–105 DOI: 10.1101/gr.082701.108.

Gaber AO, Fraga DW, Callicutt CS, Gerling IC, Sabek OM, Kotb MY. 2001. IMPROVED IN VIVO PANCREATIC ISLET FUNCTION AFTER PROLONGED IN VITRO ISLET CULTURE: Transplantation, 72(11):1730–1736 DOI: 10.1097/00007890-200112150-00005.

Gallo A, Tandon M, Alevizos I, Illei GG. 2012. The majority of MicroRNAs detectable in serum and saliva is concentrated in exosomes. In: Afarinkia K (ed) PLoS ONE, 7(3):e30679 DOI: 10.1371/journal.pone.0030679.

Garavelli S, Bruzzaniti S, Tagliabue E, Prattichizzo F, Di Silvestre D, Perna F, La Sala L, Ceriello A, Mozzillo E, Fattorusso V, Mauri P, Puca AA, Franzese A, Matarese G, Galgani M, Candia P de. 2020. Blood co-circulating extracellular microRNAs and immune cell subsets associate with type 1 diabetes severity. IJMS, 21(2):477 DOI: 10.3390/ijms21020477.

Geekiyanage H, Rayatpisheh S, Wohlschlegel JA, Brown R, Ambros V. 2020. Extracellular microRNAs in human circulation are associated with miRISC complexes that are accessible

to anti-AGO2 antibody and can bind target mimic oligonucleotides. Proc Natl Acad Sci USA, 117(39):24213–24223 DOI: 10.1073/pnas.2008323117.

Gharbi S, Khateri S, Soroush MR, Shamsara M, Naeli P, Najafi A, Korsching E, Mowla SJ. 2018. MicroRNA expression in serum samples of sulfur mustard veterans as a diagnostic gateway to improve care. In: Amendola R (ed) PLoS ONE, 13(3):e0194530 DOI: 10.1371/journal.pone.0194530.

Grunnet LG, Aikin R, Tonnesen MF, Paraskevas S, Blaabjerg L, Storling J, Rosenberg L, Billestrup N, Maysinger D, Mandrup-Poulsen T. 2009. Proinflammatory cytokines activate the intrinsic apoptotic pathway in β-cells. Diabetes, 58(8):1807–1815 DOI: 10.2337/db08-0178.

Guo L, Lu Z. 2010. The fate of miRNA* strand through evolutionary analysis: Implication for degradation as merely carrier strand or potential regulatory molecule? In: Stajich JE (ed) PLoS ONE, 5(6):e11387 DOI: 10.1371/journal.pone.0011387.

Hahn M, Krieken PP van, Nord C, Alanentalo T, Morini F, Xiong Y, Eriksson M, Mayer J, Kostromina E, Ruas JL, Sharpe J, Pereira T, Berggren P-O, Ilegems E, Ahlgren U. 2020. Topologically selective islet vulnerability and self-sustained downregulation of markers for β-cell maturity in streptozotocin-induced diabetes. Commun Biol, 3(1):541 DOI: 10.1038/s42003-020-01243-2.

Hering BJ. 2005. Single-donor, marginal-dose islet transplantation in patients with type 1 diabetes. JAMA, 293(7):830 DOI: 10.1001/jama.293.7.830.

Hering BJ, Clarke WR, Bridges ND, Eggerman TL, Alejandro R, Bellin MD, Chaloner K, Czarniecki CW, Goldstein JS, Hunsicker LG, Kaufman DB, Korsgren O, Larsen CP, Luo X, Markmann JF, Naji A, Oberholzer J, Posselt AM, Rickels MR, Ricordi C, Robien MA, Senior PA, Shapiro AMJ, Stock PG, Turgeon NA, Clinical Islet Transplantation Consortium. 2016. Phase 3 trial of transplantation of human islets in type 1 diabetes complicated by severe hypoglycemia. Diabetes Care, 39(7):1230–1240 DOI: 10.2337/dc15-1988.

Horaguchi A, Merrell RC. 1981. Preparation of viable islet cells from dogs by a new method. Diabetes, 30(5):455–458 DOI: 10.2337/diab.30.5.455.

Hu Y, Lan W, Miller D. 2017. Next-generation sequencing for MicroRNA expression profile. In: Huang J, Borchert GM, Dou D, Huan J, Lan W, Tan M, Wu B (eds) Bioinformatics in MicroRNA research. Springer New York, New York, NY, pp. 169–177 DOI: 10.1007/978-1-4939-7046-

9_12.

Huntzinger E, Izaurralde E. 2011. Gene silencing by microRNAs: Contributions of translational repression and mRNA decay. Nat Rev Genet, 12(2):99–110 DOI: 10.1038/nrg2936.

Husseiny MI, Kaye A, Zebadua E, Kandeel F, Ferreri K. 2014. Tissue-specific methylation of human insulin gene and PCR assay for monitoring beta cell death. In: Herrath MG von (ed) PLoS ONE, 9(4):e94591 DOI: 10.1371/journal.pone.0094591.

Hyöty H, Taylor K. 2002. The role of viruses in human diabetes. Diabetologia, 45(10):1353–1361 DOI: 10.1007/s00125-002-0852-3.

Iorio MV, Ferracin M, Liu C-G, Veronese A, Spizzo R, Sabbioni S, Magri E, Pedriali M, Fabbri M, Campiglio M, Ménard S, Palazzo JP, Rosenberg A, Musiani P, Volinia S, Nenci I, Calin GA, Querzoli P, Negrini M, Croce CM. 2005. MicroRNA gene expression deregulation in human breast cancer. Cancer Res, 65(16):7065–7070 DOI: 10.1158/0008-5472.CAN-05-1783.

Jin F, Hu H, Xu M, Zhan S, Wang Y, Zhang H, Chen X. 2018. Serum microRNA profiles serve as novel biomarkers for autoimmune diseases. Front Immunol, 9:2381 DOI: 10.3389/fimmu.2018.02381.

Jonas S, Izaurralde E. 2013. The role of disordered protein regions in the assembly of decapping complexes and RNP granules. Genes Dev, 27(24):2628–2641 DOI: 10.1101/gad.227843.113.

Jonas S, Izaurralde E. 2015. Towards a molecular understanding of microRNA-mediated gene silencing. Nat Rev Genet, 16(7):421–433 DOI: 10.1038/nrg3965.

Kameswaran V, Bramswig NC, McKenna LB, Penn M, Schug J, Hand NJ, Chen Y, Choi I, Vourekas A, Won K-J, Liu C, Vivek K, Naji A, Friedman JR, Kaestner KH. 2014. Epigenetic regulation of the DLK1-MEG3 MicroRNA cluster in human type 2 diabetic islets. Cell Metab, 19(1):135–145 DOI: 10.1016/j.cmet.2013.11.016.

Kanak MA, Takita M, Shahbazov R, Lawrence MC, Chung WY, Dennison AR, Levy MF, Naziruddin B. 2015. Evaluation of MicroRNA375 as a novel biomarker for graft damage in clinical islet transplantation. Transplantation, 99(8):1568–1573 DOI: 10.1097/TP.0000000000000625.

Katayama M, Wiklander OPB, Fritz T, Caidahl K, El-Andaloussi S, Zierath JR, Krook A. 2019. Circulating exosomal miR-20b-5p is elevated in type 2 diabetes and could impair insulin action

in human skeletal muscle. Diabetes, 68(3):515–526 DOI: 10.2337/db18-0470.

Kawahara DJ, Kenney JS. 1991. Species differences in human and rat islet sensitivity to human cytokines. Monoclonal anti-interleukin-1 (IL-1) influences on direct and indirect IL-1-mediated islet effects. Cytokine, 3(2):117–124 DOI: 10.1016/1043-4666(91)90031-8.

Kawamata T, Tomari Y. 2010. Making RISC. Trends Biochem Sci, 35(7):368–376 DOI: 10.1016/j.tibs.2010.03.009.

Kayton NS, Poffenberger G, Henske J, Dai C, Thompson C, Aramandla R, Shostak A, Nicholson W, Brissova M, Bush WS, Powers AC. 2015. Human islet preparations distributed for research exhibit a variety of insulin-secretory profiles. Am J Physiol-endoc M, 308(7):E592–E602 DOI: 10.1152/ajpendo.00437.2014.

Kechin A, Boyarskikh U, Kel A, Filipenko M. 2017. cutPrimers: A New Tool for Accurate Cutting of Primers from Reads of Targeted Next Generation Sequencing. J Comput Biol, 24(11):1138–1143 DOI: 10.1089/cmb.2017.0096.

Khvorova A, Reynolds A, Jayasena SD. 2003. Functional siRNAs and miRNAs exhibit strand bias. Cell, 115(2):209–216 DOI: 10.1016/S0092-8674(03)00801-8.

Kim D, Chang HR, Baek D. 2017. Rules for functional microRNA targeting. BMB Rep, 50(11):554–559 DOI: 10.5483/BMBRep.2017.50.11.179.

Kim M, Zhang X. 2019. The profiling and role of miRNAs in diabetes mellitus. J Diabetes Clin Res, 1(1):5–23 DOI: 10.33696/diabetes.1.003.

Kim S, Millet I, Kim HS, Kim JY, Han MS, Lee M-K, Kim K-W, Sherwin RS, Karin M, Lee M-S. 2007. NFκB prevents β cell death and autoimmune diabetes in NOD mice. Proc Natl Acad Sci, 104(6):1913–1918 DOI: 10.1073/pnas.0610690104.

Komatsu H, Kandeel F, Mullen Y. 2018. Impact of oxygen on pancreatic islet survival. Pancreas, 47(5):533–543 DOI: 10.1097/MPA.0000000000001050.

Korma W, Mihret A, Tarekegn A, Chang Y, Hwang D, Tessema TS, Lee H. 2020. Identification of circulating miR-22-3p and miR-93-5p as stable endogenous control in tuberculosis study. Diagnostics, 10(11):868 DOI: 10.3390/diagnostics10110868.

Kosaka N, Iguchi H, Yoshioka Y, Takeshita F, Matsuki Y, Ochiya T. 2010. Secretory mechanisms

and intercellular transfer of MicroRNAs in living cells. J Biol Chem, 285(23):17442–17452 DOI: 10.1074/jbc.M110.107821.

LaBaer J. 2005. So, you want to look for biomarkers (introduction to the special biomarkers issue) †. J Proteome Res, 4(4):1053–1059 DOI: 10.1021/pr0501259.

Lablanche S, Vantyghem M-C, Kessler L, Wojtusciszyn A, Borot S, Thivolet C, Girerd S, Bosco D, Bosson J-L, Colin C, Tetaz R, Logerot S, Kerr-Conte J, Renard E, Penfornis A, Morelon E, Buron F, Skaare K, Grguric G, Camillo-Brault C, Egelhofer H, Benomar K, Badet L, Berney T, Pattou F, Benhamou P-Y, Malvezzi P, Tauveron I, Roche B, Noel C, Frimat L, Guerci B, Pernin N, Moisan A, Persoons V, Ezzouaoui R, Gmyr V, Thony F, Bricault Y, Rodière M, Sengel C, Greget M, Enescu I, Noel C, Hazzan M, Caiazzo R, Torres F, Le Mapihan K, Raverdy V, Pierredon M-A, Valette P-J, Muller A, Champagnac J, Chaillous L, Dantal J, Cattan P, Riveline J-P, Moreau F, Baltzinger P, Bahoune T. 2018. Islet transplantation versus insulin therapy in patients with type 1 diabetes with severe hypoglycaemia or poorly controlled glycaemia after kidney transplantation (TRIMECO): A multicentre, randomised controlled trial. Lancet Diabetes Endocrinol, 6(7):527–537 DOI: 10.1016/S2213-8587(18)30078-0.

Lai Y, Brandhorst H, Hossain H, Bierhaus A, Chen C, Bretzel RG, Linn T. 2009. Activation of NFκB dependent apoptotic pathway in pancreatic islet cells by hypoxia. Islets, 1(1):19–25 DOI: 10.4161/isl.1.1.8530.

LaPierre MP, Stoffel M. 2017. MicroRNAs as stress regulators in pancreatic beta cells and diabetes. Mol Metab, 6(9):1010–1023 DOI: 10.1016/j.molmet.2017.06.020.

Latreille M, Herrmanns K, Renwick N, Tuschl T, Malecki MT, McCarthy MI, Owen KR, Rülicke T, Stoffel M. 2015. miR-375 gene dosage in pancreatic β-cells: Implications for regulation of β-cell mass and biomarker development. J Mol Med, 93(10):1159–1169 DOI: 10.1007/s00109-015-1296-9.

Lee RC, Feinbaum RL, Ambros V. 1993. The c. Elegans heterochronic gene lin-4 encodes small RNAs with antisense complementarity to lin-14. Cell, 75(5):843–854 DOI: 10.1016/0092-8674(93)90529-Y.

Lee Y. 2002. MicroRNA maturation: Stepwise processing and subcellular localization. EMBO J, 21(17):4663–4670 DOI: 10.1093/emboj/cdf476.

Lee Y, Hur I, Park S-Y, Kim Y-K, Suh MR, Kim VN. 2006. The role of PACT in the RNA silencing pathway. EMBO J, 25(3):522–532 DOI: 10.1038/sj.emboj.7600942.

Lee Y, Kim M, Han J, Yeom K-H, Lee S, Baek SH, Kim VN. 2004. MicroRNA genes are transcribed by RNA polymerase II. EMBO J, 23(20):4051–4060 DOI: 10.1038/sj.emboj.7600385.

Lenzen S. 2008. The mechanisms of alloxan- and streptozotocin-induced diabetes. Diabetologia, 51(2):216–226 DOI: 10.1007/s00125-007-0886-7.

Liu Y, Ma M, Yu J, Ping F, Zhang H, Li W, Xu L, Li Y. 2019. Decreased serum *microRNA-21* , *microRNA-25* , *microRNA-146a* , and *microRNA-181a* in autoimmune diabetes: Potential biomarkers for diagnosis and possible involvement in pathogenesis. Int J Endocrinol, 2019:1–9 DOI: 10.1155/2019/8406438.

Love MI, Huber W, Anders S. 2014. Moderated estimation of fold change and dispersion for RNA-seq data with DESeq2. Genome Biol, 15(12):550 DOI: 10.1186/s13059-014-0550-8.

Ma X, Becker Buscaglia LE, Barker JR, Li Y. 2011. MicroRNAs in NF-κB signaling. J Mol Cell Biol, 3(3):159–166 DOI: 10.1093/jmcb/mjr007.

MacRae IJ, Ma E, Zhou M, Robinson CV, Doudna JA. 2008. In vitro reconstitution of the human RISC-loading complex. Proc Natl Acad Sci, 105(2):512–517 DOI: 10.1073/pnas.0710869105.

Maedler K, Sergeev P, Ris F, Oberholzer J, Joller-Jemelka HI, Spinas GA, Kaiser N, Halban PA, Donath MY. 2002. Glucose-induced β cell production of IL-1β contributes to glucotoxicity in human pancreatic islets. J Clin Invest, 110(6):851–860 DOI: 10.1172/JCI200215318.

Malik SS, Masood N, Sherrard A, Bishop PN. 2019. Small non-coding RNAs as a tool for personalized therapy in familial cancers. In: AGO-driven non-coding RNAs. Elsevier, pp. 179–208 DOI: 10.1016/B978-0-12-815669-8.00007-5.

Marchand L, Jalabert A, Meugnier E, Van den Hende K, Fabien N, Nicolino M, Madec A-M, Thivolet C, Rome S. 2016. miRNA-375 a sensor of glucotoxicity is altered in the serum of children with newly diagnosed type 1 diabetes. J Diabetes Res, 2016:1–7 DOI: 10.1155/2016/1869082.

Markmann JF, Deng S, Huang X, Desai NM, Velidedeoglu EH, Lui C, Frank A, Markmann E, Palanjian M, Brayman K, Wolf B, Bell E, Vitamaniuk M, Doliba N, Matschinsky F, Barker CF, Naji A. 2003. Insulin independence following isolated islet transplantation and single islet

infusions. Ann Surg, 237(6):741–750 DOI: 10.1097/01.SLA.0000072110.93780.52.

Marzi MJ, Ghini F, Cerruti B, Pretis S de, Bonetti P, Giacomelli C, Gorski MM, Kress T, Pelizzola M, Muller H, Amati B, Nicassio F. 2016. Degradation dynamics of microRNAs revealed by a novel pulse-chase approach. Genome Res, 26(4):554–565 DOI: 10.1101/gr.198788.115.

Matsumoto S, Takita M, Chaussabel D, Noguchi H, Shimoda M, Sugimoto K, Itoh T, Chujo D, Sorelle J, Onaca N, Naziruddin B, Levy MF. 2011. Improving efficacy of clinical islet transplantation with iodixanol-based islet purification, thymoglobulin induction, and blockage of IL-1β and TNF-α. Cell Transplant, 20(10):1641–1647 DOI: 10.3727/096368910X564058.

Matsuoka N, Itoh T, Watarai H, Sekine-Kondo E, Nagata N, Okamoto K, Mera T, Yamamoto H, Yamada S, Maruyama I, Taniguchi M, Yasunami Y. 2010. High-mobility group box 1 is involved in the initial events of early loss of transplanted islets in mice. J Clin Invest, 120(3):735–743 DOI: 10.1172/JCI41360.

McKeon A, Tracy JA. 2017. GAD65 neurological autoimmunity: AANEM minimonograph: GAD65 neurological autoimmunity. Muscle Nerve, 56(1):15–27 DOI: 10.1002/mus.25565.

Meier JJ. 2016. Insulin secretion. In: Endocrinology: Adult and pediatric. Elsevier, pp. 546–555.e5 DOI: 10.1016/B978-0-323-18907-1.00032-9.

Meijer HA, Smith EM, Bushell M. 2014. Regulation of miRNA strand selection: Follow the leader? Biochem Soc Trans, 42(4):1135–1140 DOI: 10.1042/BST20140142.

Mi Q-S, Weiland M, Qi R-Q, Gao X-H, Poisson LM, Zhou L. 2012. Identification of mouse serum miRNA endogenous references by global gene expression profiles. In: Homberg J (ed) PLoS ONE, 7(2):e31278 DOI: 10.1371/journal.pone.0031278.

Mittelbrunn M, Gutiérrez-Vázquez C, Villarroya-Beltri C, González S, Sánchez-Cabo F, González MÁ, Bernad A, Sánchez-Madrid F. 2011. Unidirectional transfer of microRNA-loaded exosomes from t cells to antigen-presenting cells. Nat Commun, 2(1):282 DOI: 10.1038/ncomms1285.

Mokhtari D, Myers JW, Welsh N. 2008. The MAPK kinase kinase-1 is essential for stress-induced pancreatic islet cell death. Endocrinology, 149(6):3046–3053 DOI: 10.1210/en.2007-0438.

Monti P, Vignali D, Piemonti L. 2015. Monitoring inflammation, humoral and cell-

mediated immunity in pancreas and islet transplants. CDR, 11(3):135–143 DOI: 10.2174/1573399811666150317125820.

Mori MA, Ludwig RG, Garcia-Martin R, Brandão BB, Kahn CR. 2019. Extracellular miRNAs: From biomarkers to mediators of physiology and disease. Cell Metab, 30(4):656–673 DOI: 10.1016/j.cmet.2019.07.011.

Morran MP, Omenn GS, Pietropaolo M. 2008. Immunology and genetics of type 1 diabetes. Mt Sinai J Med, 75(4):314–327 DOI: 10.1002/msj.20052.

Naftanel MA, Harlan DM. 2004. Pancreatic islet transplantation. PLoS Med, 1(3):e58 DOI: 10.1371/journal.pmed.0010058.

Nagy Z, Igaz P. 2015. Introduction to microRNAs: Biogenesis, action, relevance of tissue microRNAs in disease pathogenesis, diagnosis and therapy—the concept of circulating microRNAs. In: Igaz P (ed) Circulating microRNAs in disease diagnostics and their potential biological relevance. Springer Basel, Basel, pp. 3–30 DOI: 10.1007/978-3-0348-0955-9_1.

Neiman D, Moss J, Hecht M, Magenheim J, Piyanzin S, Shapiro AMJ, Koning EJP de, Razin A, Cedar H, Shemer R, Dor Y. 2017. Islet cells share promoter hypomethylation independently of expression, but exhibit cell-type–specific methylation in enhancers. Proc Natl Acad Sci USA, 114(51):13525–13530 DOI: 10.1073/pnas.1713736114.

Nesca V, Guay C, Jacovetti C, Menoud V, Peyot M-L, Laybutt DR, Prentki M, Regazzi R. 2013. Identification of particular groups of microRNAs that positively or negatively impact on beta cell function in obese models of type 2 diabetes. Diabetologia, 56(10):2203–2212 DOI: 10.1007/s00125-013-2993-y.

Nikolov S. 2013. MicroRNA regulation, signaling pathways. In: Dubitzky W, Wolkenhauer O, Cho K-H, Yokota H (eds) Encyclopedia of systems biology. Springer New York, New York, NY, pp. 1328–1331 DOI: 10.1007/978-1-4419-9863-7_1136.

Niu Y, Wu Y, Huang J, Li Q, Kang K, Qu J, Li F, Gou D. 2016. Identification of reference genes for circulating microRNA analysis in colorectal cancer. Sci Rep, 6(1):35611 DOI: 10.1038/srep35611.

Noble JA, Valdes AM, Varney MD, Carlson JA, Moonsamy P, Fear AL, Lane JA, Lavant E, Rappner

R, Louey A, Concannon P, Mychaleckyj JC, Erlich HA, for the Type 1 Diabetes Genetics Consortium. 2010. HLA class i and genetic susceptibility to type 1 diabetes: Results from the type 1 diabetes genetics consortium. Diabetes, 59(11):2972–2979 DOI: 10.2337/db10-0699.

Norlin S, Ahlgren U, Edlund H. 2005. Nuclear factor-κB activity in β-cells is required for glucose-stimulated insulin secretion. Diabetes, 54(1):125–132 DOI: 10.2337/diabetes.54.1.125.

O'Brien K, Breyne K, Ughetto S, Laurent LC, Breakefield XO. 2020. RNA delivery by extracellular vesicles in mammalian cells and its applications. Nat Rev Mol Cell Biol, 21(10):585–606 DOI: 10.1038/s41580-020-0251-y.

Olsson R, Olerud J, Pettersson U, Carlsson P-O. 2011. Increased numbers of low-oxygenated pancreatic islets after intraportal islet transplantation. Diabetes, 60(9):2350–2353 DOI: 10.2337/db09-0490.

Paget M, Murray H, Bailey CJ, Downing R. 2007. Human islet isolation: Semi-automated and manual methods. Diab Vasc Dis Res, 4(1):7–12 DOI: 10.3132/dvdr.2007.010.

Palmer JP, Fleming GA, Greenbaum CJ, Herold KC, Jansa LD, Kolb H, Lachin JM, Polonsky KS, Pozzilli P, Skyler JS, Steffes MW. 2004. C-peptide is the appropriate outcome measure for type 1 diabetes clinical trials to preserve β-cell function: Report of an ADA workshop, 21-22 october 2001. Diabetes, 53(1):250–264 DOI: 10.2337/diabetes.53.1.250.

Papaccio G, Graziano A, d'Aquino R, Valiante S, Naro F. 2005. A biphasic role of nuclear transcription factor (NF)-κb in the islet β-cell apoptosis induced by interleukin (IL)-1β. J Cell Physiol, 204(1):124–130 DOI: 10.1002/jcp.20276.

Park NJ, Zhou H, Elashoff D, Henson BS, Kastratovic DA, Abemayor E, Wong DT. 2009. Salivary microRNA: Discovery, characterization, and clinical utility for oral cancer detection. Clin Cancer Res, 15(17):5473–5477 DOI: 10.1158/1078-0432.CCR-09-0736.

Pasquinelli AE, Reinhart BJ, Slack F, Martindale MQ, Kuroda MI, Maller B, Hayward DC, Ball EE, Degnan B, Müller P, Spring J, Srinivasan A, Fishman M, Finnerty J, Corbo J, Levine M, Leahy P, Davidson E, Ruvkun G. 2000. Conservation of the sequence and temporal expression of let-7 heterochronic regulatory RNA. Nature, 408(6808):86–89 DOI: 10.1038/35040556.

Patoulias DI. 2018. Is miRNA-375 a promising biomarker for early detection and monitoring of

patients with type 2 diabetes? amsad, 3(1):119–122 DOI: 10.5114/amsad.2018.78775.

Persaud SJ, Hauge-Evans AC, Jones PM. 2014. Insulin-secreting cell lines. In: Cellular endocrinology in health and disease. Elsevier, pp. 239–256 DOI: 10.1016/B978-0-12-408134-5.00015-9.

Pfaffl MW. 2001. A new mathematical model for relative quantification in real-time RT-PCR. Nucleic Acids Res, 29(9):45e–45 DOI: 10.1093/nar/29.9.e45.

Piemonti L. 2000. Islet transplantation. In: Feingold KR, Anawalt B, Boyce A, Chrousos G, Herder WW de, Dhatariya K, Dungan K, Grossman A, Hershman JM, Hofland J, Kalra S, Kaltsas G, Koch C, Kopp P, Korbonits M, Kovacs CS, Kuohung W, Laferrère B, McGee EA, McLachlan R, Morley JE, New M, Purnell J, Sahay R, Singer F, Stratakis CA, Trence DL, Wilson DP (eds) Endotext. MDText.com, Inc., South Dartmouth (MA) [accessed: 04/25/2021] URL: http://www.ncbi.nlm.nih.gov/books/NBK278966/.

Piemonti L, Everly MJ, Maffi P, Scavini M, Poli F, Nano R, Cardillo M, Melzi R, Mercalli A, Sordi V, Lampasona V, Espadas de Arias A, Scalamogna M, Bosi E, Bonifacio E, Secchi A, Terasaki PI. 2013. Alloantibody and autoantibody monitoring predicts islet transplantation outcome in human type 1 diabetes. Diabetes, 62(5):1656–1664 DOI: 10.2337/db12-1258.

Pileggi A, Klein D, Fotino C, Bravo-Egaña V, Rosero S, Doni M, Podetta M, Ricordi C, Molano RD, Pastori RL. 2013. MicroRNAs in islet immunobiology and transplantation. Immunol Res, 57(1):185–196 DOI: 10.1007/s12026-013-8436-5.

Pospisilova S, Pazourkova E, Horinek A, Brisuda A, Svobodova I, Soukup V, Hrbacek J, Capoun O, Hanus T, Mares J, Korabecna M, Babjuk M. 2016. MicroRNAs in urine supernatant as potential non-invasive markers for bladder cancer detection. neo, 63(5):799–808 DOI: 10.4149/neo_2016_518.

Rickels MR, Liu C, Shlansky-Goldberg RD, Soleimanpour SA, Vivek K, Kamoun M, Min Z, Markmann E, Palangian M, Dalton-Bakes C, Fuller C, Chiou AJ, Barker CF, Luning Prak ET, Naji A. 2013. Improvement in β-cell secretory capacity after human islet transplantation according to the CIT07 protocol. Diabetes, 62(8):2890–2897 DOI: 10.2337/db12-1802.

Rickels MR, Robertson RP. 2019. Pancreatic islet transplantation in humans: Recent progress and future directions. Endocr Rev, 40(2):631–668 DOI: 10.1210/er.2018-00154.

Rickels MR, Stock PG, Koning EJP de, Piemonti L, Pratschke J, Alejandro R, Bellin MD, Berney T, Choudhary P, Johnson PR, Kandaswamy R, Kay TWH, Keymeulen B, Kudva YC, Latres E, Langer RM, Lehmann R, Ludwig B, Markmann JF, Marinac M, Odorico JS, Pattou F, Senior PA, Shaw JAM, Vantyghem M-C, White S. 2018. Defining outcomes for β-cell replacement therapy in the treatment of diabetes: A consensus report on the igls criteria from the IPITA/EPITA opinion leaders workshop. Transpl Int, 31(4):343–352 DOI: 10.1111/tri.13138.

Ricordi C, Lacy PE, Finke EH, Olack BJ, Scharp DW. 1988. Automated method for isolation of human pancreatic islets. Diabetes, 37(4):413–420 DOI: 10.2337/diab.37.4.413.

Ritz C, Baty F, Streibig JC, Gerhard D. 2015. Dose-response analysis using r. In: Xia Y (ed) PLoS ONE, 10(12):e0146021 DOI: 10.1371/journal.pone.0146021.

Roat R, Hossain MM, Christopherson J, Free C, Jain S, Guay C, Regazzi R, Guo Z. 2017. Identification and characterization of microRNAs associated with human β-cell loss in a mouse model. Am J Transplant, 17(4):992–1007 DOI: 10.1111/ajt.14073.

Roggli E, Britan A, Gattesco S, Lin-Marq N, Abderrahmani A, Meda P, Regazzi R. 2010. Involvement of MicroRNAs in the cytotoxic effects exerted by proinflammatory cytokines on pancreatic β-cells. Diabetes, 59(4):978–986 DOI: 10.2337/db09-0881.

Ruby JG, Jan CH, Bartel DP. 2007. Intronic microRNA precursors that bypass drosha processing. Nature, 448(7149):83–86 DOI: 10.1038/nature05983.

Saisho Y. 2016. Postprandial c-peptide to glucose ratio as a marker of β cell function: Implication for the management of type 2 diabetes. IJMS, 17(5):744 DOI: 10.3390/ijms17050744.

Saravanan PB, Vasu S, Yoshimatsu G, Darden CM, Wang X, Gu J, Lawrence MC, Naziruddin B. 2019. Differential expression and release of exosomal miRNAs by human islets under inflammatory and hypoxic stress. Diabetologia, 62(10):1901–1914 DOI: 10.1007/s00125-019-4950-x.

Sarkar SA, Kutlu B, Velmurugan K, Kizaka-Kondoh S, Lee CE, Wong R, Valentine A, Davidson HW, Hutton JC, Pugazhenthi S. 2009. Cytokine-mediated induction of anti-apoptotic genes that are linked to nuclear factor kappa-b (NF-κb) signalling in human islets and in a mouse beta cell line. Diabetologia, 52(6):1092–1101 DOI: 10.1007/s00125-009-1331-x.

Sato Y, Inoue M, Yoshizawa T, Yamagata K. 2014. Moderate hypoxia induces β-cell dysfunction with HIF-1–independent gene expression changes. In: Minamino T (ed) PLoS ONE, 9(12):e114868 DOI: 10.1371/journal.pone.0114868.

Scharp DW, Lacy PE, Santiago JV, McCullough CS, Weide LG, Falqui L, Marchetti P, Gingerich RL, Jaffe AS, Cryer PE, Anderson CB, Flye MW. 1990. Insulin independence after islet transplantation into type 1 diabetic patient. Diabetes, 39(4):515–518 DOI: 10.2337/diab.39.4.515.

Schwarzenbach H, Silva AM da, Calin G, Pantel K. 2015. Data normalization strategies for MicroRNA quantification. Clin Chem, 61(11):1333–1342 DOI: 10.1373/clinchem.2015.239459.

Scicali R, Di Pino A, Pavanello C, Ossoli A, Strazzella A, Alberti A, Di Mauro S, Scamporrino A, Urbano F, Filippello A, Piro S, Rabuazzo AM, Calabresi L, Purrello F. 2019. Analysis of HDL-microRNA panel in heterozygous familial hypercholesterolemia subjects with LDL receptor null or defective mutation. Sci Rep, 9(1):20354 DOI: 10.1038/s41598-019-56857-2.

Sedgeman LR, Beysen C, Ramirez Solano MA, Michell DL, Sheng Q, Zhao S, Turner S, Linton MF, Vickers KC. 2019. Beta cell secretion of miR-375 to HDL is inversely associated with insulin secretion. Sci Rep, 9(1):3803 DOI: 10.1038/s41598-019-40338-7.

Serocki M, Bartoszewska S, Janaszak-Jasiecka A, Ochocka RJ, Collawn JF, Bartoszewski R. 2018. miRNAs regulate the HIF switch during hypoxia: A novel therapeutic target. Angiogenesis, 21(2):183–202 DOI: 10.1007/s10456-018-9600-2.

Shahbazov R, Kanak MA, Takita M, Kunnathodi F, Khan O, Borenstein N, Lawrence MC, Levy MF, Naziruddin B. 2016. Essential phospholipids prevent islet damage induced by proinflammatory cytokines and hypoxic conditions: Phospholipids prevent islet damage. Diabetes Metab Res Rev, 32(3):268–277 DOI: 10.1002/dmrr.2714.

Shapiro AMJ, Lakey JRT, Ryan EA, Korbutt GS, Toth E, Warnock GL, Kneteman NM, Rajotte RV. 2000. Islet transplantation in seven patients with type 1 diabetes mellitus using a glucocorticoid-free immunosuppressive regimen. N Engl J Med, 343(4):230–238 DOI: 10.1056/NEJM200007273430401.

Shapiro AMJ, Pokrywczynska M, Ricordi C. 2017. Clinical pancreatic islet transplantation. Nat Rev Endocrinol, 13(5):268–277 DOI: 10.1038/nrendo.2016.178.

Shen Y, Tian F, Chen Z, Li R, Ge Q, Lu Z. 2015. Amplification-based method for microRNA detection. Biosens Bioelectron, 71:322–331 DOI: 10.1016/j.bios.2015.04.057.

Shi R, Chiang VL. 2005. Facile means for quantifying microRNA expression by real-time PCR. BioTechniques, 39(4):519–525 DOI: 10.2144/000112010.

Sims EK, Evans-Molina C, Tersey SA, Eizirik DL, Mirmira RG. 2018. Biomarkers of islet beta cell stress and death in type 1 diabetes. Diabetologia, 61(11):2259–2265 DOI: 10.1007/s00125-018-4712-1.

Spinello I, Quaranta MT, Paolillo R, Pelosi E, Cerio AM, Saulle E, Coco FL, Testa U, Labbaye C. 2015. Differential hypoxic regulation of the microRNA-146a/CXCR4 pathway in normal and leukemic monocytic cells: Impact on response to chemotherapy. Haematologica, 100(9):1160–1171 DOI: 10.3324/haematol.2014.120295.

Tan Y, Pan T, Ye Y, Ge G, Chen L, Wen D, Zou S. 2014. Serum MicroRNAs as potential biomarkers of primary biliary cirrhosis. In: Ansari AA (ed) PLoS ONE, 9(10):e111424 DOI: 10.1371/journal.pone.0111424.

Tattikota SG, Rathjen T, McAnulty SJ, Wessels H-H, Akerman I, Bunt M van de, Hausser J, Esguerra JLS, Musahl A, Pandey AK, You X, Chen W, Herrera PL, Johnson PR, O'Carroll D, Eliasson L, Zavolan M, Gloyn AL, Ferrer J, Shalom-Feuerstein R, Aberdam D, Poy MN. 2014. Argonaute2 mediates compensatory expansion of the pancreatic β cell. Cell Metab, 19(1):122–134 DOI: 10.1016/j.cmet.2013.11.015.

Tattikota SG, Sury MD, Rathjen T, Wessels H-H, Pandey AK, You X, Becker C, Chen W, Selbach M, Poy MN. 2013. Argonaute2 regulates the pancreatic β-cell secretome. Mol Cell Proteomics, 12(5):1214–1225 DOI: 10.1074/mcp.M112.024786.

Tay JW, James I, Hughes QW, Tiao JY, Baker RI. 2017. Identification of reference miRNAs in plasma useful for the study of oestrogen-responsive miRNAs associated with acquired protein S deficiency in pregnancy. BMC Res Notes, 10(1):312 DOI: 10.1186/s13104-017-2636-3.

Tersey SA, Nishiki Y, Templin AT, Cabrera SM, Stull ND, Colvin SC, Evans-Molina C, Rickus JL, Maier B, Mirmira RG. 2012. Islet -cell endoplasmic reticulum stress precedes the onset of type 1 diabetes in the nonobese diabetic mouse model. Diabetes, 61(4):818–827 DOI: 10.2337/db11-1293.

Thorens B. 2015. GLUT2, glucose sensing and glucose homeostasis. Diabetologia, 58(2):221–232 DOI: 10.1007/s00125-014-3451-1.

Tokar T, Pastrello C, Rossos AEM, Abovsky M, Hauschild A-C, Tsay M, Lu R, Jurisica I. 2018. mirDIP 4.1—integrative database of human microRNA target predictions. Nucleic Acids Res, 46:D360–D370 DOI: 10.1093/nar/gkx1144.

Turchinovich A, Weiz L, Langheinz A, Burwinkel B. 2011. Characterization of extracellular circulating microRNA. Nucleic Acids Res, 39(16):7223–7233 DOI: 10.1093/nar/gkr254.

Vandesompele J, De Preter K, Pattyn F, Poppe B, Van Roy N, De Paepe A, Speleman F. 2002. Accurate normalization of real-time quantitative RT-PCR data by geometric averaging of multiple internal control genes. Genome Biol, 3(7):research0034.1 DOI: 10.1186/gb-2002-3-7-research0034.

Vasu S, Kumano K, Darden CM, Rahman I, Lawrence MC, Naziruddin B. 2019. MicroRNA signatures as future biomarkers for diagnosis of diabetes states. Cells, 8(12):1533 DOI: 10.3390/cells8121533.

Vendrame F, Pileggi A, Laughlin E, Allende G, Martin-Pagola A, Molano RD, Diamantopoulos S, Standifer N, Geubtner K, Falk BA, Ichii H, Takahashi H, Snowhite I, Chen Z, Mendez A, Chen L, Sageshima J, Ruiz P, Ciancio G, Ricordi C, Reijonen H, Nepom GT, Burke GW, Pugliese A. 2010. Recurrence of type 1 diabetes after simultaneous pancreas-kidney transplantation, despite immunosuppression, is associated with autoantibodies and pathogenic autoreactive CD4 t-cells. Diabetes, 59(4):947–957 DOI: 10.2337/db09-0498.

Vickers KC, Palmisano BT, Shoucri BM, Shamburek RD, Remaley AT. 2011. MicroRNAs are transported in plasma and delivered to recipient cells by high-density lipoproteins. Nat Cell Biol, 13(4):423–433 DOI: 10.1038/ncb2210.

Wahid F, Shehzad A, Khan T, Kim YY. 2010. MicroRNAs: Synthesis, mechanism, function, and recent clinical trials. Biochim Biophys Acta BBA - Mol Cell Res, 1803(11):1231–1243 DOI: 10.1016/j.bbamcr.2010.06.013.

Wahle E, Winkler GS. 2013. RNA decay machines: Deadenylation by the Ccr4–not and Pan2–Pan3 complexes. Biochim Biophys Acta BBA - Gene Regul Mech, 1829(6):561–570 DOI: 10.1016/j.bbagrm.2013.01.003.

Wang K, Zhang S, Weber J, Baxter D, Galas DJ. 2010. Export of microRNAs and microRNA-protective protein by mammalian cells. Nucleic Acids Res, 38(20):7248–7259 DOI: 10.1093/nar/gkq601.

Wang X, Li J, Wu D, Bu X, Qiao Y. 2016. Hypoxia promotes apoptosis of neuronal cells through hypoxia-inducible factor-1α-microRNA-204-B-cell lymphoma-2 pathway. Exp Biol Med (Maywood), 241(2):177–183 DOI: 10.1177/1535370215600548.

Wang Z, Lu Y, Zhang X, Ren X, Wang Y, Li Z, Xu C, Han J. 2012. Serum microRNA is a promising biomarker for osteogenesis imperfecta. Intractable Rare Dis Res, 1(2):81–85 DOI: 10.5582/irdr.2012.v1.2.81.

Winkler C, Krumsiek J, Buettner F, Angermüller C, Giannopoulou EZ, Theis FJ, Ziegler A-G, Bonifacio E. 2014. Feature ranking of type 1 diabetes susceptibility genes improves prediction of type 1 diabetes. Diabetologia, 57(12):2521–2529 DOI: 10.1007/s00125-014-3362-1.

Winter J, Jung S, Keller S, Gregory RI, Diederichs S. 2009. Many roads to maturity: microRNA biogenesis pathways and their regulation. Nat Cell Biol, 11(3):228–234 DOI: 10.1038/ncb0309-228.

Wu H, Wang Q, Zhong H, Li L, Zhang Q, Huang Q, Yu Z. 2020. Differentially expressed microRNAs in exosomes of patients with breast cancer revealed by next-generation sequencing. Oncol Rep, 43(1):240–250 DOI: 10.3892/or.2019.7401.

Xie F, Xiao P, Chen D, Xu L, Zhang B. 2012. miRDeepFinder: A miRNA analysis tool for deep sequencing of plant small RNAs. Plant Mol Biol, 80(1):75–84 DOI: 10.1007/s11103-012-9885-2.

Xu T, Liao Z, O'Reilly MS, Levy LB, Welsh JW, Wang L-E, Lin SH, Komaki R, Liu Z, Wei Q, Gomez DR. 2014. Serum inflammatory miRNAs predict radiation esophagitis in patients receiving definitive radiochemotherapy for non-small cell lung cancer. Radiother Oncol, 113(3):379–384 DOI: 10.1016/j.radonc.2014.11.006.

Yang D, Sun Y, Hu L, Zheng H, Ji P, Pecot CV, Zhao Y, Reynolds S, Cheng H, Rupaimoole R, Cogdell D, Nykter M, Broaddus R, Rodriguez-Aguayo C, Lopez-Berestein G, Liu J, Shmulevich I, Sood AK, Chen K, Zhang W. 2013. Integrated analyses identify a master MicroRNA regulatory network for the mesenchymal subtype in serous ovarian cancer. Cancer Cell,

23(2):186–199 DOI: 10.1016/j.ccr.2012.12.020.

Yang M, Chen J, Su F, Yu B, Su F, Lin L, Liu Y, Huang J-D, Song E. 2011. Microvesicles secreted by macrophages shuttle invasion-potentiating microRNAs into breast cancer cells. Mol Cancer, 10(1):117 DOI: 10.1186/1476-4598-10-117.

Yasunami Y, Kojo S, Kitamura H, Toyofuku A, Satoh M, Nakano M, Nabeyama K, Nakamura Y, Matsuoka N, Ikeda S, Tanaka M, Ono J, Nagata N, Ohara O, Taniguchi M. 2005. Vα14 NK T cell–triggered IFN-γ production by Gr-1^{+}CD11b^{+} cells mediates early graft loss of syngeneic transplanted islets. J Exp Med, 202(7):913–918 DOI: 10.1084/jem.20050448.

Yi R. 2003. Exportin-5 mediates the nuclear export of pre-microRNAs and short hairpin RNAs. Genes Dev, 17(24):3011–3016 DOI: 10.1101/gad.1158803.

Yoshimatsu G, Kunnathodi F, Saravanan PB, Shahbazov R, Chang C, Darden CM, Zurawski S, Boyuk G, Kanak MA, Levy MF, Naziruddin B, Lawrence MC. 2017. Pancreatic β-cell–derived IP-10/CXCL10 isletokine mediates early loss of graft function in islet cell transplantation. Diabetes, 66(11):2857–2867 DOI: 10.2337/db17-0578.

Yu G, Wang L-G, Han Y, He Q-Y. 2012. clusterProfiler: An r package for comparing biological themes among gene clusters. OMICS J Integr Biol, 16(5):284–287 DOI: 10.1089/omi.2011.0118.

Zeng Y. 2004. Structural requirements for pre-microRNA binding and nuclear export by exportin 5. Nucleic Acids Res, 32(16):4776–4785 DOI: 10.1093/nar/gkh824.

Zhang Y, He S, Du X, Jiang Y, Tian B, Xu S. 2017. Rapamycin suppresses hypoxia/reoxygenation-induced islet injury by up-regulation of miR-21 *via* PI3K/akt signalling pathway. Cell Prolif, 50(1):e12306 DOI: 10.1111/cpr.12306.

Zhao E, Keller MP, Rabaglia ME, Oler AT, Stapleton DS, Schueler KL, Neto EC, Moon JY, Wang P, Wang I-M, Lum PY, Ivanovska I, Cleary M, Greenawalt D, Tsang J, Choi YJ, Kleinhanz R, Shang J, Zhou Y-P, Howard AD, Zhang BB, Kendziorski C, Thornberry NA, Yandell BS, Schadt EE, Attie AD. 2009. Obesity and genetics regulate microRNAs in islets, liver, and adipose of diabetic mice. Mamm Genome, 20(8):476–485 DOI: 10.1007/s00335-009-9217-2.

Zhao S, Gordon W, Du S, Zhang C, He W, Xi L, Mathur S, Agostino M, Paradis T, Schack D von,

Vincent M, Zhang B. 2017. QuickMIRSeq: A pipeline for quick and accurate quantification of both known miRNAs and isomiRs by jointly processing multiple samples from microRNA sequencing. BMC Bioinformatics, 18(1):180 DOI: 10.1186/s12859-017-1601-4.

Ørom UA, Nielsen FC, Lund AH. 2008. MicroRNA-10a binds the 5′UTR of ribosomal protein mRNAs and enhances their translation. Mol Cell, 30(4):460–471 DOI: 10.1016/j.molcel.2008.05.001.

Declarations

Anlage 1

Technische Universität Dresden

Medizinische Fakultät Carl Gustav Carus

Promotionsordnung vom 24. Juli 2011

Erklärungen zur Eröffnung des Promotionsverfahrens

1. Hiermit versichere ich, dass ich die vorliegende Arbeit ohne unzulässige Hilfe Dritter und ohne Benutzung anderer als der angegebenen Hilfsmittel angefertigt habe; die aus fremden Quellen direkt oder indirekt übernommenen Gedanken sind als solche kenntlich gemacht.
2. Bei der Auswahl und Auswertung des Materials sowie bei der Herstellung des Manuskripts habe ich Unterstützungsleistungen von folgenden Personen erhalten:

Prof. Ezio Bonifacio

3. Weitere Personen waren an der geistigen Herstellung der vorliegenden Arbeit nicht beteiligt. Insbesondere habe ich nicht die Hilfe eines kommerziellen Promotionsberaters in Anspruch genommen. Dritte haben von mir weder unmittelbar noch mittelbar geldwerte Leistungen für Arbeiten erhalten, die im Zusammenhang mit dem Inhalt der vorgelegten Dissertation stehen.
4. Die Arbeit wurde bisher weder im Inland noch im Ausland in gleicher oder ähnlicher Form einer anderen Prüfungsbehörde vorgelegt.
5. Die Inhalte dieser Dissertation wurden in folgender Form veröffentlicht:

nicht zutreffend

6. Ich bestätige, dass es keine zurückliegenden erfolglosen Promotionsverfahren gab.
7. Ich bestätige, dass ich die Promotionsordnung der Medizinischen Fakultät der Technischen Universität Dresden anerkenne.
8. Ich habe die Zitierrichtlinien für Dissertationen an der Medizinischen Fakultät der Technischen Universität Dresden zur Kenntnis genommen und befolgt.

Ort, Datum

Unterschrift des Doktoranden

Anlage 2

Hiermit bestätige ich die Einhaltung der folgenden aktuellen gesetzlichen Vorgaben im Rahmen meiner Dissertation

- das zustimmende Votum der Ethikkommission bei Klinischen Studien, epidemiologischen Untersuchungen mit Personenbezug oder Sachverhalten, die das Medizinproduktegesetz betreffen

Aktenzeichen der zuständigen Ethikkommission

EK 502122018

20/SW/0074 (King’s college London)

- die Einhaltung der Bestimmungen des Tierschutzgesetzes

Aktenzeichen der Genehmigungsbehörde zum Vorhaben/zur Mitwirkung

DD24.1-5131/449/8

PBCFBE464 (King’s college London)

- die Einhaltung des Gentechnikgesetzes

nicht zutreffend

- die Einhaltung von Datenschutzbestimmungen der Medizinischen Fakultät und des Universitätsklinikums Carl Gustav Carus.

Dresden, den

Unterschrift des Doktoranen